A Sensor Independent Concept for the Characterisation of Imaging Spectrometers

Dissertation

zur

Erlangung der naturwissenschaftlichen Doktorwürde

(Dr. sc. nat.)

vorgelegt der

Mathematisch-naturwissenschaftlichen Fakultät

der

Universität Zürich

von

Birgit Suhr

aus Deutschland

Promotionskomitee:

Prof. Dr. Klaus I. Itten (Vorsitz)
Dr. Jens Nieke (ESA)
Dr. Matthias Kneubühler (RSL)
Dr. Peter Gege (DLR)

Zürich, 2009

Summary

This thesis describes an operational concept and the implementation of an automated process chain for the characterisation of hyperspectral sensors. The process chain includes the definition of sensor independent measurement procedures, the conduction of the measurements and the analysis of the recorded data to determine sensor parameters.

The design driver for the setup of the Calibration Home Base (CHB) was the imaging spectrometer APEX (Airborne Prism EXperiment). But the facility can also be used for the characterisation of other optical sensors like the DLR sensors ROSIS (Reflective Optics System Imaging Spectrometer), ARES (Airborne Reflective Emissive Spectrometer) and AISA (Airborne Imaging Spectrometer for different Applications).

The first part of this thesis describes the setup of the laboratory and its devices (chapter 2) as well as the operational concept for the automatic conduction of characterisation measurements (chapter 3). The concept divides the measurement process into three functional modules: a generic measurement control module (*Master*), a module for the control of the laboratory devices (*Slave*) and a sensor specific control module (*Sensor*) per sensor. The single modules interact via TCP/IP on the intranet by exchanging commands using well-defined XML formatted data. The implementation of the concept is described in Chapter 4.

Utilising the new *Slave* software the laboratory can be operated fully automated. The operator in the laboratory does not need a broad knowledge of the operation of the individual devices. The necessary manual settings are interactively reported to the operator by the *Slave* module. Furthermore the *Slave* module monitors a multitude of possible errors of the single laboratory devices. In addition the *Slave* enables external users to use the laboratory needing nothing more than the description of the interface.

The *Master* software is the central superordinate module which controls the *Slave* and the respective *Sensor* module. The *Master* hosts the various characterisation measurement procedures and executes the detailed instructions of the actual procedure(s). The *Master* offers many different options for the execution of measurements. For example, it is possible to use the emulate mode, or to control only the laboratory devices or the sensor, or to transfer data, or to carry out a data analysis. A time estimation function enables the evaluation of the estimated time for the execution of a measurement series.

The *Master* module has comprehensive monitoring functions to ensure a safe operation of the laboratory, to intercept arising errors, to interrupt the measurement process and to inform the operator immediately. Besides the monitoring functions, the *Master* stores the actual device settings in measurement logs which are necessary for the analysis software.

Summary

The current measurement process can be monitored using an internal web site. The operator has to access the laboratory only in case of a necessary manual interaction. This is beneficial for working safety aspects (dark room) and cost reasons.

Each sensor needs its individual *Sensor* module for the communication with the *Master* module, due to different internal devices which have to be controlled (sensor mirrors, internal calibration devices, shutter, etc.). The sensor control software has to provide an input interface for the communication with the *Sensor* module. If this is missing the sensor control software has to be modified. For the implementation of a new sensor, a *Sensor* module is needed and a new sensor interface and a GUI to capture the sensor parameter values have to be implemented in the *Master* module. The implementations of the two sensors AISA and ROSIS are described in chapter 4.4.

With the newly developed software modules larger measurement series can be performed automatically in less time.

The second part of the thesis was the development of generic characterisation measurement and analysis methods for imaging spectrometers in the wavelength range from 0.4 µm to 2.5 µm (chapter 5). The three main types are spectral, geometric and radiometric characterisation. Each of the defined measurement methods describes the setup of the necessary laboratory devices and explains the measurement principle. For the essential device parameters general selection criteria were defined. The developed IDL analysis procedures are generic except for the conversion of the raw data into the defined generic data format (ENVI cube format). Each analysis procedure has quality and error checks.

The first and second part of this work have been verified independently using the sensors AISA and ROSIS (chapter 6). The third part of the thesis exemplifies characterisation measurements and data analysis performed for the two above mentioned sensors intending to test the methods and to draw some conclusions from the results.

Zusammenfassung

Diese Dissertation beschreibt ein operationelles Konzept und dessen Umsetzung für eine automatisierte Prozesskette für die Charakterisierung von Hyperspektralsensoren. Diese Prozesskette beinhaltet die Definition von sensorunabhängigen Messverfahren, die automatische Durchführung der Messungen sowie die Analyse der aufgezeichneten Daten zur Bestimmung von Sensorparametern.

Maßgeblich für das Design und den Aufbau der „Calibration Home Base (CHB)“ war das luftgestützte abbildende Spektrometer APEX (Airborne Prism EXperiment). Die Einrichtung soll aber auch für die Charakterisierung von anderen optischen Sensoren genutzt werden, wie die abbildenden Spektrometer ROSIS (Reflective Optics System Imaging Spectrometer), ARES (Airborne Reflective Emissive Spectrometer) und AISA (Airborne Imaging Spectrometer for different Applications).

Der erste Teil dieser Doktorarbeit beschreibt den Aufbau des Labors und die einzelnen Geräte (Kapitel 2) sowie das Betriebskonzept für die automatische Durchführung von Labormessungen (Kapitel 3). Das Konzept unterteilt den Messprozess in drei Funktionsmodule: Ein generisches Steuerungsmodul für die Durchführung der Messungen (*Master*), ein Modul für die Steuerung und Überwachung der Laborgeräte (*Slave*) und in sensorspezifische Steuerungsmodule (*Sensor*). Die einzelnen Module kommunizieren untereinander per TCP/IP über Software-Schnittstellen und tauschen Steuerungsbefehle im XML-Format aus. Die Implementierung der Module ist in Kapitel 4 beschrieben.

Mit dem neuen *Slave*-Modul kann das Kalibrierlabor vollautomatisch betrieben werden. Der Labormitarbeiter benötigt kein umfangreiches Wissen über die Steuerung der einzelnen Geräte. Die notwendigen manuell durchzuführenden Einstellungen werden dem Labormitarbeiter von dem Softwaremodul interaktiv mitgeteilt. Darüber hinaus überwacht die *Slave* Software die einzelnen Geräte und fängt mögliche Fehler ab. Das *Slave*-Modul versetzt externe Nutzer in die Lage das Labor zu nutzen indem sie nur die Beschreibung der Software Schnittstelle benötigen.

Die *Master* Software ist das zentrale übergeordnete Modul welches sowohl das *Slave*-Modul als auch das *Sensor*-Modul steuert. Die *Master* Software verwalten die verschiedenen Messprozeduren und führt die einzelnen Steuerungsanweisungen der ausgewählten Prozedur(en) aus. Der *Master* bietet die verschiedensten Möglichkeiten der Durchführung einer Messung. Es ist zum Beispiel möglich, den Emulationsmodus zu nutzen, nur die Laborhardware oder den Sensor zu steuern, die aufgezeichneten Daten zu übertragen, oder/und eine Datenanalyse durchzuführen. Der *Master* hat eine Funktion zur Abschätzung der voraussichtlichen benötigten Messzeit einer ausgewählten Messprozedur.

Zusammenfassung

Das *Master*-Modul verfügt über umfangreiche Überwachungsfunktionen für ein sicheres Betreiben des Labors und um mögliche Fehler abzufangen; welche im Fehlerfall den Messprozess unterbrechen und den Labormitarbeiter sofort informieren.

Darüber hinaus werden alle durchgeführten Einstellungen der Geräte in Protokolldateien aufgezeichnet, welche bei der Analyse der Messdaten benötigt werden. Die aktuelle ausgeführte Messprozedur kann über eine interne Website beobachtet werden und der Labormitarbeiter braucht das Labor nur dann zu betreten, wenn ein manuelles Eingreifen notwendig ist.

Jeder Sensor benötigt ein eigenes *Sensor*-Modul für die Kommunikation mit dem *Master*-Modul, da jeder Sensor verschiedene interne Bauteile haben kann, die gesteuert werden können (z.B. Spiegel, interne Kalibrierquellen, Shutter, …). Die Steuerungssoftware des jeweiligen Sensors benötigt für die Kommunikation mit dem *Sensor*-Modul eine Schnittstelle. Für die Implementierung eines neuen Sensors ist ein *Sensor*-Modul notwendig und die *Master* Software ist um eine Schnittstelle zum *Sensor* Modul und eine graphische Oberfläche für die Schnittstellenparameter zu erweitern. Die Implementierung für die Sensoren AISA und ROSIS sind im Kapitel 4.4 beschrieben.

Mit den neu entwickelten Softwaremodulen können nun auch umfangreichere Messreihen in einer geringeren Zeit vollautomatisch durchgeführt werden.

Der zweite Teil der Arbeit umfasste die Definition von generischen Mess- und Analysemethoden zur Charakterisierung von abbildenden Spektrometern im Wellenlängenbereich von 0,4 µm bis 2,5 µm (Kapitel 5). Die drei wesentlichen Arten sind die spektrale, geometrische und radiometrische Charakterisierung. Diese sollten möglichst für jeden Sensor durchgeführt werden. Jeder der definierten Messmethoden beschreibt den Messaufbau und das Prinzip. Es werden die benötigten Geräte und deren Parameter beschrieben. Die entwickelten ENVI/IDL Analyseprozeduren sind ab der Rohdatenkonvertierung sensorunabhängig. Jede Analyseprozedur verfügt über Qualitäts- und Fehlerkontrollen.

Der erste und zweite Teil dieser Arbeit wurde anhand exemplarischer Messungen für die beiden Sensoren AISA und ROSIS getestet. Der dritte Teil der Arbeit (Kapitel 6) beschreibt diese Messungen und die Ergebnisse der Datenanalysen für die beiden Sensoren mit dem Ziel die beschriebenen Methoden und die Anwendbarkeit der Software zu testen. Darüber hinaus werden einzelne Analyseergebnisse diskutiert.

Table of Contents

List of Figures

List of Figures

List of Tables

List of Abbreviations

ADC	Analog-to-digital Converter
AIS	Airborne Imaging Spectrometer
AISA	Airborne Imaging Spectrometer for different Applications
APEX	Airborne Prism EXperiment
API	Application Programming Interface
Ar	Argon
ARES	Airborne Reflective Emissive Spectrometer
ASI	Airborne Hyperspectral Imager
AVIRIS	Airborne Visible/Infrared Imaging Spectrometer
AVIS	Airborne Visible / Infrared imaging Spectrometer
BIL	Band Interleaved by Line
BIPM	Bureau International des Poids et Mesures
CAF	Cluster Angewandte Fernerkundung
CASI	Compact Airborne Spectrographic Imager
CCD	Charge Coupled Device
CEOS	Committee on Earth Observing Satellites
CHB	Calibration Home Base
CHRIS	Compact High Resolution Imaging Spectrometer
CNES	Centre National d'Études Spatiales
CORBA	Common Object Request Broker Architecture
CSL	Centre Spatial de Liège
DAIS	Digital Airborne Imaging Spectrometer
DAQ	Data acquisition
DLR	German Aerospace Center
DN	Digital Numbers
DSU	Data Storage Unit
EnMAP	Environmental Mapping and Analysis Program
ENVI	Environment for Visualizing Images
ESA	European Space Agency
FODIS	Fiberoptic downwelling irradiance sensor
FOV	Field of View
FTP	File Transfer Protocol
FWHM	Full Width at Half Maximum
GPS	Global positioning system
GUI	Graphical user interface
Hg	Mercury
HTTP	Hypertext Transfer Protocol
HyMAP	Hyperspectral Maper
IDL	Interactive Data Language
IFC	In flight calibration
IFOV	Instantaneous Field of View
INI	Initialization
INMS	Institute for National Measurement Standards
IP	Internet protocol address
JAXA	Japan Aerospace Exploration Agency
JPL	Jet Propulsion Laboratory
Kr	Krypton
LAN	Local area network
LSF	Line spread function
MFC	Microsoft Foundation Class
MTF	Modulation Transfer Function
NASA	National Aeronautics and Space Administration
Ne	Neon

NERC	Natural Environmental Research Council
NIR	Near-infrared part of the electromagnetic spectrum
NIST	National Institute of Standards and Technology
NMI	National Measurement Institute
NPL	National Physical Laboratory
NRC	National Research Council
OSI	Open Systems Interconnection
PC	Personal computer
PCI	Peripheral Component Interconnect
PGP	Prism-Grating-Prism
PROBA	Project for On Board Autonomy
PSF	Point spread function
PTB	Physikalisch-Technische Bundesanstalt
PV	Peak to Valley
QTH	Quartz Tungsten Halogen
RMI	Remote Method Invocation
RMS	Root mean square
ROSIS	Reflective Optics System Imaging Spectrometer
RPC	Remote Procedure Calls
SI	International System of Units
SOAP	Simple Object Access Protocol
SRF	Spectral Response Function
SSI	Spectral Sampling Interval
SWIR	Short-wave Infrared part of the electromagnetic spectrum
TCP	Transmission Control Protocol
TIR	Thermal Infrared
UDP	User Datagram Protocol
VIS	Visible part of the electromagnetic spectrum
W3C	World Wide Web Consortium
WGCV	Working group on calibration and validation
Xe	Xenon
XHTML	Extensible HyperText Markup Language
XML	Extensible Markup Language
XSD	XML Scheme Definition
XSLT	Extensible Stylesheet Language Transformations

1 Introduction

In recent years the demand for improved and reliable Earth observation data has increased. Motivations are to understand better the functioning of the Earth systems, the impacts of the climate change, improvements of models and the reliance on data combination of different sensors and sources. Data combination can only be conducted if each data set has a clear and reliable uncertainty specification [1]. Geospatial information is growing dramatically, in governmental and private areas. Many Earth observation applications have advanced to the point where high quality digital image products are essential for success. Raw or uncorrected imagery can no longer be used to provide meaningful information for natural resource management. It is important to ensure that Earth observation data can be used by non-specialists in the government and private sectors. This data has to be reliable and quantitatively usable which requires standardised procedures for the data processing [2].

It has been an issue in the Earth observing community for over two decades to have terms for consistency in sensor calibration. Characterisation is an essential component of any remote sensing system [1]. Sensor characterisation, calibration and validation, data standardisation and quality assurance play integral roles in strengthening the various links in the chain from remote sensing and other data to information of value to users. When a new Earth observation sensor (spaceborne or airborne) is being built, characterisation and validation research must be undertaken to provide acceptable results for the new capability [2].

During the last 15 years, various studies have covered data standardisation. Many committees and groups are involved in sensor characterisation and data quality evaluation. One of them is the working group on calibration and validation (WGCV) of the Committee on Earth Observing Satellites (CEOS). In 1992, the European study “Research Needs to Encourage the Growth of the Earth Observation Applications Market” [2] identified a lack of proper standardisation in diverse applications. A second Canadian study in 1995 a remote sensing market analysis for calibration and validation revealed that Earth Observation data would only become a mainstream technology if a consistent data quality will be available which implicates appropriate standardisation tools. Based on this item, three national Canadian workshops between 1996 and 1998 established strategic priorities for the Canadian calibration and validation efforts. The latest user requirement study from 2004 countersigned that there is a definitive need for standardisation and calibration of Earth Observation data [2].

The CEOS formally recognised in November 2000 the resolution that “Pre-launch calibration should be performed using equipment and techniques that can be demonstrably traceable to, and consistent with, the SI system of units; and traceability should be maintained throughout the lifetime of the mission” [1], p. 31). WGCV defined calibration as “the process of quantitatively defining the system response to known, controlled signal inputs” [3].

The following two sections give a brief overview about the history of hyperspectral sensors and the main characterisation aspects.

Airborne Imaging Spectrometers

Early remote sensing multispectral sensors record data at several wavelengths and hyperspectral imaging spectrometer collect data of hundreds of spatial pixels and channels. Imaging spectroscopy is a technique for collecting many, very narrow, contiguous bands in the visible, near-infrared (IR), mid-IR and thermal IR of the electromagnetic spectrum.

Most sensors use either a whiskbroom or pushbroom technique for the collection of data. A whiskbroom spectrometer has an opto-mechanical scanner where a mirror tilts to different angles perpendicular to the forward motion of a platform. Each band is represented by one detector element. The pushbroom approach collects all across track pixels (column) at the different viewing angles, perpendicular to the forward motion, simultaneously. Pushbroom sensors use 2D detector arrays for the spatial information in one dimension and the spectral information in the other [4].

One of the first hyperspectral sensors was the Airborne Imaging Spectrometer (AIS) developed by the Jet Propulsion Laboratory (JPL), first flown in 1982. It collected data in 128 spectral bands with a band width of 9.3 nm in the spectral range from 1.2 to 2.4 µm and was a pushbroom scanner. The airborne visible/infrared imaging spectrometer (AVIRIS) developed by NASA and JPL was tested in 1987 and placed in service 1989. AVIRIS operates in the spectral range from 400 nm up to 2.5 µm with 224 channels, each 10 nm wide and has 614 across track pixels [5, 6]. The first civilian space borne hyperspectral sensors are HYPERION on the EO-1 platform, launched in 2000 by NASA, and the Compact High Resolution Imaging Spectrometer (CHRIS) on the Project for On Board Autonomy (PROBA) platform, run by European Space Agency (ESA) since 2001 [7].

The German hyperspectral satellite mission Environmental Mapping and Analysis Program (EnMAP) from the German Aerospace Center (DLR) space agency is envisaged to be launched in 2012. Examples of airborne sensors are DAIS 7915 [8-11] (DLR, GE), HyMAP [12] (Integrated Spectronics, AU), ROSIS [13, 14] (DLR, DE), CASI [15] (ITRES, CA), AISA [16] sensors from SPECIM, FI and ASI/HySpex [17] (Norsk Elektro Optikk AS (NEO), No) and AVIS (Ludwig-Maximilians-University Munich, GE) [18]. Future sensors are the Airborne Prism Experiment (APEX) [19] developed by a Swiss / Belgium consortium and the DLR Airborne Reflective Emission Spectrometer (ARES) [20].

Laboratory characterisation

Generally the calibration and characterisation is an essential part of any imaging spectrometer. Calibration can comprise issues such as conversion from raw data to physical units, laboratory devices, calibration standards, vicarious calibration, in-flight-calibration, sensor models or the measurements to determine a sensor parameter, each of these issues is an own subject [1].

Calibration in this thesis means the conversion of sensor signals into physical units. Whereas characterisation means the determination of sensor parameters like across track Line Spread Function (LSF) or Spectral Response Function (SRF). Ideally sensors are characterised under controlled conditions in the laboratory (e.g. temperature, humidity, pressure). A full characterisation of a sensor is very time and cost intensive. Characterisation takes place before the sensor is operational. In case of spaceborne sensors laboratory measurements can only be performed before launch. Normally airborne sensors are calibrated in regular intervals between flight cycles in the laboratory [21]. Those characterisation measurements are necessary for the monitoring of the sensor properties and the detection of discrepancies (e.g. misalignments or contaminations). Those problems can be caused by transportation, installation or operation in an aircraft by physical stresses (vibrations, collisions, shocks, dust, etc.). In case of discrepancies, the actual calibration loses its validity and new characterisation measurements are necessary. But those frequent monitoring calibrations are often omitted due to their enormous time and cost effort.

The sensor scan method (whiskbroom or pushbroom) has an influence on the characterisation strategy of imaging spectrometers [4, 22]. The across track pixels of a whiskbroom scanner are observed by the same spectrometer. Therefore the assumptions are: the response functions as well as the dark signal don't vary with the scan angle and can be characterised only for the nadir position. The radiometric response will vary smoothly across the field of view. Since a pushbroom sensor has different light paths, more than one scan angle position and channel has to be characterised. The characterisation of a pushbroom sensor is more complex and time- and cost-intensive than for a whiskbroom scanner [4].

In general, laboratories equipped for the entire characterisation represent a big advantage in reducing the risk associated with multiple transportations and handling of the instrument. Additionally the time and cost factor, as well as the consistency in test conditions, utilised standards and equipment, are significantly reduced when performing the entire procedure at the same time and in the same facility. Most of the calibration laboratories are setup for a specific instruments located close to the place where the sensor was built or is being hosted. Laboratories equipped for the characterisation of spectrometers are listed in Table 1.1.

Table 1.1: Calibration laboratories

Country	**Organisation**
Australia	National Measurement Institute (NMI) [23]
UK	NERC Field Spectroscopy Facility (FSF) [24]
UK	National Physical Laboratory (NPL)
France	Onera, Toulouse [25]
France	Centre National d'Études Spatiales (CNES), Toulouse
Japan	JAXA, Earth Oberservation Research Center (EORC) [26]
Belgium	Centre Spatial de Liège (CSL) [27]
German	German Aerospace Center (DLR), Oberpfaffenhofen and Berlin
Italy	Thales Alenia Space
US	NASA, Jet Propulsion Laboratory [28]

A major challenge for the near future will be to standardise the technology in order to make characterisation of different sensors and different laboratories comparable and compatible. With the advent of new instruments such as ARES and APEX, an increased calibration accuracy and an intrinsic data quality must become standard in imaging spectrometry [4].

1.1 Problem Description

The DLR Oberpfaffenhofen operates two calibration facilities for airborne imaging spectrometers. Both laboratories are equipped with hardware for the geometric, spectral and radiometric characterisation. The older laboratory, where ROSIS was characterised, has a tilt and rotating stage, which can tilt sensors with a mass up to 50 kg [4]. The concept for the new laboratory is a tilting mirror under a fixed sensor with a weight up to 350 kg including interface [21].

At the beginning of the thesis manufacturer characterisation concepts are sensor specific in the majority of cases. An analysis of the sensor specific characterisation concepts for DAIS [10],[9, 29], ROSIS [13, 14, 30, 31], AREX [32] and APEX [33] result in the use of different laboratory components, measurement procedures, analysis methods, software programs and level of automation during the measurements and analysis. Figure 1.1 illustrates the differences and complexity revealed at the time of the analysis. The dashed lines are manual interactions and the solid lines are automated ones. Not all existing devices are represented in the diagram.

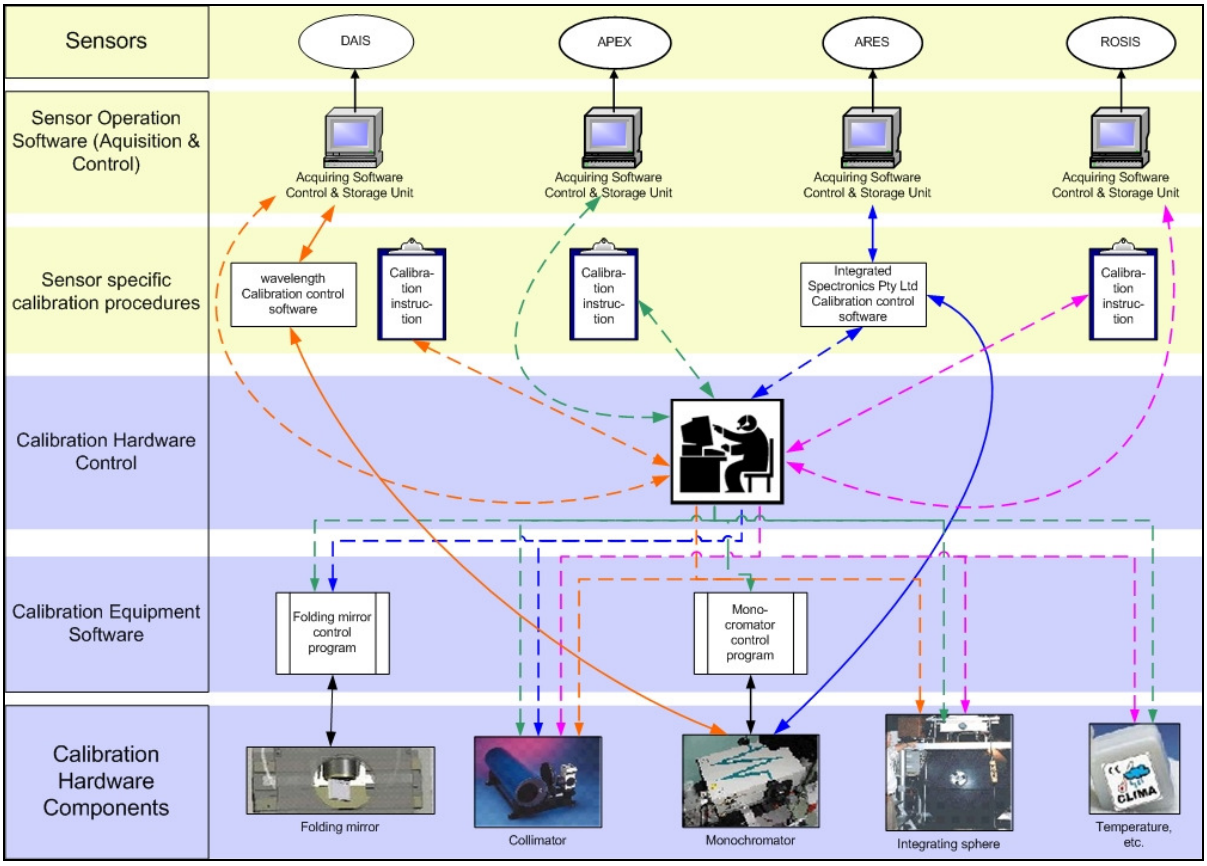

Figure 1.1: Overview of the existing characterisation workflows for different sensors

The percentage of manual intervention in the workflows is remarkably high. Different laboratory devices are used for the same purpose (e.g. monochromator for spectral measurements for ROSIS and DAIS). A complete characterisation of the DLR sensors (DAIS, ROSIS) has not been performed up till now. One of the reasons is the enormous expenditure of time for the execution of the characterisation measurement and the use of multiple programs for the analysis.

The existing sensor-specific characterisation concepts differ in their methods and they are mostly not comparable to each other. A major future challenge is to use standardised characterisation methods to get a better basis for comparability and interoperability for different sensors [4, 34]. The present characterisation methods are sensor dependent. A generalised concept does not exist [35].

This work focuses on the imaging spectrometers which will be characterised in the new DLR calibration facility. The involved DLR sensors are ROSIS-03 [14, 31], AISA 1710 [36] and ARES, but the demanding requirements of the new facility arose from APEX [19]. Table 1.2 contains some parameters of these sensors.

Table 1.2: Specifications of the sensors for the characterisation at the DLR laboratory

Parameter	ROSIS-03	AISA 1710	ARES	APEX
FOV (°)	16	57.6 / 21.7	65	28
IFOV (mrad)	0.56	2.4 / 0.9	2	0.49
Number of spatial pixel	512	364	813	1000
Spectral Range (µm)	0.43 – 0.86	0.42 – 0.89	VIS: 0.47 – 0.89 NIR: 0.89 – 1.35 SWIR1: 1.36 – 1.80 SWIR2: 2.00 – 2.42 TIR: 8.10 – 12.1	VNIR: 0.38 – 1.0 SWIR: 0.95 – 2.5
Number of channel	115	286	VNIR & SWIR: 115 TIR: 30	VNIR: 313 SWIR: 221
Spectral sampling interval (nm)	4	1.6 to 9.8	VIS: 15 – 16 NIR: 14 – 16 SWIR1: 15 – 17 SWIR2: 13 – 16 TIR: 115 – 130	5 10
Dynamic range (bit)	14	12	14..16	VNIR: 12 SWIR: 14
Sensor type	Pushbroom	Pushbroom	Whiskbroom	Pushbroom
In-Flight Calibration (IFC) facility	Mercury vapour lamp		3 Blackbodies, calibration lamp	QTH lamp, Rare earth filter, 3 band pass filters, NG4 attenuation filter

1.2 Objectives and Structure

Taking into consideration the above mentioned challenges and the planned use of the DLR laboratory facility for the characterisation of DLR and external sensors a new concept is necessary. This thesis addresses questions related to the laboratory characterisation of airborne imaging spectrometers. This work focuses on the DLR calibration facility Oberpfaffenhofen and on the sensors to be calibrated in the future.

Based on the above described state (Figure 1.1) the objective of this thesis is the establishment of a complete characterisation process chain beginning with the definition of generic measurement methods, an automatic execution of the measurements, and the application of the developed generic analysis methods and procedures. Generic means in the context of this thesis the definition of measurement and analysis methods which are applicable for a variety of hyperspectral sensors.

Automation of the characterisation process chain
The goal is the automatic control of all devices of the laboratory and the minimising of the manual tasks to ensure fast execution of characterisation measurements under constant quality standards. It is intended to use the laboratory as a universal facility for the characterisation of the current sensors (APEX, ROSIS and AISA) and for further airborne imaging spectrometers. A main goal is the development of an operational concept which considers the integration of the different laboratory devices as well as the spectrometers, enables a parameterised command access and provides logging and control functions. An issue is the definition and establishment of an interface for external laboratory operators, which allows a simple control of the different devices. There will be investigation into which parts of the control can be automated and which would be better kept manual.

Sensor independent measurement methods
Certain sensor property parameters can be determined by standardised procedures. Others have to be characterised with specific sensor procedures. Based on the analysis of the existing concepts, standard characterisation procedures will be defined. The focus of this thesis will be the definition of generic procedures for regular sensor characterisation which are applicable for hyperspectral sensors in the wavelength range from 0.4 µm up to 2.5 µm. A set of sensor property parameters will be defined which can be determined from the generic spectral, geometric and radiometric procedures. These procedures will take into account the existing laboratory devices with its hardware restrictions.

Sensor independent analysis methods
Generic analysis methods will be developed and implemented for the determination of the defined sensor parameters. The execution of analysis procedures should be automated and parameterised. The implementation of error- and quality checks, output functions for suitable result figures and standardised measuring logs, are major objectives of this thesis.

Application of the defined methods

The different spectral, geometric and radiometric characterisation methods are developed for sensors with a spectral range from 0.4 µm to 2.5 µm. The applicability of the methods will be demonstrated for two different sensors. Example measurements and analysis will be performed with the DLR available sensors AISA and ROSIS. Both sensors are pushbroom sensors recording data in the spectral range from 0.4 µm to 0.9 µm. Finally, it will be investigated whether it is possible to define sensor independent characterisation procedures or not.

Structure of this work

The devices of the Calibration Home Base (CHB) laboratory are described in detail in chapter 2. The chapter explains the concept behind the optical bench and the setup of the single devices of the three main characterisation groups (spectrometry, geometry and radiometry).

The ideas of the operational concept are explained in chapter 3. This chapter describes the network and communication issues, describes the partial aspects of the tasks and points out the requested functionalities of the three areas of responsibilities (CHB hardware control, measurement process, sensor control). An additional section specifies the general ideas and functional requirements for the data analysis. Chapter 4 gives a detailed description of the implementation of the operational concept.

The defined measurement methods for the determination of spectral, geometric and radiometric sensor properties are explained in chapter 5. The sections for each measurement method group give a description of the necessary laboratory devices, the measurement principles and the requested settings followed by the details of the relevant analysis method.

The execution of the characterisation measurements and analysis are demonstrated with the two pushbroom sensors AISA and ROSIS. The measurement setups are explained and the results are discussed in chapter 6. Chapter 7 draws conclusions on the results achieved by this work.

2 DLR Calibration Laboratory

Within the framework of the pushbroom sensor Airborne Prism Experiment (APEX) project the European Space Agency (ESA) has co-funded parts of the new characterisation and calibration facility located at DLR Oberpfaffenhofen. The scope of the new calibration facility is to perform a variety of characterisation measurements for the verification of the instrument performance. During the operational phase of APEX regular instrument checks will be performed, such as on-board characterisation, pre and post-flight laboratory characterisations and vicarious calibrations. The new laboratory was designed to fulfil the requirements for APEX performance checks, but it can also be used for other imaging spectrometers. The facility also hosts additional equipment for other sensors such as thermal sources for the DLR sensor ARES. The laboratory is located in a large semi-clean, temperature-controlled, dark room (see Figure 2.1).

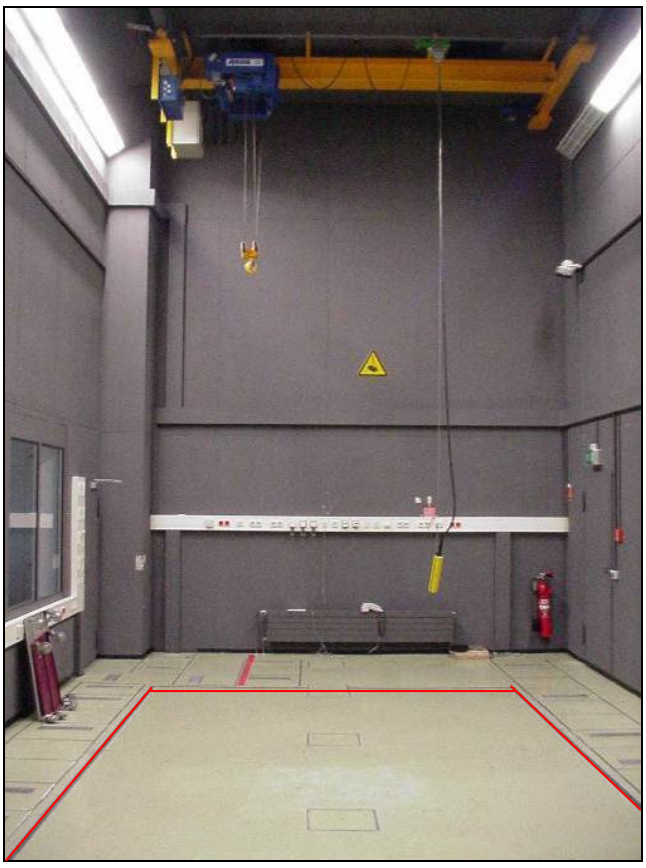

Figure 2.1: Laboratory room before setup

Figure 2.1 gives a view of the situation before the setup. In the middle of the floor is a ~51 t foundation (8.3 m × 3.5 m × 0.8 m) which is de-coupled from the building to avoid vibrations. This “seismic block” (red line) is isolated from vibrations from the building and from underground. The taken Seismometer measurements demonstrated that the vibrations are insignificant for the foreseen characterisation and characterisation processes [37]. Beyond that the laboratory is equipped with a crane, has a broad entrance door, is easily accessible (no steps and elevators) and it is close to the airfield. All detail requirements, based on the APEX statement of work [38], are listed in Table 2.1.

Table 2.1: Laboratory requirements and premises ([37], modified)

Requirements	Calibration Laboratory at Oberpfaffenhofen, Germany
Room size	12.8 m × 5.5 m, height: 8 m
Crane	Lifting capacity up to 2 tons, the traverse path covers almost the total length and width of the room
Darkroom	No outside windows, shutters on all internal windows, dark wall paint
Semi Clean Environment	Air filters and air flow control installed
Temperature control	85 kW air-conditioning, temperature control (22 ± 1 °C)
Humidity control	Humidifier installed
Vibration damping	de-coupled 52 ton seismic block (size 8.25 m × 3.6 m, 0.8 m height)
Accessibility	Outside ramp, laboratory door size 2.3 m width & 4.1 m height, no steps
Infrastructure	Power supply (240 / 380 V), independent power supply, compressed air, Local Area Network (LAN), GPS antenna
Vicinity to airfield	Approx. 100 m driveway

An overview of the whole setup of the laboratory is given in Figure 2.2.

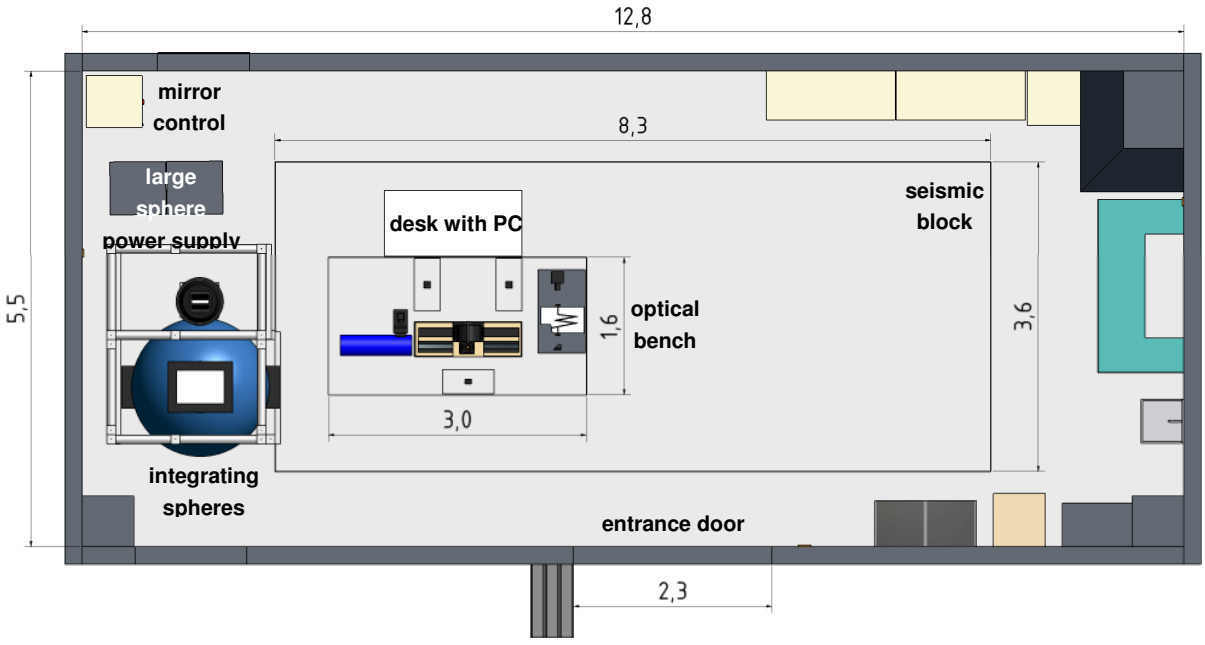

Figure 2.2: Laboratory Sketch

The following subchapters describe the optical bench and hardware interface followed by the hardware components for each of the three main characterisation groups (spectral, geometric and radiometric). The last section contains a description of the additional necessary components.

2.1 Optical Bench

The existing geometric characterisation equipment at DLR Oberpfaffenhofen, conceived for ROSIS, can carry sensors with a mass of up to 50 kg.

For the APEX sensor a new design was necessary since APEX has a higher mass and size. The initial design for a new optical bench was a stage which moves the sensor to dedicated viewing angles. With the increase of mass (from ~100 kg up to 260 kg) during the sensor design phase an alternative stage design was necessary.

The new concept [39] is to fix the sensor and the laboratory devices and to move and tilt only a mirror. The principle is shown in Figure 2.3. The sensor is mounted in a fixed position looking downwards to a mirror. The mirror reflects the light from the monochromator into the sensor. The mirror can be moved along the linear stage and tilted in the across track direction of the sensor to set an angle of incidence. The light can also be provided from the geometric characterisation side (collimator) by tilting the mirror to the other side.

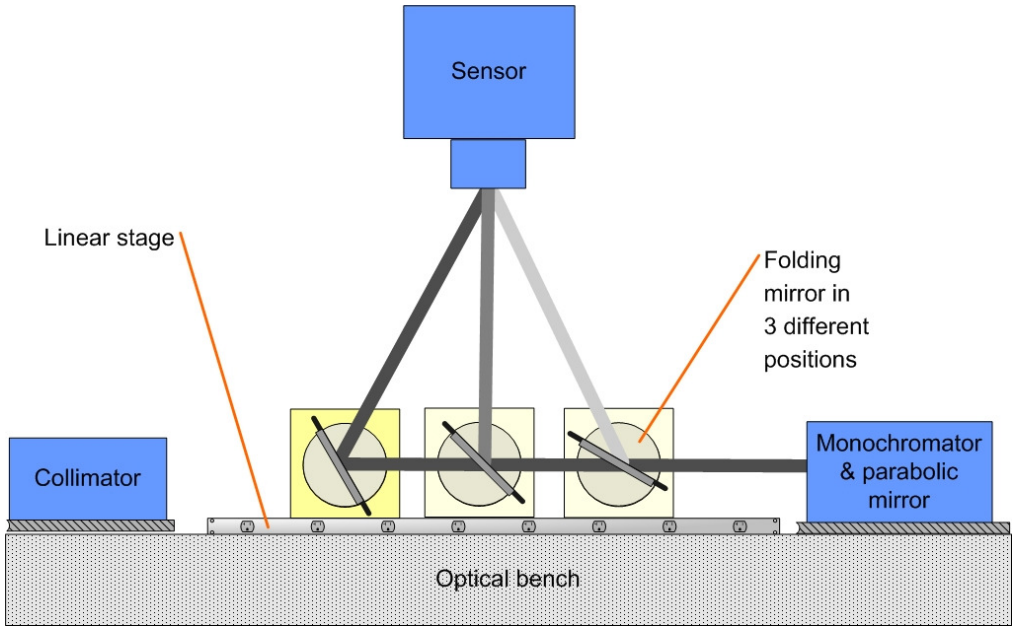

Figure 2.3: Folding Mirror Principle

The complete setup of the individual hardware components on the bench is illustrated in Figure 2.4. The optical bench (1) comprises, in addition to the folding mirror (4), the geometric (5) and spectral (6) characterisation hardware components. The adapter plate (3) with the sensor is mounted on top of three pillars (2) looking downwards to the middle of the linear stage (4).

The optical bench is a black 6.4 t granite block (3.0 m × 1.6 m × 0.4 m) with three pillars (0.6 m × 0.3 m × 0.67 m) produced by J. Fischer, Aschaffenburg, Germany. The flatness of the polished surface is less than 1.24 µm at the linear stage mounting area.

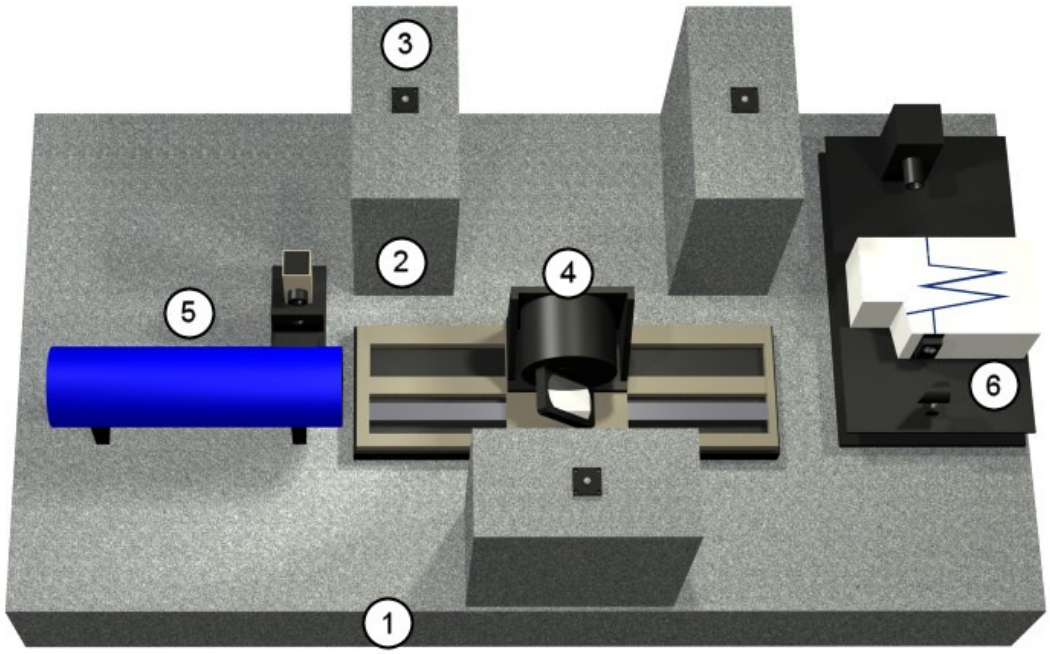

Figure 2.4: Draft of the optical bench [34]

The folding mirror (4) consists of two air-bearing stages and a mirror. The rotary stage (ABR1000) with the mirror is mounted on the linear stage (ABL80075-LC). The assembly was manufactured by AEROTECH GmbH (Nürnberg, Germany). The linear stage is moveable from -375 mm up to +375 mm. The mirror can be rotated by 360°. The home position of both stages is at 0° (face up to the sensor) and 0.0 mm (centre of the linear stage). The accuracy is ±0.025 mm for the linear and ±0.007 mrad for the angular stage.

The elliptical size of the folding mirror is 180.04 mm × 119.85 mm. The surface is a special kind of silver coating on Zerodur substrate (Optical Surfaces Ltd, Kenley, England). The root mean square (RMS) deviation determined for a sensor aperture of 200 mm × 10 mm at 632.8 nm test wavelength is 0.010 wavefront [40].

The mechanical interface between the bench and a sensor adapter plate is the V-groove on the three pillars (see Figure 2.5). The spheres can either directly be attached to the plate or they can be loose. The distance between the folding mirror and the adapter plate level is 200 mm.

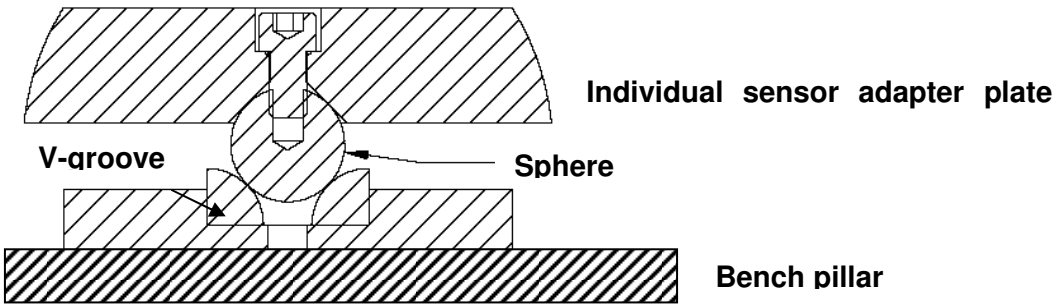

Figure 2.5: Mechanical interface between optical bench and sensor plate ([40])

Universal DLR adapter

A sensor can be aligned and attached on the optical bench by using the DLR universal adapter (see Figure 2.6). It was manufactured by Mühlbauer Maschinenbau GmbH (Runding, Germany) in May 2008 and can carry loads up to 150 kg. The adapter has four adapter rings to fit the opening. Each ring has several threads to mount a sensor on the adapter (see App. A, Figure A.1).

The adapter has three possibilities to align a sensor (see Figure 2.6). The sensor can be moved in flight direction (X-axis) and rotated in Y and Z direction. The X-axis (1) is adjustable from -50 mm up to +50 mm in steps of 0.01 mm. The pitch angle β (Y-axis) can be changed with the handwheel (2) in the middle of the adapter and the yaw angle γ (Z-axis) with the left one (3). The β and γ angles can be changed in the range from -1° up to +1° with an increment of 0.2 mrad.

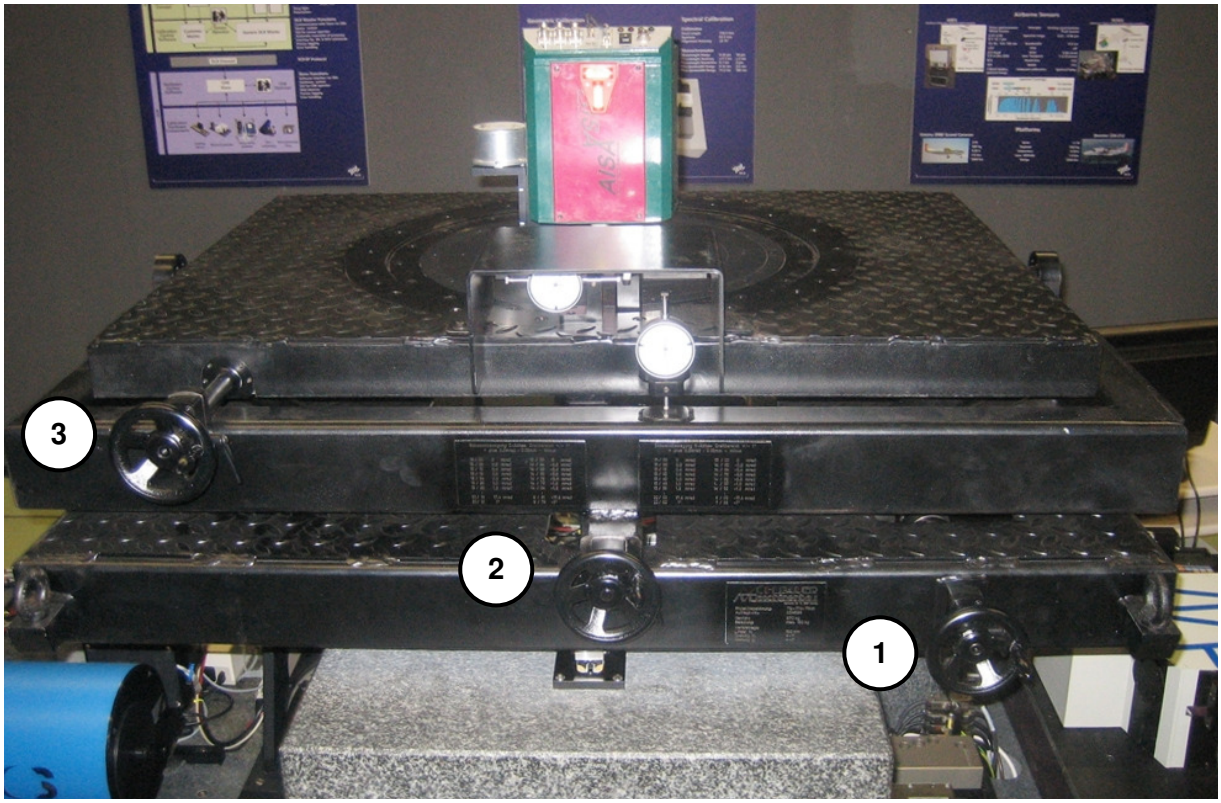

Figure 2.6: DLR universal adapter with the AISA sensor

The next two sections describe the components (5) and (6) on both sides of the optical bench (see Figure 2.4).

2.2 Spectral Measurement Components

A 1/4-m ORIEL monochromator MS257™ is a wavelength standard for spectral measurements [41]. It is an F/3.9 asymmetric in-plane Czerny-Turner instrument with an exit focal length of 257.4 mm. Stray light is negligible. Additional parts of the monochromator are two automatic switching fourfold grating turrets (see Table 2.2) and a wheel with long pass filters (see Table 2.3) suitable to the wavelength range of each grating [42].

The used input and exit slits are precision micrometers which can continuously vary the slit width from 40 µm to 3 mm. The input slit height is fixed (15 mm) and the exit slit can be set to 1, 2, 4 or 10 mm. The shutter at the entrance of the monochromator can be closed automatically for dark measurements.

The MS257™ uses a high speed stepper motor. The wavelength accuracy is ±0.1 nm and the repeatability is 0.06 nm for a 1200 l/mm grating. The wavelength step size is 0.028 nm and the wavelength temperature change is 0.01nm/°C [41]. The monochromator has been calibrated by the manufacturer by measuring hundreds of points with an interferometer. A software correction algorithm is implemented into the monochromator. The automatically controllable filter wheel (ORIEL model 77737) can hold up to five 25.4 mm diameter filters with a 22 mm aperture.

Table 2.2: Monochromator turrets and gratings

Turret No.	Grating No.	Oriel No.	Wavelength range (nm)*	Blaze wavelength (nm)	Line density (lines/mm)	Reciprocal dispersion (nm/mm)**	Minimum bandwidth (nm)***
1	1	77752	450 — 1400	750	1200	3.1	0.12
1	2	77745	600 — 2500	1000	600	6.4	0.26
1	3	77748	1100 — 3400	2000	300	12.9	0.52
1	4	77751	4500 — 20000	7000	75	51.7	2.07
2	1	77742	200 — 1400	350	1200	3.2	0.13
2	2	77752	450 — 1400	750	1200	3.1	0.12
2	3	77768	900 — 3000	1600	600	6.2	0.25

*Primary wavelength region is where the grating efficiency is ≥20%. **At blaze wavelength. ***Calculated as slit width / dispersion for 40 µm slit width.

Table 2.3: Long pass filter glasses

No.	Part No.	Diameter (mm)	Thickness (mm)	Cut-on wavelength (nm)	Use with grating no.	Use with turret no.
1	305FG01-25, (L.O.T.-Oriel)	25	3	305	1	2
2	550FG05-25, OG, (L.O.T.-Oriel)	25	3	550	2 1	2 1
3	830FG07-25, RG, (L.O.T.-Oriel)	25		830	2	1
4	3-51362, RG-1000, (L.O.T.-Oriel)	25.4	3	1000	3	2
5	50933, LWP-1405-25, (L.O.T.-Oriel)	25	3	1450	3	1
6	50831-FK, IR long pass, (L.O.T.-Oriel)	25	3	2500	-	-
7	50834-FK, IR-long pass, (L.O.T.-Oriel)	25	2.5	7300	4	2
8	582330, JB450, (Laser Components)	25	3	450	-	-

Two Quartz Tungsten Halogen (QTH) lamps with different power (12 V/100, 15 V/150 W, L.O.T.-Oriel) used for the wavelength range between 0.35 µm and 3.0 µm.

The light source is used with a current-controlled stabilised power supply (TOE 8851, Toellner). For the wavelength from 3 µm up to 14 µm the light source can be changed to an infrared ceramic element (ORIEL model 6575). For the infrared source in addition a reflector (ORIEL model 7295, focal length = 86 mm) is needed to focus the collimated beam from the ceramic light source onto the entrance slit of the monochromator. The ceramic source is a borosilicate glass substrate, cemented to a mirror mount [43].

Five neutral density filters (Laser Components) are available for the monochromator (see Table 2.4). Each filter is 3 mm thick and has a diameter of 25 mm. A filter wheel with four filters is mounted behind the exit slit of the monochromator and wheel position five is not equipped with a filter. The filter wheel is computer controlled.

Table 2.4: Neutral density filters

Part No.	Transmission (%)	Wheel Position
LCQ-400-F	0.01	—
LCQ-300-F	0.1	1
LCQ-200-F	1.1	2
LCQ-100-F	10	3
LCQ-30-F	50.12	4

A parabolic mirror is mounted in front of the exit of the monochromator slit to parallelise the beam. This off-axis paraboloidal reflector (L.O.T.-Oriel, no. 45347) has an aperture of 63.5 mm and a focal length of 119.4 mm. It has a wideband rhodium coating. A technical drawing of the mirror is shown in App. A, Figure A.2.

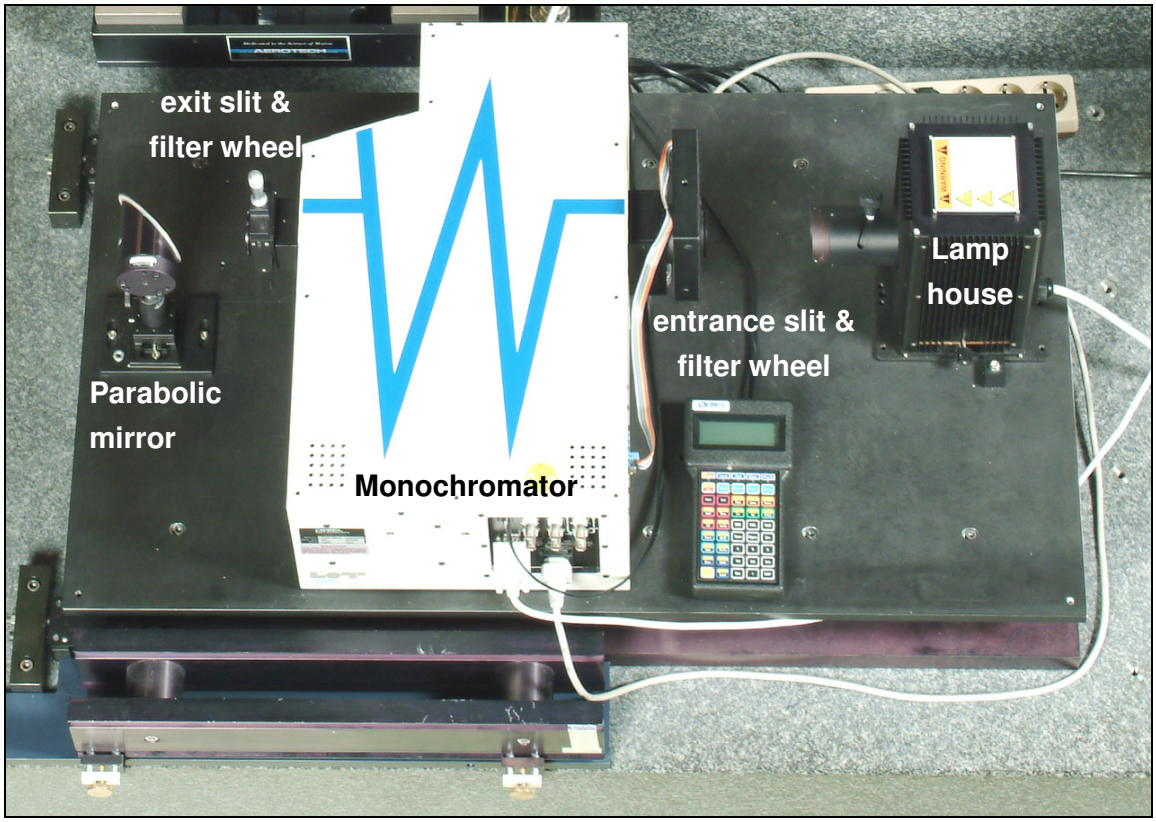

Figure 2.7: Adjustment of spectral characterisation components

All hardware (monochromator, lamp house and parabolic mirror), described above, are mounted on a base plate (ASTRO Feinwerktechnik, Berlin, Germany) which is attached on the optical bench (see Figure 2.7).

2.3 Geometric Measurement Components

Components for the geometric characterisation are a collimator, a slit wheel and a light source (see Figure 2.8). The main part is an off-axis collimator with a focal length of 750 mm and an aperture of 120 mm (Optical Surfaces Ltd.). The wavefront accuracy is lambda/5 peak to valley (PV) at 633 nm in the field centre. The slit wheel has three horizontal and three vertical slits with different slit width (50 µm, 100 µm and 1000 µm). Each slit has a length of 10 mm. The slits are arranged on a slice driven by a stepper motor (Optical Surfaces Ltd.) with a resolution of 0.01° = 0.17 mrad for one movement step. The 100 Watt QTH lamp is mounted in a fan cooled housing and stabilised by a dual-output power supply (TOE 8852, Toellner). The slit wheel assembly is mounted in the focal plane of the collimator.

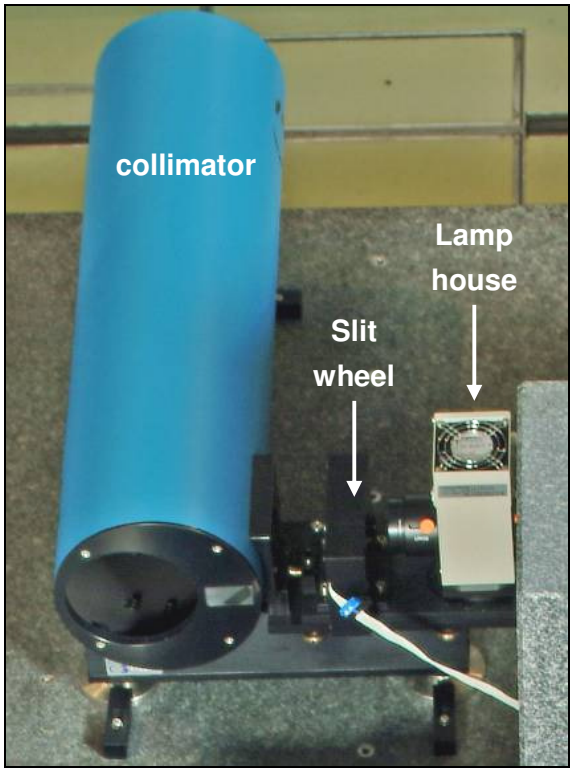

Figure 2.8: Adjustment of the geometric characterisation components

Instead of the QTH lamp an auto-collimation head (RET-02, Trioptics, Wedel, Germany) with a 5 W bulb can be mounted at the collimator entrance. The head is equipped with an eyepiece and a cross line reticle inside. The reticle has a dark cross and an illuminated background. The reticle has a line width of 0.02 mm and a diameter of 12 mm.

2.4 Radiometric Measurement Components

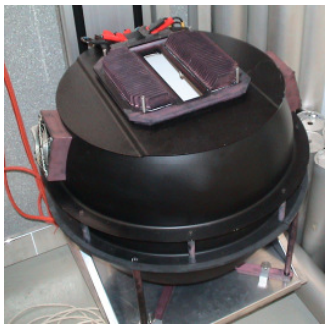

For radiometric measurements two integrating spheres are available. The small sphere (PRC Krochmann, Berlin) has a diameter of 50 cm and an output port of 4 cm × 20 cm. Its four 100 Watt QTH lamps are operated by a stabilized power supply (TNs 25-1000, Heinzinger). It is periodically calibrated against a national standard at a national certified laboratory (Physikalisch-Technische Bundesanstalt (PTB), Berlin, Germany). This sphere is used for absolute radiometric calibration.

The large integrating sphere (SC-5000, Labsphere) has a diameter of 1.65 m and an output port of 55 cm × 40 cm. It is equipped with 18 QTH lamps, each lamp has is own stabilized power supply (LPS-200-H, Labsphere). The lamps have different lamp types from 45, 100 and 200 Watt, which can be combined to get different radiant exitance (lamp assembly see App. A, Figure A.4). An inside looking photodiode monitors the light intensity of the sphere (Labsphere SC-5000 system control with 16 bit ADC, 12 Hz). This sphere is used during relative radiometric measurements.

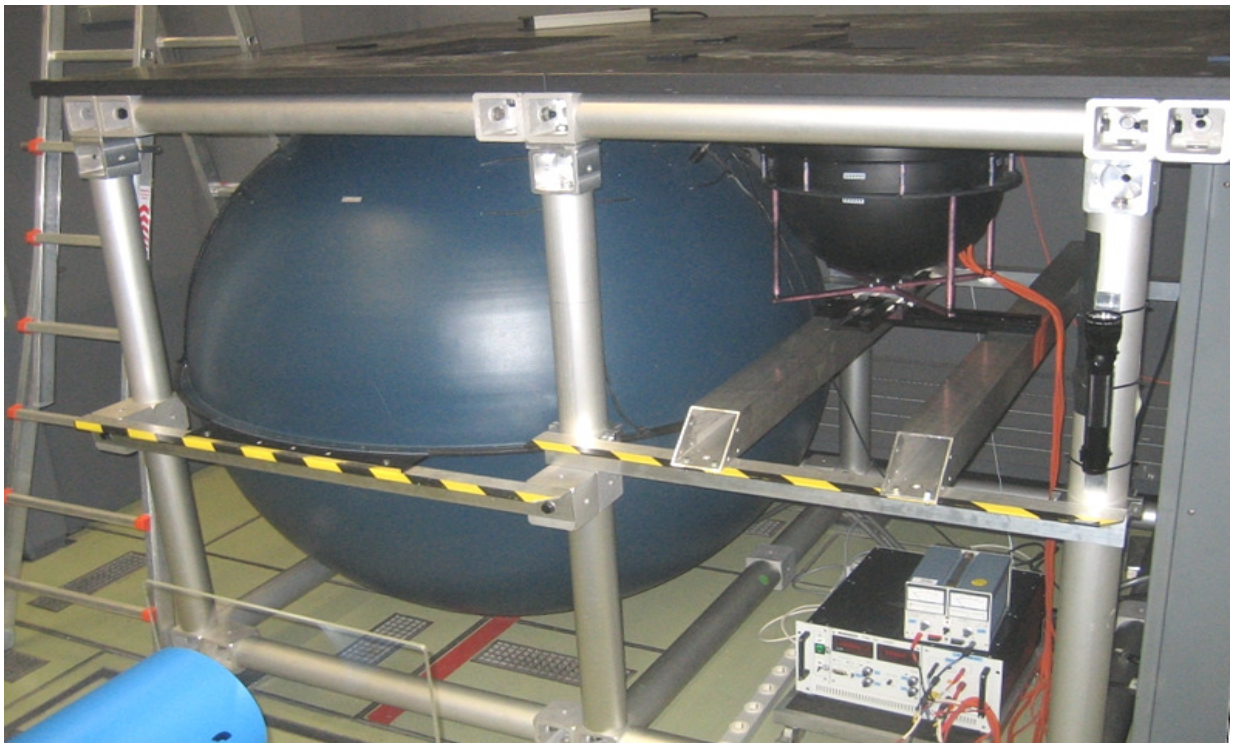

Figure 2.9: Left: Large integrating sphere; right: small sphere

The small and large spheres are shown in the Figure 2.9. The sensor has to be mounted above one of the spheres looking downwards into the sphere. Both spheres cover the wavelength range between 350 nm and 2500 nm. The radiance exitance of the small sphere is stable after a warm-up time of 10 minutes. The warm-up time of the large sphere is 20 minutes. The intensity variations of the large sphere are monitored by a photodiode installed in one side of the sphere (Labsphere SC-5000, 16 bit ADC).

Depending on the FOV of the sensor and the opening of the sphere different numbers of sensor pixels will be illuminated.

2.5 Auxiliary Components

This chapter describes additional hardware, which is necessary during a characterisation measurement and for additional sensor characterisation measurements (e. g. stray light, polarisation effects).

Weather station

The laboratory is equipped with a weather station to monitor the environmental conditions. It measures temperature, humidity and air pressure inside the room close to the optical bench. The station provides the measured data together with the received DCF-77 radio signal. The station is connected to the CHB computer via serial interface. The recording interval can be set from 1 minute to 60 hours.

Illuminance meter

The illuminance meter (“testo 545”, TESTO, Lenzkirch, Germany) monitors the ambient light in the laboratory [44]. This measurement is used to check whether the room light in the laboratory is switched on during a characterisation process. The instrument measures irradiance in the range of 0 to 100,000 Lux. It consists of a sensor head and a hand held controller. The sensor head has a 3.5 cm diameter diffuser and a silicon photo diode. The diffuser provides angle-dependent weighting according to the cosine law at an accuracy of 5 %. The photo diode converts the measured irradiance to voltage according to DIN 5032 (part 6) at an accuracy of 8 %. The data are transferred to the laboratory computer via RS232 interface.

Polarisation Measurement Equipment

For checking the sensor polarisation sensitivity a set of three linear polarisers (CODIXX, Barleben, Germany) covering the spectral range from 475 nm to 2500 nm is available. A special design allows placing the polariser in the parallel beam in front of the sensor entrance aperture. It is behind all optical components of the calibration bench, so all surfaces are included which might influence the radiation. Each filter has an aperture of 27.5 mm and a diameter of 32.5 mm. The polariser specifications are listed in the Table 2.5.

Table 2.5: Polariser specifications

No.	Type	Wavelength range	Thickness	Transmission	Contrast
1	VIS 500 BC3	475 — 650 nm	280 ± 20 µm	55 — 81 %	> 1000 : 1
2	IR 1300 BC5	650 — 850 nm 850 — 1600 nm	220 ± 20 µm	76 — 87 % 82 — 86 %	> 1000 : 1 > 100 000 : 1
3	IR 2000 BC2 HT	1600 — 2500 nm	220 ± 25 µm	> 90 %	> 100 : 1

The polariser is clamped in a filter holder which is attached to a rotary arm. This assembly can be attached temporarily during the polarisation measurements at the backside of the folding mirror stage. It automatically performs the same linear movements as the mirror.

To follow the rotary movements of the mirror, the rotary arm can be turned manually around the rotary stage axis from -20° to +20° in steps of 2.5° (see b of Figure 2.10). The angle mismatch up to 1.25° between mirror orientation and polariser has a negligible effect on intensity and polarisation. The filter holder can be rotated over 360° and has 4 lock points at the sensor along track angles of 0°, 45°, 90° and 135°. Polariser and lock point exchanging has to be done manually. The setup is shown in the following Figure 2.10.

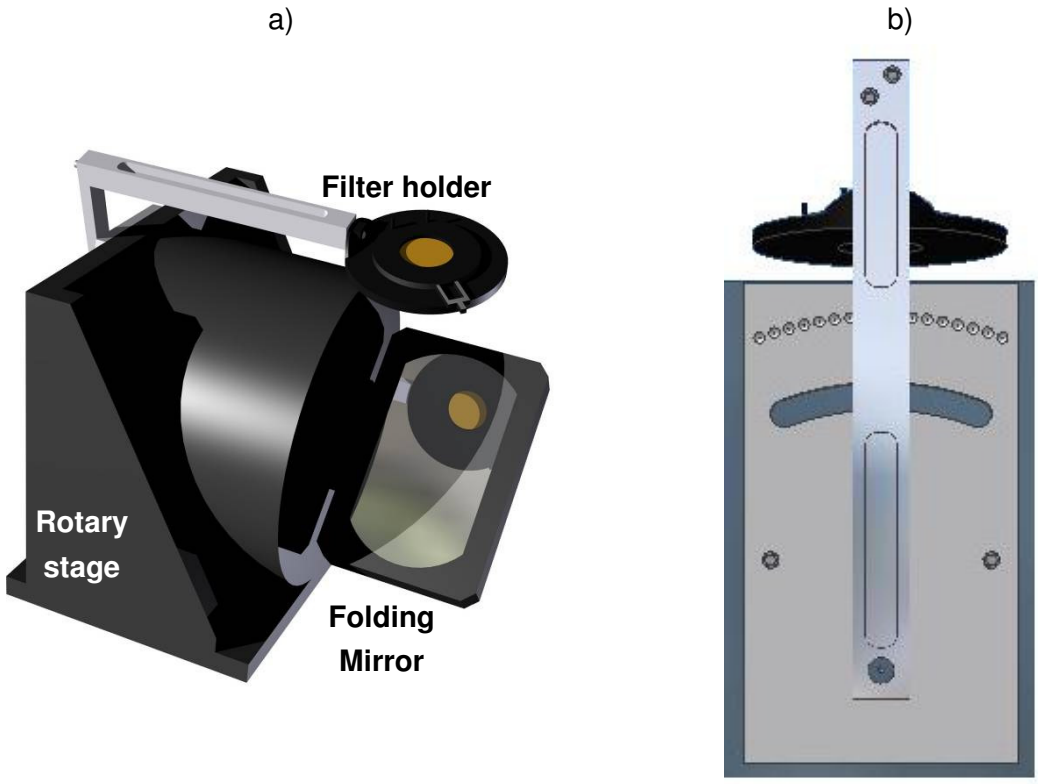

Figure 2.10: Polariser mounted over the folding mirror, a) isometric view, b) backside

Optical Meter

For measuring the optical power and energy of the monochromator output an optical meter is used. The single channel optical meter (model 1935T-C, Newport) has a built-in detector cooler controller. It is equipped with two low power detectors. The first is a 918D-IG-C1 cooled Indium Gallium Arsenide detector with a thermo-electric cooler working in the wavelength range between 1.2 µm and 2.5 µm. The second, a silicon detector 918D-SL-OD3, covers the wavelength range from 400 nm up to 1100 nm. The detectors are calibrated against National Institute of Standards and Technology (NIST) standard and comply with ANSI/NCSL Z540-I-1994 and ISO 9001.

Table 2.6: Uncertainty over the range (calibration date: June 2007)

Wavelength range (nm)	Uncertainty without Attenuator	Detector
400 — 940	± 1%	918D-SL-OD3
941 — 1100	± 4%	
1200 — 1390	± 5%	918D-IG-C1
1400 — 2520	± 4%	
2530 — 2540	± 8%	

The measurements of the optical meter can be displayed in W, Joule, Ampere, Volt, Hertz, or relative units, either directly or as relative ratio measurements from present or stored values. It provides also statistical functions like the computation of Min, Max, Max-Min, Mean and Standard Deviation. In the detector head is a 0.01 % attenuator which can be mechanically switched on and off.

“ZuckerWürfel”

The so called ‘”ZuckerWürfel” (type ZW clima, Meilhaus Electronic) is a small cube (31 mm edge length) which measures and logs the temperature and humidity over a long time period (Meilhaus Electronics, Germany). It covers a temperature range from -20.0°C up to +85.0°C with 0.1°C resolution and the relative humidity from 2 up to 99 % with 0.1% resolution [45].

3 Operational Concept

Sensor characterisation is complex and varies for each sensor. In the past each of the imaging spectrometers of DLR's Remote Sensing Technology Institute had its own characterisation procedures, software, and equipment. A sensor characterisation consists of the determination of different sensor parameters. The calculated coefficients are required for the calibration of flight data. The characterisation of one parameter can be divided into the definition of the characterisation procedure, the selection of the laboratory hardware, the executing of the characterisation measurements and the analysis of the recorded data. This chapter explains the higher-level concept for the execution of the measurements and the data analysis. The measurement process consists of the adjustment of the hardware, the setting of the sensor and the data recording.

Laboratory characterisation is cost and time complex. In the past the characterisation measurements of a sensor were predominantly accomplished with a lot of manual interactions. These manual measurements were time consuming and costly in terms of labour. With the setting-up of the new calibration laboratory a new concept for the execution of the characterisation measurements was necessary. The new concept should achieve the highest possible level of automation with regard to the following goals:

- Reduction of manual interceptions
- Reduction of measurement time
- Establishment of an environment for the external laboratory user
- Avoidance of errors
- Automatic execution of characterisation measurements
- Generation of a standardised but flexible environment for the handling of the characterisation processes.

Beside these goals there are different responsibilities and conditions which have to be considered in the concept. DLR is responsible for the laboratory devices and they are only operated by staffs from DLR. The sensor operator is responsible for the sensor and takes over the control of the sensor. Because most of the sensors are one-off products each sensor has its own control software. Since the laboratory should be open for external users it should be possible for them to use their own characterisation concept and control software. Furthermore for the external users a safe and simple possibility of controlling the laboratory devices is needed. All DLR sensors should be calibrated with one characterisation control software.

Considering the mentioned points the decision was to divide the characterisation process into the following main functions: The control of the characterisation process, the control of the laboratory devices, the sensor control including data recording and the data analysis. The four software modules are:

Master This is the main module which manages the characterisation processes. The *Master* handles the chronology of the process steps and synchronises the communications. The steps are the adjustment of the laboratory hardware, the setting up of the sensor and the data recording. For the setting of the CHB hardware the *Master* communicates with the *Slave* module and for the two others steps with the *Sensor* module.

Slave The *Slave* controls all devices of the calibration laboratory. It receives, interprets and performs the instructions of the *Master* and reports the actual settings back to the *Master*.

Sensor This module controls a specific sensor by receiving and performing the instructions of the *Master*. It is responsible for the recording of the measurement data.

Analysis This module analyses the recorded data and provides the results.

Figure 3.1 gives an overview of the concept with the involved parties, responsibilities, hardware, networks, and modules.

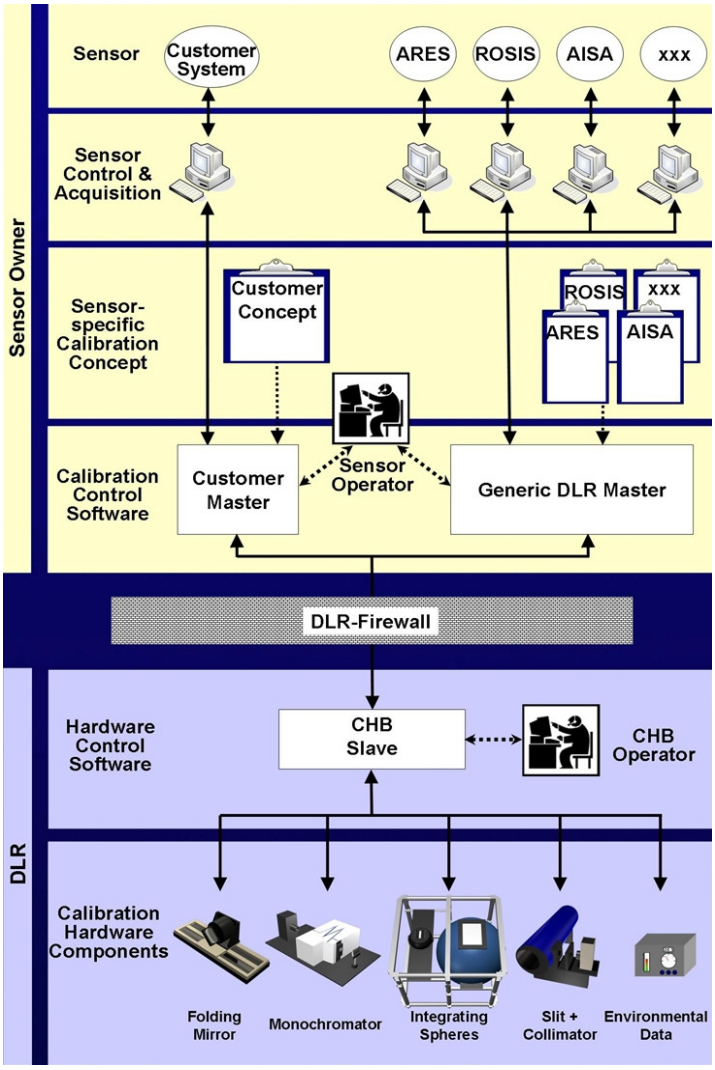

Figure 3.1: Responsibilities, hardware, parties and modules involved in sensor characterisation

There is a clear separation of the responsibilities between operating the laboratory hardware (DLR, blue boxes) and operating the sensor (Sensor owner, yellow boxes). The laboratory devices can only be controlled by the *Slave.* Figure 3.1 illustrates examples of the existing devices. A sensor operating company can be either DLR or an external company (e. g. APEX team). External users can use their own *Master* or the DLR *Master* without a direct control of the sensor. The DLR *Master* has the possibility to control the DLR sensors (ROSIS, ARES, AISA …). Each sensor will need its own *Sensor* module, because most sensors are one-off products with unique control programs.

The separation of the responsibilities is also reflected by different networks. The hardware control computer with the *Slave* software is in the DLR intranet and protected by the DLR firewall. PCs of external laboratory users can only be operated in a secure network environment (DLR security policy [46]). Therefore the sensor control PCs and the PC with the *Master* software have to be in a separate network. The different modules (CHB *Slave*, generic DLR *Master* / customer *Master* and the *Sensor* control and acquisition modules) need adequate software interfaces for the communication between the two networks.

The terms “request” and “response” are used in the following chapters. A request is an instruction of the *Master* to the *Slave* or *Sensor*. A request contains the desired settings of the hardware (sensor or laboratory devices). A response is the return of the *Slave* or *Sensor* containing the current status of the devices.

Operation Modes

In addition to the major function - the execution of a measurement cycle (“automatic” mode) - further functions are necessary. For time optimisation a function which estimates the duration of a measurement cycle is essential, since characterisation measurements are often time consuming. In addition, a function is needed for testing the communication and the instructions of the *Master*. The time estimation and test function is termed “emulation” mode.

Automatic mode

In the automatic mode all device settings are handled by the *Slave* or *Sensor* fully automatically, except for those that can only be executed manually. Only devices with changed parameter values have to be set to reduce the setting time of the devices. The response has to contain the current settings of all devices including the environmental data (temperature, humidity, etc.).

Emulation mode

In this mode there is no interconnection between the *Sensor* / *Slave* and the devices. The response contains the extracted parameter values from the *Master* request except for the environmental data. The environmental data are default values. Basis for the time calculation are the averaged setting times for each device (CHB hardware and sensor). The *Master* summarises all measurement times and averaged setting times of the devices for a measurement cycle and displays the cumulated amount.

The requirements for all software modules are re-usability, expandability, user-friendliness, modular programming and parametric coding. The aim is to use external configuration files as much as possible to minimise the number of software compilations.

In the following sections the ideas of the four modules are explained as well as the network concept. The implementation of the whole concept is described in chapter 4.

3.1 Communication

For the communication between the different modules (*Master* ↔ *Slave*, *Master* ↔ *Sensor*) software interfaces have to be defined. An interface needs a possibility of exchanging data between two PCs which are in two networks. The *Master* controls the measurement process and takes over the role of a client, whereas the *Slave* and *Sensor* are servers (client-server architecture). The communication between the three modules can be synchronous and asynchronous. The *Master* sends a request to the *Slave* or *Sensor* and has to wait for the response before the next step can be performed (synchronous communication). In case of an abrupt error on the *Slave* or *Sensor* side the *Master* has to get an immediate message without waiting for a *Master* request (asynchronous communication). The communication between the *Master* and the *Slave*, as an example, is shown in Figure 3.2. The *Slave* can only communicate with one *Master*.

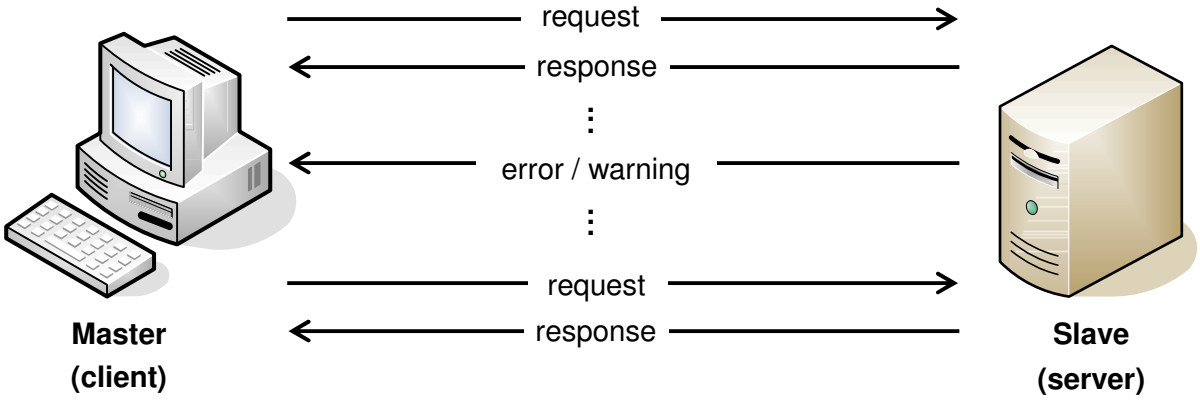

Figure 3.2: Communication between *Master* and *Slave* ([47])

The demand for the transmission protocol is to select an existing technology for distributed systems which can be implemented on established network layers. Additional criteria are: security, complexity, development effort, flexibility, and platform independence.

Beside the protocol the data format of the interfaces between the three modules is important. The interface between *Master* and *Slave* is most complex, because wide varieties of parameters of the different hardware devices have to be interchanged. Selection criteria of the format are a suitable interface format, the ability to upgrade easily, readability in plain text and the use of a standardised format. The data format of the interface should be well structured and interpretable when given to third parties. The following criteria should be achieved for the interface format:

- Clear and understandable specification
- Easy implementation (concerning time and knowledge)
- Allow interoperability
- Robustness

For the communication between the *Master* and *Slave* / *Sensor* a precise allocation technique between a request and a response is needed as well as for the mapping of the measured data to the laboratory device and sensor settings during the data analysis.

For the parameters of an interface unique names and scopes have to be defined and stored in external formats which can be easily modified.

3.2 Hardware Control

The control of all laboratory hardware components is realised by the *Slave* module. Only this software is permitted to operate the devices in order to protect the hardware against incorrect handling. Potential sources of errors have to be intercepted by the *Slave* software and the laboratory assistant has to be informed accordingly. The number of manual interactions has to be reduced to a minimum. The *Slave* has to request the assistant to perform the necessary manual tasks in the correct order. In general nobody should be present in the laboratory during a measurement. The actual device settings, errors and messages have to be provided outside of the laboratory to avoid an on-site supervision. The *Slave* has to provide a software interface for the *Master.*

In addition to the calibration devices, environmental sensors are installed in the laboratory (see chapter 2.5). The *Slave* has to monitor these data and to inform the *Master* in the case of an exceeded threshold. The actual device setup values and the environmental data (e. g. laboratory temperature, ambient light level) have to be transmitted to the *Master*. New hardware should be easily implemented in the *Slave* module.

3.3 Sensor Control

The scope of the *Sensor* module is to control the sensor and to record data. Since the sensors are different, each sensor needs its own *Sensor* module and interface, but all sensor modules need a network connection for the communication with the *Master*. A major aspect is the automation of the data recording with regard to the reduction of manual engagements. A transfer function for the recorded data from the sensor PC to the data analysis PC is useful. Due to an enormous growth in file size only a limited amount of measurement data can be recorded and the disk capacity should therefore be constantly monitored.

Usually sensors have interactive data acquisition and control software built for use in an aircraft but not for an automatic use in a laboratory. Ideally the existing sensor control software can be modified by implementing an interface for the *Master* and a network communication possibility.

If this is not possible, a *Sensor* module with a network communication possibility and an interface for the *Master* module is needed. This module has to take over the control of the sensor and to trigger the data recording.

3.4 Measurement Process Control

The central part is the DLR *Master* module, because it manages the measurement process and instructs the *Slave* and the *Sensor*. The *Master* module has to be flexible since it has to handle a wide variety of characterisation measurement processes. A complete characterisation process step includes the setting-up of the laboratory hardware (*Slave*), the instruction of the sensor including a data recording (*Sensor*) and the execution of actions. Action can be a data transfer, a display of a message, a data analysis or the execution of a program. It should also be possible only to setup the laboratory hardware without using a sensor but to perform actions.

In the “automatic” mode all hardware parameters (laboratory and sensor) are set and the data is recorded. In the “emulation” mode the *Master* has to accumulate the received setup times from the *Slave* and *Sensor* and to display the overall time (see chapter 3.1).

In order to optimise the administration of the measurement series the execution of loops are necessary. Loops are useful for the setting of the folding mirror, the monochromator wavelength and the slit wheel angle. For a loop a range and an increment are needed. A characterisation measurement process can contain one or multiple single measurement steps or loops. For the execution of a measurement process a selection of the required measurement steps and loops is useful. An easy selection of the operation mode is essential.

The *Master* module has generic and specific parts. The parts affecting the sensor are specific. Generally each sensor has its own interface with different setting parameters which have to be implemented in the *Master*. In addition each sensor will need its own user interface. Generic parts are

- The management of the measurement process,
- User interface for the administration of the laboratory devices,
- User interface for the administration of actions,
- Communication with the *Slave* and *Sensor*,
- automatic execution of parts or of a whole characterisation process,
- warning and error handling,
- and parameter logging.

All the mentioned points apply to the DLR *Master* and can be different from the needs of customer *Masters*.

3.5 Data Analysis

The major part of sensor characterisation processing chain is the analysis of the recorded laboratory data since the analysis results are the required for the calibration of the raw data (e.g. centre wavelength, FWHM, radiometric response function). The characterisation processing chain ends with the output of the calibration results in generic file formats. An objective of this thesis is the definition and implementation of sensor independent analysis procedures for the spectral, geometric, and radiometric characterisation as well as for the sensor alignment.

It is indispensable to use a sensor independent data format in the procedures and functions. Since each sensor has its own raw data format, the first step of data analysis is to convert raw data into a sensor independent file format. To implement sensor independent procedures it is necessary to split the recorded data into the different data types. The different kinds are image data, in-flight calibration data, dark current data or housekeeping data. These data can differ from sensor to sensor. However, the assignment of the additional data to the image data is necessary to avoid manual interactions during the data analysis.

For the data analysis, in addition to the recorded sensor data, the hardware settings of the laboratory devices and the sensor are needed. The recorded settings have to be converted into a generic data format. The data content is dependent on the characterisation measurement type (spectral, geometric and radiometric). An allocation of the single measurement data and the respective hardware settings is required.

For the analysis of the data a software program is required, which is able to process large data files in an efficient way. General routines for reading and writing data or for printing plots and for writing measuring logs have to be developed. In each analysis procedure data quality functions, error checks and logging functions have to be implemented. The analysis programs for the spectral, geometric and radiometric characterisation measurements are described in chapter 5.

4 Implementation of the Concept

This chapter describes the realisation of the concept explained in chapter 3. It is divided into the sections communication, control of the laboratory hardware (*Slave*), sensor control (*Sensor*), measurement control (*Master*), and data analysis. In the separate sections the implementation of the concept ideas and demands are explained. The *Master*, *Slave* and *Sensor* software modules have been developed with Microsoft Visual Studio .NET 2003 and the GUIs with the Microsoft Foundation Class (MFC) library [48]. The data analysis procedures are implemented with IDL 6.3 / ENVI 4.3 from ITT Visual Information Solutions.

Concerning the rules for the use of PCs in the DLR network environment three networks were installed (see chapter 3). The three networks are the intranet of the "Cluster angewandte Fernerkundung" (CAF), a private virtual network (DLR-VLAN) and an external network (F-LAN). The network setup of the CHB laboratory is shown in Figure 4.1. The CAL-Slave PC which interacts directly with the laboratory devices and the folding mirror control PC (CAL-Aerotech) are in the CAF intranet protected by the C-AF firewall. The computer with the *Master* software and the sensor control computer(s) are in the DLR-VLAN. The private network is isolated from the DLR intranet and from the Internet. The F-LAN was setup for the APEX sensor and is equipped with its own firewall.

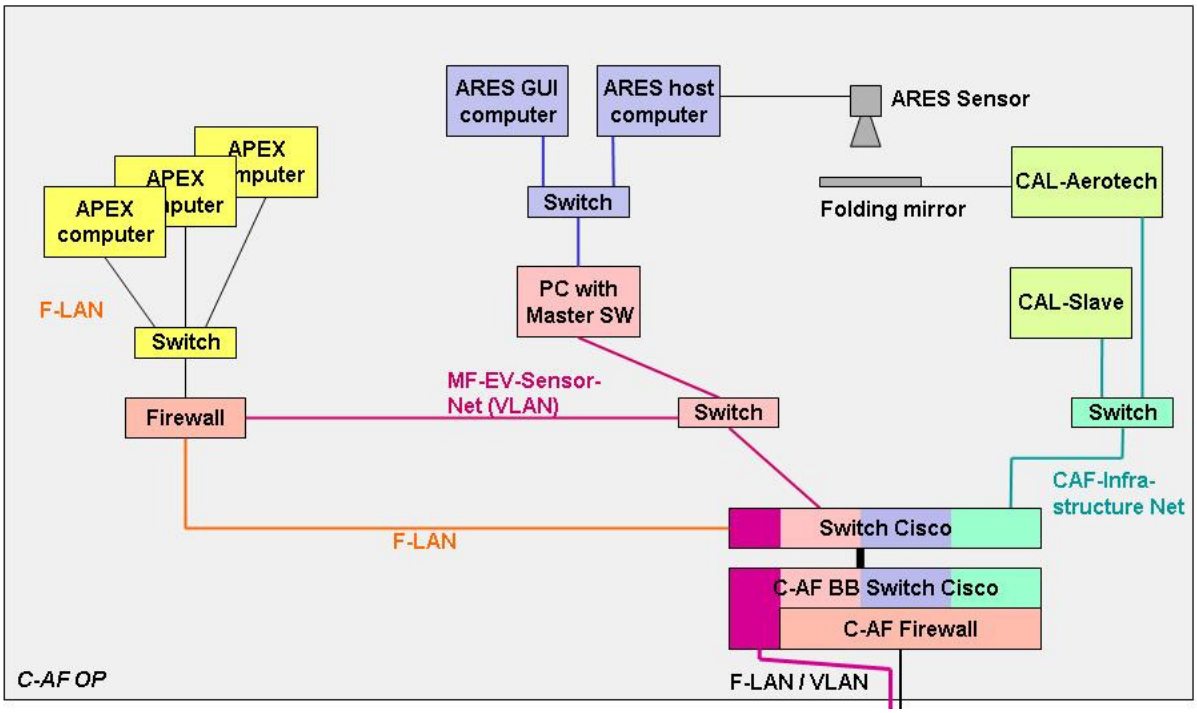

Figure 4.1: Network design of the CHB laboratory

Figure 4.1 shows the DLR network design of the calibration laboratory for DLR and external sensors (APEX). The C-AF network with the DLR laboratory PCs are coloured in light green, the VLAN with the ARES computers are marked in purple and pink, and the F-LAN with the APEX PCs are signed in yellow.

The communication between the three networks is restricted. Computers in the VLAN can only communicate with one port of the CAL-Slave computer in the CAF network. The data packages from F-LAN computers are routed across the VLAN to the CAL-Slave PC.

4.1 Communication

Several technologies exist for the realisation of the communication between the three modules (*Master*, *Slave* and *Sensor*). A possible solution has to communicate on established network layers with a proprietary protocol or an existing technology for distributed systems. The Open Systems Interconnection (OSI) model is the standard model for network protocols and distributed applications and consists of seven network layers [49]. The first four layers are the basis for the data transmission. Applications are based on the layers five to seven.

There are two common protocols available for the transport (layer 4), the Transmission Control Protocol (TCP) and the User Datagram Protocol (UDP). Layer 5 is responsible for the session management. Techniques for this layer are the Common Object Request Broker Architecture (CORBA), Remote Procedure Calls (RPC), Remote Method Invocation (RMI), Simple Object Access Protocol (SOAP), and sockets.

TCP versus UDP
UDP is an unacknowledged transmission protocol, which neither controls the data package receiving nor checks the sequence of the packets. Because of these points it is an unreliable protocol, but it is faster due to a minimal overhead. TCP provides a reliable transmission. It guarantees the transmission of the data packages in the right order and condition as the packages were sent. TCP provides extensive error detection functions. In the case of an error, e.g. collapse of the connection, the connection will be reset and the data package will be sent again. Considering these factors TCP has been chosen as the appropriate transmission protocol.

Sockets
Sockets are Application Programming Interfaces (APIs), which provide a simple way to create and manage a network connection (e.g. TCP/IP connection). A socket implementation (e.g. of Berkeley, Microsoft [50]) can be assigned to the layers 5 to 7 of the OSI model. Likewise there are functions for server programming, as well as for transmission and reception. The choice of network communication via sockets has obvious advantages in relation to other techniques like CORBA etc.:

- less complexity
- asynchronous communications can easy be impelemted
- available for nearly all standard platforms and operating systems

By choosing sockets for the connection the data format is not determined, so the developer has free choice. The simplest way is the definition of a serialization instruction, which specifies the order in which the data fragments are transmitted.

Sockets can handle the transmission of both binary data and plain text. Due to the minimal overhead binary data can be transmitted efficiently over the network. The disadvantage of this approach is the need for a routine for the extraction and validation of the received data. Between the *Master* and the *Slave* many parameters in different combinations have to be exchanged. For the variety of the CHB modules the combination of sockets with Extensible Markup Language (XML) is the best choice [51, 52].

Interface Format

The simplest format is a binary one, but a plain text format is more comfortable and more easily readable. A binary format enables the most time efficient transfer because it contains only the pure parameter values and has no format overhead. But the data examination is time consuming, because extra software must be developed for this purpose. The data transmission time is not a critical aspect, because the data volume is low.

A more useful format than the binary format is the eXtensible Markup Language (XML) text format. The XML is a standardised technology for reading, writing, transforming and validation of data [51]. XML is a plain text readable format, which consists of a name and a value for each parameter. The benefit is robustness since a misinterpretation of the data can be excluded. Indeed the data volume increases because of the additional information, but allows the use of already existing parsers for the data validation.

The XML scheme definition (XSD) is used for the specification of the XML data structure [52]. A XSD includes elements and data types as well as ranges. A XML parser translates the XML data, checks the structure and validates the data against the XML scheme [53]. Parsers are available as open source and are freely adaptable (e. g. TinyXML [54], Apache Xerces C++ [53]). The Xerces parser is used in the three applications (*Master*, *Slave* and *Sensor*). Therefore the development of individual program tools for data access and validation is not necessary.

For the mapping of the *Master* request and the *Slave* / *Sensor* response a unique identifier is needed. Therefore each XSD contains a parameter “request-id”. The “request-id” is a consecutive number, initiated and handed over by the *Master* during an instruction of the CHB devices (*Slave*) and the spectrometer (*Sensor*). On the basis of this “request-id” an allocation of the measured data to the settings of the laboratory devices and the sensor can be done, which is essential for the data analysis afterwards.

4.2 Hardware Control Software

The *Slave* provides the interface to the calibration laboratory. Its primary task is the controlling of the hardware according to the parameters received from the *Master*. Afterwards the *Slave* sends the actual settings of the devices back to the *Master*. The work flow of the hardware setting performed by the *Slave* module is illustrated in Figure 4.2. Most of the laboratory devices are directly connected with a serial interface to the CAL-Slave computer.

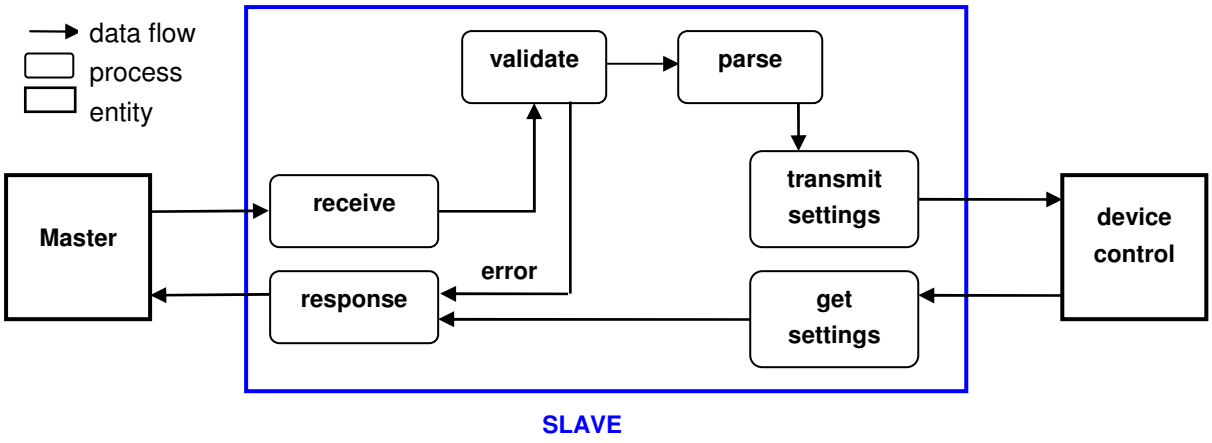

Figure 4.2: Slave work flow for the setting of the laboratory devices ([55], p. 18, modified)

The *Master* module communicates with the *Slave* module over a static IP address and port number. All changeable program parameters (e.g. COM-port numbers of the devices, network settings, and environmental data thresholds) are stored in an external configuration file. The contents of the INI-files are listed in App. B, Table B.3. Only the requested *Master* parameters which are different to the current settings are adjusted by the *Slave* module. This minimises the device setting time.

In the emulation mode the *Slave* checks the parameter values and sums the setting time of the required devices on the basis of the averaged setting time of each device. Since there are no current settings the *Slave* responses the received parameter values to the *Master.* The environmental data (temperature, humidity, pressure, ambient light) contain default values (INI-file).

The laboratory components are split into the groups folding mirror, spectral, geometric, radiometric, and environment (see Table 4.1). For each group initialisation and shut-down procedures are implemented in the *Slave* module. These procedures are stored in external files and contain the sequential manual tasks. The manual tasks instruct the laboratory assistant during power-on / shut-down (e. g. power-on of the monochromator or removing of the folding mirror coverage). The advantage is that the operator does not have to care about the sequencing and completeness of the required steps. The *Slave* module uses the generic dialog procedures to display the instructions. Each instruction has to be acknowledged with an “OK” or “error”, triggering a reaction of the *Slave* software.

Error handling plays a major role in the automatic operation of the laboratory. The manual engagement of the laboratory staff is reduced to a minimum. If an error cannot be solved by the software, manual interaction by an operator is required. An example for a software-solved problem is the reconnection of a lost communication. A loss of air pressure can only be solved by the laboratory staff. If the error can’t be solved the *Master* gets an error message. The *Master* gets also an error message if any of the requested interface parameters are not valid.

Monitoring of the *Slave* activities (Observer)

Additional to the *Slave* software a web front-end was developed with the current hardware settings from the *Slave*, the *Master* requests and the *Slave* error messages. For the web page an Apache web server was implemented on the CAL-Slave computer. The current device settings are sent from the *Slave* to the web server as XML files. The web server converts the files into Extensible Hypertext Markup Language (XHTML) [56]. Presently three XML files (last request, last response and current errors) are stored in the web server folder. The conversion EXtensible Stylesheet Language Transformations (XSLT) [57] processor Xalan [58] from Apache Software Foundation transfers the three files into the frames of the web page (see App. B, Figure B.12).

To avoid any on-site supervision the actual hardware settings, including errors and messages, are provided in a web page (see App. B, at the bottom of Figure B.12). This can be called from any PC in the DLR intranet and the characterisation process can be controlled from a remote office.

Implementation of the device Groups

Table 4.1 contains the single devices of the groups divided into software controllable and non-controllable components. In the following the integration of the single devices are explained.

Table 4.1: Overview of the device groups and its components

Device group	Controllable components	Non-controllable components
Folding mirror	Folding mirror	Air pressure, coverings, power supply, polarisation filters
Geometric	Slit wheel: slit	Lamp, power supply, auto-collimation head
Spectral	Monochromator: Filter wheels, grating and shutter	Entrance and exit slit, lamps, turret, power supply
Radiometric	Large integration spheres: lamps	Power supply, filters, targets
Environment	Illuminance meter, weather station	

Folding mirror

The folding mirror has a rotation axis (A) and a linear axis (Y) controlled by the CAL-Aerotech computer. The manufacturer supplied a driver library (AUTOMATION, Aerotech GmbH) with specified functions for the control of the two axes. The execution of a command runs asynchronously and it is possible to execute more than one command at a time, e. g. the rotating and the moving of the mirror. The mirror may not be moved without compressed air under any circumstances. This is constantly monitored in a dedicated thread to provide quick interaction.

The main software function is the setting of the folding mirror. The primarily used functions are enabling and disabling of the drives, moving to the home position, rotation or moving of the mirror. A special function is the setting of a viewing angle.

For the setting of a viewing angle the mirror will be rotated and moved to the right position in dependence to the given “sensor height”. Depending on the selected characterisation side (spectral or geometric, see Figure 2.4) the mirror has to be moved to the corresponding viewing direction.

During initialisation the mirror will be moved to its home position (A = 0°, Y = 0.0 mm). In this position the mirror looks face up to the sensor in the centre of the linear desk. The shut-down procedure moves the mirror to its stand-by position at the border and disables the drives.

On the back side of the folding mirror a holder for polarisation filters can be mounted (see Figure 2.10). The assembly and shifting of the filter has to be done manually, whereas the *Slave* program displays the necessary tasks to the operator.

Geometry

The only automatically controllable device of the geometric group is the slit wheel with six different slits at intervals of 60° (see App. A, Figure A.3). The wheel is driven by a stepper motor connected to a Peripheral Component Interconnect (PCI) card in the CAL-Slave computer. The delivered driver library (PCISM32.dll, OWIS GmbH) can only initiate commands, but gives no acknowledgement [59]. Therefore an own thread has been established to detect whether the motor is still running. The *Slave* compares the queried actual step position with the target position and adjusts until the target position is reached. The motor works with full and slice steps whereas the *Slave* commands with slice steps.

Slit parameters are the slit number and an offset angle, which is limited to ± 10°. Greater angles cannot be used since theses angles are covered by the wheel housing. For the movement to the new wheel position the steps are calculated based on the actual position. The smallest possible step size is 0.01°. It takes approx. one minute to move from one slit to the next. All angle movements are performed in relative slice steps.

During the execution of the initialisation routine the wheel will be moved to the home position (see App. A, Figure A.3). The home position is the 50 µm vertical slit at an angle of 60°. The shut-down process moves the slit wheel to the home position.

Instead of the slit wheel an auto-collimation head can be mounted. The switching of the light source and the adjustment of the power are manual activities.

Spectral

The only controllable device is the monochromator, which is directly connected to the CAL-Slave computer via serial interface. The main used functions are the opening or closing of the shutter, selection of the filter, selection of the grating and the adjustment of the wavelength [60]. The entrance and exit slits are actual manually adjustable components, but an automatic control is possible. The complete setting sequence is shown in Figure 4.3.

The left side of the figure illustrates all single adjustment steps and the right side shows an example of a single step. The right figure is split into the manual steps and the automatic steps of the adjustment of the slit respectively.

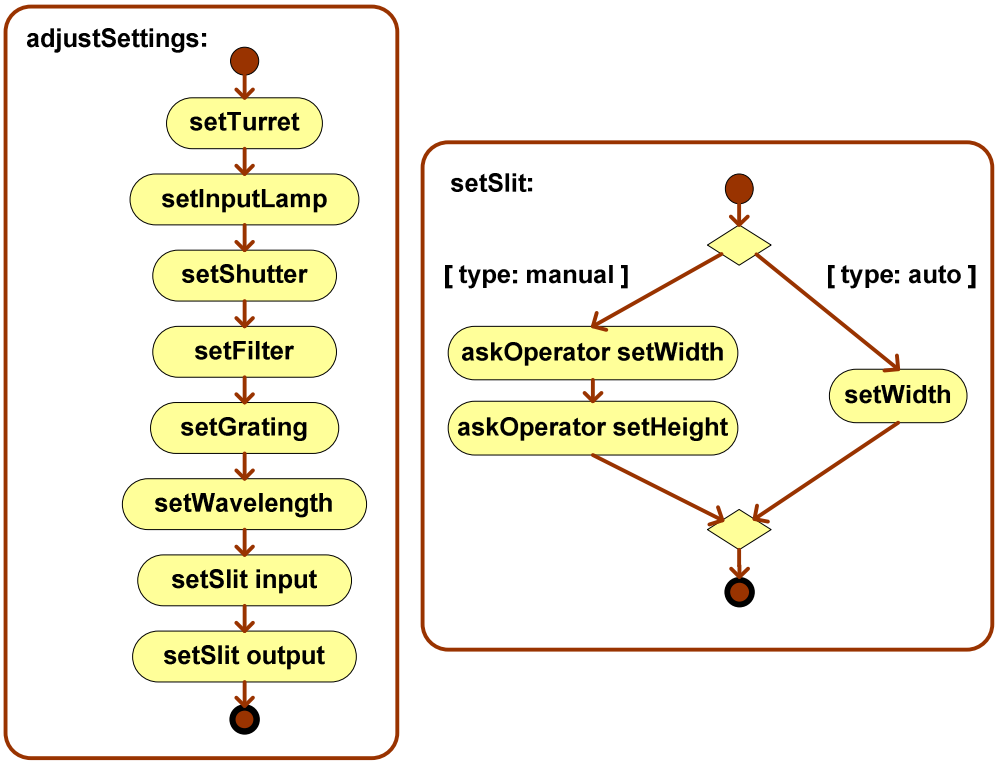

Figure 4.3: Monochromator instruction sequence ([47])

The monochromator itself will be calibrated with pencil lamps [61, 62] several times per year to monitor and maintain the accuracy. The calibrations are performed separately for each grating and the results for each grating are stored in a settings file. This file is loaded at run time and the wavelength settings are performed in four steps (left line of Figure 4.4).

a) Steps

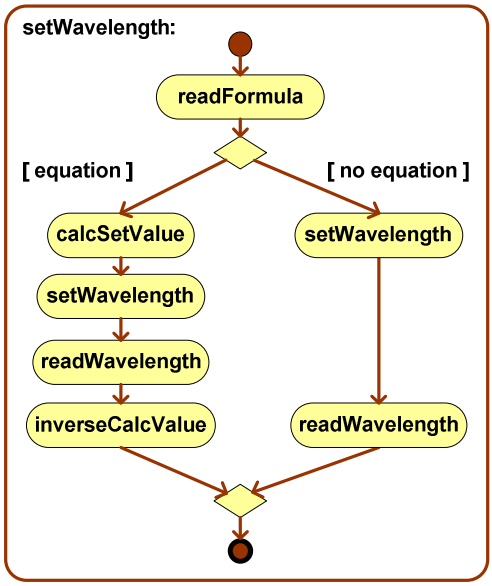

b) Equations

Calculate wavelength for monochromator setting

$$\lambda_{mono} = (\lambda_{des} - C_{offset}) / (1 + C_{gain})$$

Correct the wavelength after monochromator setting

$$\lambda = C_{offset} + \lambda_{act} * (1 + C_{gain})$$

where

λ : corrected wavelength (nm)

C_{gain} : gain of the monochromator calibration

C_{offset} : offset (nm) of the monochromator calibration

Figure 4.4: Steps of the wavelength setting (a) ([47]) and conversion equations (b)

The first step after the import of the formula is the calculation of the monochromator wavelength (λ_{mono}) on the basis of the desired wavelength (λ_{des}) by using the first equation (see right side of Figure 4.4). Then the calculated wavelength is set and the actual wavelength setting is read which differs about small values. The last step is the calculation of the corrected wavelength (λ) by using the second equation. The calculations are performed with an mathematics library (muparser [63]). In case of no wavelength correction only the setting and reading of the wavelength are performed (see right path of a) of Figure 4.4).

Additional manual tasks are the powering on or off of the monochromator and its power supply and the setting of the lamp power supply current. Activities which are rarely necessary and time consuming are the changing of the turret and the light source.

Radiometry

Only the large integrating sphere has a serial interface and can be controlled automatically. The small sphere has only a power supply, which has to be switched on or off. The large sphere has 18 lamps of different power. Each lamp has its own power supply, which has to be power-on or -off. For the large sphere 12 lamp combinations are defined to provide different radiant exitances (see App. A, Table A.1). The sphere can be controlled but gives no return whether the settings were successful. Errors are only shown on the control unit display. But it is possible to monitor the signals of the sideways-installed photodiode and to write the data into a text file. The control program checks if the values of the photodiode can be read. In accordance with the required lamp combination the control units of the necessary lamp power supplies will be activated and all other are deactivated. The lamp combinations are stored in a separate file which can be upgraded easily.

Environment

The devices of this group check the environment of the laboratory, which may have an influence on the measurements. The data are provided from a weather station and an illuminance meter which are connected to the CAL-Slave PC with a serial interface. For the monitoring of the environmental data (temperature, air pressure, humidity and ambient light) a GUI was implemented in the *Slave* application (see App. B, Figure B.13). Each of these data has a defined threshold and if one of them is exceeded, the *Slave* sends a warning to the *Master* and informs the laboratory staff. The alarm function can be switched on or off. The alarms for temperature, pressure and humidity can only be handled together. The data of the weather station and illuminance meter can be stored in text files. The *Master* is able to set the recording interval for the weather station and or the illuminance meter.

The weather station stores the temperature, air pressure and humidity with a minimum interval of one minute on an internal device. For the reading of the stored data an open source program is used [64].

The ambient light in the laboratory is monitored by the illuminance meter which is placed between the two bench pillars. It measures the room light in lux. If all room lamps are switched off, the opening of the door cannot be detected because the illuminance is < 1 lx.

4.3 Measurement Process Control Software

The *Master* module is the main module of the characterisation process, because it handles the execution of characterisation measurements. The *Master* is the central instance controlling the *Slave* and the *Sensor*. In addition it has functions for the collection, administration and execution of characterisation measurement instructions. A characterisation measurement process usually consists of several measurement instructions. One measurement instruction is denoted as “Scan Batch” and several “Scan Batches” are stored in a “Scan Suite”. For the administration of the instructions of a measurement process the following input tasks are possible. The mandatory task is the setting of the CHB devices.

- Setting of the CHB devices (*Slave*)
- Setting up the sensor and performing a measurement (*Sensor*)
- Execution of action(s) after one measurement step
- Execution of action(s) at the end of one measurement series

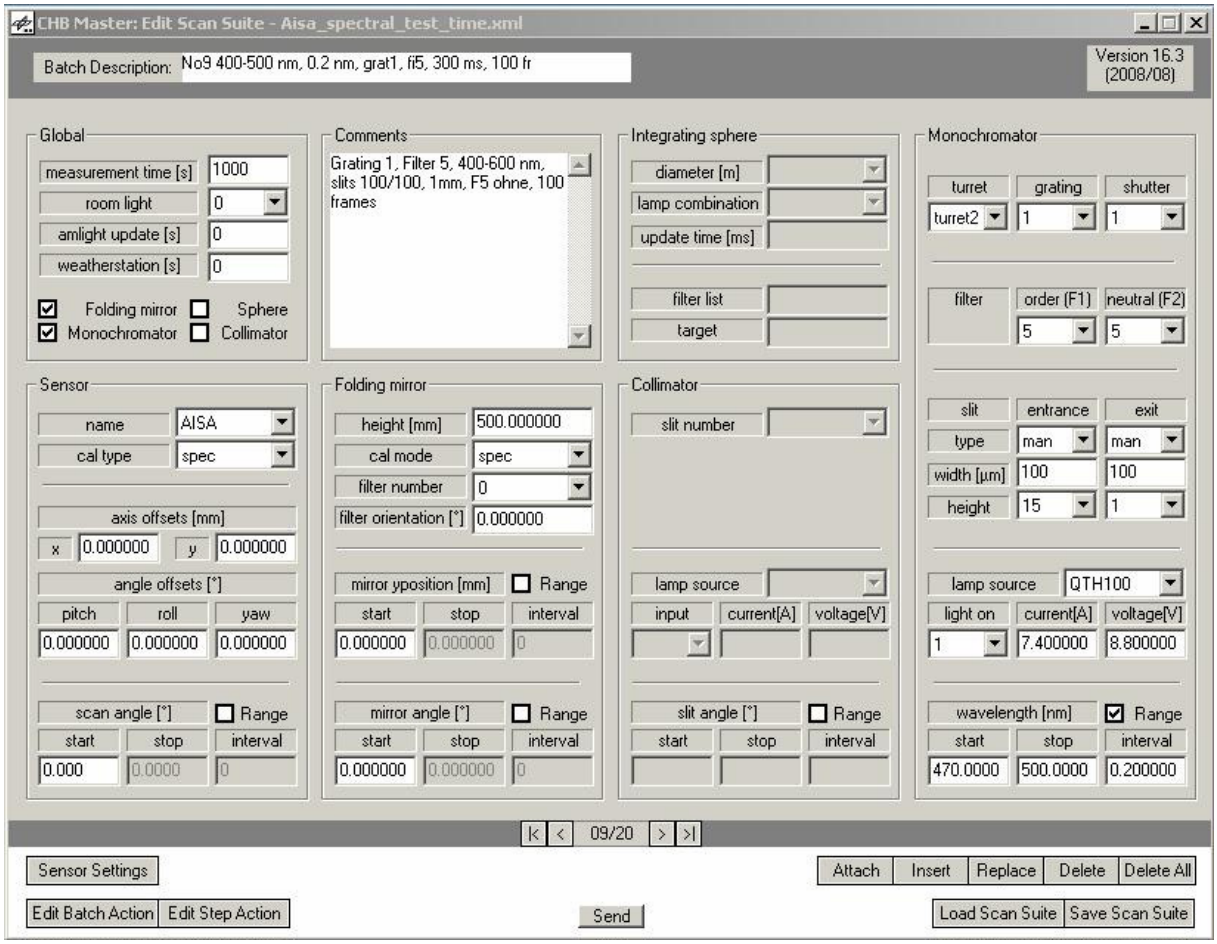

Figure 4.5: *Master* GUI for characterisation instructions

Figure 4.5 shows the administration GUI of the *Master* software with the possibility to insert, edit or delete a measurement instruction (“Scan Batch”). Each of the tasks a) to d) can be managed in this GUI.

In the main part of the GUI the settings of all devices can be defined and adjusted (task a). This part and the administration GUIs for the step and batch actions (task c and d) are identical for all sensors. The GUIs are displayed in Figure B.9 of Appendix B. The sensor parameters are not implemented in this GUI since these differ from sensor to sensor. Each sensor has its own GUI which will be opened according to the selected sensor name. Figure B.7 and Figure B.8 of Appendix B show the sensor input parameters of ROSIS and AISA.

For an efficient handling of the characterisation processes, loops with a range and increment are implemented in the *Master* module. Loops are executable for the parameter “sensor viewing angle”, “folding mirror angle”, “folding mirror linear movement”, “monochromator wavelength”, and “slit wheel angle” (see Figure 4.5). In addition a combination of two loops is possible for the sensor viewing angle with a monochromator wavelength range or slit wheel angle range. In this constellation the sensor viewing angle is the outer loop and the monochromator / slit wheel the inner loop.

For a quick setting of the CHB devices the GUI has a function to send the start field values to the *Slave* (“Send” button of Figure 4.5).

***Master-Slave* interface**

The *Master* sends XML coded strings with the desired CHB device settings to the *Slave*. The *Slave* answers likewise in a XML coded format and communicates the current settings of the devices to the *Master*.

The *Slave* interface is divided into the groups “Global”, “Sensor”, “Folding mirror”, “Integrating sphere”, “Collimator” and “Monochromator”. The “Global” group contains general data for the room light monitoring or the recording interval for the environmental data. The “Sensor” group covers sensor relevant information like sensor name, viewing angle, characterisation type and axes offsets (see App. B, Figure B.6). The parameters of all groups are listed in Appendix B, Table B.7. Each *Master* request must contain the “Global” and “Sensor” group. All other groups are optional.

***Master-Sensor* interface**

Unlike the communication between *Master* and *Slave* the *Sensor* interface is less complex. Since the sensors are different their parameters are also different except for the network parameters (IP address and port number). Each sensor needs its own XML coded interface and GUI in the *Master* module. Example GUIs are shown in Appendix B (see Figure B.7 and Figure B.8). The main function of the sensor part in the *Master* module is to adjust the sensor and to initiate the data recording.

Scan actions

Implemented action types are the display of a message, the execution of a system command, the data transmission or the execution of an IDL program. In the *Master* software step actions can be added for each “Scan-Batch”. During the execution of a “Scan-Batch” the measurement series will be interrupted after each step and all added actions will be performed either directly or in the background. The execution of actions in the background is only possible for the actions “system command”, “data transmission” and “run IDL program”. In the case of a direct execution of an action the actual measurement process will be interrupted, the actions will be performed and the measurement series will be continued afterwards.

Display a message

The action “add display” shows a message for the laboratory assistant which has to be acknowledged afterwards. Such as the display of a message to inform the laboratory assistant to mount a transmission filter.

System Commands

During a characterisation process it is possible to run system commands and/or call external programs.

Data transmission

The data transmission is useful for moving the recorded data from the sensor PC to the computer with the *Master* software in order to analyse the measured data. For the data transmission three options are implemented in the *Master* software, a local copy, FTP or HTTP [65, 66]. The selection of the data transmission type depends on the network infrastructure of the sensor computer. Table B.8 of Appendix B contains further information of the three options. For all data transmission actions the file name of the recorded data is not needed since the name is a return parameter and will be provided by the *Sensor* software.

Run Interactive Data Language (IDL) programs

IDL has an Application Programming Interface (API) for C++. The *Master* program can call IDL programs and perform three types of actions according to the return parameter. Possible actions are:

- The *Master* performs the action “Display a message” where the return parameter contains the message.
- The *Master* sends a valid XML request to the *Slave*. After the setting of the CHB devices the last *Sensor* request will be repeated, as well as the step actions.
- The *Master* sends a request to the *Sensor*. Afterwards the last step actions will be performed again.

Execution of characterisation processes

The *Master* has different strategies for the execution of “Scan Batches”. The strategies are selected on the basis of the included tasks (CHB settings, sensor settings and actions). The four possible strategies are:

- Adjustment of the laboratory devices.
- Adjustment of the device and execution of step actions.
- Adjustment of the device settings and recording of the sensor data.
- Adjustment of the device settings, recording of the sensor data and execution of step actions.

An example of the workflow for the last strategy is shown in Figure 4.6. The work flow of a single measurement is as follows: The *Master* sends the required settings for the laboratory devices (1) to the *Slave* and waits for the response. In the case of an error the *Master* displays an error message. In case of no error, the *Master* sends the required sensor parameters to the *Sensor* module (2) and waits for a response from the *Sensor*. After each measurement step one or more actions (3) are performed. In this example the transfer of the recorded data (red / black picture) to the PC with the *Master* software, the deletion of the copied data and the execution of the conversion program is shown.

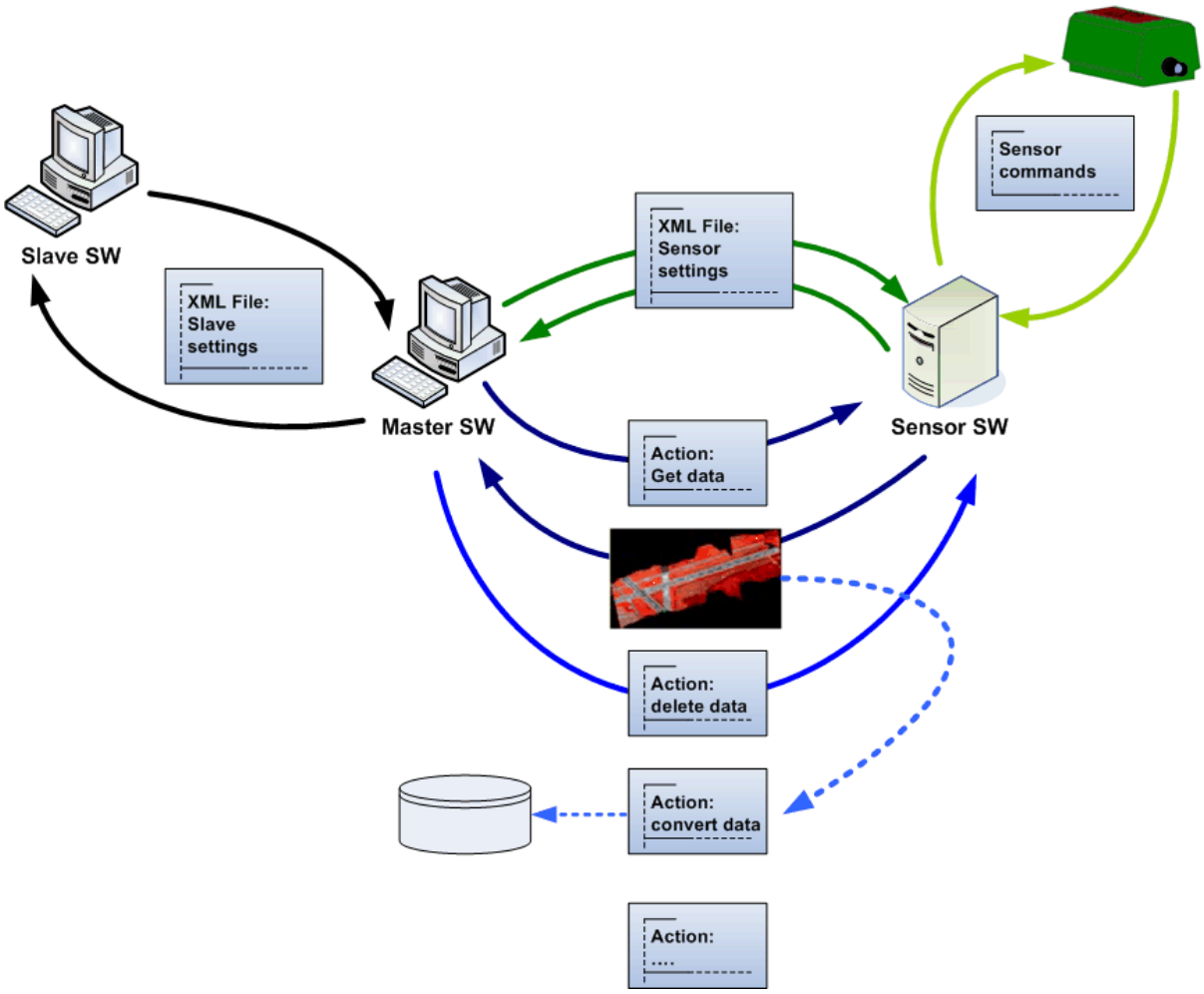

Figure 4.6: Work flow with all possible tasks of one measurement step

The *Master* provides a GUI for the execution of selected “Scan Batches” of a “Scan Suite” in “auto” or “emulation” mode (see GUI of App. B, Figure B.11). In the “auto” mode all settings are performed from the *Slave* and *Sensor*.

In the “emulation” mode the *Slave* and *Sensor* modules emulate the device settings by sending the default values of the parameters including the estimated duration for the device settings back to the *Master*. The *Master* accumulates all setting times and displays the total duration. This mode is useful for the calculation of an estimated duration of a characterisation process.

Parameter ranges for CHB devices can only be set in the execution function of the *Master*. In the case of a combination of two ranges the *Master* starts with the setting of the first viewing angle and performs afterwards all single steps of the wavelength range and the slit angle range respectively before the next viewing angle is set. If actions are included in the characterisation process the step actions are performed after each single step and the batch actions are executed after the complete range has been performed. In the GUI of the execution function it is possible to select whether the actions should be performed or not.

Measuring logs

Each XML request and response is logged by the *Master* software (see App. B, Figure B.10). In order to be able to assign a request and its response each measurement step has a continuous number, the parameter “Request-ID”. This ID is generated by the *Master* software and is the main parameter in the *Slave* and the *Sensor* interface. All XML requests and responses of the two interfaces are stored in log files (see left side of Table 4.2). These files are created for each performed Scan-Batch and the file names are extended by the “Scan Suite” name and “Scan Suite” number. These log files are necessary during the analysis of the measurements for the assignment of the data and to the device settings.

Table 4.2: Log files created by the *Master* software

Master interface log files		**Additional log files**	
File name	**Content**	**File name (chbmaster*.log)**	**Function**
SlaveTX_*	Slave request parameters	-access	All informative entries
SlaveRX_*	Slave response parameters	-warn	All warnings
SensorTX_*	Sensor request parameters	-error	All errors
SensorRX_*	Sensor response parameters		

The additionally created logs of the *Master* are listed on the right side of Table 4.2.

4.4 Sensor Control Software

For a fully automatic characterisation measurement chain a control module for the respective sensor is necessary. In most cases a new sensor has to be implemented in the *Master* software and new *Sensor* control software has to be developed or the existing sensor control software has to be modified. This chapter describes the implementation of the *Sensor* module in accordance to the explained concept in 3.3. The *Sensor* modules for AISA and ROSIS are described in the following.

In general the *Sensor* module has the following work flow: The *Sensor* receives the XML string from the *Master* and validates it. Before the data acquisition can start the sensor settings have to be performed. Settings can be done directly by the *Sensor* module or by an existing sensor controlling software with an interface, with which the *Sensor* communicates. Only if all settings have been made the sensor control program receives the instruction to start the measurement. The sensor control program stops the data recording after collecting a defined number of frames. Afterwards the *Master* receives a response whether the measurement was successful or not.

The whole *Sensor* module can be divided into

- a communication part to the *Master*,
- a communication part to the data acquisition software and
- a data recording part.

Communication parts

In the normal case the *Sensor* module itself is a server program, which communicates with a client and provides a specific service for automatic data recording. The server establishes a TCP/IP network communication on a defined port for the *Master* and opens a network connection to the data acquisition software (DAQ) of the sensor. The IP addresses and the port numbers of both connections are loaded from an external XML file at runtime. The incoming XML string is validated by an XML parser. If a request is not valid, the *Master* receives an error response. In the valid case the data recording will be performed and the *Master* gets a response afterwards. Figure 4.7 gives an overview of the client / server architecture and the communication parts.

Data recording

Depending on the DAQ software the *Sensor* module sends control commands. Before the data recording can start, the sensor has to be prepared for the data acquisition. Initialisation parameters can be, for example, the integration time, the acquisition mode or the file name. For some sensors the file name can be freely selected, for others the acquisition software defines the file name. However it is important to know the exact file name for the automatic data analysis; therefore the name is a return parameter of the *Sensor* interface.

AISA

The Airborne Imaging Spectrometer for different Applications (AISA) is described in detail in chapter 6.1. The AISA was delivered with two programs: A DAQ software from the manufacturer of AISA and sensor control software written by the previous owner of the AISA sensor. The DAQ software communicates via serial interface with AISA and is an executable program which cannot be modified. The *Sensor* module was developed in C++ [67] based on the existing sensor control program.

Normally the *Sensor* software is only a server but for AISA the software acts as a server and as a client with respect to the DAQ software (see Figure 4.7). The AISA S*ensor* server GUI contains only the port number and a start / stop button. In the simulation mode no connection to the DAQ server will be established and the communication with the DAQ server is emulated in the *Sensor* program.

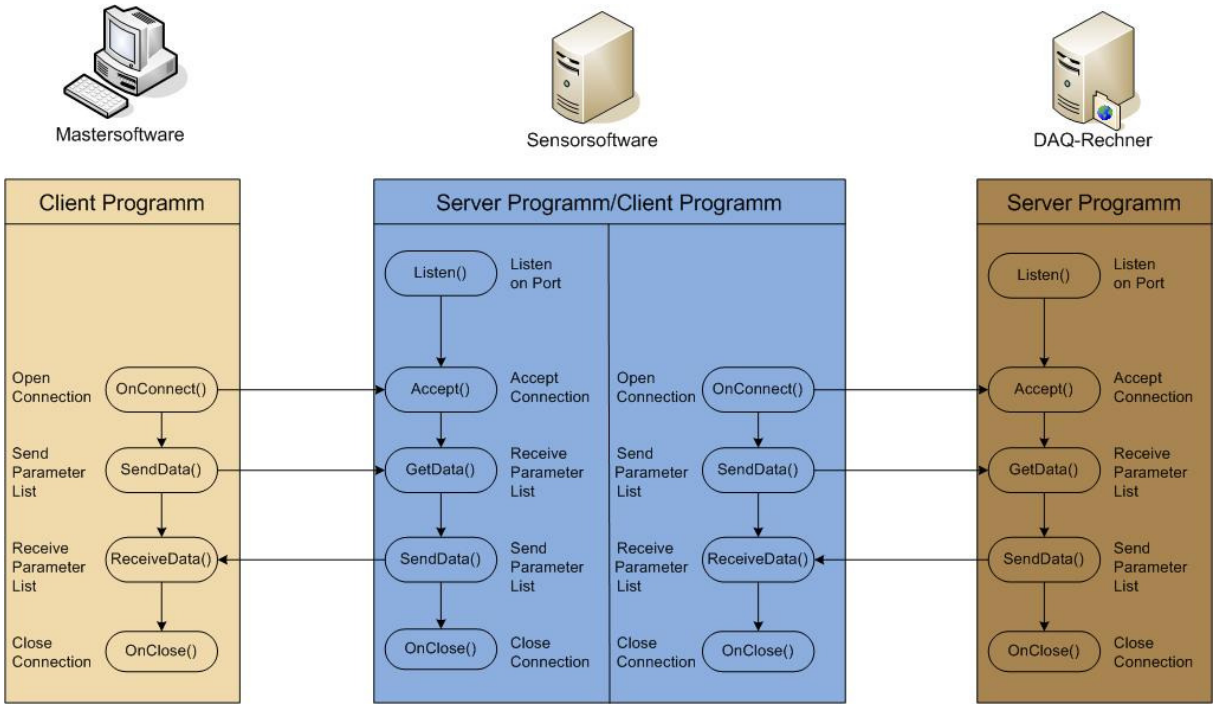

Figure 4.7: AISA client / server architecture ([67], p. 32)

AISA has four acquisition modes and the data acquisition is flexibly programmable by using a configuration file. The four different selectable modes are [68-71]:

- Mode A: All spatial and spectral pixels of the CCD array are stored. This mode requires the longest integration time due to the data transmission rate.
- Mode B: The number of channels and the width for all spatial pixels can be selected. The width is selectable between 1.6 and 9.4 nm.
- Mode C: The information of all channels for 47 (every 9th pixel) spatial pixels is recorded.
- Mode D: In this mode the channels and spatial pixels can be selected.

A configuration file contains the integration time, the acquisition mode, and the number of channels and pixels.

The *Sensor* XML interface contains the name of the configuration file, the lens, the shutter status, the number of frames, comments, the data file name pre-fix, and network settings (see App. B, Figure B.8). *Master* response parameters are the data file name, the integration time and the status of the data recording.

The interface to the DAQ software is a 1024 byte array with a header, a command code, a data field and an error field [72]. The data field is used for sending the name of the data file or configuration file. The DAQ software has single commands for starting or stopping an acquisition, sending a configuration file, toggling the shutter or setting the file name prefix [67]. The data recording sequence is the following: Loading of the configuration file, toggling of the shutter, setting the data file name, and starting of the acquisition. Since the DAQ software has no function for an automatic stop after a certain number of frames have been collected, the *Sensor* software calculates the measurement time and sends the stop command after this time has expired.

ROSIS

The Reflective Optics System Imaging Spectrometer (ROSIS) is described in detail in chapter 6.1. ROSIS has an internal tiltable mirror controlled by a stepper motor. The motor can be steered in full steps but returns the adjusted half steps. There are three essential mirror positions corresponding to the line of sight downwards (nadir), to the mercury-vapour lamp (spectral) and to the inside of the sensor body (dark). The last mirror position is needed for dark current measurements, since ROSIS has no shutter.

The existing ROSIS Data Storage Unit (DSU) control software (from Schneider, Germany) is used in airplanes and in the laboratory. The software has different operation modes. For the laboratory a semi automatic mode is used, which records data at five mirror positions. The sequence consists of the defined number of frames at the nadir position and 500 dark and 100 spectral frames at the beginning and end of each measurement series. The data recording in the nadir position must be stopped manually after the desired number of frames has been recorded. Afterwards the 100 spectral and 500 dark current frames are recorded automatically. This kind of automation is unsuitable for the automated characterisation process in the CHB, since manual interactions are necessary.

The existing DSU software was upgraded. A network connection and interface were implemented directly in the DSU software for the communication with the *Master*. The sequence of one measurement is as follows: The DSU software receives the XML string, parses and validates the parameters, sets the file name and performs the fiver sequence. The DSU software moves the ROSIS mirror to the desired positions and records the desired numbers of frames. After all measurements have been performed the DSU software transmits the parameters in XML format back to the *Master* and waits for the next request.

For some measurements, like the spectral characterisation, the moving of the mirror to the five positions is not necessary, because the dark current and spectral data are not needed.

Therefore the DSU software has been upgraded accordingly. In the new version the software records only the data and does not tilt the mirror. Before the characterisation process can start, the ROSIS mirror has to be moved to the nadir position manually. With the new function the measurement time can be reduced dramatically. The spectral and dark current measurement times as well as the tilting of the mirror are omitted.

The *Sensor* XML interface of ROSIS contains the number of frames and the mirror positions in motor steps for each of the five mirror positions, a data file pre-fix, and the scan frequency (see App. B, Figure B.7). Return parameters are the file name, the available disk space of the ROSIS computer and the mirror position in full steps.

The measured signals are split and stored on two hard disks. The files have to be merged with a specific DSU program before the files can be moved.

4.5 Data Analysis

This chapter describes the implementation of the data analysis concept explained in chapter 3.5. The analysis processes (spectral, geometric and radiometric) are developed under IDL/ENVI. This is a common software program for the analysis of hyperspectral data and has standard functions for the reading, writing and creation of large data files.

The first task of each analysis process is the conversion of the measurement data into a generic data file format. Since the most sensors are one-off products the raw data formats differ in the data types, numbers of pixels and header information. Therefore it is not possible to develop an independent conversion program. Each sensor needs its own program. The generic approach is to store the converted measurement data as IDL files and split the different data types (nadir data, dark current, IFC data) into single files.

Generic File structure

The converted data are stored as ENVI files in the Band Interleaved by Line (BIL) format consisting of a header and a data file. The structure of data file is a three dimensional data cube. The spatial pixels are stored in the rows (X), the channels in the columns (Z) and each line (Y) contains the main CHB device parameter value (see Figure 4.8). This main parameter depends on the type of characterisation (spectral, geometric or radiometric). Examples for the main CHB parameters are the wavelength for the spectral characterisation analysis, the viewing angle for the geometric analysis or the request-id for the raw data. The single CHB parameter values of each line are stored in a separate text file and are used in the analysis programs.

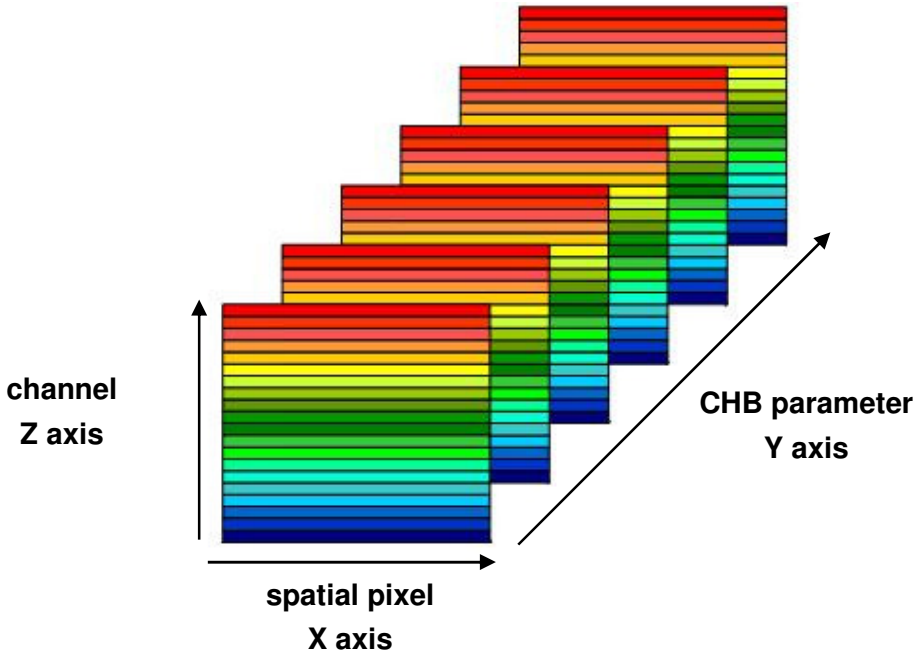

Figure 4.8: Data cube structure for the stored measurement data

Sensor conversion programs

The implemented conversion programs are for AISA and ROSIS. The AISA conversion program reads and converts the raw data of the 286 spectral and 392 spatial pixels. The 392 pixels consist of 364 spatial pixels, 20 fiberoptic downwelling irradiance sensor (FODIS) pixels and 8 dark current reference pixels. The created data cube has 364 columns, 286 rows and x lines according to the measured frames. For each frame the eight dark current pixels and four of the FODIS pixels (pixel 378 to 381) [69] are averaged and stored in two text files. Since AISA has a shutter, dark current measurements are performed with a closed shutter and the data are stored in separate marked files.

The ROSIS conversion program converts the maximum quantity of spectral and spatial pixels. An interpretation of the timing file has not been implemented yet. From the ROSIS CCD array (552 columns and 124 rows) only 512 spatial and 115 spectral pixels are used and converted. The spatial pixels start at pixel number 25 and the spectral at row 3. The modified acquisition software (DSU) can record dark current, spectral lamp and nadir measurement data in one file. The ROSIS conversion program separates these data types according to the parameters of the *Sensor* software measurement log file, which contains the number of frames of each data type. The twice-measured dark and spectral data are combined, separated, averaged and stored in two data files.

Analysis programs

Each analysis program requires the converted measurement data and measurement logs (*Master* requests, *Master* replies and *Sensor* replies). For the analysis of the measurement data the data are allocated with the sensor and the CHB hardware settings. The allocation parameter is the “request-id” which is in each log file.

For each analysis program input parameters with default values are defined to minimise the interaction during the execution of an analysis program. The user can overwrite the default parameter values at the call of the program.

The analysis programs for the different characterisation processes are sensor independent. But for quality and error checks the sensor specific parameters are needed (e. g. centre pixel, dynamic range). These parameters are stored for each sensor in an external text file and are loaded at run time. The sensor independent programs are modularly structured and use generic programs:

- Averaging of the measured data
- Conversion of the measurement logs s
- Combining of the averaged data of one measurement series into a data cube
- Creation of uniform plots,
- Creation of analysis logs
- Import of different text or ENVI files.

Each analysis procedure generates graphics and text files, and stores the results in a sensor and characterisation type specific data cube file. The structure and content of the analysis log files are defined in external style sheets. The style sheets are line-based with a description and a field part. Each log file is divided into four blocks. The first block contains the program settings like the file path and the input parameter values. The second block covers the hardware settings of the CHB devices and of the sensor. The third block contains the program control parameter like threshold, the selected pixel or errors of the analysis of a single channel or a spatial pixel. The last block lists the analysis results depending on the characterisation process type.

Spatial pixel calculation program

For the evaluation of the measured data it is necessary to know which spatial pixel should be illuminated in the measured data according to the folding mirror settings. Relevant for the calculation are the parameters “scan angle” and “roll angle offset” in the *Slave* measurement log file, as well as the “Instantaneous Field of View (IFOV)” and ”centre pixel” parameter from the sensor parameter file. The viewing angle is the angle from where the light comes. If a roll angle offset has been used during the measurement the viewing angle has to be corrected by subtracting the offset from the viewing angle. The affected spatial pixel (P_{aff}) can be calculated according to the centre pixel (P_{center}), the viewing angle (δ_{corr}) and the IFOV with the equation:

(4-1)

$$P_{aff} = P_{center} - round(\frac{\delta_{corr}}{IFOV})$$

5 Characterisation Methods

Imaging spectrometers are designed to collect the spectral and geometric characteristics of an image scene. The most used approach is to use a line scanner with a monochromator whose entrance aperture is located at the primary focal plane. The incoming light is dispersed into its spectral bands using prisms, gratings or filters and the detector arrays sense the dispersed radiation. Two scanning techniques are used. A mechanical (whiskbroom) scanner changes the viewing angle by rotating a mirror in cross-track direction. While opto-electronic (pushbroom) sensors are parallel line-scanning systems with no moving parts. The radiation in across track direction is being imaged simultaneously for all detector elements [73-76].

Hyperspectral sensors provide a large amount of spectral and spatial information. The whiskbroom spectrometer records the spectral information into a linear detector array for one spatial pixel at a time. Pushbroom sensors sense the spectra for hundreds of spatial pixels at the same time. A comparison of the characterisation strategies of the two sensor types show varieties. For example, the spectral and geometric characterisations are often performed only for the nadir pixel assuming that all across track pixels of a whiskbroom sensor are observed by the same spectrometer [4, 9, 77]. Anyway sensor characterisation is extremely time consuming. With the traditional strategies only the mandatory characterisation measurements are performed (spectral and radiometric). Recent studies demonstrate that non-uniformities and detector imperfections have an impact on the data quality if they are not known or not corrected [78-81].

Calibration Standards

For the execution of accurate characterisation measurements calibration standards are used. Generally standards are be distinguished in three types [15, 35, 75]:

- Primary: mostly located and calibrated by national standardising agencies
- Secondary: calibrated by secondary laboratories which use primary standards to establish traceable standards
- Working: in house calibrated as compared to primary or secondary

Table 5.1: National standardisation institutes (Walker et al. 1991)

Country	Organisation
Canada	National Research Council (NRC) - Institute for National Measurement Standards (INMS) [82]
Germany	Physikalisch-Technische Bundesanstalt (PTB), Division 4 – Optics [83]
UK	National Physical Laboratory (NPL) [84]
USA	National Institute of Standards and Technology (NIST) [85]
France	Bureau International des Poids et Mesures (BIPM) [86]

Most laboratories use different types of secondary and working standards like wavelength standards (e.g. monochromator, pencil lamps) for spectral measurements or radiance standards (e.g. integrating sphere) for radiometric measurements.

This chapter describes major characterisation processes for hyperspectral sensors divided into the main groups: spectral, geometric, and radiometric. The three sections contain the laboratory setups for the measurements, the necessary CHB device and its parameters, recommendations for the setting of the parameters, as well as the description of the analysis processes. The specified measurement and analysis methods are sensor independent.

5.1 Sensor Alignment

Before the spectral and geometric characterisation measurements can be performed the sensor has to be aligned on top of the optical bench using an adapter. An exact alignment of the sensor is necessary for the spectral and geometric measurements. For the radiometric measurements the CHB adapter with the sensor can be carried from the optical bench to the frame of the spheres and a new alignment is not necessary.

The coordinate system of the optical bench is defined like in the aircraft (see Figure 5.1) [87]. The across track axis of the sensor corresponds to the linear axis (Y) of the folding mirror and the roll angle (α) to the angle of the folding mirror. A sensor mounted on the CHB adapter can be moved in along track direction (X-axis) and rotated around the Y- and Z-axes. The pitch (β) and yaw angle (γ) have to be aligned manually using the handwheels of the DLR adapter (see Figure 2.6).

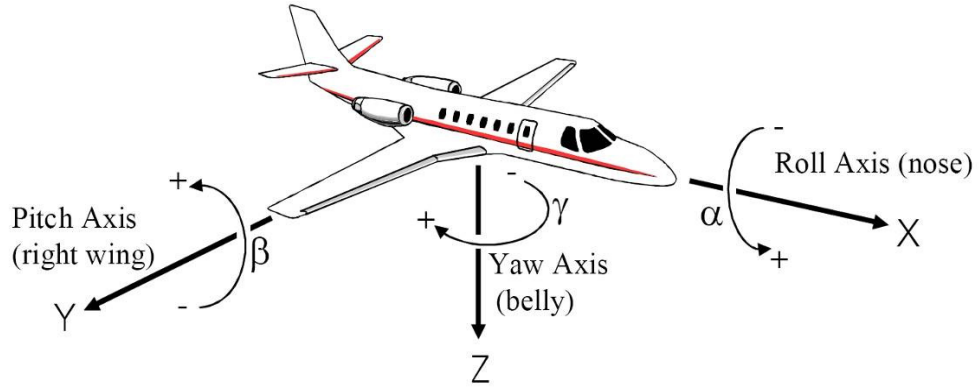

Figure 5.1: Coordinate system definition [88]

Sensor height is defined as the distance from the aperture of the sensor downwards, along the Z axis, to the folding mirror (see Figure 5.2). It determines the linear movement of the folding mirror for a specific viewing angle. Y, Z, and α are parameters of the *Slave* interface and are adjusted by the *Slave* software.

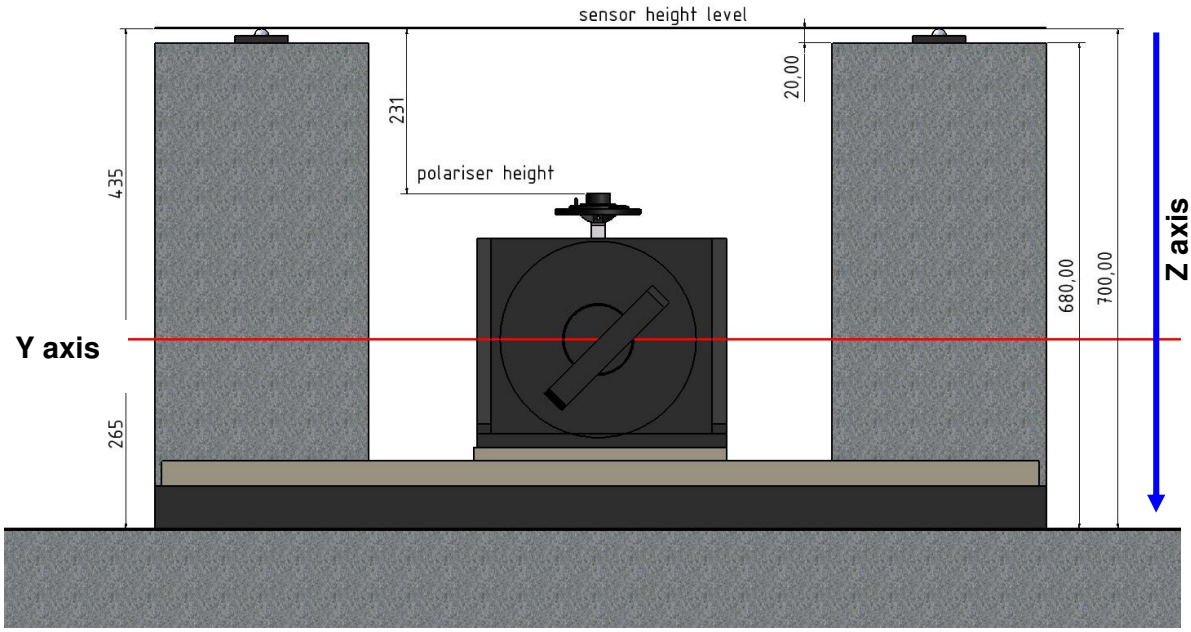

Figure 5.2: Relevant interface frame dimensions in mm [40]

The goal of alignment is to adjust the optical axes of the bench and the sensor parallel to each other and to meet the entrance aperture near its centre. The alignment procedure describes the adjustment of the six degrees of freedom.

Alignment procedure

a) For a first rough alignment the sensor aperture is illuminated with white light produced by the monochromator at none dispersed throughput. The light spot is moved along the sensor FOV by changing the angle of the folding mirror to control the alignment. The spot should cover the entrance optics of the sensor at the different positions (borders and nadir). The sensor has to be aligned by moving it along the X-axis and rotating it around the Z-axis (yaw angle γ) until the FOV is illuminated.
b) Perform two measurements for the pixels near the borders by using the 50 µm horizontal slit and the folding mirror. Compare the illuminated pixel number with the calculated pixel number of the two border pixels. Adjust the height parameter until the correct border pixels are illuminated.
c) Determine the Y-axis offset by equalising the number of pixels between the two border pixels and the nadir pixel. Perform measurements with the 50 µm horizontal slit and move the folding mirror in small steps along the Y-axis with a fixed mirror angle.
d) The roll angle offset can be determined from measurements using the 50 µm horizontal slit and the folding mirror. This can be done by rotating the folding mirror in small steps around the viewing angle of 0° and recording data at each position. The viewing angle of the measurements with the highest signal corresponds to the roll angle offset.

e) Maximise the signal of the nadir pixel by changing the pitch angle of the DLR adapter using the 100 µm vertical slit and the folding mirror. Check again the roll angle offset by performing step d).
f) The following steps are performed iteratively for the border pixels of the sensor FOV. The process can be finished when the signals of both pixels differ less than 10 % using the 100 µm vertical slit and the folding mirror.
    - Record data of two symmetric pixels close to the border and compare the signals of the two measurements.
    - Rotate the sensor around the Z-axis to adjust the yaw angle using the adapter.

A real-time display of the sensor signals is advantageous during the alignment procedure. Suitable are graphical displays of a two dimensional image and horizontal plots with zoom functionality.

5.2 Spectral Characterisation

This chapter refers to the determination of spectral properties of imaging spectrometers. The main parameters are: the spectral resolution, the centre wavelengths and spectral sampling interval. It is essential to know, for a spectrometer, how well the sensor wavelength reading agrees with the true wavelength [76]. The spectral response function (SRF) of a sensor channel describes the response of the sensor to narrow spectral band radiances at various wavelengths [35, 89]. This function is basically a function of the spectral filter, grating and detector [9]. The spectral separation into channels can be done by a dispersion element (grating/prism) or a filter based system [76]. In case of an imaging spectrometer the incoming radiation is separated in distinct angles, dispersed and focused on different locations of the detector array (row) [90].

The spectral parameters of a sensor, which can be determined from the spectral characterisation measurements, are:

- Spectral range (nm)
- Centre wavelength of each channel (nm)
- FWHM of each band (nm)
- Spectral sampling interval (nm)
- Channel overlap (%)

In most cases the spectral response is not a rectangular function [76], but a good approximation is a Gaussian function [9]. Assuming a Gaussian function the spectral resolution is defined as the full width at half maximum (FWHM) of the function [35]. The peak of the response is the centre wavelength [9, 35]. The spectral sampling interval is the distance between two adjacent channel centre wavelengths. The channel overlapping parameter is defined as the overlap of the FWHM of two adjacent channels.

This parameter should be ≤ 50 %. If there are overlaps above 50 %, the spectrum is oversampled. The spectrum is undersampled if the FWHM of two adjacent channels do not overlap [35]. The out-of band response is the spectral range where the response of a channel is less than 0.001 of the peak spectral response [75]. The spectral parameters are illustrated in Figure 5.3.

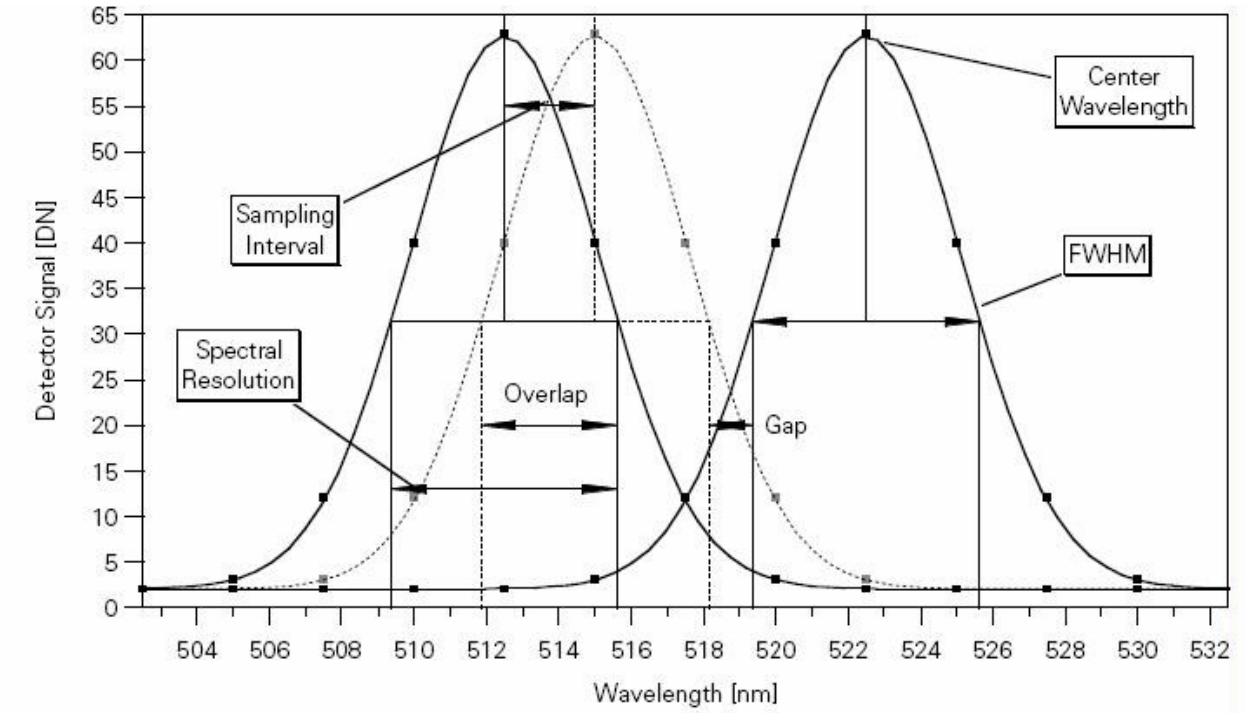

Figure 5.3: Spectral parameters of a sensor ([35], p 38)

This chapter is divided in two sections. The first section describes the measurements setup, explains the necessary laboratory devices and CHB parameter for the measurements as well as the main selection criteria for the parameter settings. The second section explains the analysis methods.

5.2.1 Measurement Materials and Methods

For the characterisation of the spectral parameters of a sensor a wavelength standard is needed. There are many wavelength standards available. The characterisation can be done by using a known wavelength of either spectral emission or absorption lines. These are obtained by gas discharge lamps, gas cell absorption lines, gas laser lines, neutral density filters and Fabry-Pérot etalon and interferometers. Gas-discharge lamps contain rare gases like argon, krypton, neon, mercury or xenon. These lamps provide narrow well-known emission lines. A monochromator illuminated by a tungsten lamp provides narrow spectral bands out of a bright spectral range of the light source [35, 75]. Criteria for the selection of a wavelength standard are the wavelength range, the spectral bandwidth to provide narrow line width, the uncertainty, and the irradiance must be high enough to provide enough signal.

Measurement Setup

The CHB devices for the spectral characterisation measurements are a monochromator, a light source (tungsten halogen or ceramic lamp) and a folding mirror. The monochromator, which is a working standard, is calibrated at DLR with gas emission lamps (Hg, Ne, Ar, Kr, Xe). The monochromator provides a narrow-band of the light source and illuminates the entrance aperture at a defined angle by using the folding mirror.

The setup is illustrated in Figure 5.4 .The source (1) illuminates the entrance slit (3) of the monochromator. An order filter (2), if selected, removes shorter wavelengths of light. The main components of the monochromator are the entrance slit (3), the turret with its gratings (4) and the exit slit (5).

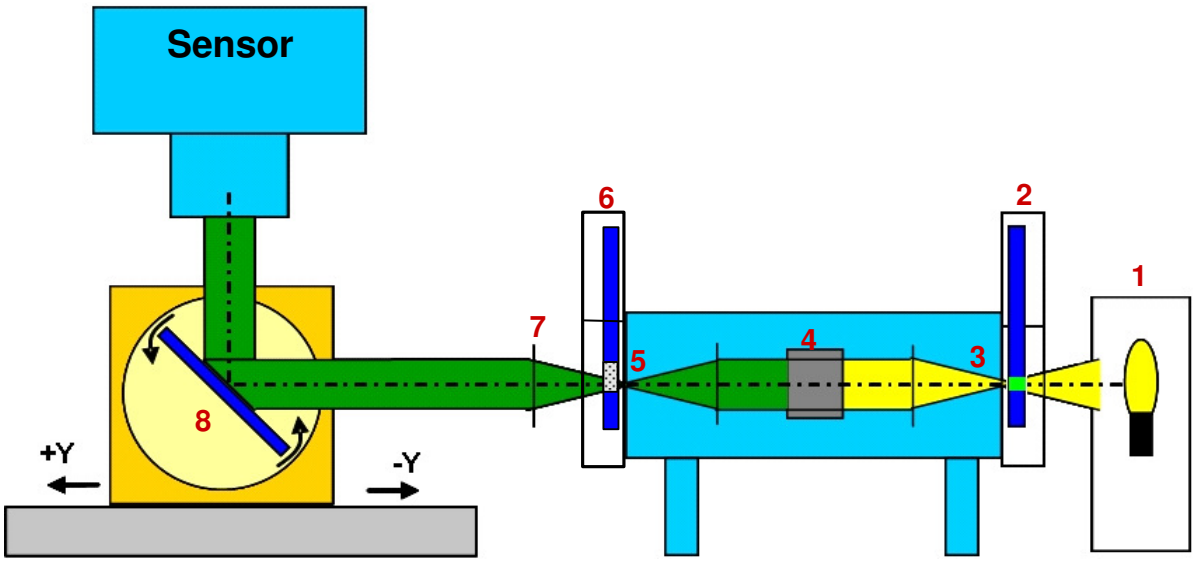

Figure 5.4: Spectral measurement setup ([88] modified): 1 = source, 2 = wheel (blue) with order filters (green), 3 = entrance slit, 4 = grating, 5 = exit slit, 6 = wheel with neutral density filters (gray), 7 = collimator, 8 = folding mirror

The monochromatic light can be attenuated by using a neutral density filter (6). The turnable wheel (6) is equipped with four filters which have a transmission between 0.01 % and 50 %. The beam out of the monochromator is collimated by the parabolic mirror (7) and reflected by the folding mirror (8) to the sensor aperture. These devices are described in detail in chapter 2.2.

Methods

Hyperspectral sensors can have more than 100 spectral and spatial detector elements. Ideally the spectral characterisation has to be performed for each channel and each spatial pixel. Due to the huge amount of measurements and data which are necessary for this task, in most cases rather a few detector elements are characterised. The parameters of the omitted elements are interpolated.

The amount of pixels (channels at different viewing angles) depends on the sensor properties and the required accuracy. This should be defined by the instrument manufacturer and is not part of this thesis. In a first step elements can be selected by using a raster among all elements. At least the selected elements should cover the centre and border of the single detector array. For the determination of the spectral sampling interval, measurements of adjacent channels of one spatial pixel element have to be performed.

The measurement cycle for one spatial pixel and a defined wavelength range is as follows. The signal of the selected spatial pixel has to be optimised to its maximum. For this step an across track LSF measurement for the selected pixel can be performed (see chapter 5.3). One analysis result of the LSF measurements is the viewing angle of the folding mirror, which is a required parameter for the setup of spectral characterisation measurements. After the setup of the folding mirror the monochromator wavelength is increased stepwise while the sensor collects the data.

Predefinition of the measurement settings

Table 5.2 includes the parameters, which are needed for the setup of the spectral characterisation measurements referring to one spatial pixel and one or more spectral pixel element. Gratings and filter changes should be reduced to a minimum and the wavelength range of one detector should be covered by one monochromator grating and one order filter. The sensor response to the incoming light should be checked to avoid saturation and low signals.

Table 5.2: Setup parameters for the spectral characterisation measurements

Monochromator	**Folding mirror**	**Sensor**
Wavelength range (nm)	Z axis (mm)	Integration time (ms) / frequency (Hz)
Wavelength interval (nm)	Viewing angle (°)	Frame numbers
Grating no.	Roll angle offset (°)	Interface
Filter no.	Y axis offset (mm)	Neutral density filter
Slit width (µm)		
Lamp current (A)		
Neutral density filter		

The following conditions have to be satisfied for the definition of setup of CHB parameters.

1. The wavelength range setting (λ_{start}, λ_{end}) of each selected channel has to cover the whole wavelength range where the channel has a signal (i.e. it should include wavelengths with out of band response). Since the response function is usually similar to a Gaussian function the range for one channel is approximately six times the spectral sampling interval (SSI) [91].
2. The selected wavelength range has to be covered by the wavelength range of the light source.
3. The illumination of the monochromator should provide enough light to produce an acceptable SNR for the entire wavelength range. The flux can be reduced by using a neutral density filter, or the integration time of the sensor can be adjusted.

4. The spectral response of each channel should be measured with less than 1/5 (optimal 1/10) of the spectral resolution (FWHM) of the channel ([75]). The spectral band width (b) is provided by the monochromator exit slit width (s_{mono}) in dependence of the grating dispersion (d). The slit width of the monochromator can be calculated on the basis of the required spectral bandwidth:

(5-1)

$$S_{mono} = \frac{b}{d}$$

5. The monochromator step width should be less than, or equal to, the selected spectral band width of the monochromator.
6. The collimated beam should completely fill the sensor entrance aperture.
7. The monochromator slit width has to be set in a way that it guarantees full geometrical coverage of the sensor IFOV (θ_{IFOV}). The factor (c) should be greater than 1.0 to illuminate the whole IFOV. The monochromator slit width (s_{mono}) can be calculated for a IFOV, considering the focal length of the parabolic mirror (f_p), with the equation:

(5-2)

$$s_{mono} = \theta_{IFOV} \cdot f_p \cdot c$$

5.2.2 Analysis Materials and Methods

This chapter describes the analysis of the spectral characterisation measurements. It is divided into the sections materials, restrictions, pre-processing, quality and error checks, and analysis. The section “Materials” contains all items needed during the process. Preparatory tasks are explained under “Pre-processing”.

For the analysis of the SRF the Gaussian function is used to determine the centre wavelength and FWHM.

(5-3)

$$R_i(\lambda) = \frac{1}{\sigma\sqrt{2\pi}} e^{-0.5(\lambda-\mu)^2/\sigma^2}$$

where

λ: wavelength
μ: centre wavelength
σ: standard deviation

(5-4)

$$FWHM = 2\sigma\sqrt{2\ln(2)}$$

where

σ: standard deviation

Materials

The required inputs of the analysis process are the measured sensor data and the measuring logs (*Slave* and *Sensor* logs). The sensor data have to be converted and averaged. From the *Slave* log, the parameter settings of the monochromator and folding mirror are needed. If the monochromator wavelength was not corrected during the measurement process by the *Slave*, the monochromator wavelength has to be corrected during the analysis. Therefore the monochromator calibration values are necessary. Since the intensity of the monochromator output may vary for different wavelengths the signals of the sensor data have to be corrected accordingly. If a neutral density filter was used the transmittance values of the filter are needed for a correction of the signals. The monochromator signal outputs of the different gratings were measured with the power meter. These measurements should be used for the correction of the sensor signals. The following items are needed for the analysis of the spectral characterisation measurements:

Data:

- Converted and averaged measurement data
- Converted *Sensor* and *Slave* measuring logs
- Input parameter values
- Monochromator calibration values
- Monochromator irradiance measurements
- Neutral density filter transmittance values

Software:

- IDL program “chbmo01_008_spectral” and several procedures (see App. B, Table B.4)
- The IDL Gaussian fit function “GAUSSFIT” has been modified to return an error if the curve fit has a failure.

Restrictions

The spectral characterisation analysis program can analyse the data of one spatial pixel with the same monochromator settings for the grating, exit slit width, order filter, neutral density filter and lamp.

Pre-processing

For the data analysis the converted and average sensor data and the converted measurement log files are needed. The conversion program for the measured data depends on the sensor (see chapter 4.5). Whereas the averaging and the creation of the data cube are sensor independent. The cube structure corresponds to Figure 4.8 and the CHB parameter (Y axis) is the “wavelength” of the monochromator. The additional possible preparative procedures are explained below.

Wavelength correction

The wavelength correction is only necessary if this was not performed by the *Slave* software during the characterisation measurement process. The correction has to be selected at the beginning of the analysis. The current monochromator calibration results are stored in a file. This file contains for each grating a gain and an offset value of a linear fit function. The following equation is used for the wavelength correction:

$$\lambda = C_{offset} + \lambda_{mono} \cdot (1 + C_{gain}) \tag{5-5}$$

where

λ_{mono} : monochromator wavelength

λ : corrected wavelength

C_{gain} : gain of the monochromator calibration

C_{offset} : offset of the monochromator calibration

Signal correction

The signal produced by the monochromator is not constant at all wavelengths. This effect can be corrected by irradiance data recorded by the power meter at different monochromator wavelengths. The measurements are performed with the same monochromator settings (grating, slit width, lamp current, and filters) as for the sensor measurements. The power meter data are interpolated according to CHB wavelengths. The relative correction is a division of the sensor data by the interpolated data.

Transmission correction

The transmission correction is necessary if a neutral density filter has been used for the measurements. The correction is a multiplication of the sensor signals by the transmission coefficients.

Selection of the spatial and spectral pixels

For the analysis of the data one spatial pixel has to be selected. The spatial pixel will be calculated based on the sensor viewing angle (see chapter 4.5) and compared with the maximum illuminated pixel. This spatial pixel is the pixel with the maximum signal in the whole data cube. If the calculated pixel differs from the illuminated pixel the user has to select the pixel. For the analysis the relevant channels have to be selected. The selection is performed on the basis of a signal threshold. The threshold is a multiplication of the minimum signal by a factor. All channels of the selected spatial pixel, with a greater signal as a threshold are selected for the analysis. The threshold factor is an input parameter and default is 2.0. Due to the low threshold also channels with low signals are selected. The user can ignore the selected channels and chose other channels.

Quality and error checks

The implemented quality and error checks are the saturation control, the check of the amount of data points, and a stray light control. All these checks are performed for each selected channel. Errors are saturated data points or channels where the number of measurement points is below a threshold. Channels with an error will not be analysed.

Saturation control

The analysis program checks the measured signals on saturation. A measurement is saturated if one signal is at its maximum. The maximum value is a sensor parameter (see chapter 3.5), which is in most cases the bit digitisation value. If any data point is saturated the analysis of the channel will not be performed and identified with an error.

Check number of data points

There are two tests controlling the number of data points. The first check is implemented in the modified IDL Gaussian fit function. The IDL function returns an error if there are not enough data points and the channel will not be analysed. The second control is implemented in the analysis program itself. For this check the total amount of data points in the affected spectral range of one channel is required. This is the range where a channel has a response higher than the dark current signal. Since this range can vary from channel to channel an estimated spectral range is calculated by multiplying the SSI by a factor. The default value is six which is three times the SSI to each side of a peak. The total number of data points in the range is calculated with regard to the wavelength step interval (*Master* log file).

On the basis of the total points the minimum needed data points are computed by multiplying the total points by a factor. Each channel with less data points will be analysed but signed. Investigations results in a default value for the factor of 0.75 which equates to ¾ of the total amount of data points. This number of data points is adequate to get a data Gaussian fit curve where the sensor signal decreases to the borders of the range.

Stray light control

The rough stray light control checks spatial and spectral stray light. Spatial stray light is, in this context, when a pixel other than the selected one is illuminated. Spectral stray light in this context is when a channel which is not one of the selected channels is illuminated. All pixels with a signal greater than a threshold are identified. The threshold is a multiplication of the minimum signal by a factor. This factor is an input parameter and the default value is 1.1.

Analysis

The analysis program for the spectral characterisation asks for the required input parameters (see Table 5.3) and computes the program control parameters, such as the spectral range and thresholds. The input parameters, device settings, monochromator calibration values, and program control parameters are written in the log file. Table 5.3 contains the input parameters of the spectral analysis. Parameter e) and f) have no default values, because these parameters have to be selected by the user.

Table 5.3 Input parameters for the spectral characterisation analysis

Input parameter	Default value
a) Channel spectral range factor	6
b) Data point factor	0.75
c) Pixel selection threshold factor	2.0
d) Stray light threshold factor	1.1
e) Correct the wavelength	-
f) Intensity correction	-

After the pre-processing and error checks the data analysis for each selected channel is performed. The centre wavelength and the FWHM are determined for each channel by the IDL Gaussian fit function. Input parameters for the Gaussian fit are the corrected wavelength and the corrected measurement data of the channel. Return values are the peak value, the amplitude and constant term of the function as well as the standard deviations of the single parameters.

If the measurement series cover more than one channel the spectral sampling interval and the channel overlap parameter is determined. The spectral sampling interval can be calculated by subtracting the centre wavelengths of two adjacent channels. The channel overlap parameter (*CUS*) is calculated with equation:

(5-6)

$$CUS_i = \frac{(\lambda_{i-1} + 0.5 \cdot FWHM_{i-1}) - (\lambda_i - 0.5 \cdot FWHM_i)}{(\lambda_i + 0.5 \cdot FWHM_i) - (\lambda_{i-1} - 0.5 \cdot FWHM_{i-1})} * 100$$

where

CUS_i : channel under sampling

λ_i : centre wavelength

$FWHM_i$: FWHM

i : channel number

The errors and results of each channel are written in an analysis log file, graphs with the raw data and Gaussian curves are plotted, and the analysis results are transferred to a sensor result cube. Each sensor has its own result cube. Only results of channels with no error are stored. The user has to choose whether existing results are overwritten or not. The result cube structure is according to the cube structure in Figure 4.8. The dimension in X direction is equal to the spatial pixel number and Z equates to the channel number. The parameters of the Y-axis are:

- Centre wavelength (nm) and its standard deviation (nm)
- FWHM (nm) and its standard deviation (nm)
- Standard deviation (nm) of Gaussian function
- Constant term (DN)
- Altitude of the Gaussian function (DN)
- Spectral sampling interval (nm)
- Channel overlap (%)

Additional to the plotted curves the measurement and Gaussian fit data are written in a text file which can be used for further processing in other programs (i.e. TechPlot, Excel). Examples of the program outputs are shown in Appendix C.

5.3 Geometric Characterisation

A good indicator for the image transfer quality of a sensor is the Modular Transfer Function (MTF), which measures the contrast in an image [76]. The MTF measures the spatial resolution of a sensor image and can be determined by a Fourier transformation of a Point Spread Function (PSF) or LSF [34, 75]. The LSF measures the sensor response to a slit illumination [76]. Measurements can be performed by scanning a slit image across the detector array or by imaging a knife edge. The slit methods are described in ISO standard 15529:1999 ("Optical transfer function – principles of modular transfer function (MTF) …") [76].

The following sensor parameters can be examined from the geometric characterisation measurements:

- Field of View (FOV) (°)
- Instantaneous Field of View (IFOV) (mrad, °)
- Across and along track LSF
- Viewing angle of a spatial pixel (°)
- Across track sampling distance (mrad)

The FOV is the difference between the viewing angles of the first and the last spatial pixel through which a spectrometer detects the radiance [35]. The across and along track IFOV is identical to the FWHM of the LSF [34]. The viewing angle of a spatial pixel corresponds to the peak of the LSF. The sampling distance is the distance between the viewing angles of two adjacent spatial pixels.

5.3.1 Measurement Materials and Methods

The signal responses of a slit illumination performed at different viewing angles can be used to determine the LSF. The geometric characterisation measurements can be performed with a collimated light source in combination with a slit in the direction of the scan.

Measurement Setup

For the geometric characterisation in the CHB a lamp, a collimator and a slit are used (device description see chapter 2.3). The setup of the geometric characterisation components is shown in Figure 5.5. The light source (1) illuminates one of the six slits (2) in the rotating slit plate. There are three horizontal and three vertical slits with different slit widths. These slits are used as characterisation target. The illuminated slit, on the top position of the wheel, is located at the focal plane of the collimator (3). Its off-axis parabolic mirror parallelises the beam and the folding mirror (4) reflects this into the entrance aperture of the sensor. The illuminated channels correspond to the wavelength range of the light source.

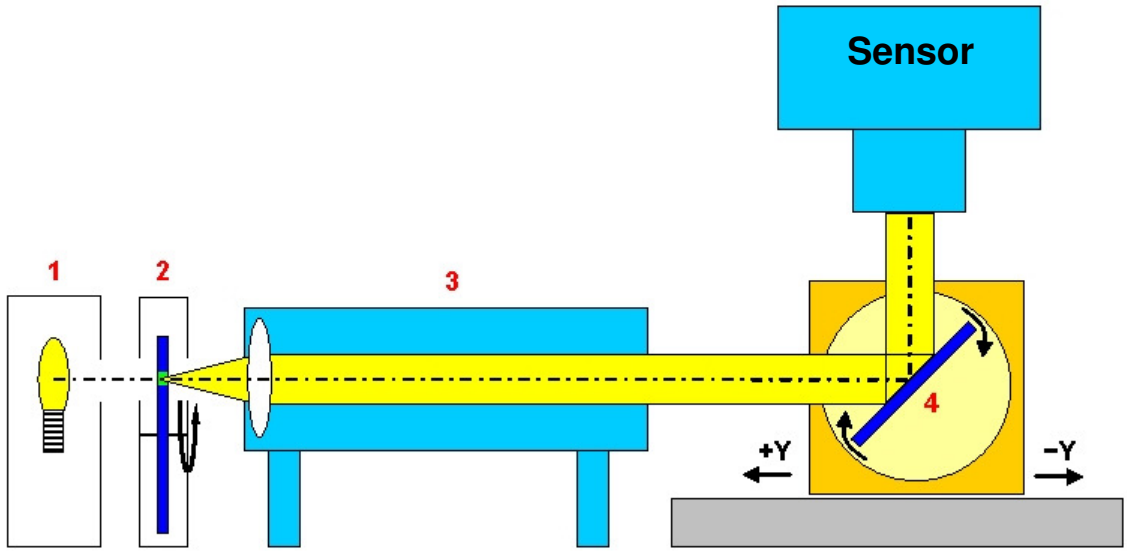

Figure 5.5: Setup of the geometric characterisation devices 1 = lamp, 2 = slit (green) in a rotating slide plate (blue), 3 = collimator, 4 = folding mirror

Methods

The focal plane of a sensor is illuminated by a narrow line, produced by one of the slits. The narrow line is moved in small angle steps in the scan direction (across or along). The across (top) and along track (bottom) measurement principles are illustrated in Figure 5.6 for a camera and an imaging spectrometer.

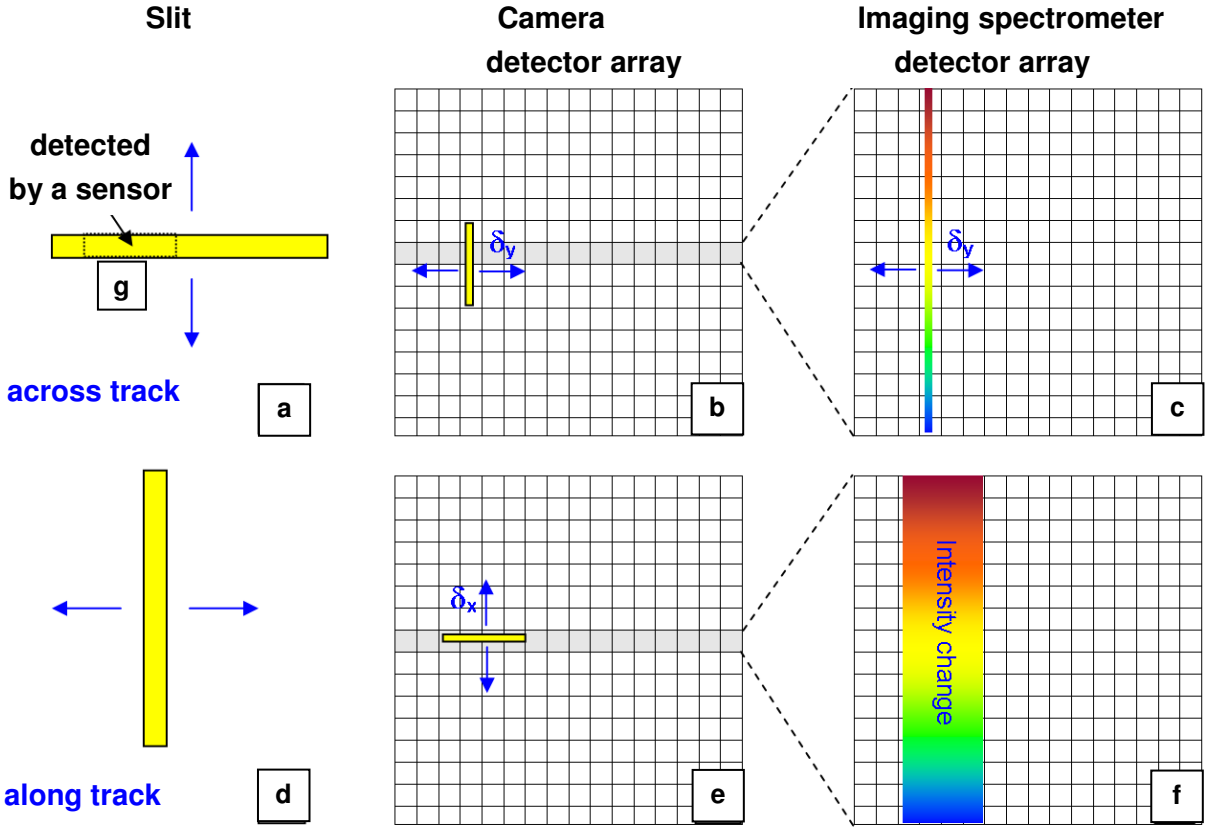

Figure 5.6 Principle of the geometric characterisation – across track: a, b, c and along track: d, e, f

The horizontal slit illuminates only a small area of a spatial pixel (b) and the vertical slit several spatial pixels (e) depending on the IFOV of a sensor. The direction of the horizontal and vertical slit movements are marked with blue arrows (see b and e of Figure 5.6). The images of the horizontal (a) and vertical (d) slit are turned at an angle of 90° (see b and e of Figure 5.6) since the components are mounted on the bench at 90° relative to the sensor (see Figure 5.5). In the case of a camera, the slit image (b, e) is similar to the target itself (a, d). Since imaging spectrometers are line scanners only that part (g) of a target which is inside the along track FOV is detected (see grey line in the two arrays of b) and e)). The spectrum of the QTH lamp is received by the spectrometer which splits it into the different wavelengths (c, f).

The selection of the amount of characterisation pixels (channel and spatial pixel) depends on the sensor property and the required accuracy. Due to the broad-band spectrum of the lamp all channels in the spectral range of the lamp are illuminated and determined. A full characterisation of all elements of a detector array is highly time-consuming and cost-intensive. For a first characterisation of the whole detector array measurements at different angular positions have to be performed. Therefore several spatial pixels across the swath have to be selected, particularly the centre and border pixels. For the determination of the across track sampling distance adjacent pixels have to be characterised as well.

The following descriptions explain the different setups of the along track and across track characterisation. The characterisations of the two types are performed for an individual detector element by setting its corresponding viewing angle of the folding mirror. The roll angle and Y-axis offsets are determined during the execution of the sensor alignment.

Across track measurements: The principle is shown in the top frame of Figure 5.6 (see a, b and c). The horizontal slits are the targets for this type of measurement. At the beginning of the measurements the slit wheel turns to the selected horizontal slit. The slit is fixed for the measurement cycle. The slit image is moved vertically across the detector element in Y-direction by using the folding mirror. The movements are realised by changing the sensor viewing angle in narrow steps. The slit height of 10 mm has a beam divergence of 13 mrad in the along track direction (X). This overfills the IFOV of most imaging spectrometers, while the slit width illuminates a small part of the IFOV in Y-direction. The necessary devices with their parameters are listed in Table 5.4.

Table 5.4: Setup parameters of across track characterisation measurements

Folding mirror	Slit wheel & lamp	Sensor
Viewing angle range (°)	Horizontal slit	Integration time / scan frequency
Angle interval (°)	Slit angle (°)	Frame numbers
Z axis (mm)	Lamp type	Interface
Roll angle offset (°)	Current (A)	Neutral density filter
Y axis offset (mm)		

Along track measurements: For the along track characterisation measurements the vertical slits are used as targets. The measurement begins with the movement of the folding mirror to the desired viewing angle to illuminate the selected detector element. The viewing angle is fixed for the whole measurement cycle. The horizontal slit image is moved in sub-pixel steps along the X axis (flight direction). The movements are realised by turning the slit wheel in narrow angle steps. D, e and f of Figure 5.6 illustrate the principle. The movements are nearly parallel.

Table 5.5: Setup parameters of along track characterisation measurements

Slit wheel & lamp	Folding mirror	Sensor
Slit angle range (°)	Viewing angle (°)	Integration time / scan frequency
Angle interval (°)	Z axis (mm)	Frame numbers
Vertical slit	Roll angle offset (°)	Interface
Lamp type	Y axis offset (mm)	Neutral density filter
Current (A)		

The following conditions have to be considered for the selection of the parameter values for the CHB setup.

1. The collimated beam should completely fill the sensor entrance aperture.
2. The slit angular dimension should be 1/10 of the nominal detector IFOV [75]. The parallel beam should illuminate in minimum 1/3 of the IFOV. The focal length of the collimator f_{colli} produces a beam with a divergence of 2 arctan(s_{width}/2 f_{colli}) where s_{width} is the width of the selected slit.
3. **Across track LSF:** The folding mirror viewing angle range should cover the FOV of the selected spatial pixel where the sensor detects the light. A good estimation for the range is six times the IFOV.

   Angle interval: The interval can be calculated by dividing the range by the desired numbers of steps.

   Slit angle: The slit angle is constant during the whole along track measurement series.

4. **Along track LSF:** The slit angle range should cover the whole viewing angle of the selected spatial pixel, where the light can be detected. A good estimation for the slit angle range is three times IFOV. For the along track LSF measurement setup the viewing angle range has to be converted into a slit angle range. The starting and endpoint angles of the range can be calculated by:

(5-7)

$$\alpha = \arctan(\frac{\theta * f_c}{r_s})$$

where

θ: viewing angle (°)

r_s radius of the slit wheel (mm)

f_c collimator focal plane (mm)

α slit angle (°)

The maximum slit angle range is ±10.0°, where the 10° correspondents to a sensor viewing angle of 0.4378° (7.641 mrad).

Slit angle Interval: The slit angle interval can be calculated with equation (5-7). The minimum slit angle interval is 0.01°.

Rough measurements to check the angle range can help to save time before a complete measurement cycle is performed.

5.3.2 Analysis Materials and Methods

In face of progressive manufacturing technologies, lenses can still vary considerably in imaging quality because of manufacturing errors. The Modulation Transfer Function (MTF) is a good indicator for the characterisation of the image transfer performance. The MTF describes how the image contrast varies with the spatial frequencies. The MTF can be determined from the Fourier transform of a point spread function (PSF) or line spread function (LSF). Focus in this work is on the determination of the LSF. Assuming a Gaussian function for the determination of the LSF the spatial resolution is identical to the FWHNM of the function. The pixel response for the across track characterisation is determined as a function of the viewing angle and for the along track characterisation as a function of the slit angle.

Materials

The required inputs of the analysis process are the converted sensor and measuring log data (*Slave* and *Sensor* logs). The required parameters of the log file are the settings of the folding mirror and the slit wheel. If a neutral density filter was used the transmittance values of the filter are needed for a correction of the signals. The following items are necessary for the analysis of the geometric measurements.

Data:

- Converted and averaged measurement data
- Converted *Sensor* and *Slave* measuring logs
- Input parameter values
- Sensor parameter values
- Neutral density filter transmittance values

Software:
The "chbmo01_001_across_track_lsf" and "chbmo01_009_along_track_lsf" programs are used for the determination of the across respectively along track LSF. All subroutines of the two programs are listed in App. B, Table B.5.

Pre-processing

The pre-processing procedures are the conversion of the measurement and measurement log data as well as the correction of the signals (neutral density filter). The relevant CHB parameter (Y-axis) of the data cube is the sensor viewing angle (see Figure 4.8). For the along track LSF analysis the slit angle has to be converted into the viewing angle. The angle θ can be calculated by multiplying the tangent of the slit angle α by the division of the slit wheel radius r_s with the focal plane of the collimator f_c.

Selection of the pixels

For the analysis of the measurement data the spatial pixel numbers are necessary. The analysis program calculates the pixel number depending on the viewing angle range (see chapter 4.5). The calculated pixels are compared with the illuminated pixels and if the pixel numbers differ, the user has to select the pixel numbers. All pixels with a higher signal as the threshold are selected (see chapter 5.2.2). The analyses are performed for the selected channel numbers chosen by the user.

Quality and error checks

The implemented quality and error checks are saturation control, quantity of data points and stray light. The saturation control is already explained in chapter 5.2.2. All checks and controls are performed for all selected spatial pixels. Errors are saturated data points or Gaussian fit errors. Spatial pixels with errors are not be analysed.

Check number of data points

This check is similar to the control described in chapter 5.2.2. The relevant CHB parameter for the calculation of the data points is the viewing angle. For the calculation of the range the pixel analysis interval (input parameter a) is multiplied by the IFOV (sensor parameter). The minimum number of data points is calculation by the data point factor (input parameter b).

Spatial stray light control

The rough stray light control checks if any other spatial pixel, other than the selected ones, has a signal higher than the stray light threshold. The threshold is calculated by multiplying the minimum DN by a factor (input parameter d). The default value for this factor is 1.1.

In the case of an error the results of the spatial pixels will not be transferred into the result data cube.

Analysis

The analysis program for the geometric characterisation asks for the required input parameters (see Table 5.6) and computes the program control parameters, such as the viewing angle range and thresholds.

Table 5.6 outlines the input parameters for the across and along track LSF analysis explained in detail above.

Table 5.6 Input parameters for the geometric characterisation analysis

Input parameter	Default value
a) Pixel analysis interval factor	6
b) Data point factor	0.75
c) Pixel selection threshold factor	2.0
d) Stray light threshold factor	1.1

After the data conversion the analysis of each selected spatial pixel is carried out. The centre viewing angle and the FWHM are determined by the Gaussian fit function. The pixel response (averaged data) is determined as a function of the viewing angle. For the along track characterisation the slit angles are converted to viewing angles.

The analysis is executed for each single spatial pixel and the selected channels. Before the determination of the Gaussian function the error and quality checks are performed, the angle range is calculated and the quantity of existing data points is checked. Only faultless pixels are analysed. The analysis results for each selected spatial pixel are stored in a result data cube. Each sensor has its own geometric characterisation result cube. The Y-axis frames correspond to the following result parameters:

- Viewing angle (°)
- FWHM (mrad)
- Standard deviation of peak (°)
- Standard deviation of FWHM (mrad)
- Constant term (DN)
- Height of the Gaussian function (DN)
- Spatial sampling distance (°)

The analysis log contains the input parameters, major device settings, errors and the main results of the selected spatial pixel and channels. In addition plots and text files with the results are created. Examples of logs, text files and diagrams are listed in Appendix C).

5.4 Radiometric Characterisation

The main task of the radiometric characterisation is the determination of the coefficients for the conversion from digital numbers (DN) into physical units L (spectral radiance, W / m²·sr·nm). Sensors are designed to provide a linear relationship between DN and L. The conversion coefficients are calculated for each spatial pixel and each channel. The signals are expected to increase linearly with the integration time (electronic property) and as such are independent from the wavelength and pixel number. In principle the radiometric responses are determined for one illumination intensity. Since non-linearity effects cannot be excluded characterisation measurements with different illumination levels are necessary.

The parameters discussed in this thesis are the determination of the radiometric response matrix, the control of linearity with the integration time and the linearity between sensor response and radiance.

5.4.1 Measurement Materials and Methods

For the radiometric calibration radiance standards are used, which should be stable, uniform and a Lambertian source. Integrating spheres are often used as radiance standards. Such a hollow sphere has standard lamps and is internally coated with a diffusing white coating (i.e. Barium sulphate or Spectraflect [92]). The radiation across the exit port is uniform and therefore independent of the viewing angle [15, 75].

For the radiometric characterisation two integrating spheres are available at DLR Oberpaffenhofen. The small sphere (0.5 m Ø) is used for absolute radiometric calibration to determine the conversion coefficients. The large sphere (1.65 m Ø) is used for relative radiometric calibration to determine the response differences of the individual detector elements. The small sphere is periodical calibrated by Physikalisch Technische Bundesanstalt (PTB, Germany's national metrology institute) in the spectral range from 350 to 2500 nm. The radiance of the sphere and uncertainty is shown in App. A, Figure A.5. The uncertainty is 1% in the wavelength range between 390 and 1700 nm.

Measurement Setup

The two spheres are mounted in a frame as shown in Figure 5.7. The CHB adapter with the sensor is placed on top of the frame during the measurements. The sensor is located at the centre of the selected sphere looking downwards into the sphere. On top of the frame is a plate with the pick-up points of the interface such as that of the optical bench (see Figure 2.5).

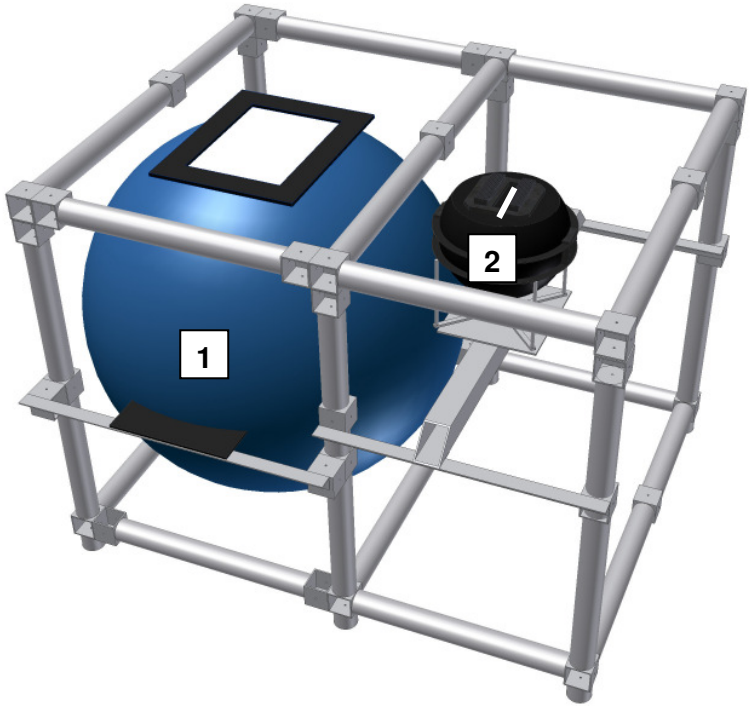

Figure 5.7: Setup of the radiometric measurement devices: 1 = large and 2 = small integrating sphere

The small sphere can be moved on a bar along the FOV of a sensor. The radiance exitance of the large sphere can be changed in various steps between 20 and 1640 W m^{-2}. The spheres are described in detail in chapter 2.4. The radiance variations of the small sphere can be monitored by using the Zeiss MCS 501 UV-NIR spectrometer.

Methods

For the execution of the radiometric measurements the sensor is mounted on top of the selected sphere. For the three types of measurements in addition to the measurements on the sphere, dark current measurements are performed after the sphere measurements.

Determination of the radiometric response

The small sphere is the calibration standard for the determination of the radiometric response function (absolute calibration). The measurements can be performed for the channels which are covered by the spectral range between 350 and 2500 nm. The number of illuminated spatial pixels depends on the FOV and the distance between sensor and sphere (output port of the sphere). The relative responses for all spatial pixels and channels are measured by using the large sphere. This sphere has an extended exit port and illuminates all spatial pixels of a typical sensor.

Check the linearity of the sensor response to intensity

The linearity of a sensor between response and radiance can be checked by performing measurements at different intensity levels. The intensity levels can be realised by using different neutral density filters or illumination intensities. Both spheres can be selected for the measurements.

Only for the large sphere the radiant exitance can be changed by selecting different lamp combinations (see chapter 2.4). For the small sphere nine different neutral density filters can be placed in the spheres opening. Some sensors have their own filters placed in front of the lens or in the optical path.

Check the linearity with the integration time

The sensor signal is expected to increase nearly linearly with the increase of the integration time. The relationship between the integration time and the measured signal (DN) is an electronic characteristic. It is independent from the spatial pixel and channel number. For the determination of this linearity, measurements with different integration times are performed. The integration time has to be varied between minimum and maximum. For these measurements both spheres can be used.

Predefinition of the measurement settings

Table 5.7 contains the *Slave* parameters, which are needed for the setup of measurements. If neutral density filters are used for measurements the filter has to be mounted manually before the measurements can be performed. The intensity of the large sphere can be set automatically by selecting the lamp combination. The measurements can be performed after the warm up time of the sphere.

Table 5.7: Setup parameters for the radiometric measurements

Integrating sphere	**Sensor**
Size	Integration time (ms) / frequency (Hz)
Lamp combination	Number of frames
Power (W)	Neutral density filter
Neutral density filter	Data type (nadir or dark current)

The following terms have to be considered before the measurements are performed:

1. The used radiance level should be similar to that during the flight campaigns [15].
2. The integrating exit opening should fill the sensor aperture [75].
3. The sphere should be a good Lambertian source with a low degree of polarisation [75].
4. A direct view of the sensor to the sphere lamps should be prevented [75].
5. Ensure that the instrument is not in saturation by choosing a suitable integration time and illumination level of the sphere. Perform integration time control measurements before to avoid saturation.
6. For the absolute radiometric calibration use the small integrating sphere since this sphere is calibrated against a standard. Check the sensor signal to avoid saturation.
7. If neutral density filters are used during the characterisation the transmission coefficients of the filter have to be known for the analysis of the measurements.
8. For the flat-field image an integration time should be selected which records signals between 50 % and 75 % of the maximal signal.

5.4.2 Analysis Materials and Methods

This chapter explains the analysis for the determination of the radiometric response and the control of the sensor linearity to the integration time and to different intensity levels. In addition a flat-field image can be generated on the basis of the performed measurements. The chapter is divided into the sections materials, pre-processing and analysis.

Materials

Basis for the analysis process are the converted and averaged measured data as well as the device settings. If a neutral density filter was used, the transmittance values of the filter are needed for a correction. For the determination of the conversion coefficients the radiance values of the small sphere are necessary. The following list contains all items needed for the spectral characterisation analysis process.

Data:

- Converted and averaged measurement data (nadir and dark current)
- Converted *Sensor* and *Slave* measuring logs
- Sensor requirement parameters
- Neutral density filter transmittance values
- Radiance data of the sphere
- Centre wavelength of each channel

Software:

For the different analyses the IDL programs “chbmo01_004_linearity”, “chbmo01_006_radiometric_response” and several subroutines (see App. B, Table B.6) are used.

Pre-processing

After the conversion of the log data and measurement data the average dark current data are subtracted from the averaged nadir data. The Y-axis parameter of the created data cube can be the lamp combination number, filter transmittance or the integration time. The implemented quality check is a saturation control described in chapter 5.2.2. If the measurements are performed with a neutral density filter, the measured data are corrected.

Analysis of the radiometric response

The radiometric responses $R_{x,c}$ of each pixel (x) and channel (c) can be determined, in the units of DN / mW m^{-2} nm^{-1} $sr^{-1}ms^{-1}$, by the quotient of the measured signals (DN) and the product of the filter transmittance T_c, the sphere radiance L_c and the integration time t_{int}. The measured sensor signals $DN_{x,c}^{meas}$ are subtracted by the dark current $DN_{x,c}^{dark}$. The transmittance values and the radiance are computed on the basis of the allocation from the channel number to the centre wavelength. The equation for the determination of the response is:

(5-8)

$$R_{x,c} = \frac{DN_{x,c}^{meas} - DN_{x,c}^{dark}}{t_{\text{int}} * T_c * L_c}$$

The radiometric response for each spatial pixel and channel are computed according to equation (5-8) assuming the response is linear to the integration time and to the radiance. The transmittance and radiance data of the small sphere are interpolated for each channel according to the centre wavelength of each channel. The result is a response matrix for each spatial pixel and channel.

Analysis of the linearity with the integration time

For each integration time measurement the dark current and transmittance corrected data are divided by the integration time and stored in a data cube. The line of the data cube contains the DN for 1 ms integration time. The results of the centre pixel and all channels for each integration time are plotted in one diagram. The result of the centre pixel for each integration time is plotted for all channels. The differences between the single results are then computed.

Analysis of the linearity of the sensor response to intensity

The recorded data are dark current and transmittance corrected. Results are the signal response of each pixel and channel for the different intensity level. The Y-axis parameter can be the lamp combination number of the large sphere or a transmittance of the filter. The results of each intensity level are plotted for the centre pixel against the wavelength.

Creation of a "flat field" image

Additional to the response matrix a flat field image can be plotted from the radiometric measurements. A flat field image can be used to show artefacts like vignetting, reflection of optical elements and dust. A "flat field" $DN(x,c)_{flat}$ is created by a dark current corrected "white" measurement $DN(x,c)_{corr}$ normalised to the mean value of the total dark current corrected image. A "white" image can be produced by performing a measurement with the integrating sphere. Each spatial pixel (x) of one channel (c) is normalised to the $\max_c$ – $\min_c$ value of all spatial pixels of the channel:

(5-9)

$$DN(x,c)_{flat} = \frac{DN(x,c)_{corr}}{\max_c - \min_c}$$

6 Verification of the Characterisation Methods

The aim of this chapter is to illustrate the applicability of the defined measurement and analysis methods of chapter 5 as well as the verification of the operationality of the complete process chain for the characterisation of hyperspectral sensors. Example spectral, geometric and radiometric measurements were performed for the two DLR sensors AISA and ROSIS. The sensors and their parameters are described in the following section. In the characterisation sections the selected CHB devices parameter, and sensor parameter values of the different measurements are listed and the results are illustrated by figures. In the last subchapter of each section the results are discussed and some conclusions are drawn.

6.1 Sensors for the verification

The two available sensors at DLR Oberpfaffenhofen are the AISA 1710 (Airborne Imaging Spectrometer for different Applications) and the ROSIS-03 (Reflective Optics System Imaging Spectrometer) are used for the verification of the methods. These sensors are pushbroom scanners measuring light in the wavelength range between 430 nm and 900 nm. The specifications of the sensors are explained in the following section.

AISA model 1 (ID 1710)
The model 1 AISA with the ID 1710 is a compact light-weight imaging spectrometer which is being operated since 1996 [36]. The sensor is equipped with a Thomson TH7863 CCD silicon detector array of 288 * 384 pixels [74]. Each pixel has a size of 23 µm * 23 µm. The instrument records the spectral range from 430 nm to 900 nm in up to 286 pixels (spectral axis). The imaging spectrometer has 364 spatial pixel and 20 FODIS (fiberoptic downwelling irradiance sensor) pixels. Additional to the 384 pixels the signals of 8 masked dark reference pixels are collected for each channel (spatial axis).

Optical system
The fore optics is a standard C-mount camera lens. Two lenses [93, 94] from Schneider Optics are available with a focal length of 8.3 (Cinegon f/1.4 [95]) and 22.5 mm (Xenoplan f/1.4 [96]). The dispersion component is a prism-grating-prism (PGP) element [68]. A PGP element uses a holographic transmission grating between two protective glass plates with high diffraction efficiencies. The typical absolute diffraction efficiencies of gratings (without optics) for non polarised light are listed in App. A, Table A.2 [68]. The radiation entering the spectrometer slit is collimated by the first lens and refracts at the prism surface (see Figure 6.1). The grating disperses the light so that the central wavelength passes symmetrically through the PGP (see Figure 6.2).

Four neutral density filters are available which can be mounted in front of the lens. These filters reduce the incoming signal by factors of 2, 4, 8 or 64.

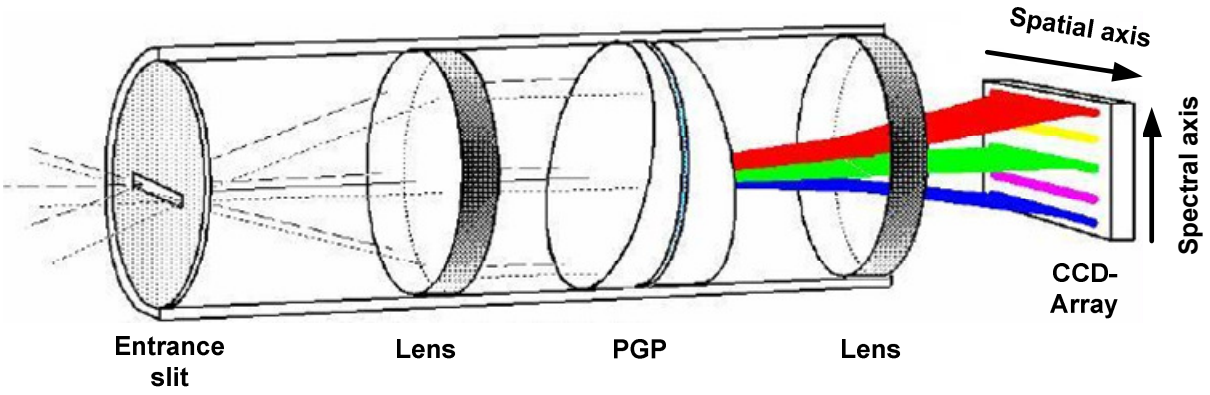

Figure 6.1: Scheme of the components of an imaging spectrometer and mapping to the CCD pixels [68]

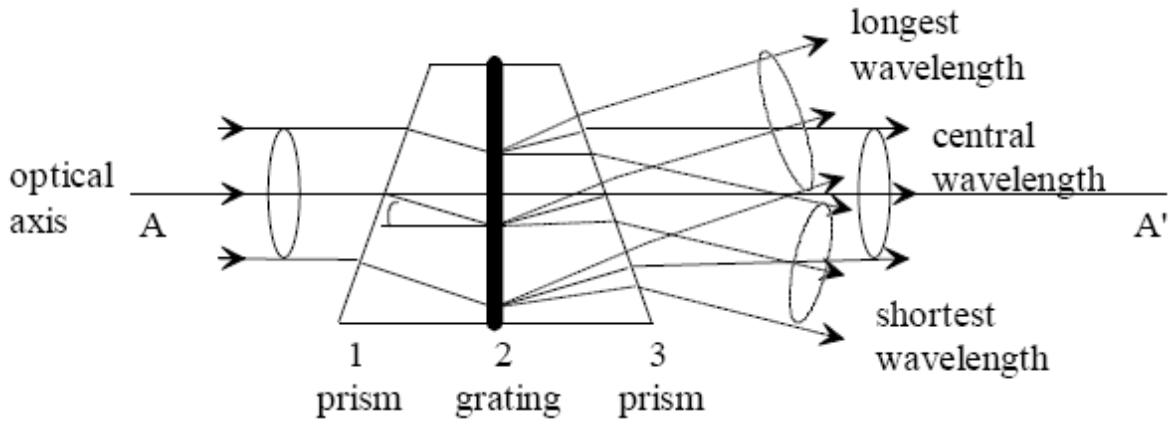

Figure 6.2: Basic principle of the prism-grating-prism element [68]

Characterisation

The former owner (Airobotics GmbH) delivered AISA with calibration coefficients from SPECIM. The last wavelength and radiometric characterisations for the two lenses were performed in July 2000 [93, 94]. Afterwards the sensor was not any more at SPECIM for calibration purposes. For the wavelength calibration a Helium-Neon laser and a fluorescent lamp (20 W) were used. The laser produces a monochromatic light at 632.8 nm. The light was projected on different spatial pixels, with the result that the illuminated channel differs around 1 channel from the centre to the border (channel no. 124 at the borders and 125 in the middle). The centre pixel of the spatial plane is pixel no. 192. A two-piece linear model, split at 611 nm, was used for the wavelength calculation of all channels. For radiometric characterisation a radiance standard was used [97].

Measurement process aspects

For all performed measurements the data acquisition mode A has been selected. This mode records the information of all spatial and spectral pixels (see chapter 4.4). During long series measurements the data files are transferred to the computer with the *Master* software. Therefore the measurement process contains in addition to the *Slave* settings, two actions (see chapter 4.3). A FTP data transfer and a file delete command are performed directly after each measurement.

Sensor parameters

Table 6.1 summarizes the sensor parameters for the AISA 1710 given by the manufacturer (SPECIM Ltd.) [36, 74, 95]. The table contains the specification of the 8 mm lens since this has been used for the performed measurements.

Table 6.1: AISA sensor parameters

Spectral		**Geometric**	
Parameter	**Value**	**Parameter**	**Value**
No. of bands	286	No. of spatial pixel	364
Wavelength range (nm)	430 – 900	FOV (°)	57.6
Spectral sampling interval (nm)	1.63	IFOV (mrad / °)	2.6 / 0.15
		No. of centre pixel	192
		Focal length (mm)	8.3

ROSIS-03

ROSIS was developed in a cooperation between German industry (EADS, Ottobrunn), DLR in Oberpfaffenhofen and GKSS in Geesthacht. ROSIS is a light-weight and compact instrument. The sensor has a tiltable mirror capability in flight direction of ± 20° and binning functionality. The Thomson THP 7895 detector is a two-dimensional CCD array [31]. The rows contain the spatial and the columns the spectral information. A single row of the detector consists of 552 elements of which 512 are used for spatial information and the other pixels are foreseen for system corrections [14, 31].

Optical System

The optical assembly of ROSIS is shown in Figure 6.3. The mirror (2) can be tilted to different positions to record dark current, spectral or nadir data information. Since ROSIS has no shutter dark current measurements are performed by tilting the mirror in the opposite viewing direction to the CCD. To perform in-flight calibration (IFC) measurements the mirror moves to the position where the mercury vapour lamp (3) illuminates the CCD (13). Between the tilt mirror and the second mirror is a long pass filter (5) which transmits only wavelengths greater than 430 nm (Schott GG 420) [30]. For reduction of the intensity neutral density filters can be used in the filter holder (4). Available are 10%, 31% and 63% transmittance filters.

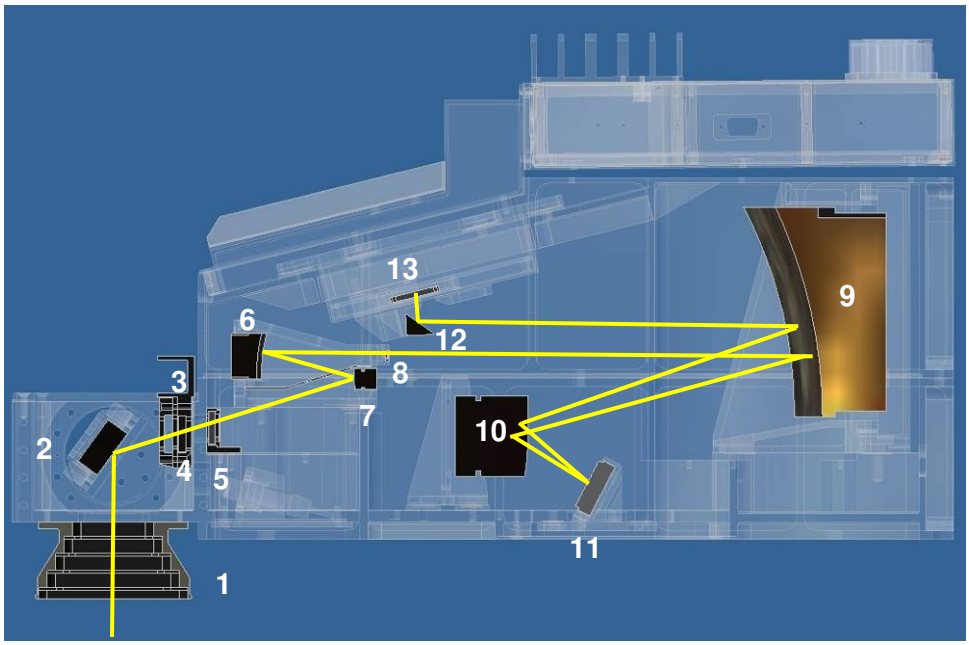

(1) Baffle
(2) Movable mirror
(3) Mercury lamp
(4) Filter holder
(5) Long pass filter
(6,7) Telescope
(8) Slit
(9,10) Collimator
(11) Grating
(12) Mirror
(13) CCD

Figure 6.3: ROSIS optical assembly [98]

Characterisation

ROSIS is inhouse characterised at DLR Oberpfaffenhofen. The spectral, geometric and radiometric measurements were performed in the second laboratory [4, 21]. The spectral measurements were executed with a monochromator and the radiometric calibration with the small integrating sphere. First spectral resolution measurements where performed for the wavelength 600 nm in 2001 and continued in 2002 for the wavelengths 500, 600, 700 and 800 nm [99]. Further measurements are made in 2003 for defined wavelengths (450nm, 500nm, 550nm, 600nm, 650nm, 700nm, 762nm, 800nm) [100]. The radiometric calibration measurements are executed close before or after flight activities. The geometric characterisation measurements were performed on the tilt and rotation stage for sensors with a weight up to 50 kg [101].

Measurement process aspects

Two different types of measurement modes (automatic and nadir) were used for the execution of the characterisation measurements. The automatic mode performs measurements at five mirror positions by tilting the mirror to desired positions. In the nadir mode the sensor records only data at the actual manually adjusted mirror position. The different acquisitions modes are explained in chapter 4.4. For the execution of automatic measurements with the *Master* software the nadir mode of the DSU software is required.

Sensor parameters

The necessary sensor parameters for the characterisation measurements and analysis are listed in Table 6.2.

Table 6.2: ROSIS sensor parameters

Spectral		Geometric	
Parameter	**Value**	**Parameter**	**Value**
No. of bands	115	No. of spatial pixel	512
Wavelength range (nm)	430 – 860	FOV (°)	16.0
Bandwidth (nm)	4	IFOV (mrad / °)	0.54 / 0.03
		No. of centre pixel	258

6.2 Alignment

This chapter describes measurements for the determination of the folding mirror offsets necessary for the following spectral and geometric measurements. The measurements are performed during the alignment of AISA. The roll angle offset can be determined by performing across track LSF measurements. The method is described in chapter 5.3.1.

Determination of the roll angle offset

Across track LSF measurements are performed for the nadir pixel (192). For the measurements AISA was mounted on top of the DLR universal adapter. The first measurement series was performed without a roll angle offset and for the second series the determined offset of the first measurement series was used (see a) and b) of Table 6.4). The integration time and number of frames were reduced to a minimum to reduce the measuring time. The viewing angle range of the second measurement series b) was reduced for time reducing aspects. The range is five times the previously determined IFOV (0.138° [102]). The fixed measurement parameter values are listed in Table 6.3 and the variables ones in Table 6.4.

Table 6.3: AISA alignment measurement setups (fixed parameters)

Folding mirror		Slit wheel	
Parameter	**Settings**	**Parameter**	**Settings**
Viewing angle interval (°)	0.01	Slit angle (°)	90.0
Height Z axis (mm)	777.0	Slit	50 µm, vertical
Y axis offset (mm)	0.0		

Table 6.4: AISA alignment measurement setups (variable parameters)

	Viewing angle range (°)	Roll angle offset (°)	Z axis (mm)	Current (A)	Integration time (ms)	Number of frames	Measurement date
a	-1.0 – 1.0	0.0	777.0	6.3	260	20	2008-06-04
b	-0.34 – 0.34	-0.3219	777.0	8.33	300	100	2008-06-16

The measurements are analysed with the across track LSF program and the default input parameter values (see chapter 5.3.2).

Results

Figure 6.4 shows the measurement results of the centre pixel 192 and the channel 143 of the alignment measurements a) and b). The peak of the Gaussian fit of measurement a) was -0.3219° and for measurement b) 0.0018°. The blue curve (without offset) shifts to the magenta curve (with offset). The FWHM difference between a) and b) is 0.027 nm (0.471 mrad). The results of the two measurements are listed in Table 6.5.

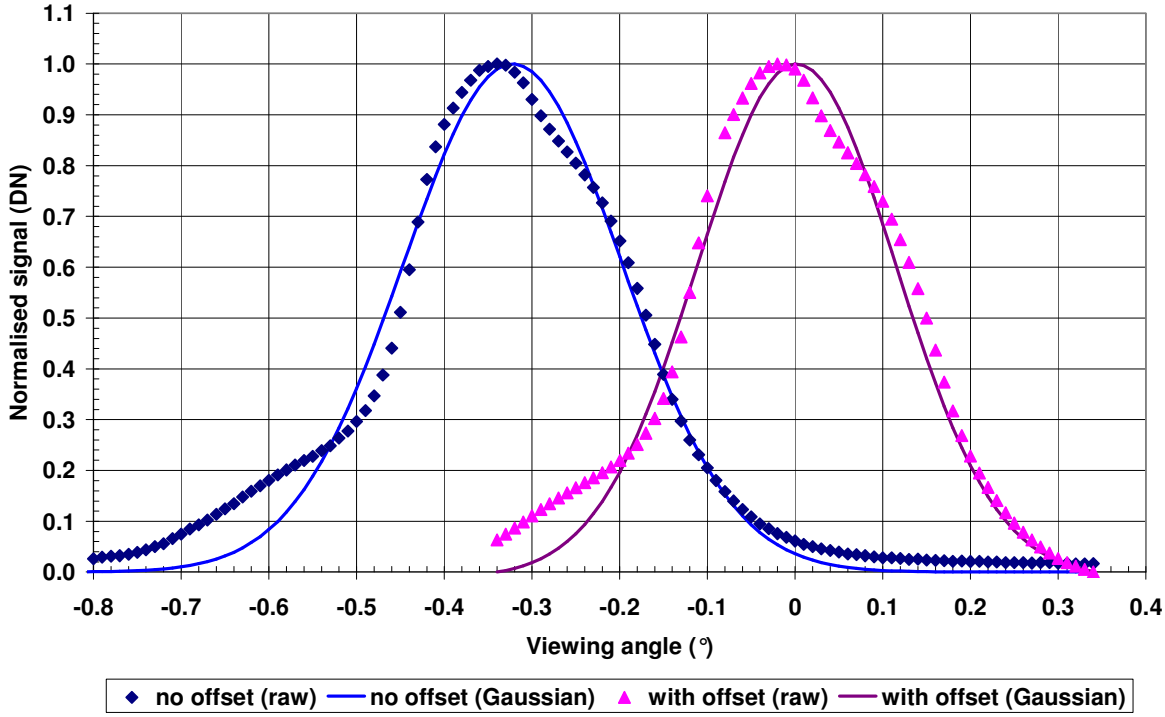

Figure 6.4: Across track LSF measurements of pixel 192 and channel 143 without and with a roll angle offset

Table 6.5: Results of the across track characterisation of pixel 192 and channel 143

Values for pixel 192 and channel 143	With no offset (a)	With -0.3219° offset (b)
Viewing angle peak (°)	$-0.3219 \pm 1.22 \cdot 10^{-3}$	$0.0018 \pm 1.8 \cdot 10^{-3}$
FWHM (°) FWHM (mrad)	$0.294 \pm 1.31 \cdot 10^{-3}$ $5.131 \pm 2.29 \cdot 10^{-2}$	$0.267 \pm 2.92 \cdot 10^{-3}$ $4.66 \pm 5.1 \cdot 10^{-2}$

The roll angle offset of measurement series a) was used for the following spectral and geometric measurements.

6.3 Spectral Characterisation

This chapter describes examples of spectral characterisation measurements and results for AISA and ROSIS. The relevant spectral properties are the spectral resolution, spectral sampling interval and the centre wavelength. A spectral characterisation (determination of the centre wavelengths) is essential for the usage of data because an inaccurate wavelength calibration can produce significant errors in the interpretation of data.

A complete spectral characterisation for the nadir pixel was performed for AISA as well as measurements for a few channels and a few spatial pixels over the FOV. For ROSIS only a few measurement series were performed to test the updated ROSIS software and to compare the measurement results. The measurement setup and the methods are defined in chapter 5.2.1. The used analysis methods are described in chapter 5.2.2.

While the measurement setup is more general (see chapter 5.2.1), decisions concerning the sensor parameters were necessary for the accomplished measurements and analyses. The necessary parameters are given in the column “spectral” of Table 6.1 (AISA) and Table 6.2 (ROSIS). Starting with the measurement setup, suitable monochromator gratings and order filters have to be selected according to the wavelength range of the two sensors. The wavelength range between 400 nm and 900 nm is covered by the gratings 1 and 2 of both turrets (see Table 2.2), but smaller band widths are possible with the gratings of turret two. Table 6.6 shows the two necessary gratings and the selected long pass filters of Table 2.3 on the basis of the grating wavelength ranges. The suitable wavelength ranges for the gratings are defined by the grating efficiency curves.

Table 6.6: Mapping of the selected gratings (turret 2) and the order filters

Grating no.	Dispersion (nm/mm)	Suitable wavelength range (nm)	Filter cut-on wavelength (nm)	Filter no.	Wheel position
1	3.2	350 — 600	305	1	1
2	3.1	550 — 1300	550	2	2

Previous measurements with the 100 Watt QTH lamp for AISA and ROSIS illustrate the need of neutral density filters. The filter wheel was equipped with a 0.1%, 1.1%, 10% and 50% filter. All necessary CHB device parameters are listed in Table 5.3. For all spectral characterisation measurements turret 2 and the 100 Watt QTH lamp were used. All other parameter settings are given in the following sections.

For all measurements the wavelength correction was performed during the data analysis, because the monochromator wavelength correction was not executed by the *Slave* software (see chapter 4.2). The used correction values are listed in Appendix C, Table C.9.

6.3.1 Spectral Response function

For the determination of the spectral properties the spectral response function (SRF) was used. Example measurements are performed for AISA and ROSIS. For AISA a complete spectral characterisation for the nadir pixel and all channels were performed and analysed. The spectral properties like the centre wavelength, FWHM, spectral sampling interval and channel overlapping for all channels were determined. ROSIS measurements were performed for the nadir and border pixels for different wavelength ranges. This subchapter explains in detail the measurement setup, analysis, results and measurement time.

AISA

This section describes the measurement settings and analysis results for the nadir pixel and all channels. The necessary *Slave* parameters for spectral characterisation measurements are given in Table 5.3. The two involved CHB device groups are the folding mirror and the monochromator. The folding mirror offset parameters were determined during the sensor alignment. Main parameters of the monochromator are the grating and the order filter according to the desired wavelength range as well as the slit width. The selected gratings and filters are listed in Table 6.6. Grating 1 can be used with the order filter number 1 or with no filter.

The slit width of 100 µm was calculated for a bandwidth of 0.32 (equation (5-1)). This bandwidth corresponds to 1/10 of the FWHM determined in previous measurements for a few channels (75 to 78). The monochromator beam, provided by the 100 µm slit, covers ~1/3 IFOV (equation 5-2) behind the parabolic mirror. For covering the whole IFOV the slit width has to be set to 330 µm which correspondent to a bandwidth of 1.056 nm (~½ of the FWHM). A slit width of 100 µm was selected based on the 1/10 FWHM principle.

Previous spectral measurements were performed to check the sensor signal at different lamp settings and with different neutral density filters. These measurements over the whole wavelength range were performed with an interval of 10 nm. Based on the previous measurement results the necessary neutral density filters and different lamp settings were selected (see Table 6.7).

Long measurement times can cause a change of the centre wavelengths (channel displacement). Therefore the whole wavelength range was divided into 10 measurement series performed on several days. The recorded data of the channels 31 to 51 of measurement a) are saturated. These erroneous measurements are repeated by measurement b) with a reduced lamp power. All variable parameter values are listed in Table 6.7 and the fixed CHB setups are given in Table 6.8.

Table 6.7: AISA spectral characterisation measurement setups (variable parameters)

	Wavelength range (nm)	Grating no.	Order filter no.	Neutral density filter (%)	Current (A)
a	400.0 – 500.0	1	none	-	8.4
b	470.0 – 498.8	1	none	-	7.9
c	500.0 – 549.8	1	none	-	6.3
d	542.0 – 586.8	1	none	-	7.4
e	580.0 – 649.8	2	2	10	6.3
f	650.0 – 679.8	2	2	10	6.3
g	680.0 – 692.2	2	2	10	6.3
h	692.4 – 799.8	2	2	10	6.3
i	800.0 – 869.8	2	2	10	6.3
j	867.0 – 909.8	2	2	10	6.3

Table 6.8: AISA spectral characterisation measurement setups (fixed parameters)

Monochromator		Folding mirror		Sensor	
Parameter	**Value**	**Parameter**	**Value**	**Parameter**	**Value**
Wavelength interval (nm)	0.2	Z axis (mm)	500.0	Integration time (ms)	300
Entrance & exit slit width (µm)	100	Viewing angle (°)	0.0	Number of Frames	100
		Roll angle offset (°)	0.0	Interface	Aeroetech
		Y axis offset (mm)	0.0		

The 10 measurement series were analysed with the spectral characterisation program described in chapter 5.2.2. For the analysis the default input parameter values of Table 5.3 were used except for the wavelength and intensity correction parameters. The wavelength correction was performed during the analysis. The intensity correction was omitted because a comparison of the measurement results with a correction and without a correction resulted in a deviation of 0.007 nm for the centre wavelength and a deviation of 1.5 ‰ for the FWHM. An example for channel 1 and spatial pixel 192 is shown in App. C, Figure C.17.

Results

This section describes analysis results of the 10 measurement series of Table 6.7. The illustrated results for all channels of the nadir pixel are the centre wavelength, the FWHM, the spectral sampling interval and the channel overlap.

The wavelength range of measurement series a) covers the first 50 channels of AISA. The spectral properties of the first 35 channels were determined and listed in App. C, Table C.11 as an example. The properties for the channels 36 to 51 were not analysed since the recorded data are saturated. The FWHM values increase from 1.52 nm to 2.53 nm. The sampling distances range from 1.47 nm to 1.62 nm and the mean value is 1.55 nm. Figure 6.5 is an example of a single measurement result of the first two channels. The figure shows the recorded data (DN) and the calculated Gaussian fit values. The determined centre wavelengths are 419.77 nm (channel 1) and 421.24 nm (channel 2). The spectral sampling interval between both channels is 1.47 nm. The FWHM for both channels is 1.52 nm and the channel overlap is 1.9 %.

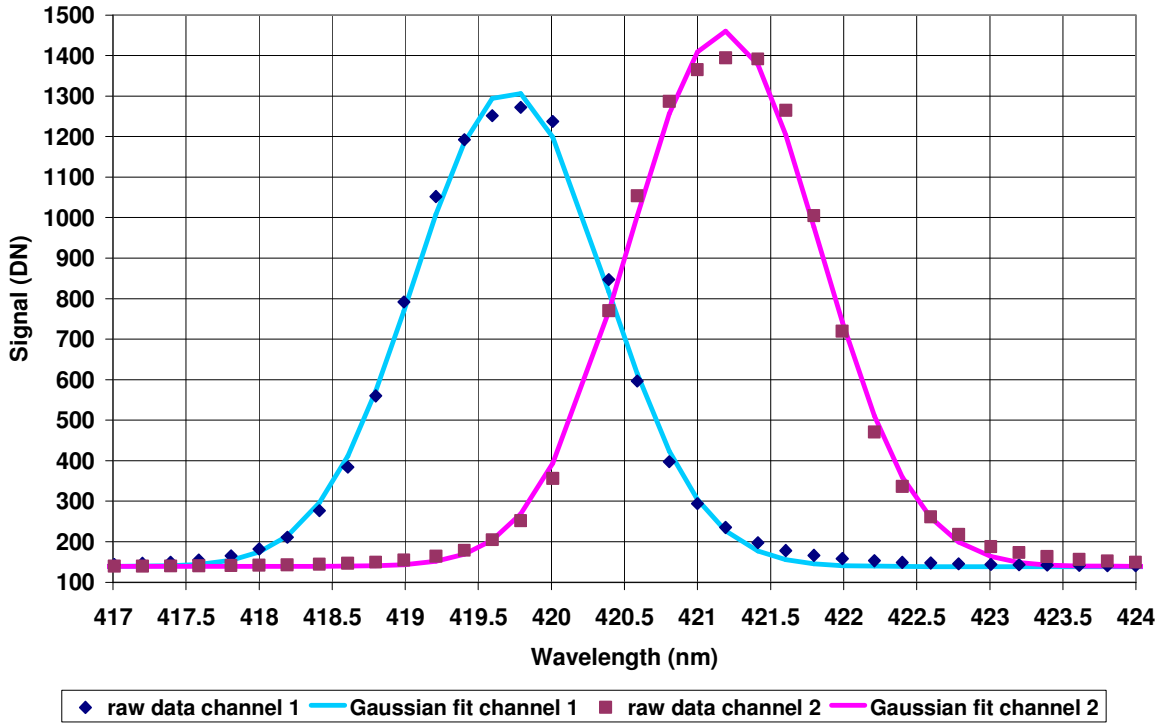

Figure 6.5: AISA spectral characterisation results of the nadir pixel and channel number 1 and 2

The following figures show the determined spectral properties of all measurements for the nadir pixel and 258 of the 286 channels. For 28 channels no properties were computed because of saturated data or missing measurements caused by a data transfer problem.

The centre wavelengths of the nadir pixel and all channels are shown in Figure 6.6. The black ascending line corresponds to a linear fit function. The centre wavelengths are in the range from 419.77 nm to 895.71 nm.

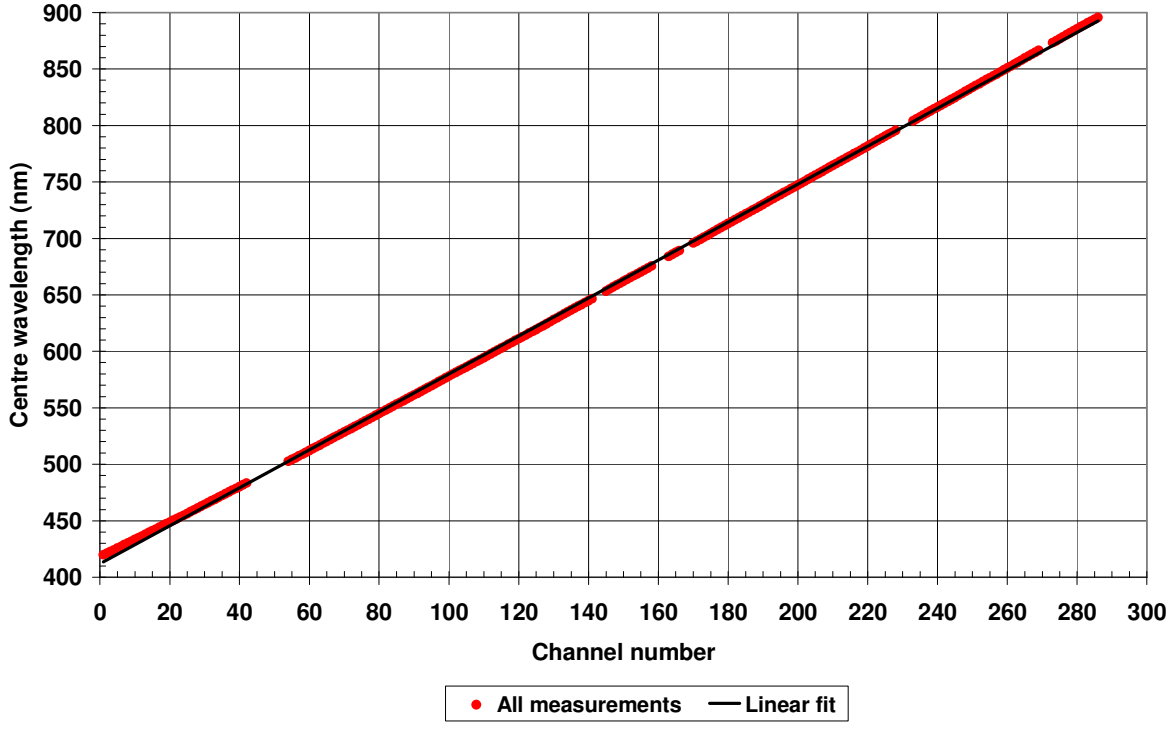

Figure 6.6: AISA centre wavelengths of the nadir pixel and all channels (March 2008)

Since the centre wavelengths do not fit very well with the linear function, polynomial functions up to the 4th degree were calculated. The function equations are listed in Table 6.9. The differences for the linear fit are in the range from -2.62 nm to +6.08 nm and the average deviation is 1.8 nm. The deviations of the 2nd degree function vary between -1.33 nm and +1.56 nm, the averaged deviation is 0.44 nm. The deviations of the 3rd function are in the range from -0.20 nm to +0.37 nm and the averaged deviation is 0.08 nm. The 4th degree function vary between -0.25 nm and +0.22 nm and the averaged deviation is 0.07 nm. The differences between the measured and the calculated wavelengths of the polynomial functions are plotted in Figure 6.7 and Figure 6.8 (only the 3rd and 4th polynomial functions).

Table 6.9: Polynomial functions for the determination of the centre wavelength

	$\lambda_{CW}(c) = a_0 + a_1 \cdot c + a_2 \cdot c^2 + a_3 \cdot c^3 + a_4 \cdot c^4$					
Polynomial	**a_0**	**a_1**	**$a_2\ 10^{-4}$**	**$a_3\ 10^{-6}$**	**$a_4\ 10^{-9}$**	**σ (nm)**
linear	412.014	1.68	—-	—-	—-	2.154
2nd degree	416.629	1.583	3.369	—-	—-	0.514
3rd degree	417.868	1.530	8.090	-1.105	—-	0.104
4th degree	418.037	1.518	10.011	-2.143	1.8	0.088

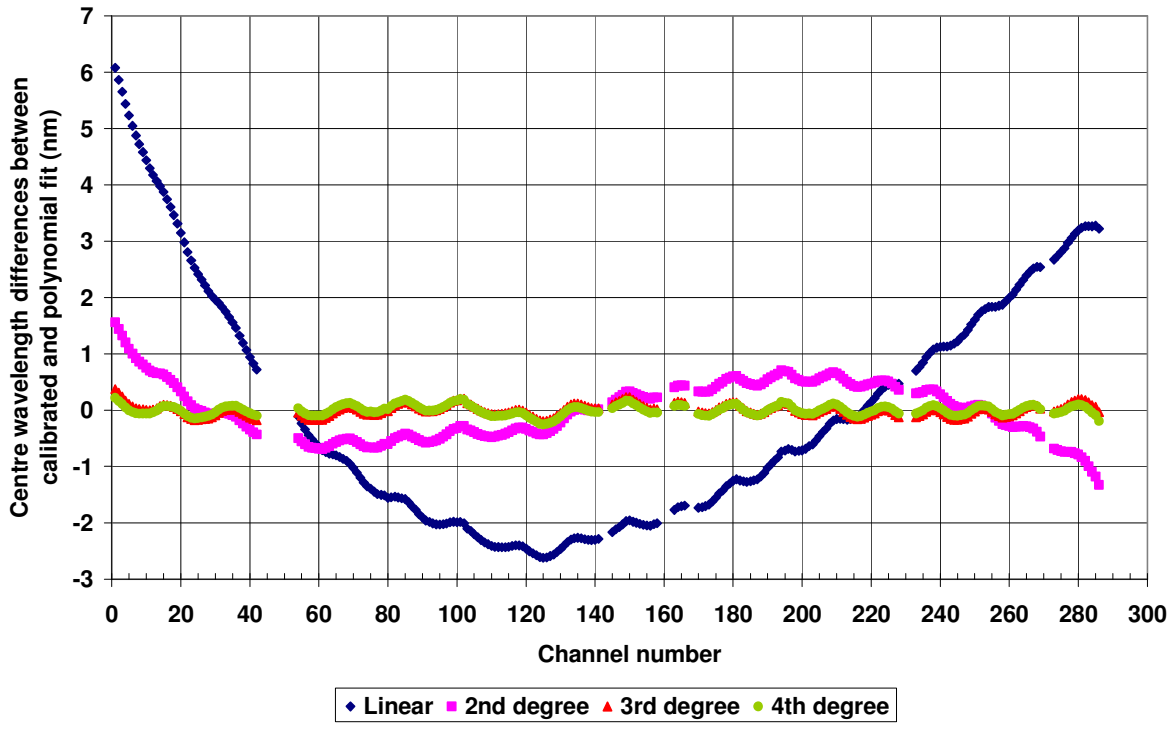

Figure 6.7: Differences between the calibrated and calculated centre wavelengths of polynomial fits

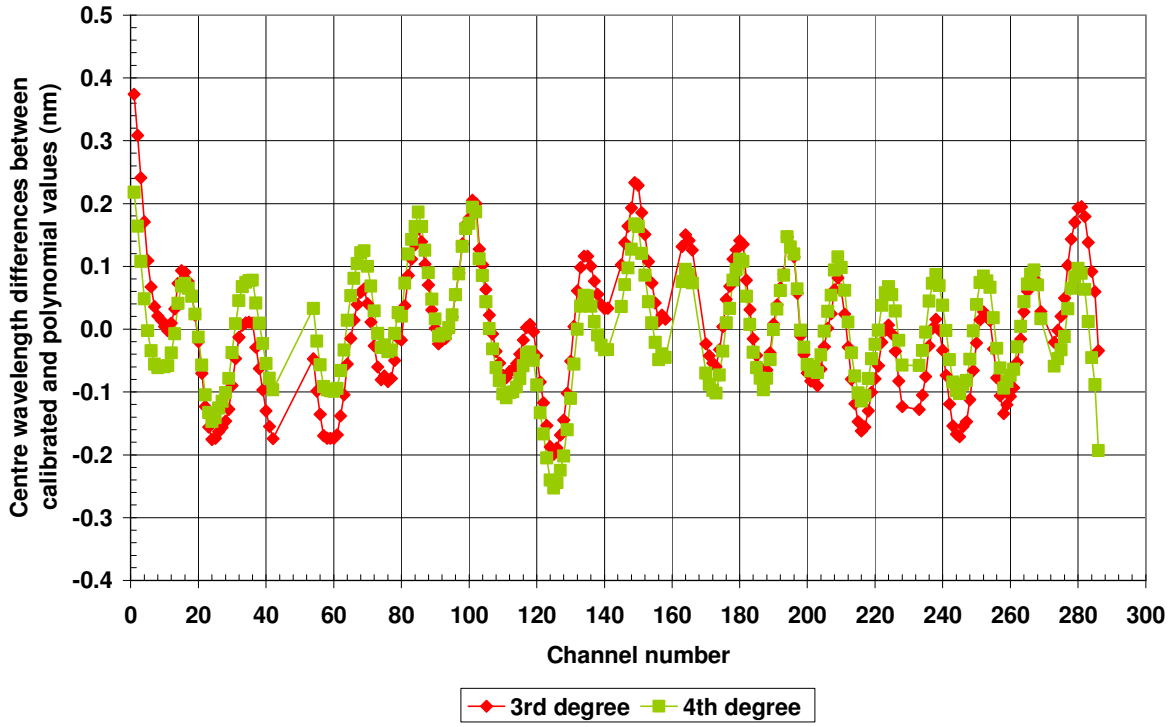

Figure 6.8: Centre wavelength differences between the measured and calculated values of 3rd and 4th degree polynomial functions (section of Figure 6.7)

The FWHM values of the centre pixel and all channels are shown in Figure 6.9. The values are in the range from 1.52 nm to 3.48 nm. Figure 6.9 shows a peak at channel number 130 in the middle of the figure. The FWHM values are results of measurement e) of Table 6.8. The responses of the channels 115 to 133 show artefacts (see App. C, Figure C.18) and the standard deviation values of these channels vary between 0.009 nm and 0.017 nm. The mean standard deviation value of all channels is 0.006 nm.

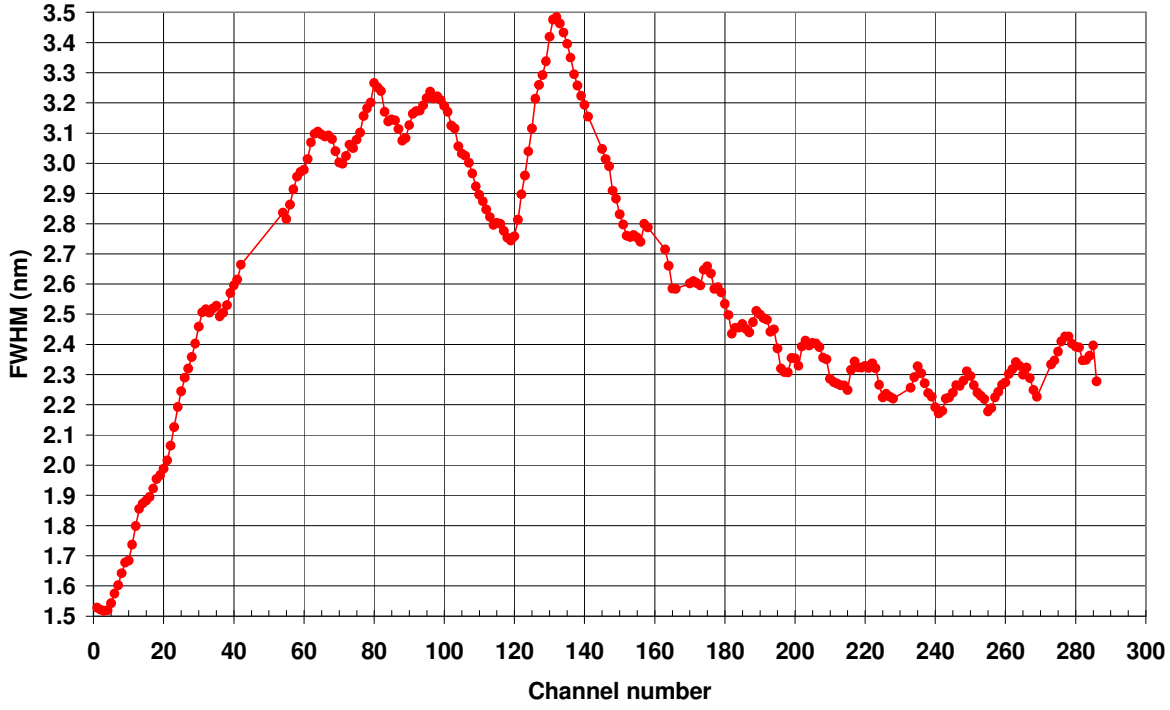

Figure 6.9: AISA FWHM values of the nadir pixel and all channels (March 2008)

Figure 6.10 shows the spectral sampling intervals of the nadir pixel and all channels. The black line is the 4th degree polynomial function. The values vary from 1.47 nm to 1.78 nm.

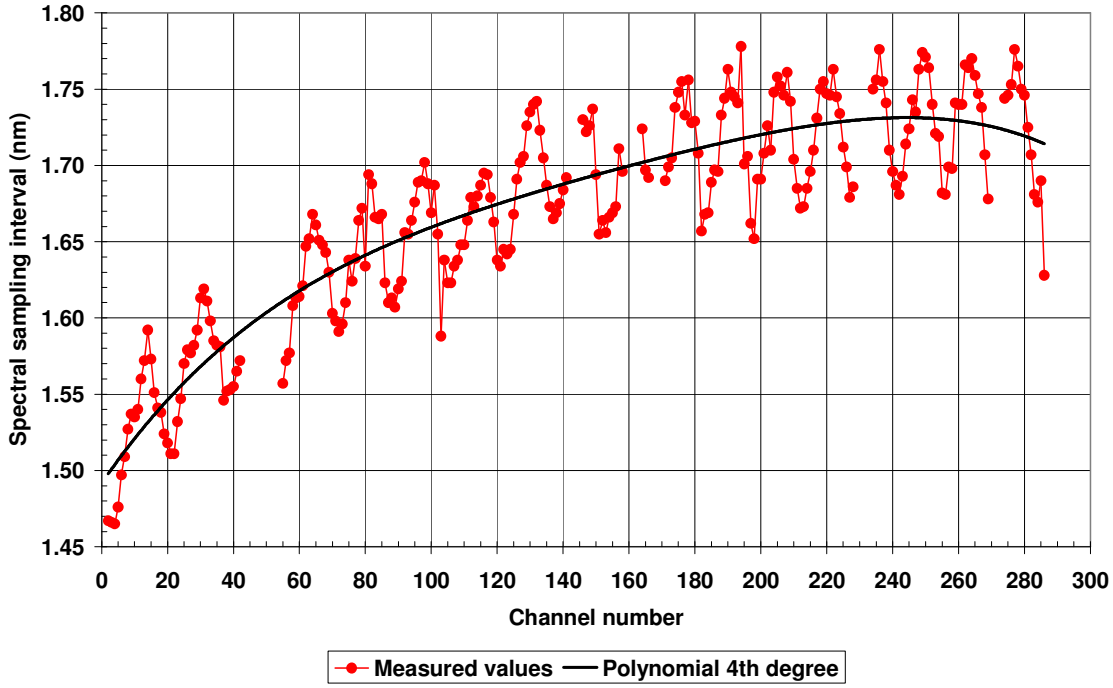

Figure 6.10: AISA spectral sampling intervals of the nadir pixel and all channels (March 2008)

The spectral sampling interval of each channel can be calculated with the equation $ssi(c) = 1.492 + 3.130\ E^{-3} \cdot c - 2.191\ E^{-5} \cdot c^2 + 8.773\ E^{-8} \cdot c^3 - 1.394\ E^{-10} \cdot c^4$. The intervals themselves vary about ±0.05 nm from the fitted line.

Figure 6.11 illustrates the channel overlap values of the nadir pixel and all channels. The values are in the range from 1.8% to 33.9%. There is no gap between any channels.

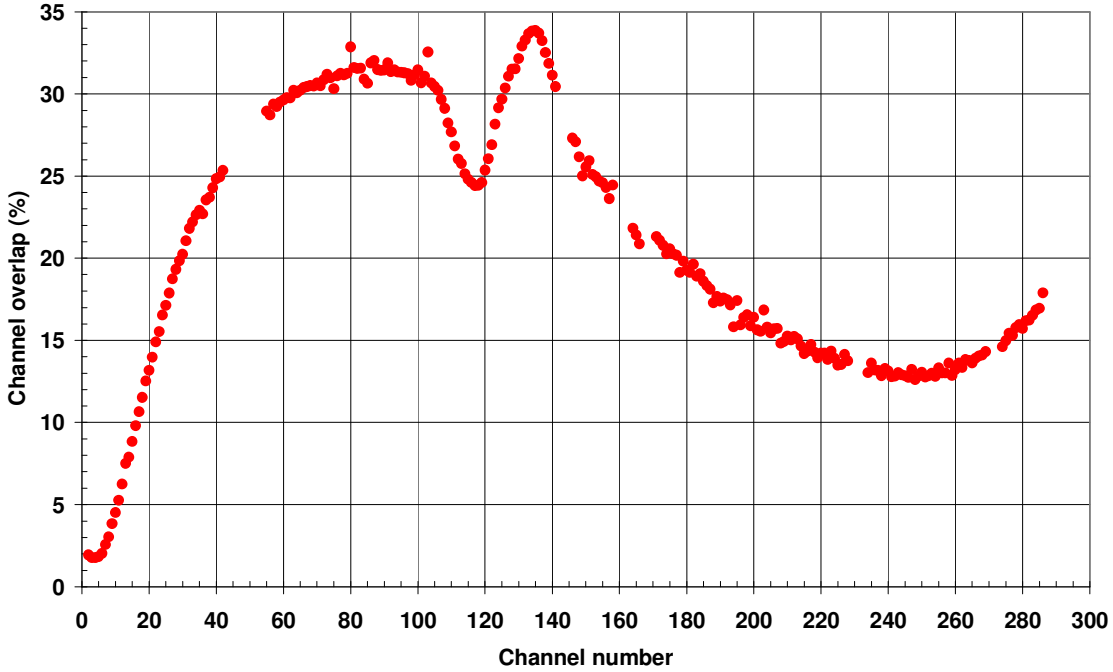

Figure 6.11: AISA channel overlaps of the nadir pixel and all channels (March 2008)

The manufacturer of AISA carried out three linear fits with different sampling distances [69] for the mapping of the channel number to the centre wavelength. The three segments begin at 421.4 nm, 594.14 nm and 700.56 nm with the spectral sampling intervals of 1.598, 1.715 and 1.725 nm.

The AISA 1710 operates in a wavelength region between 419.8 nm and 895.7 nm with a mean spectral resolution of 2.59 nm and a mean spectral sampling interval of 1.7 nm. In Table 6.10 the overall AISA spectral characterisation results of the nadir pixel and all channels are listed. The centre wavelengths for all channels are calculated on the basis of the 4th degree polynomial function since this is the function with minimal differences. The wavelength for each channel number was written in a file for future use.

Table 6.10: AISA spectral characterisation results for the nadir pixel

Number of channels	Wavelength range (nm)	FWHM (nm)	Spectral sampling interval (nm)	Channel overlap (%)
286	419.8 – 895.7	Min: 1.52 Max: 3.48 Mean: 2.59	Min: 1.47 Max: 1.78 Mean: 1.67	Min: 2 Max: 34 Mean: 21

For the 10 measurement series of Table 6.7 the total measuring times, the quantity of the recorded data points and the average measuring time for one data point are listed in App. C, Table C.13. The average measuring time for one data point composed of the time for the setting of the CHB devices, the setting of the sensor, the data recording and the data transfer. The averaged measuring time of all measurement series for one data point was 43 seconds. The averaged times for the sensor setup and the data recording (100 frames) was about 34 seconds and the data transfer time was 4 seconds. The mean time for the setup of the monochromator was 2 seconds. The measurement time for one channel with 50 data points (10 nm in 0.2 nm steps width) needs approx. 36 minutes. The 10 measurement series were performed on seven days and the 2777 measurements required a total measuring time of 34 hours.

ROSIS

The spectral measurements for ROSIS were performed with a fixed sensor mirror to compare and validate the updated software. The data recording of the measurements a) to c) of Table 6.12 were accomplished manually whereas the CHB device settings are performed by the *Master/Slave* software. The measurements d) and e) are performed with the *Master/Slave* software and the updated ROSIS control software where the software records the data. The 5 measurement series were performed on different days in September 2008. After each restart of the ROSIS computer the ROSIS mirror was moved to the nadir position manually and the sensor was aligned by optimising the signal.

The fixed and variable CHB device parameter settings are listed in Table 6.11 and Table 6.12. Since the recorded data of measurement a) were saturated for the following measurements the 50 % neutral density filter was used.

Table 6.11: ROSIS spectral characterisation measurement setups (fixed parameters)

Monochromator		Folding mirror		Sensor	
Parameter	**Value**	**Parameter**	**Value**	**Parameter**	**Value**
Entrance & exit slit width (µm)	150	Z axis (mm)	1400.0	Frequency (Hz)	40
Current (A)	8.5	Roll angle offset (°)	0.0	Interface	Universal
		Y axis offset (mm)	0.0		

Table 6.12: ROSIS spectral characterisation measurement setups (variable parameters)

	Wavelength range (nm)	Interval (nm)	Grating no.	Order filter no.	Sensor neutral density filter (%)	Viewing angle (°)	Neutral density filter (%)	No. of frames
a	785.0 – 815.0	1.0	2	2	63	0.0	—	500
b	693.3 – 709.3	1.0	2	2	10	0.0	50	500
c	485.0 – 514.6	0.8	1	5	10	-7.0	50	500
d	693.3 – 709.3	1.0	2	2	10	0.0	50	500
e	690.0 – 712.0	0.5	2	2	10	0.0	50	1000

For the measurement series a) to d) the ROSIS mirror position was -1139 and for measurement e) it was -1138. All measurements were analysed with the spectral analysis program and the default input parameter values as described in chapter 5.2.2. The wavelength correction was performed in the analysis process.

Results

For the measurement series a) of Table 6.12 no spectral properties were determined since the Gaussian fits failed. Figure 6.12 shows the recorded data of pixel 258 results and the channels 103, 104, 105 und 106. The recorded signals of the four channels decrease to a continuous signal of ~10300 DN. A closer examination of the spatial pixels near the illustrated pixel and channels resulted in recorded signals with the maximum digital number of 16383 (2^{14} bit).

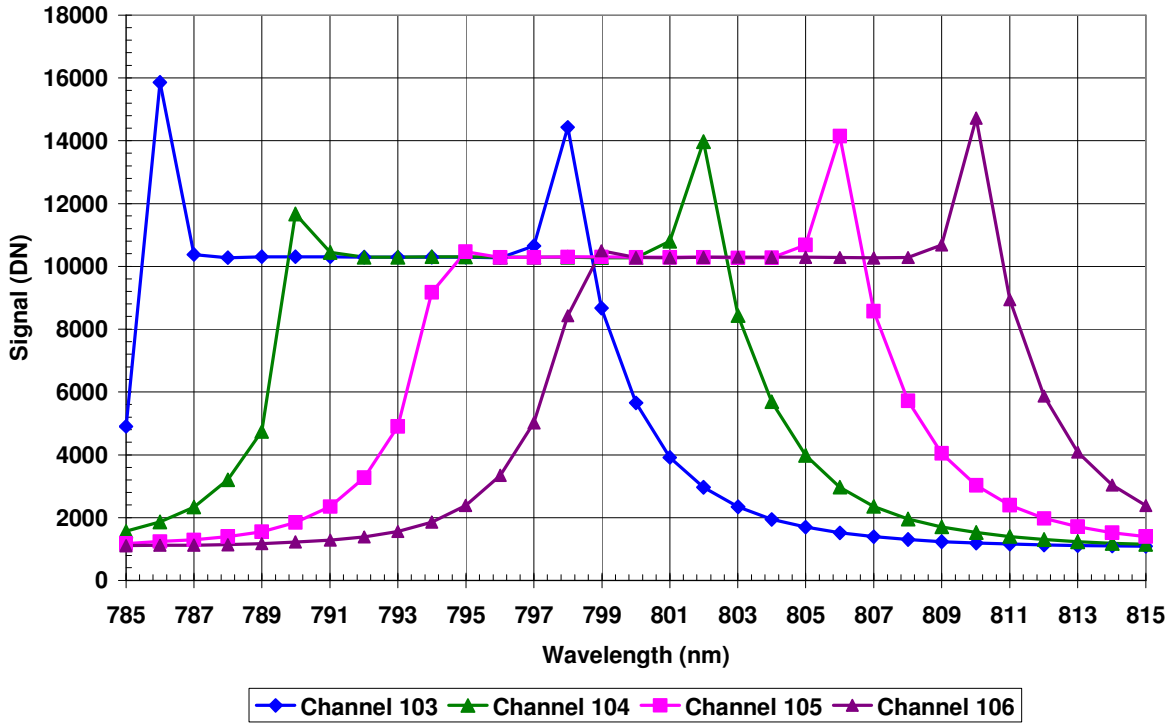

Figure 6.12: ROSIS recorded signals of pixel 258 and several channels (erroneous measurement a)

The measurement series b), d) and e) were performed for the nadir pixel in the same wavelength range with varying step intervals. These measurements were performed on three consecutive days with a re-alignment of the sensor. The nadir mirror position of ROSIS for series e) differ about 1 step. The analysis results of the measurements of pixel 259 and channel 80 are shown in Figure 6.13. The centre wavelengths, FWHM values as well as the signal peaks of the three measurements are different.

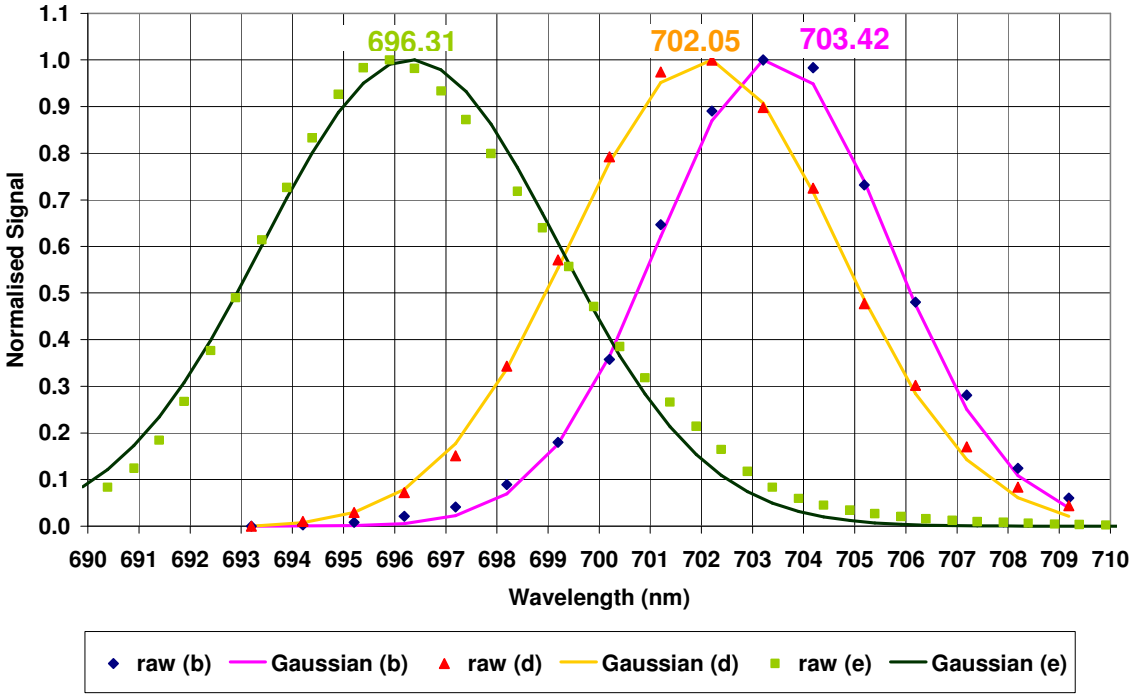

Figure 6.13: ROSIS spectral characterisation results of pixel 259 and channel 80

The centre wavelength differences of channel 80 and pixel 259 between the measurements b) to d) is 1.38 nm, between b) and e) is 7.11 nm and between d) and e) 5.73 nm. The determined FWHM values are 5.3 nm (b), 6.2 nm (d) and 6.8 nm (e). The difference between b) to d) is -15.8% and between d) and e) -10.2% and between b) and e) -27.6%. The maximum signals (DN) are 6379 (b), 1786 (d) and 13657 (e). Since the wavelength range of measurement series e) was larger as the two others, in addition the spectral properties for pixel 259 and channel 81 and 82 were determined. The centre wavelengths, FWHM values and spectral sampling intervals are listed in App. C, Table C.16.

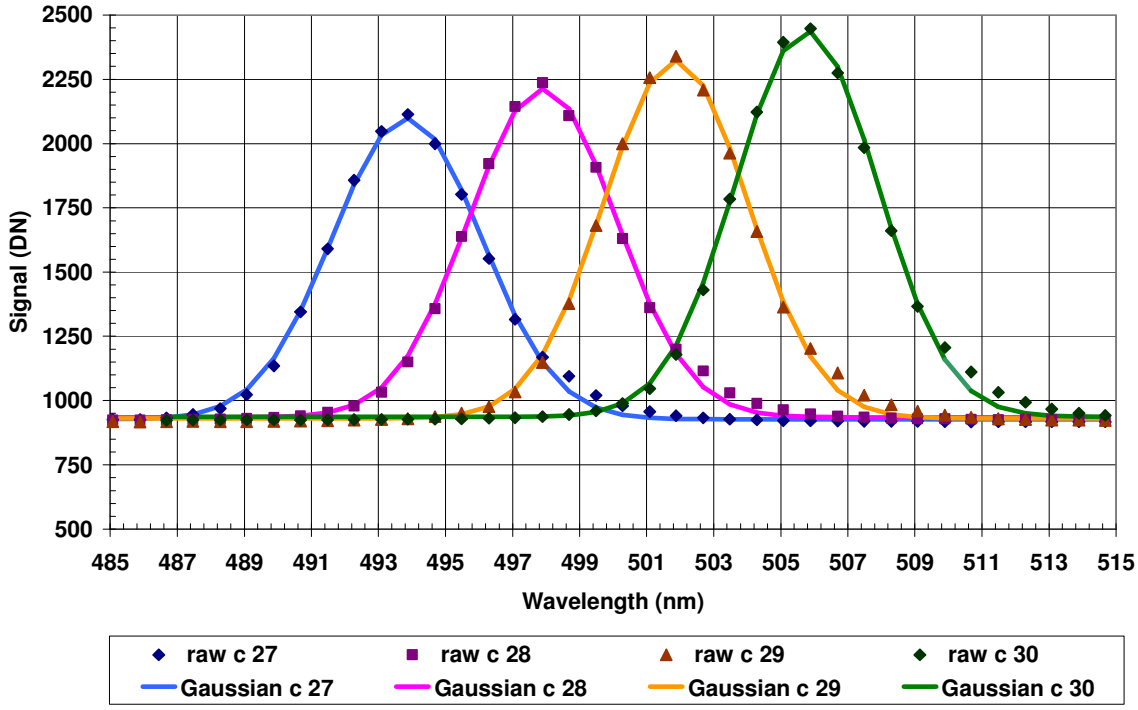

Figure 6.14: ROSIS spectral characterisation results of pixel 18 and the channels 27 to 30 (measurement c)

Figure 6.14 shows the recorded data and the Gaussian fit results of measurement series c) for the spatial pixel number 18 and the channels 27 to 30. The determined spectral properties of the series c) and e) are listed in App. C, Table C.16.

The measuring times, the quantity of the recorded data points and the averaged measuring time for one measurement with 500 frames are listed in App. C, Table C.15. The averaged measuring time for one data point was 28.6 seconds for the measurement series a) to c) and 13.7 seconds for the series d) and e). The data recording of the first three measurements was performed manually whereas the last two were executed with the updated ROSIS software. With a completely automated measurement process using the *Slave*, *Master* and *Sensor* software, the measuring time can be reduced about 50 %. The detailed analysis of the *Master* / *Slave* measurement logs of measurement series c) and d) result in an averaged time period for the setting of the monochromator of 2 seconds. The averaged time for the manual data recording of 500 frames was 28 seconds and for the automated acquisition 14 seconds.

6.3.2 Spatial Pixel Dependency of one Channel

For AISA characterisation measurements were carried out for three channels and for seven spatial pixels evenly spread over the FOV. The purpose of these spectral measurements was the investigation of a smile effect [103]. The selection criteria of the necessary CHB parameters are analogous to that of chapter 6.3.1. The relevant CHB parameters (fixed and variable) are listed in Table 6.13 and Table 6.14.

Table 6.13: AISA spectral characterisation measurement setups for different viewing angles (fixed parameters)

Monochromator		Folding Mirror		Sensor	
Parameter	**Value**	**Parameter**	**Value**	**Parameter**	**Value**
Wavelength range (nm)	540.0 – 551.8	Z axis (mm)	500.0	Integration time (ms)	300
Wavelength interval (nm)	0.2	Roll angle offset (°)	0.0	Number of frames	100
Entrance & exit slit width (µm)	100	Y axis offset (mm)	0.0	Interface	Aeroetech
Grating no.	1				
Order filter	none				
Current (A)	6.3				

Table 6.14: AISA spectral characterisation measurements setup for different viewing angles (variable parameters)

Measurement series	**a**	**b**	**c**	**d**	**e**	**f**	**g**
Viewing angle (°)	16.432	10.962	5.515	0.0	-5.515	-10.962	-16.432
Pixel number	74	114	153	192	231	270	309

The measurement series were analysed with the spectral analysis program and the default input parameters as described in chapter 5.2.2. The monochromator wavelengths were corrected during the analysis.

The measurement series were conducted on two days in June 2008 with a total measuring time of approx. 4.5 hours. Each series records 60 data points accordingly to the single wavelength settings. The mean measuring time for one data point with 100 frames was 39.4 seconds. The detailed information regarding the measuring time and numbers of data points are listed in App. C, Table C.14. As an example the analysis log of measurement series g) were analysed to compute the time periods for the setting of the CHB devices and the data recording. The one-time adjustment time of the folding mirror was 3 seconds and the averaged time period for the setting of monochromator was 2 seconds. The averaged time for the setup of the sensor and the data recording was 34 seconds. The averaged time for the data transfer was 4 seconds.

Results

The centre wavelengths of the channels 79, 80 and 81 for the spatial pixels 74, 114, 153, 192, 231, 270 and 309 are shown in Figure 6.15. The three fit lines are 5th degree polynomial functions (functions see Table 6.11). The figure illustrates a smile and frown effect. For the 3 channels the minimum centre wavelength is at the nadir pixel (192) and the maximum at pixel 309. The difference between the minimum and maximum wavelength is ~1.4 nm of the three channels. The averaged distance between two channels is ~1.68 nm (spectral sampling interval).

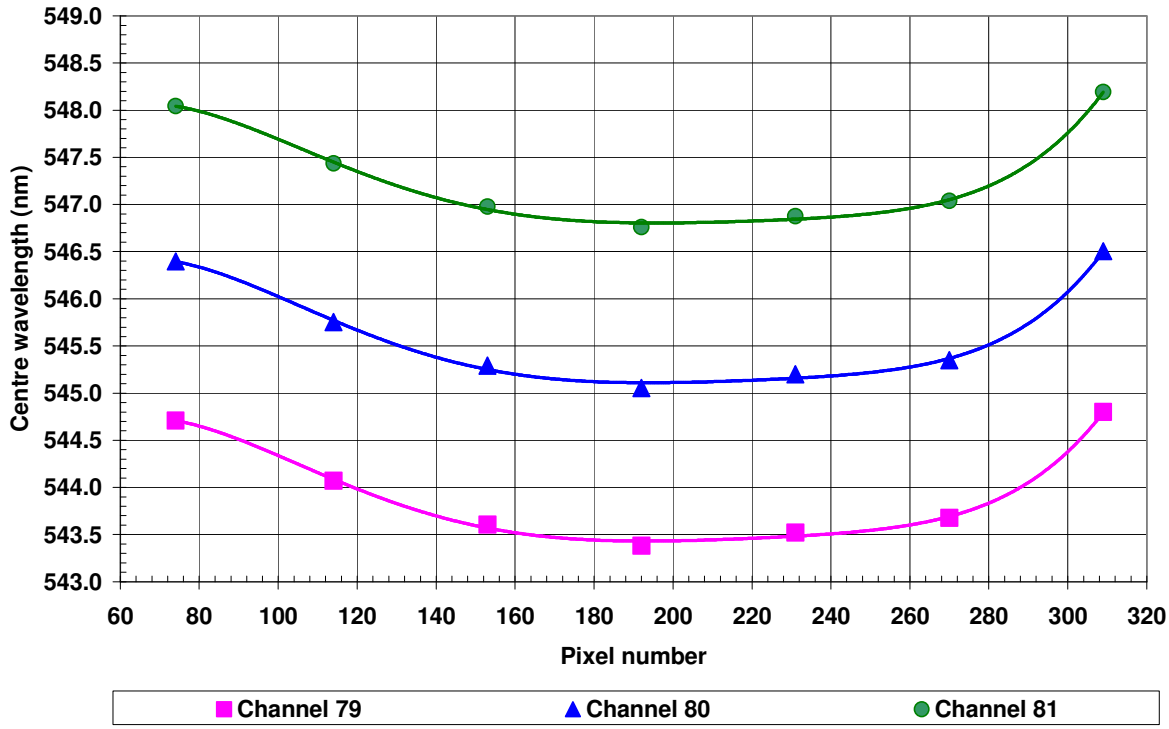

Figure 6.15: AISA centre wavelengths for the channels 79, 80 and 81and seven spatial pixels

Table 6.15: Polynomial function 5th degree for the calculation of the centre wavelength for 3 channels

	$\lambda_{CW}(p) = a_0 + a_1 \cdot p + a_2 \cdot p^2 + a_3 \cdot p^3 + a_4 \cdot p^4 + a_5 \cdot p^5$					
Channel no.	a_0	a_1	$a_2\ 10^{-3}$	$a_3\ 10^{-5}$	$a_4\ 10^{-8}$	$a_5\ 10^{-11}$
79	539.67	0.206	- 2.94	1.81	-5.20	5.73
80	541.24	0.211	- 3.02	1.87	-5.34	5.87
81	542.98	0.207	- 2.96	1.83	-5.24	5.74

The centre wavelengths and the FWHM values of the three channels and the seven spatial pixels are listed in App. C, Table C.12. The FWHM values are in the range between 3.3 nm and 4.8 nm. The FWHM values of the pixels to the right side of the CCD array increase from 3.4 nm (centre pixel) to 4.8 nm for pixel 309. Figure 6.16 shows the recorded signals of channel 80 and the seven spatial pixels. The curve shapes differ from each other as well as the signal levels of the seven pixels.

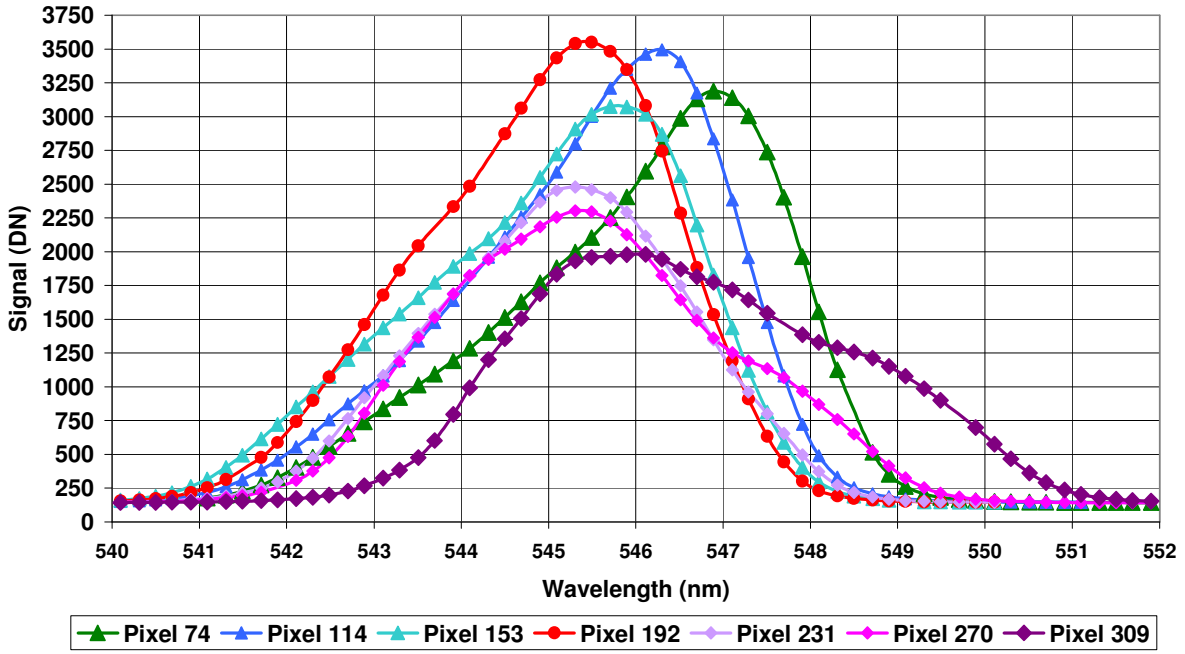

Figure 6.16: Measurement data (raw) of channel 80 for the seven spatial pixels

The standard deviations of channel 80 and the seven pixels range from 0.017 nm to 0.085 nm. The signal curve with the strongest deviation from a Gaussian curve form is that of pixel 309. The standard deviations of the FWHM values for this pixel are the largest ones of the seven pixels.

6.3.3 Discussion

The executed spectral measurements for AISA and ROSIS document the applicability of the described measurement and analysis methods for sensor characterisation (chapter 5.2). For AISA a complete spectral characterisation of the nadir pixel and all channels was carried out. In addition measurements for the determination of smile and frown were performed for selected pixels. For verification and comparison ROSIS measurements were done.

AISA

Neither the determined centre wavelengths nor the spectral sampling intervals of AISA are a linear function of the channel number as approximated by the manufacturer who uses three linear functions. The centre wavelengths of the spectral measurements of the AISA nadir pixel and all channels illustrate a non linear relationship between the channel number and the centre wavelength (Figure 6.7, Figure 6.8). The centre wavelengths of each channel are calculated on the basis of a 4^{th} degree polynomial function (Table 6.9). Also the spectral sampling intervals are fitted by a 4^{th} degree polynomial function (Figure 6.10). The ups and downs (±0.1 nm) of the measured intervals could be noise. The determined FWHM values of all channels vary widely (Figure 6.9). Noticeable is the peak in the middle of the figure at channel 130 (628 nm). The signal curves of the channels 115 to 133 are not Gaussian. The response curves show artefacts like a “bulge”, therefore the determined FWHM values are larger than for the remaining channels.

The current analysis software has no quality flag which marks channels with signal curves which differ from a Gaussian shape. For an identification of channels with no “proper” Gaussian fit curves, increased standard deviations of the Gaussian fits can be used. For the future a quality check for the response curves should be implemented in the analysis software.

The measurement results of the channels 79 to 81 and the evenly spread 7 spatial pixels from pixel 74 to pixel 309 obviously indicated a “smile” and “frown” effect (Figure 6.15). The wavelengths of the spatial pixels near to the centre differ to those near the borders (± 16.4°) of the CCD array with a shift of ~1 sampling distance (1.4 nm). How large the “smile” effect for the total field of view is, has to be determined with further measurements for more spatial positions especially near to the borders. “Smile” and “frown” effects can be caused by dispersion properties of the prism-grating-prism element or by a misalignment of the optical components. In addition to the “smile” effect the FWHM values of the 7 spatial pixels vary strong as well as the shapes of the response curves (Figure 6.16). The FWHM difference from the lowest to the largest value is 46%.

Currently the calibration software of AISA uses the same centre wavelengths and FWHM values for all spatial pixels. “Smile” and “frown” effects should be corrected during the calibration of raw data. Ideally the centre wavelengths and FWHM values for each spatial pixel and each channel should be computed and used for the radiometric calibration.

The characterisation measurements of the AISA nadir pixel and all channels were performed on seven different days over two weeks. The time for the performance of all measurement series took 33 hours and 44 minutes in total. The longest measuring time for one day took approx. 9 hours for 750 measurement steps. Altogether 2777 single measurements were accomplished. The averaged times for the setup for each wavelength at the monochromator was 2 seconds, the automated sensor setup and the data recording required 35 seconds (100 frames) and the data transfer time was 4 seconds. The net data transfer time of all series was approx. 3 hours (2777 * 4 sec) which was ~9 % of the total time. A reduction of the time is only possible with a reduction in the quantity of recorded data.

On the basis of the accomplished measurement, a complete characterisation of the 364 spatial pixels and 286 channels of AISA would require 516 days (364 * 34 hours) for the execution of the measurements. Such extensive measurements are not realisable and meaningful. The recording of data (35 sec) requires the main part of the measuring time. With the programmable configuration mode for AISA only a few selected spatial pixels and channels can be recorded. Thereby the recording time can be reduced to a minimum. Further investigations should be accomplished on this aspect regarding the comparability of the results and the information loss (e.g. stray light, saturated neighbour pixels). For the selection of the necessary spatial pixels and channels a sensor model which doesn’t exist for AISA yet could be helpful.

The performed measurement series demonstrate the operationality of the developed characterisation software for a fully automated execution of a spectral characterisation of one spatial pixel and all channels. Manual interactions were only necessary at the beginning of the measurements for the setup of the monochromator slits and the lamp power unit as well as the changing of the lamp currents during the complete measurement series. Measurements during the night are possible if no manual interactions are necessary (e.g. lamp current change).

ROSIS

The performed ROSIS measurements were the first ones with the modified ROSIS control software with the aim to validate the manual and automated measurement processes and their results.

The results of the performed spectral measurements of ROSIS illustrate different effects. The measurements results of pixel 258 and channels 103 to 106 (693 nm – 709 nm) show data curves with an “enclosed basin” (Figure 6.12). The recorded signals of the “basin” are ~2/3 of the maximum value (14 bit). Saturation could be the cause for this, because the measurements were performed with the 63 % filter and the following ones with the 10 % filter. The recorded signals of the analysed pixel 258 itself and the channels 103 to 106 are not saturated but spatial pixels nearby are, for example pixel 263. Hence the measurements are erroneous. As a result it is important to check all recorded data against saturation and not only the data of one spatial pixel and one channel. The current analysis software should be updated with a saturation check for all spatial pixels and channels.

The analysis of the three measurement series of spatial pixel 259 and channel 80 illustrates the problem with the repeatability of measurement results (Figure 6.13). The three measurement series were performed on different days each time with a new positioning of the sensor mirror and a re-alignment of the sensor. There is the large difference between the centre wavelengths of the measurements (~1.8 times the spectral sampling interval). A wavelength shift caused by temperature and pressure is known from earlier longer characterisation measurement series but the ambient temperature was +22° and the pressure varied between 946 (hPa) and 953 (hPa) for the 5 measurement series. Also the longest measuring time on one day was only 26 minutes. Another cause could be an unprecise alignment of the sensor after the moving of the ROSIS mirror. An incorrect alignment results in erroneous spectral measurements. A partial illumination of the IFOV or the aperture results in a partial illumination of the grating and mirror. Remarkable also the large differences of the response curve signals (between 1786 (DN) and 13657 (DN)).

The mirror problem makes a re-alignment of ROSIS necessary. This task is time-consuming since the ROSIS control software has no proper graphic user interface to control the recorded signals for one spatial pixel and a few channels.

For the future a new program with selectable pixels and 3D graphics will be available to optimise the alignment. New measurements will be performed after the modification of the ROSIS system (enhancement of hard- and software).

The spectral characterisation measurements of ROSIS were executed semi-automated and automated. For both types the CHB devices (monochromator and folding mirror) were adjusted with the *Slave* software instructed by the *Master* software. But the data recording was performed once manually and once with the ROSIS *Sensor* software. A comparison of the measuring time for both types show that with a fully automated measurement process, by using the *Slave*, *Master* and *Sensor* software, the time can be reduced by about 50 %. The required time for an automated data recording was approx. 14 seconds instead of 28 seconds for a manual recording. An automation of the measurement workflow results in a large reduction of the measuring time. The time for setting the monochromator was identical to that of AISA (2 seconds).

6.4 Geometric Characterisation

This chapter describes selected examples of geometric characterisation measurements and results of AISA and ROSIS. The measurements are used for the verification of the specified characterisation methods. The methods specified in chapter 5.3 are used for the determination of the sensor parameters (Field of View (FOV), instantaneous field of view (IFOV), spatial resolution across and along track, spatial sampling distance, and frown effects).

The relevant sensor parameters are given in the columns “geometric” of Table 6.1 (AISA) and Table 6.2 (ROSIS). The focus in this chapter is placed on AISA. The laboratory setting parameters for the geometric characterisation measurements are listed in Table 5.4 and Table 5.5. The selected parameter settings are given in the following sections. For all geometric measurements the 100 Watt QTH lamp was used.

6.4.1 Field of View, Instantaneous Field of View

The FOV of a sensor can be determined by performing across track LSF measurements for the border pixels. The method is described in chapter 5.3.1. FOV measurements are described here for AISA. The measurement setup parameters for the FOV determination are listed in two tables. Table 6.16 contains the parameters which were fixed during the measurements. Table 6.17 includes the changing parameters except for the last two columns which contain the spatial pixel number and the measurement date.

For all measurements the smallest vertical slit (50 µm) was selected. The measurement setups of a) to c) cover the left border of the FOV and d) to e) the right border. Previous measurements showed a viewing angle of ~25° at the left and ~23° at the right border. This indicates a smaller FOV than the FOV (57.6) given by the manufacturer [104].

The measurements a) and d) of Table 6.17 are performed with a large interval to estimate the required viewing angle ranges for the left and right border. The viewing angle ranges of measurements b) and e) are the results of the previous measurements. Further measurements (c, f of Table 6.17) were made with the DLR universal adapter and a new alignment was necessary. The roll angle offset for these two measurement series were determined during the alignment of the AISA (see chapter 6.2).

Table 6.16: AISA FOV measurement setups (fixed parameters)

Folding mirror		**Slit wheel**		**Sensor**	
Parameter	Value	Parameter	Value	Parameter	Value
Y axis offset (mm)	0.0	Slit angle (°)	90.0	Integration time (ms)	300
		Slit	50 µm, vertical	Number of frames	100

Table 6.17: AISA FOV measurement setups (variable parameters)

	Viewing angle range (°)	**Angle step interval (°)**	**Roll angle offset (°)**	**Current (A)**	**Z axis (mm)**	**Interface plate**	**Spatial pixel no.**	**Measurement date**
a	25.00 – 26.95	0.05	0.0	6.7	500	Aerotech	1 – 3	2008-03-07
b	25.00 – 26.19	0.01	0.0	6.7	500	Aerotech	1 – 4	2008-03-11
c	25.40 – 26.00	0.01	-0.3219	7.0	777	universal	1 – 5	2008-06-13
d	-24.00 – -22.00	0.05	0.0	6.7	500	Aerotech	361 – 364	2008-03-07
e	-24.00 – -22.80	0.01	0.0	6.7	500	Aerotech	362 – 364	2008-03-10
f	-24.04 – -22.80	0.01	-0.3219	7.0	777	universal	364	2008-06-16

The analysis of all recorded data has been performed with the across track LSF program described in chapter 5.3.2. The used input parameters are the default values of Table 5.6.

Results

Selected analysis results like a comparison of the viewing angles and the FWHM values of the three measurements of different pixels are shown and described.

The results of the first three measurements a) to c) of Table 6.17 are plotted in Figure 6.17. The figure shows the maxima of the Gaussian fits (viewing angles) of the pixel number 1 (left border) and all channels. The channel viewing angles of measurement a) and b) range from ~25.68° to ~25.90°. The difference is 3.91 mrad which is approximately 1.5 IFOV. The results of the first 22 channels of measurement b) are not in Figure 6.17 since the Gaussian fits failed. A fit fails if the signal difference between dark current and signal is too low (< 10 DN). The viewing angles differences among a) and b) are between -0.006° to 0.002° and for a) and c) are between -0.008° and 0.013°. Hence the maximum error is 0.013° (0.225 mrad) and the averaged deviation is 0.003° (0.053 mrad). The channels with the maximum viewing angle are channel no. 42, 48 and 41 for the three first measurements. The three measurement results demonstrate the reproducibility of the results.

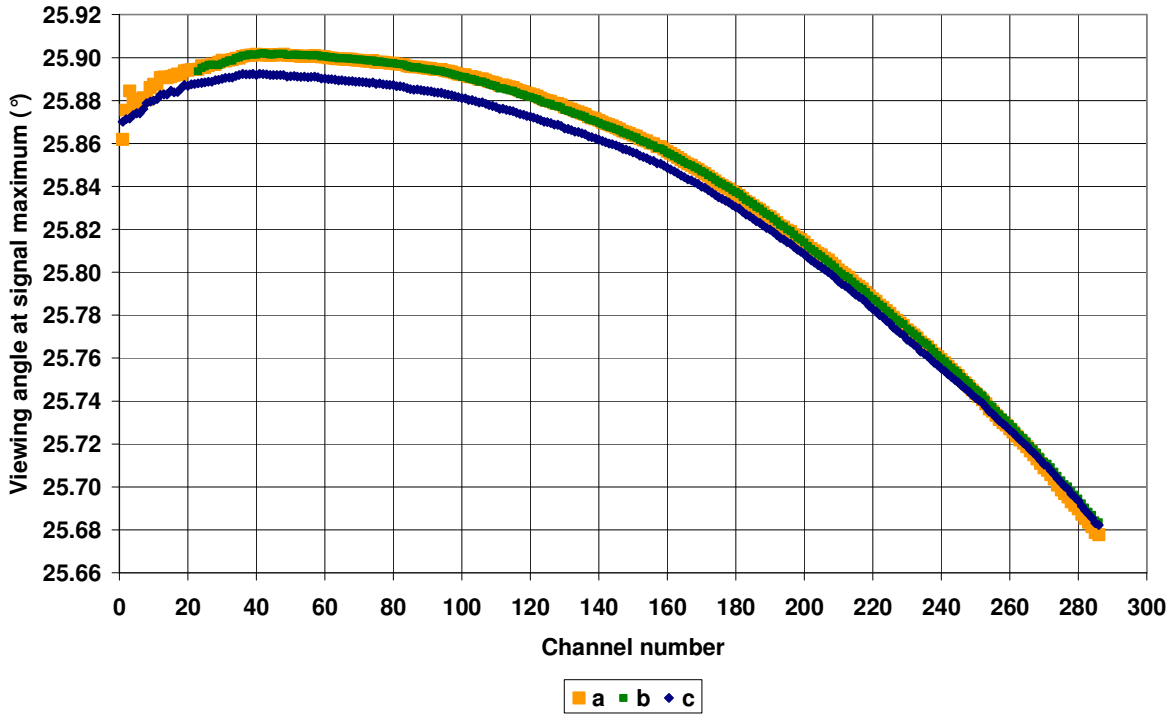

Figure 6.17: Across track viewing angles of pixel number 1 and all channels performed at different days and with different settings (results of the measurements a) to c) of Table 6.17)

Figure 6.18 shows the viewing angles (maximum of the Gaussian fit) of pixel 364 and all channels of the measurements d) to f) of Table 6.17. The viewing angles of the measurements d) and e) are in the range from -23.32° to -23.47°. The difference is 2.5 mrad which is ~1 IFOV. The viewing angles of the measurements d) and e) differ between -0.008° and 0.007°.

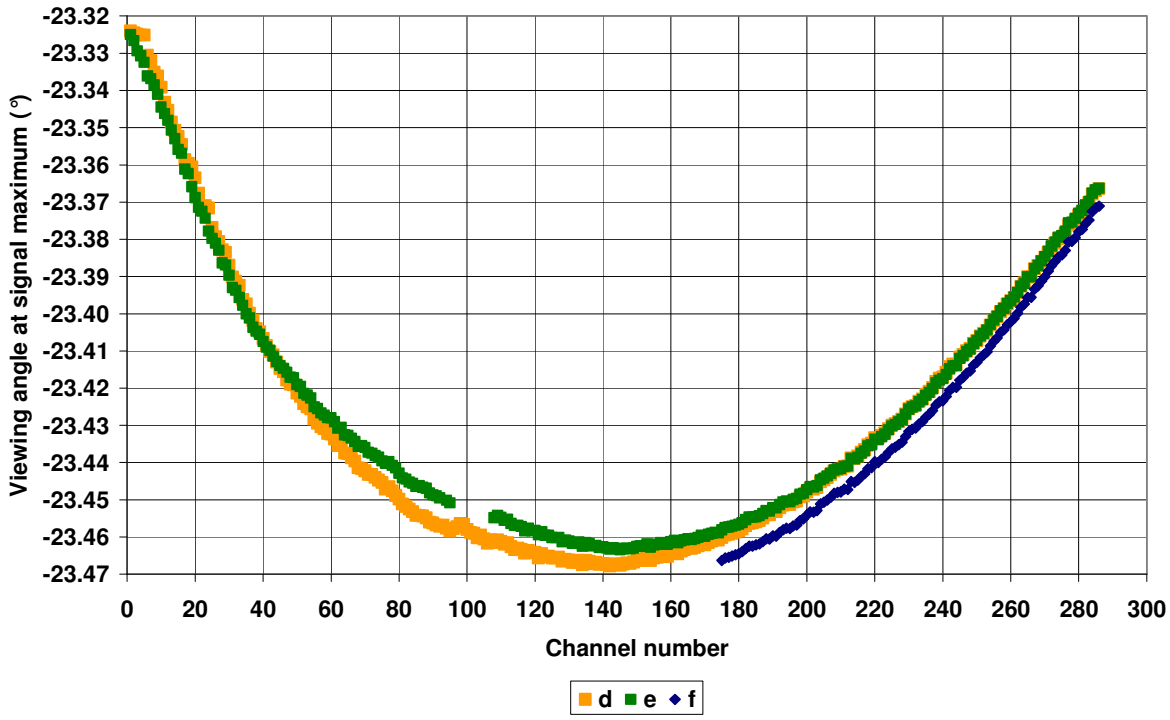

Figure 6.18: Across track viewing angles of pixel number 364 and all channels performed at different days and with different settings (results of the measurements d) to f) of Table 6.17)

The channels with the minimum viewing angle are number 142 and 144 for the measurement series d) and e). The results of f) are incomplete since the measurement stops at viewing angle -23.2° (planned -22.8°) due to an AISA computer problem. The recorded data curves of the three measurements of the channels below 200 have two maxima. An example with two maxima for the centre channel 143 and pixel 364 is shown in Figure 6.20. The single recorded data of the three measurements d) to e) agreed well with each other.

The FOV measurements of Table 6.17 were performed on different days using various interface plates associated with a new alignment of the sensor. The results shown in Figure 6.17 and Figure 6.18 agree very well with each other.

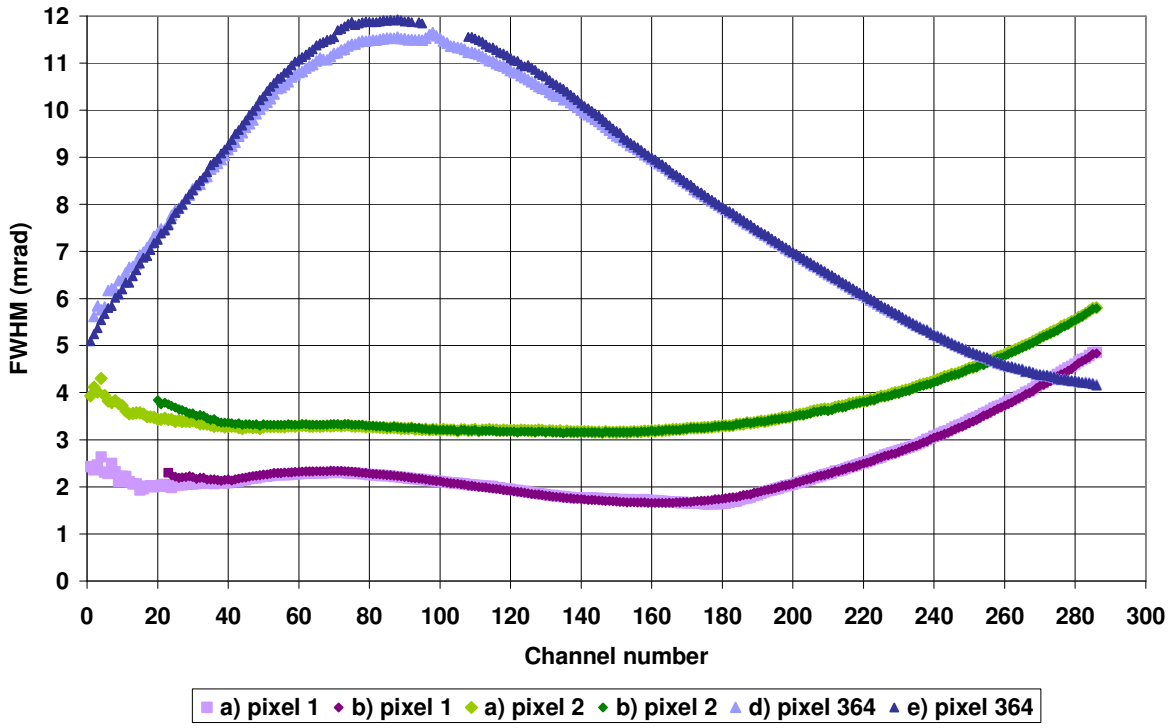

Figure 6.19: FWHM of all channels for different spatial pixels, all channels and different measurements

Figure 6.19 shows the determined FWHM values of pixel 1, 2 and 364 of the measurement series a), b), d) and e) of Table 6.17. The results of the measurements c) and f) are incomplete. The FWHM values of the shown pixel vary between ~1.7 mrad and ~12 mrad. The FWHM values of pixel 1 of measurement a) and b) ranges from 1.633 mrad to 4.855 mrad. The differences of the two measurements are between -0.292 mrad to 0.063 mrad and the averaged deviation is 0.04 mrad. For pixel 2 the FWHM values are in the range between 3.142 mrad and 6.683 mrad. The pixel 2 differences of the measurements a) and b) are in the range from -0.404 mrad to 0.037 mrad and an averaged deviation of 0.039 mrad. The FWHM values of pixel 364 are among 4.146 mrad and 11.926 mrad. The differences of the two measurements d) and e) are between -0.481 mrad and 0.475 mrad. The averaged deviation is 0.133 mrad.

The standard deviations of the plotted FWHM values of Figure 6.19 are shown in Appendix C, Figure C.14. The pixels 363 and 364 are the pixels with the greatest standard deviations.

Figure 6.20 shows the results of the three (d to f) measurements of pixel 364 and channel 143 from Table 6.17. Since measurement f) was incomplete no Gaussian fit was performed. The figure contains the recorded and the Gaussian fit data in the viewing angle range from -24.0° up to -22.8°. The recorded signals of the three measurements have two maxima and the signals are similar. The maxima of two Gaussian fits are at viewing angle -23.465 respectively -23.463 for measurement e. The FWHM is 0.565° (9.859 mrad) for measurement d) and 0.572° (9.983 mrad) for measurement e). The difference between the two measurements is 1.3 %.

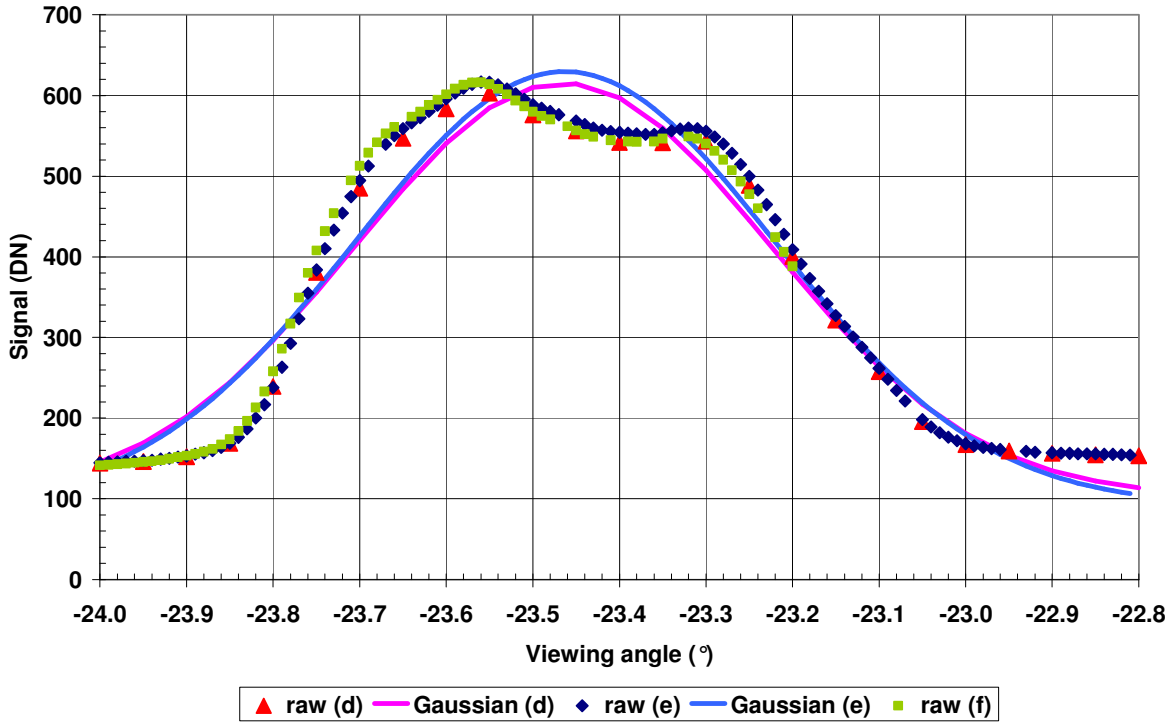

Figure 6.20: Across track signals and Gaussian fits of pixel 364 and channel 90

The overall FOV results of the FOV across track LSF measurements a) and d) are listed in Table 6.18. The measurements a) and d) are selected because results are available for all channels.

Table 6.18: AISA FOV measurement results of a) and d) from Table 6.17

	On the left	On the right
Pixel number	1	364
Viewing angle (°) of channel 143	$25.87 \pm 9.35 \cdot 10^{-4}$	$-23.47 \pm 7.95 \cdot 10^{-3}$
FWHM (mrad) of channel 143	$1.778 \pm 1.74 \cdot 10^{-2}$	$9.069 \pm 1.62 \cdot 10^{-1}$
Minimum viewing angle (°)	$25.68 \pm 7.11 \cdot 10^{-3}$	$-23.47 \pm 8.05 \cdot 10^{-3}$
Maximum viewing angle(°)	$25.90 \pm 1.80 \cdot 10^{-3}$	$-23.32 \pm 5.08 \cdot 10^{-3}$
Frown (mrad)	3.91	2.51
Frown (IFOV)	1.5	1.0

The determined FOV of the 8 mm lens of all channels range from 49.04° to 49.35° and is 49.34° for the centre channel (143). The asymmetry between the viewing angles of the border pixels is 2.4° (left: 25.87°, right: -23.47°).

On the right side of the CCD array 20 columns of the 384 are reserved for FODIS data. Based on the centre pixel number 192 [105] the right side has only 172 columns for spatial information compared with the 192 columns for the left side.

6.4.2 Across track Line Spread Function

Geometric measurements for the determination of the across track LSF were performed for AISA and ROSIS. The methods for the measurement and analysis are described in chapter 5.3. The necessary CHB parameters are listed in Table 5.4. For all across track measurements the small vertical slit and the folding mirror were used.

AISA

Across track characterisation measurements were performed for seven spatial positions over the FOV excluding the borders. The border pixels were measured during the FOV determination (see chapter 6.4.1).The fixed measurement setup parameters are listed in Table 6.19. Table 6.20 contains the different viewing angle ranges and the illuminated pixels. The roll angle offset was determined during the sensor alignment (see chapter 6.2). The viewing angle range was defined as five times the calculated IFOV of 0.136° (see results of chapter 6.4.1). The measurements were performed with the DLR universal adapter. The Y, Z and roll angle (α) *Slave* parameters were determined during the sensor alignment (see chapter 6.2).

Table 6.19: AISA across track LSF measurement setups for seven pixels (fixed parameters)

Folding mirror		Slit wheel & lamp		Sensor	
Parameter	**Value**	**Parameter**	**Value**	**Parameter**	**Value**
Step interval (°)	0.01	Slit angle (°)	90.0	Integration time (ms)	300
Z axis (mm)	777.0	Slit	50 µm, vertical	Number of frames	100
Roll angle offset (°)	-0.3219	Current (A)	7.0	Interface	universal
Y axis offset (mm)	0.0				

Table 6.20: AISA across track LSF measurement setups for seven spatial pixels (variable parameters)

	Viewing angle range (°)	Pixel no.
g	16.03 — 16.71	72 — 73
h	10.55 — 11.23	113 — 114
i	5.12 — 5.80	152 — 153
j	-0.34 — 0.34	191 — 192
k	-5.80 — -5.12	230 — 231
l	-11.23 — -10.55	269 — 270
m	-16.72 — -16.04	310 — 311

The seven measurements were analysed with the across track LSF program (see chapter 5.3.2). The used input parameters are the default values of Table 5.6.

Results

The viewing angles of the seven measurements of Table 6.20 and the two border pixel measurements b) and e) of Table 6.17 are shown for channel 250 in Figure 6.21. The viewing angles, FWHM values and sampling distances of the shown spatial pixels are listed in Appendix C,

Table C.10. A viewing angle θ_p of a spatial pixel p can be calculated with the linear fit function 26.128 – 0.1365 * p (black line of Figure 6.21). The differences between the measured and the viewing angles calculated by using the linear function are in the range from -0.25° to 0.23°.

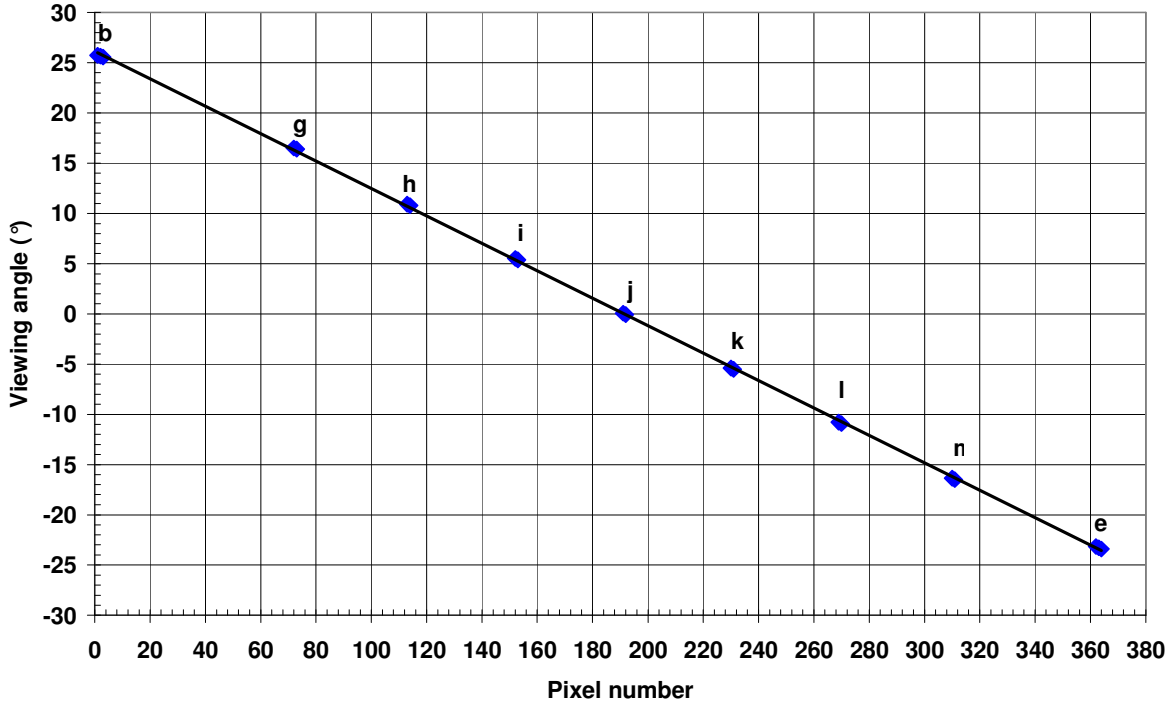

Figure 6.21: Viewing angles of channel 250 and several spatial pixels

The relative viewing angles of all channels of the spatial pixel 73, 113, 153 and 192 are plotted in Figure 6.22. The viewing angles are relative to the maximum viewing angle of each of the four spatial pixels. The other three characterised spatial pixels are not plotted because of missing Gaussian fit results for all channels. The channel numbers with the maximum viewing angles for the four spatial pixels are between 38 (pixel 192) and 65 (pixel 73). All curves have a sharp bend at channel 163. The frown values for the four pixels are in the range from 3.9 mrad to 2.6 mrad. These values are approx. 1.5 IFOV for pixel 73 and 1 IFOV for pixel 192.

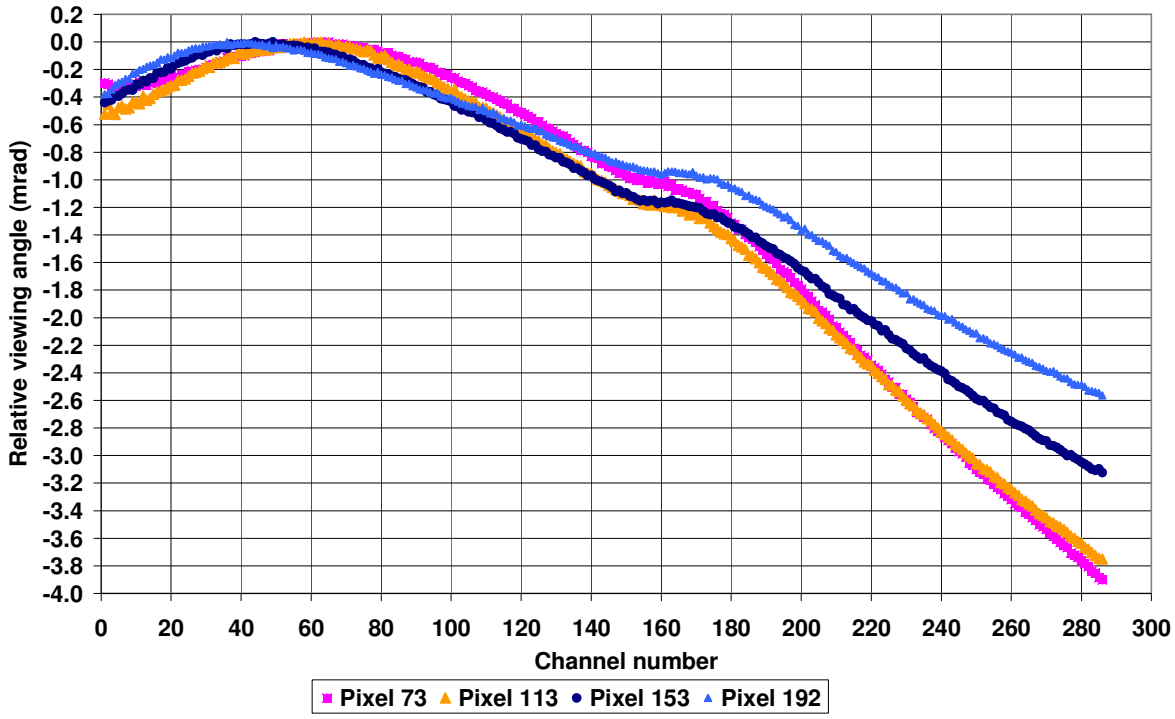

Figure 6.22: AISA relative viewing angle at signal maximum for all channels for four spatial pixels

The FWHM values of the spatial pixels 73, 113, 153 and 192 are plotted in Figure 6.23. The vales range from 4.28 mrad (~1.7 IFOV) to 5.64 mrad (~2.2 IFOV). The differences between the minimum und maximum values of each channel are in the range from 0.11 mrad to 0.5 mrad. The recorded data for the channels in the range from 160 to 215 have two peaks. An example of pixel 153 and channel 179 is shown in App. C, Figure C.16. The standard deviation values of the FWHM of the four pixels are plotted in Appendix C, Figure C.14. The values differ between 1.3 *10^{-2} mrad and 9.3 *10^{-2} mrad.

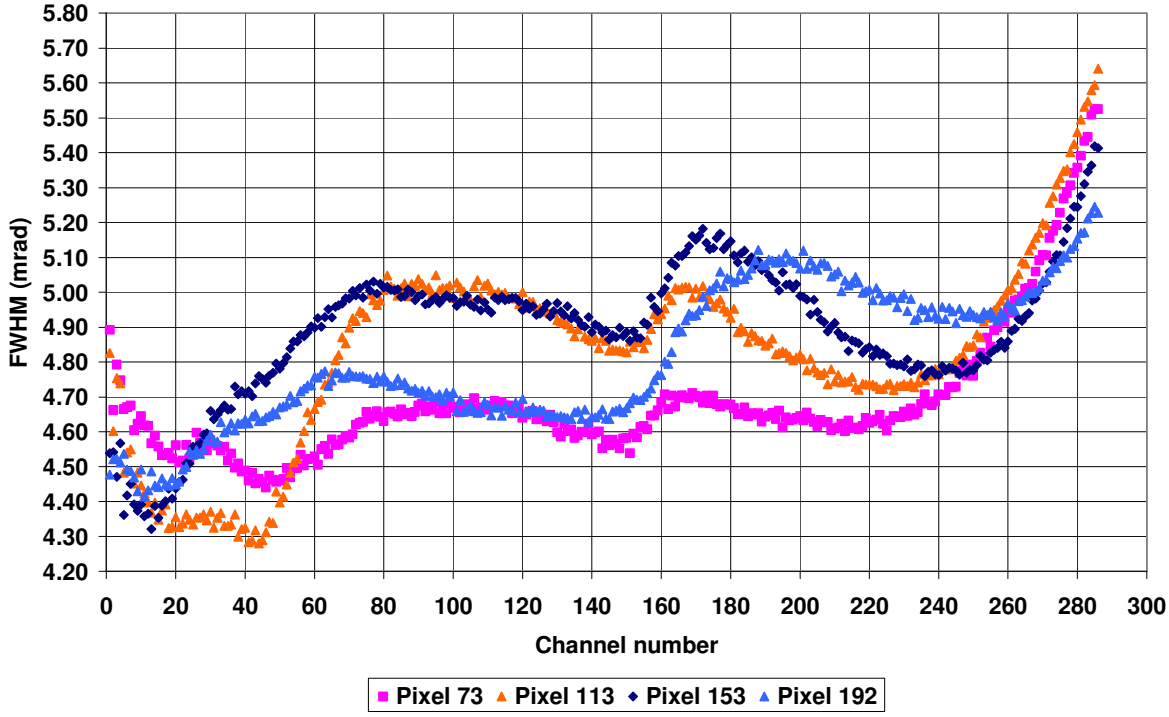

Figure 6.23: Across track FWHM values of all channels of four spatial pixels

ROSIS

There was the assumption that the internal ROSIS mirror causes difficulties with the positioning of the mirror. Therefore across track LSF measurements were performed with two different data recording types. The first two measurement series were performed with the automatic mode “A”. In this mode the data acquisition software automatically changes the mirror position and records the three data types (dark current, spectral and nadir data, see chapter 4.4). The other two measurements were conducted manually (mode “M”) at different days. Therefore the mirror was tilted to the nadir position and the data was recorded manually for all measurements of the two series whereas the folding mirror was adjusted by the *Slave* software. The two types of measurements are performed to check the sensor response for a tilting and fixed mirror to verify the mirror position problem.

The fixed CHB parameters are listed in Table 6.21 and the variable ones in Table 6.22. For the measurements the smallest vertical slit was selected. The range of measurement a) equates approx. 3 times IFOV. For the following measurements a range of two times IFOV are selected.

Table 6.21: ROSIS across track LSF measurement setups for different settings (fixed parameters)

Folding mirror		**Slit wheel**		**Sensor**	
Parameter	**Value**	**Parameter**	**Value**	**Parameter**	**Value**
X axis (mm)	1400.0	Slit angle (°)	90.0	Frequency (Hz)	40
Interval (°)	0.003	Slit	50 µm, vertical	Interface	Universal
				Neutral density filter	63 %

Table 6.22: ROSIS across track LSF measurement setups for different settings (variable parameters)

	Viewing angle Range (°)	**Roll angle offset (°)**	**Y axis offset (mm)**	**Current (A)**	**Frame No.**	**ROSIS mirror position**	**Mode**	**Measurement date**
a	-0.10 – 0.10	0.0	0.0	6.3	100	-1138	A	2008-08-25
b	-0.06 – 0.06	-0.007	0.0	8.4	200	-1138 / -1139	A	2008-08-28
c	-0.06 – 0.06	-0.007	0.0	7.0	500	-1139	M	2008-09-05
d	-0.06 – 0.06	-0.007	0.0	7.0	500	-1139	M	2008-09-09

The data were analysed with the across track LSF program and the default input parameter values.

Results

The recorded data of the centre pixel (258) and channel 80 of the automatic performed measurements (a) and b) of Table 6.25 are shown in Figure 6.24. The mirror position in steps is a return value of the automatic data acquisition software and was -1138 (nadir) for all measurements of series a). The mirror step of measurement b) ranges between -1138 and -1139. The shown measurement data in Figure 6.24 illustrate the mirror problem. The two curves are not identical as was expected (see AISA measurement Figure 6.20).

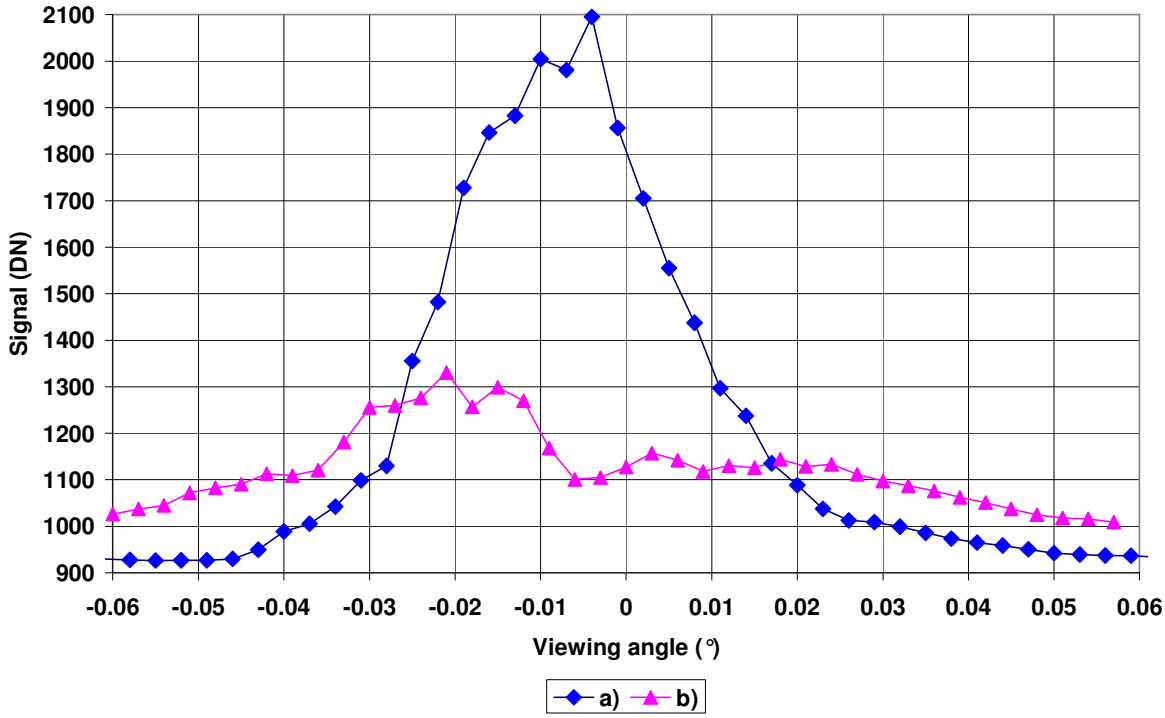

Figure 6.24: ROSIS across track LSF measurement data of pixel 258 and channel 80 of erroneous measurement a) and b) of Table 6.22

The results of the measurements with a fixed mirror position are shown in Figure 6.25. The recorded data and Gaussian fits of pixel 258 and channel 80 of measurements c) and d) of Table 6.22 are displayed. The maximum of the Gaussian fits of both measurements are -0.01064° and -0.00345°. The difference is 0.0072° (0.125 mrad). The FWHM values are 0.6153 mrad and 0.7700 mrad which is a difference of 0.1548 mrad (~25%).

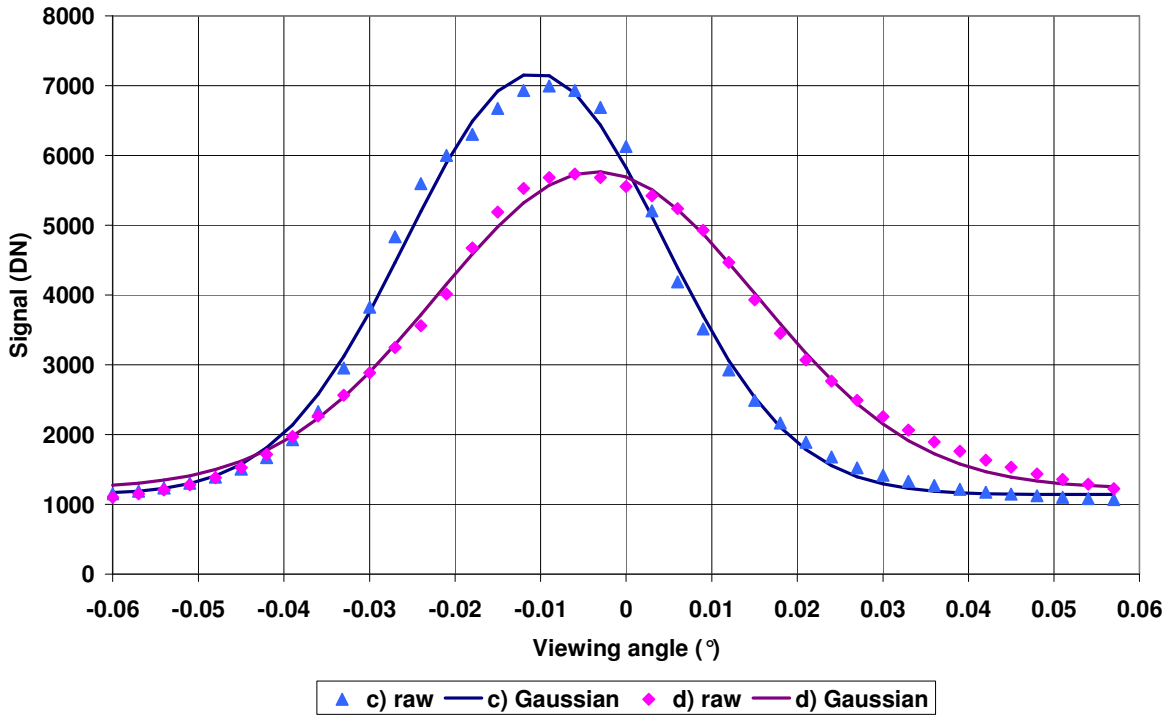

Figure 6.25: ROSIS across track LSF measurement of pixel 258 and channel 80 (manually recorded)

Figure 6.26 shows the viewing angles of the centre pixel (258) and all channels higher than 24 for measurement c) and d) of Table 6.22. The results of the first 23 channels are omitted because these channels are affected by the implemented long-pass filter (see 6.1). The viewing angles of measurement c) are in the range from -0.034° to 0.004° and for measurement d) between -0.025° and 0.012°. The range is 0.668 mrad for measurement c) and 0.634 mrad for measurement d) which is approx. 1.2 IFOV (see Table 6.2). The viewing angle differences between the two measurements range from -0.0097° to -0.007° and the mean value is -0.0073° (0.128 mrad).

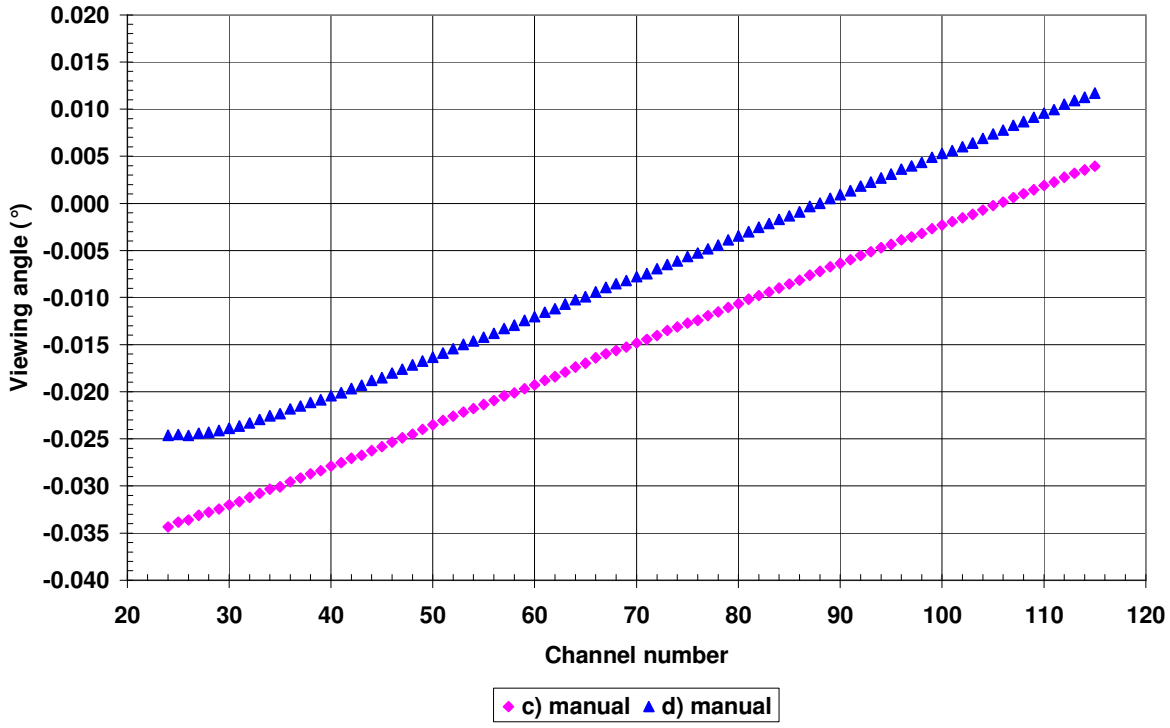

Figure 6.26: ROSIS viewing angles of spatial pixel 258 and all channels (measurement c and d)

The FWHM values of the two measurements are not shown because of the different data curves (see Figure 6.25) which seem to be incorrect and which may be a problem of incorrect alignment of the sensor.

6.4.3 Along track Line Spread Function

The second geometric property is the along track FOV. The measurement and analysis methods are described in chapter 5.3. Along track LSF measurements were performed for the nadir pixel of AISA.

The measurements were performed with the smallest horizontal slit and a slit angle range of ±9°. The slit angle of 9° corresponds to a sensor viewing angle of 0.39° (6.807 mrad) calculated according to equation (5-7). A slit angle interval of 0.1° was selected which corresponds to a viewing angle interval of 0.076 mrad. The Y-axis and roll angle offsets were determined during the alignment measurements (see chapter 6.2). A 2-fold neutral density filter was installed in front of the lens. The necessary CHB parameters for the along track LSF measurements are given in Table 6.23.

Table 6.23: AISA along track LSF measurement parameters

Folding mirror		Slit wheel & lamp		Sensor	
Parameter	**Value**	**Parameter**	**Value**	**Parameter**	**Value**
Viewing angle (°)	0.0	Slit angle range (°)	-9.0 – 9.0	Integration time (ms)	260
Z axis (mm)	777.0	Step interval (°)	0.1	Frame no.	20
Roll angle offset (°)	-0.327	Slit	50 µm, horizontal	Interface	universal
Y axis offset (mm)	0.0	Current (A)	6.6	Filter	2-fold

The recorded data were analysed with the along track LSF measurement program and the default input parameter values (description see chapter 5.3.2).

Results

For the first 140 channels no results were computed because the Gaussian function failed. The data signals of the Gaussian peaks of the computed channels are in the range from 450 DN to 915 DN. Figure 6.27 shows normalised recorded data of the nadir pixel for selected different channels.

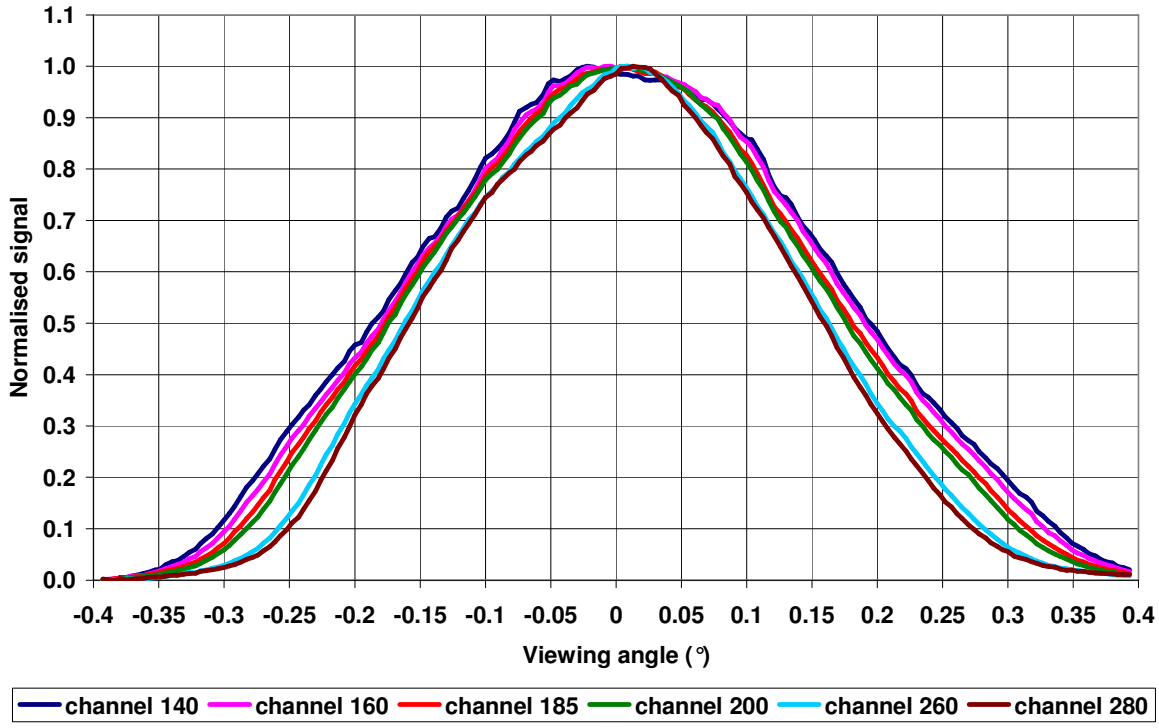

Figure 6.27: AISA along track measurement data of pixel 192 for different channels

The FWHM for channel 140 is 0.714 mrad and for channel number 280 5.62 mrad. The difference between both is approx. 21 %. All determined FWHM values of the channels with a channel number greater than 140 are shown in Figure 6.28. The FWHM values range from 5.62 mrad to 7.14 mrad.

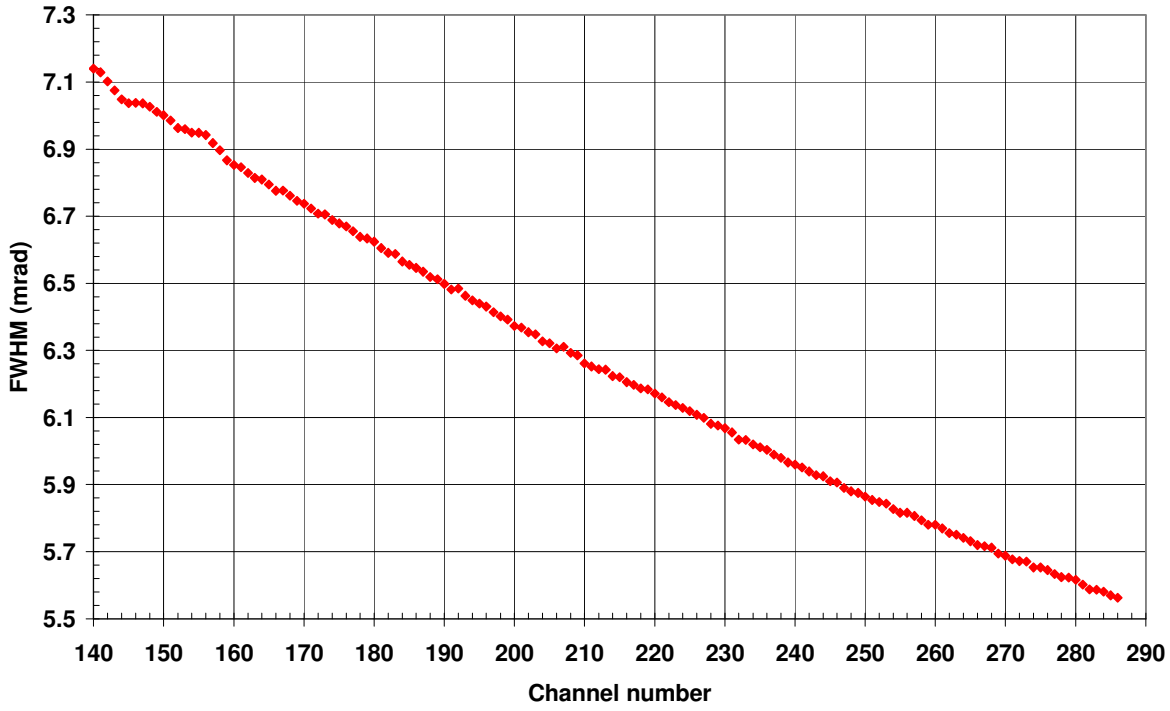

Figure 6.28: AISA along track FWHM results of pixel 192

6.4.4 Discussion

The performed geometric measurements have demonstrated the applicability of the methods described in chapter 5.3. Across track LSF measurements and their analyses were performed for ROSIS and AISA, along track measurements only for AISA. All these geometric measurements are the first ones which were executed with the automated software modules (*Master*, *Sensor* and *Slave*). The *Master* software is flexible and makes also measurements without an automated control of the sensor possible. An across track LSF measurement was performed in this way for ROSIS. The measurement setups and results are the basis for further measurements and analyses.

AISA

The across and along track measurements were carried out to determine the FOV and IFOV. The resulting FOV of 49.3° (see Table 6.18) differs from the manufacturer FOV (57.6°) by about 8.3°. The viewing angles of the border pixels differ. Pixel number 1 has a viewing angle of 25.9° and the angle of pixel 364 (right border) is -23.5°. The number of pixels between the centre pixel (192) and the border pixels differs (left side: 191, right side: 172). On the right border the last illuminated spatial pixel of the 288 * 384 detector array is pixel number 364 (see chapter 6.1). The remaining 20 pixels on this side are reserved for the FODIS information. These 20 pixels correspond to a viewing angle of 3° using the manufacturer IFOV of 0.15°. However the determined IFOV from the measurements is 0.1365° (see linear fit in Figure 6.21). The difference between the determined and given IFOV calculated with 364 pixels corresponds to an angle of 4.9°.

The across track FOV measurements of Table 6.17 were performed several times on different days and with different interface plates associated with a new alignment of the sensor. The determined border pixel viewing angles and FWHM values for each channel of the different measurement series agree very well with each other (see Figure 6.17, Figure 6.18 and Figure 6.19). This indicates that the defined measurement and alignment procedures allow highly reproducible results.

Across track LSF measurements over the whole FOV were performed for nine viewing angles (Figure 6.21). Seven of the nine angle positions have a successive interval of 5° from nadir. The two other measurements are at the border pixels. The calculated viewing angles on the basis of the linear fit differ from determined viewing angles about ± 0.2° which is approx. 1.5 IFOV. Additional across track LSF measurements should be performed in the future to improve the fit. This should be done especially for spatial pixels at the borders because of their greater differences.

The relative viewing angles of four spatial pixels (73, 113, 153 and 192) are shown in Figure 6.22. The frown is in the range from 1 IFOV (2.6 mrad) to 1.5 IFOV (3.9 mrad) where the values increase from the nadir pixel to the borders. The effect may be caused by the dispersive element (Grating-Prism-Grating) of the AISA sensor. The shapes of the frown curves vary for the different spatial pixels. Additional measurements have to be carried out in the future to get results for the spatial pixels greater than 192 and to determine the frown.

The FWHM values of the different spatial pixels vary substantially between the channels and the spatial pixels (see Figure 6.23). The difference can be explained by the curve shapes of the single channels. Some of the channels have response curves with two peaks (Figure 6.20) or the curves are not like a Gaussian function. The cause hasn't yet been established. Anyway, the determined FWHM values should be used for the raw data calibration and not the same FWHM value for all channels as in the past. The standard deviations of the Gaussian fit can be a first quality indicator for varying response curves. The standard deviations of the measurements are shown in App. C, Figure C.15. The existing analysis software should be upgraded with a quality flag which marks channels with a greater than standard deviation. In addition, channels with more than one peak should be marked as well.

Some of the measurements could not be analysed because the Gaussian fit failed due to an insufficient number of data points. This was in particular the case for the response curves with two peaks. For those measurements the viewing angle range has to be expanded to cover the whole viewing angle of a selected pixel. An enlargement of the range leads however to extra time for the measurements and this should be taken into account.

Concerning the time for data recording, the angle interval is the import parameter as well as the number of frames and the data transmission. If a sensor becomes unstable during a long measurement series the data transfer should be performed at the end of the measurement series.

The results of the along track LSF measurements for the channels greater than 140 are shown in Figure 6.27. The lower channels were not analysed since the signals were too low. For some channels the signals at the borders are not at dark current level which indicates that the slit angle range was too small. Additional measurements should be performed in the future with the 100 µm slit and the maximum angle range of ±10°. In general, for sensors like APEX or ROSIS the maximum slit range of ±10° is not a problem since these sensors have a small IFOV. Only for sensors like AISA with a larger IFOV the along track LSF can be difficult to measure.

ROSIS

The manual and automatic measurements were performed to investigate the problem of moving the ROSIS mirror during a measurement series. In the automatic mode the mirror of ROSIS was changed at every single measurement. The analysis of the measurement data resulted in non Gaussian response curves (see Figure 6.24). Whereas the manually performed measurements, with a fixed ROSIS mirror showed a Gaussian curve shape (see Figure 6.25). This comparison discloses that there exists a problem with the positioning of the mirror in the automatic mode.

The two manual measurements (Figure 6.25) were made without additional alignment of the sensor after the setting of the ROSIS mirror. The signal levels from the two measurements differ and the maxima are at different viewing angles. Both measurements seem to be incorrect because of an incorrect alignment. An alignment of ROSIS (pitch angle) is necessary after each re-start of the ROSIS system or movement of the mirror. For this the ROSIS mirror has to be tilted to the nadir position and the signal has to be optimised to its maximum by tilting the sensor around the Y axis (pitch angle) with the universal adapter.

The viewing angles for all channels (Figure 6.26) of the measurements with the fixed mirror don't show a frown effect but a linear function with a slope. The relative range of the viewing angle is 0.67 mrad which is approx 1.2 IFOV. This effect could be caused by an improper alignment of the detector (rotation).

Based on the measurement results the ROSIS data acquisition software was modified. In the upgraded software the tilting of the mirror was skipped and the automatic mode includes "only" an automatic data recording. An upgrade of the ROSIS system including the software and the control of the mirror is planed for 2009. A stepper motor for the mirror with a smaller step size and a well-defined home position would be ideal. With the new control software it should be possible to allow a repeatable setting of a mirror position.

A statement concerning the reproducibility of the measurements is not possible due to the mirror problem. But the manually performed measurement series illustrates the flexibility of the software modules. The execution of a characterisation measurement of a sensor can be performed with the *Master* SW without a communication with a *Sensor* module.

The CHB devices are automatically set by the *Master* which informs the operator to record data at the right moment.

6.5 Radiometric Characterisation

This chapter describes the setups and analysis results of the performed radiometric characterisation measurements for AISA. The corresponding methods are defined in chapter 5.4. The performed measurements are used for the determination of the radiometric response function and for the control of the linearity with the integration time.

The different characterisation types are executed together. Therefore the selected device parameter values are described at this point. The analyses and results are explained in the following sections.

For the measurements the small integrating sphere was used since this sphere is calibrated against a national standard. The sphere illuminates all spatial pixels of AISA and overfills its aperture. Since the radiance of the sphere saturates some of the channels a neutral density filter was used to reduce the incoming light. The four available filters for AISA reduce the light by a factor of 2, 4, 8 and 64. Previous measurements showed a need of the 64-fold neutral density filter for the recording of unsaturated data. Hence this filter was mounted in front of the lens. AISA itself was mounted without an adapter plate above the opening of the small sphere.

The fixed parameter settings of the CHB devices and the sensor are listed in Table 6.24. The only variable parameter is the integration time (see Table 6.25) with its minimum value of 260 ms.

Table 6.24: AISA radiometric characterisation measurement setups (fixed parameters)

Integrating sphere		**Sensor**	
Parameter	**Value**	**Parameter**	**Value**
Size	Small	Number of frames	250
Power (W)	400	Interface	no
Current (A)	34.7	Transmittance filter	64-fold
		Data type	Dark current and nadir data

Table 6.25: AISA radiometric characterisation measurement setups (variable parameters)

Integration time (ms)					
a	b	c	d	e	f
260	300	350	400	450	500

The measurements were performed manually in January 2008 by a colleague (W. Vreeling), no *Master* software was used. The dark current data were recorded after each data file, with the same integration time as the data file. The measuring log file with the sensor information was manually created afterwards.

The dark current corrected measurements were analysed with the radiometric characterisation program as described in chapter 5.4.2. This analysis program computes the radiometric response, the linearity and creates a “flat-field” image. Table 6.26 contains the program input parameters used for the analyses.

Table 6.26: Radiometric characterisation analysis input parameter values

Program input parameter	Input value
a) Sensor name	AISA
b) Check linearity	Yes
c) Use of neutral density filter?	Yes
d) Selected filter transmittance file	MO08_64x.prn
e) Selected integration time	300 ms

The transmittances of the filters were determined with the two-beam spectrometer Varian CARY-1 in the wavelength range between 190 and 900 nm with a resolution of 1 nm [102]. The curve of the transmittance of the filter is plotted in App. C, Figure C.19.

6.5.1 Radiometric Response Function

For the determination of the radiometric response function the measurement with the integration time of 300 ms was selected (b of Table 6.25). This integration time was selected because it is used mostly during field measurements.

The responses for each spatial pixel and channel are calculated according to equation (5-8). The dark current corrected signal of each pixel element was divided by the transmittance value, the integration time and the radiance of the sphere. The transmittance and the radiance values are interpolated (spline function) according to the centre wavelength of the channels. The spectral radiance of the small sphere is plotted in App. C, Figure C.20.

The following figures show the radiometric responses for several spatial pixels, the signals of several channels and all spatial pixels, and a flat-field image.

Results

The results of the measurement with the 300 ms integration time (b of Table 6.25) are shown in Figure 6.29. This figure contains the radiometric responses of the border pixels, the centre pixel and the averaged response over all spatial pixels (red line). The radiance values of the first 34 channels (< 472 nm) are sinking fast and rise steadily up to ~681 nm. The responses of channel 162 of the border pixels are ~71 % (pixel 1) and ~35 % (pixel 2) less than the response of the centre pixel. The results of the pixel 363 are not in Figure 6.29 because they are similar to that of pixel 364. The responses decrease significantly for the channels with a wavelength above 700 nm.

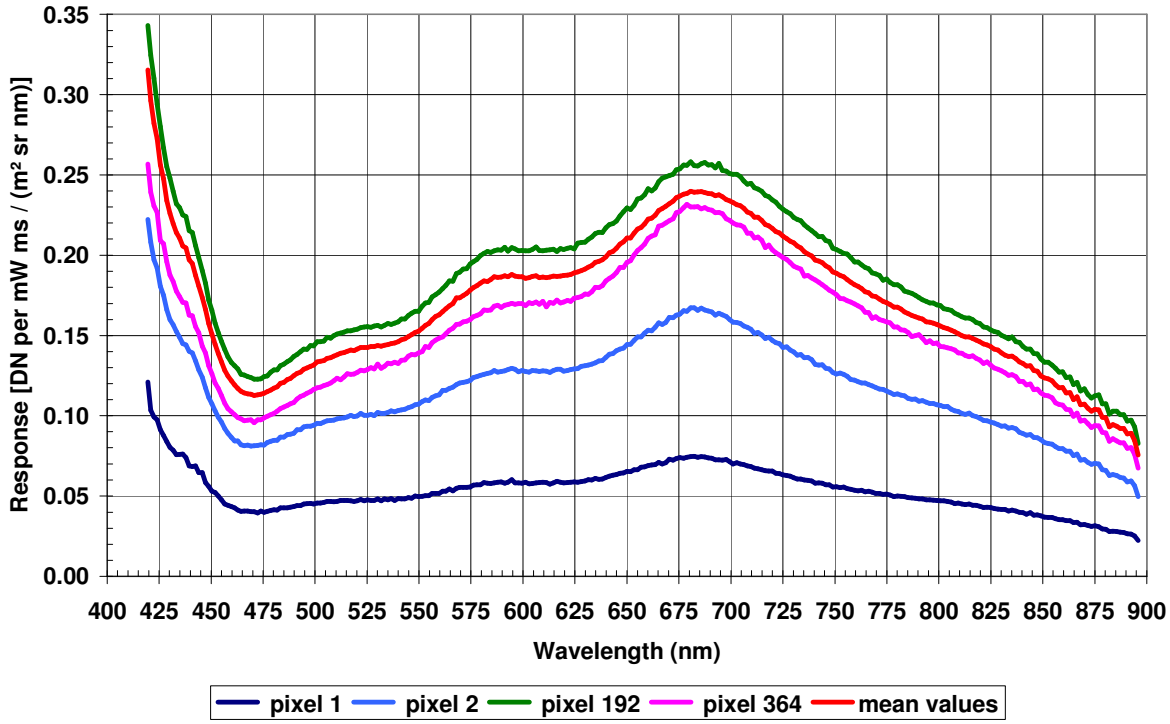

Figure 6.29: Radiometric responses of different spatial pixels and mean values of all spatial pixels

The sensitivity of a detector element depends on the wavelength and the spatial pixel. In Figure 6.30 the normalised signals of six selected channels are displayed. These are the results of measurement f) of Table 6.25.

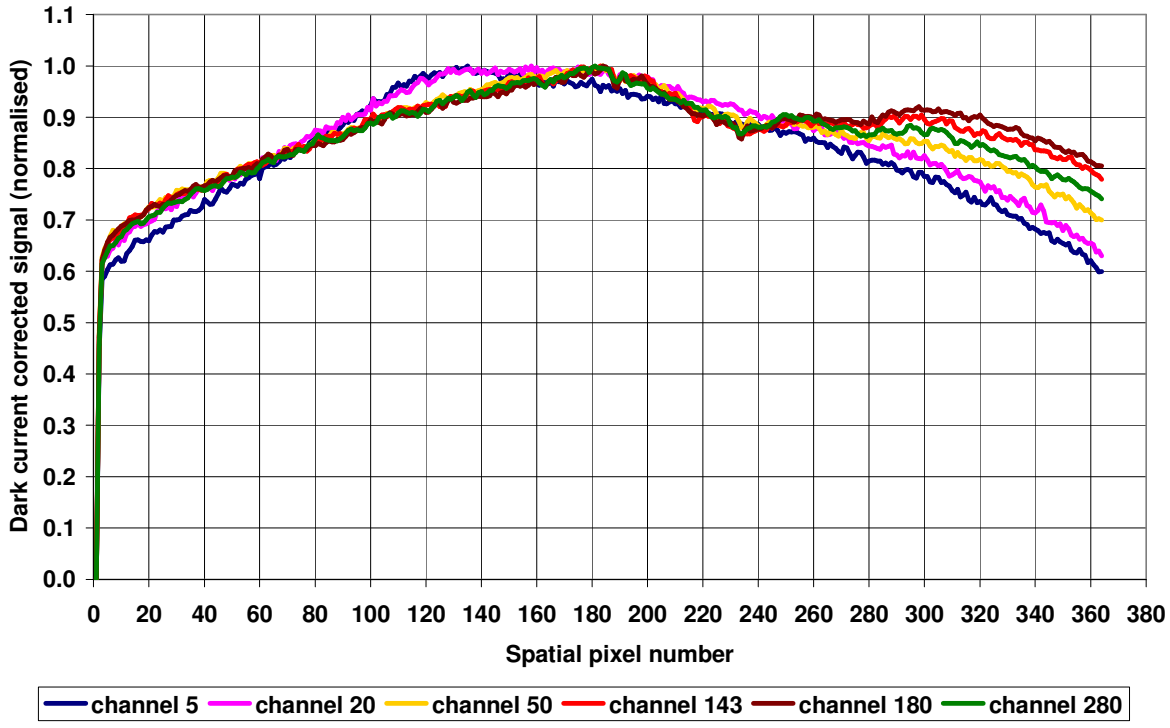

Figure 6.30: Pixel dependency of relative responses of selected channels

The normalised signals vary between the spatial pixels of the different channels. The characteristics of the curves are different.

The signals of the first spatial pixel are 50 % less than those of pixel 2. The spatial pixel of channel 5 with the maximum value is pixel 135 and for channel 20 it is pixel number 158. For the other channels the peaks are around the spatial pixel number 183. The curves of channel 50, 143, 180 and 280 show a local minimum at pixel 235.

In addition to the radiometric response function a flat-field image of measurement b) was created. Figure 6.31 shows the normalised dark current corrected signals for each channel and each spatial pixel.

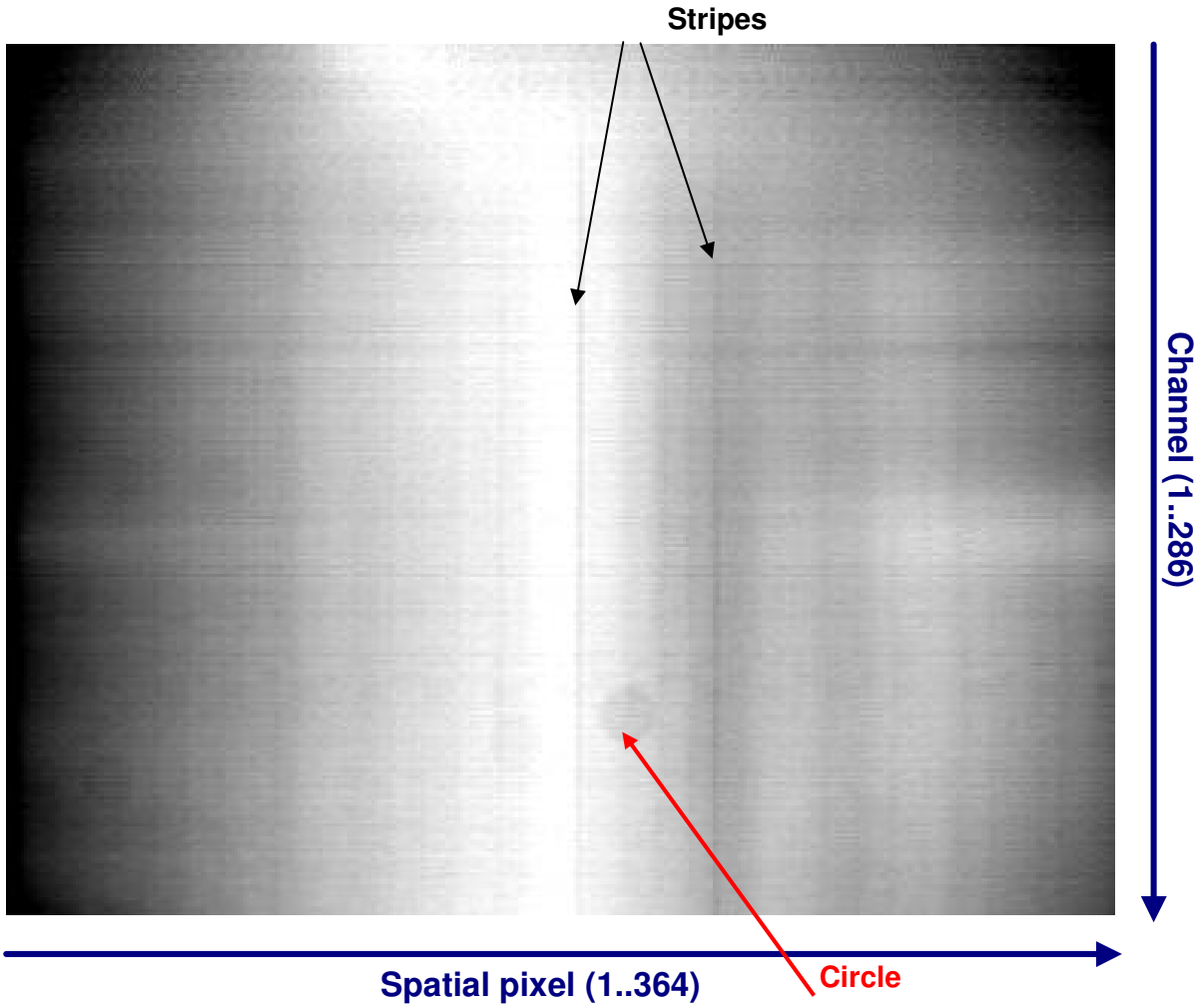

Figure 6.31: AISA "flat-field" image

The image shows horizontal and vertical stripes and circles as well as the brightness variations between the centre and the borders. At the middle of the top a bright spot can be seen.

6.5.2 Integration time linearity

Six measurements series were executed to check the signal linearity with the increase of the integration time of the AISA sensor. The different integration times are in the range between 260 ms and 500 ms (see Table 6.25). All measurements were performed using the calibrated small integrated sphere. The values of the fixed measurement parameter are listed in Table 6.24.

For the verification of the linearity of the signal with the integration time the recorded signals were normalised to one millisecond. The dark current corrected data are divided by the integration time. The normalised signals for the six integration times for the centre pixel and all channels are shown in Figure 6.32. The maximum values vary between 5.79 DN/ms for the integration time of 260 ms and 5.91 DN/ms for the 500 ms measurement. The minimum value for all integration time measurements is 0.12 DN for one millisecond.

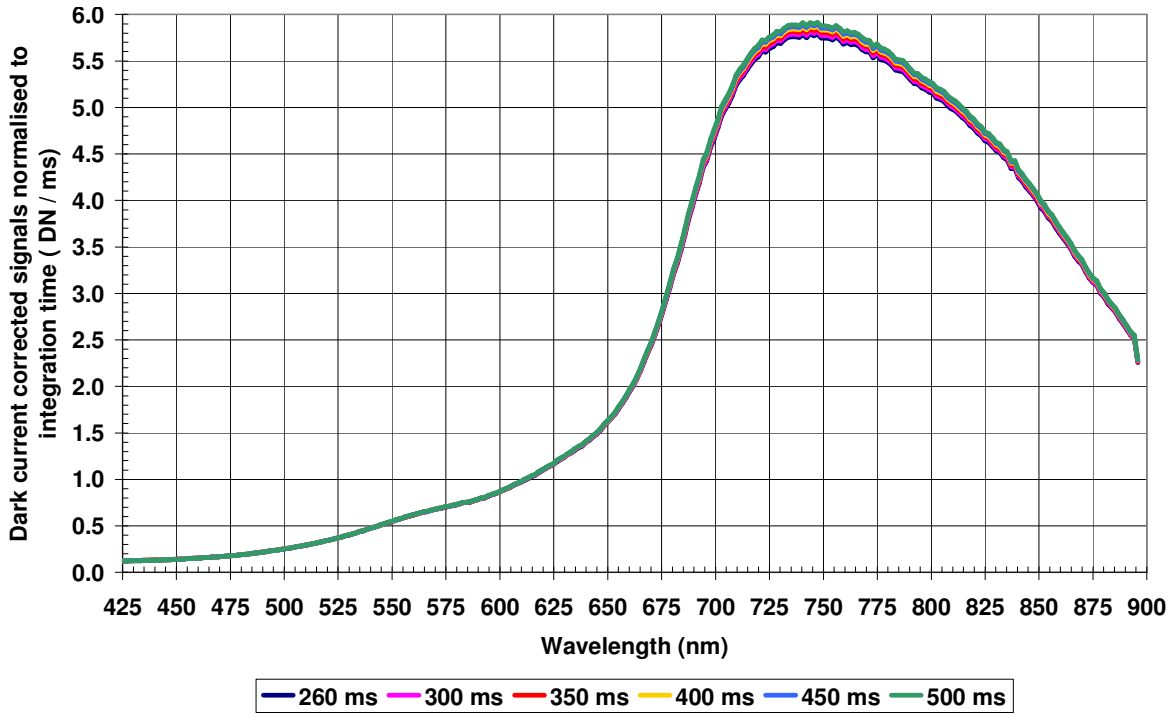

Figure 6.32: Normalised dark current corrected signals of pixel 192 for different integration times

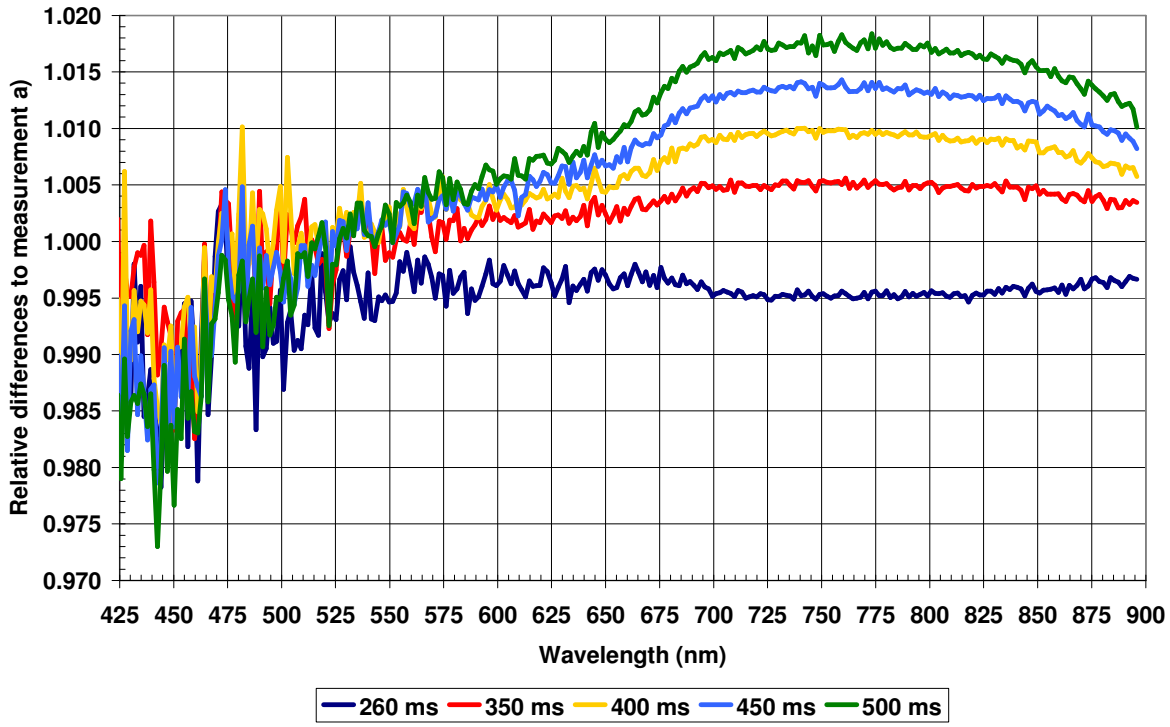

Figure 6.33: Relative differences between the varying integration time measurements normalised to measurement a) (260 ms)

Figure 6.33 shows the differences between the measurements normalised to measurement a) with the lowest integration time of 260 ms. Differences are visible in the wavelength range between 700 nm and 850 nm which are the channels with the higher responses (see Figure 6.32). The standard deviations are in the range from 0.0002 DN/ms to 0.0499 DN/ms.

6.5.3 Discussion

The radiometric responses curves for different spatial pixels (Figure 6.29) show a significant increase towards shorter wavelengths below 472 nm (channel 35). This may be an effect of the quantum efficiency of the silicon detector which decreases in this range. A bandpass filter often blocks radiation below 430 nm - this effect is probably caused by stray light. The responses of the channels higher than 700 nm continuously decrease. This could be an effect of the lower diffraction grating efficiencies. Typical absolute grating efficiencies of the wavelengths higher than 800 nm are between 35% and 45% (see App. A, Table A.2) compared with the efficiency from 70% to 75% for 600 nm [68]. The responses of the border pixels on the left and right side vary widely. The lower signals of the first border pixels (1 and 2) can be an effect of mechanical vignetting caused by obstructions (e. g. lens hood or filter frame). The signals of the spatial pixel on the right side of the FOV are higher than the signals of the pixels on the left side since the last pixel (364) is 20 pixels away from the “real” border of the CCD array detector size of 288 * 384.

A comparison of the dark current corrected signals of different channels for all spatial pixels shows signal distinctions (Figure 6.30) beside the light fall-off to the borders (Figure 6.31). Remarkable is a sink for the spatial pixels between 195 and 230 and the channels greater than 35 (472 nm). The cause hasn’t yet been established. The response curves for these channels are quite similar up to pixel 230. But the responses for the greater pixels vary. The signals and the curve shapes of the channels lower than 35 are really different to the other channels. Older measurement results, performed with the 23 mm lens, did not show a sink [102]. Therefore additional measurements and analyses should to be performed with the 23 mm lens to compare the results.

The responses of each spatial pixel and each channel illustrate a light fall-off from the centre to the borders of the FOV and artefacts (Figure 6.31). The light fall-off is caused by the mechanical vignetting (blocked light) and the natural vignetting ($\cos^4$ law). The vertical stripes in the image may be an indicator for a non uniform plain slit. The bright spot at the top of the image could be stray light. The different effects can be corrected by using correction values for each spatial pixel and each channel during the data processing from raw data into level 1 data.

Figure 6.32 and Figure 6.33 show differences between the six measurements particularly for the channel numbers above 113. These are the channels with the higher responses. Further measurements and analysis have to be performed in the future.

7 Conclusions

It has been the goal of this work to establish a process chain for the characterisation of hyperspectral sensors beginning with the definition of the measurement procedures, followed by the automatic execution of the measurements and the analysis of the recorded data. A substantial goal was the automation of the characterisation measurement process. For this an operational concept was developed. It groups the necessary steps into three scopes of functions: the control of the CHB devices (*Slave*); the execution of the measurements (*Master*); and the control of the sensor (*Sensor*). The subdivision of the modules and the definition of software interfaces for the modules enabled a parallel and independent development of the three modules. Furthermore the individual modules can be modified independently from each other. This was particularly for the CHB control module an advantage (*Slave*) during testing the software interface of APEX at an early stage. In addition the “emulation” mode of the *Slave* module was very helpful for the interface tests. The APEX sensor has been characterised several times in the CHB facility. Thus one of the essential aims of the laboratory automation is fulfilled.

Regarding the aim of automating the CHB, this has been shown to be possible and has subsequently been implemented (all devices can now be controlled automatically). The necessary manual interactions are limited to the switching on and off of the devices. An extension of the module with further devices is unproblematic. This was demonstrated with the implementation of an additional filter wheel of the monochromator. The currently implemented *Sensor* modules are for AISA, ROSIS, ARES and the lock-in amplifier in combination with a photo diode (used for calibration of the monochromator). These examples show the usability of the sensor part of the operational concept.

The central part of the automatic execution of measurements is the *Master* module. It offers many additional options besides the execution of the measurements. For example the data transfer functions, the execution of programs or system commands both directly or in the background. In particular the possibility of executing programmes (e.g. raw data conversion) in the background function (parallel job) offers additional time saving potentialities.

The second main goal was the definition of generic measurement and analysis methods for spectral, geometric and radiometric characterisation for hyperspectral sensors. For each of the three measurement groups the measurement setups were described. The required devices and their parameters were defined. The defined sensor independent measurement methods have been successfully applied for the both test sensors. The various control commands for the different measuring tasks, consisting of settings for the CHB devices and the sensor, could be collected, and consequently it is now possible to perform the measuring sequences automatically. Measuring tasks over many hours have been executed without any problem and with only a few interactions of the CHB operator at the beginning of the measuring tasks.

The developed analysis procedures are generic after the conversion of the raw data into the generic data format (ENVI/IDL) since the raw data formats are sensor specific. The analysis procedures can be performed fully automatically due to their parameterisation. The *Master* records all sensor and laboratory device settings (e.g. sensor name, viewing angle) of the measurements which are necessary for the analysis procedures. Erroneous measurements caused by saturation, or incomplete measurements, can be easily identified on the basis of the analysis logs. The generated plots are useful for the recognition of artefacts. For each sensor three files were created which contain the analysis results of all spectral, geometric and radiometric measurements. The performed characterisation measurements and analyses for ROSIS and AISA showed the applicability of the sensor independent measurement and analysis methods.

Main accomplishments:

- A complete process chain has been established for the characterisation of hyperspectral sensors.
- The full automation of the CHB facility was implemented and the time effort to carry out the measurements decreases up to 50% depending on the measurement type. The manual interactions of the operator are reduced to a minimum (switching on and off of the devices, alignment of the sensor).
    - The *Master* and *Slave* software modules are expandable by the addition of new sensors and devices with minimal effort.
    - The *Master* module offers a high flexibility for the execution of most diverse characterisation measurements.
- Standard measurement and analysis methods for regular spectral, geometrical and radiometric characterisation for imaging spectrometers in the wavelength range from 0.4 µm up to 2.5 µm have been defined and were verified with two sensors (AISA and ROSIS).

Outlook

The planed upgrade of the ROSIS system (e.g. controlling system of the internal mirror, extension of the disk space, new graphic user interface) represents an improvement for future characterisation measurements. The following aspects should be considered for the design of future sensors: sufficient disk storage, a suitable graphical user interface and functions and features for a proper alignment of the sensor (e.g. alignment mirror) and possibilities for a direct data processing.

An important point for the future is an error estimation of the laboratory. The accuracies of the single devices in this thesis have been provided by the manufacturers. These have to be improved and further investigations on error propagation are planed for the future.

Acknowledgements

This work has been carried out with the support of scientist of DLR and from several other individuals which work at different institutions.

My special thanks go to Prof. Klaus I. Itten, supervising this work and Dr. Peter Gege for continuous support. Many thanks go also to Dr. Peter Haschberger, Jochen Fries, and Dr. Horst Schwarzer for additional feedback on this work. Special thanks go to Dr. Georg Wagner and Dr. Daniel Hoja for reading parts of the manuscript and motivation talks. I am grateful to Willem Vreeling supporting me with laboratory measurements. Sincere thanks also to the people from RSL for sharing knowledge and fruitful discussions, especially Francesco Dell'Endice. I thank all other people at DLR/IFM and temporarily present students for their contributions and the nice working ambience at the IFM.

Very special thanks are due to my husband and my mother for their encouragements and the facilitation to create this work.

It is impossible to prepare a complete list of all people contributing this work. Thank you all!

Appendices

Appendix A. Technical information

Optical Bench

Figure A.1 show the opening of the DLR universal adapter where a sensor can be mounted on. The flanges have hole pattern as Leica's PAV30 [106].

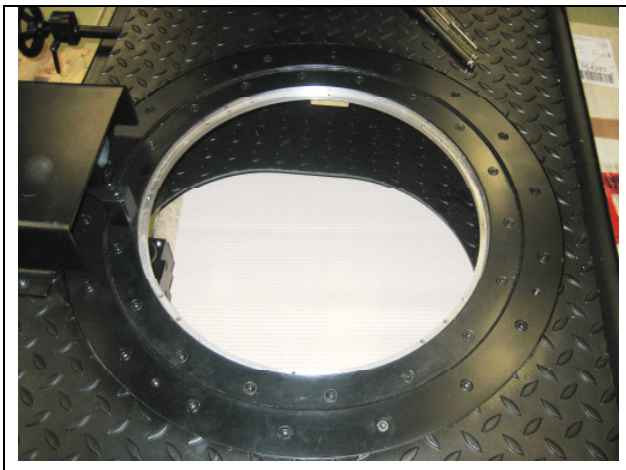

a) Maximum opening of 443 mm

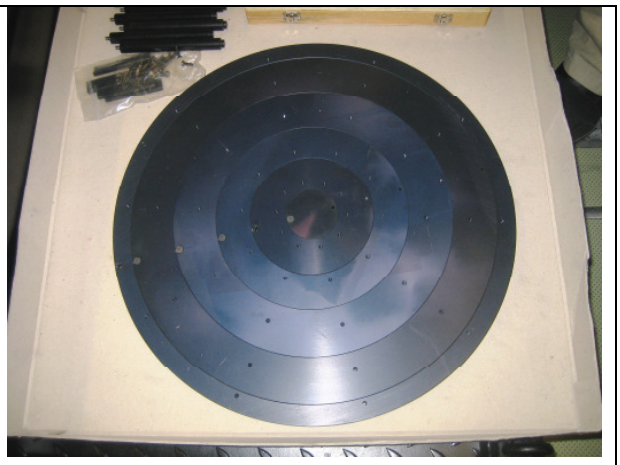

b) Adapter flanges

Figure A.1: DLR universal adapter with rings

Figure A.2 show technical drawings of the off-axis parabolic mirror at the exit slit of the monochromator.

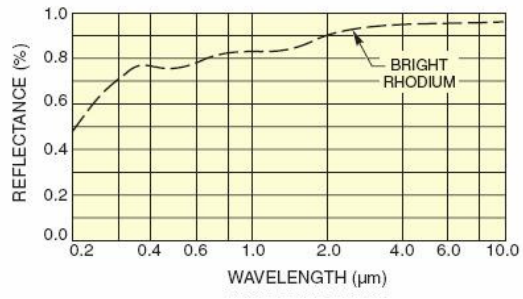

a) Reflectance of bright rhodium

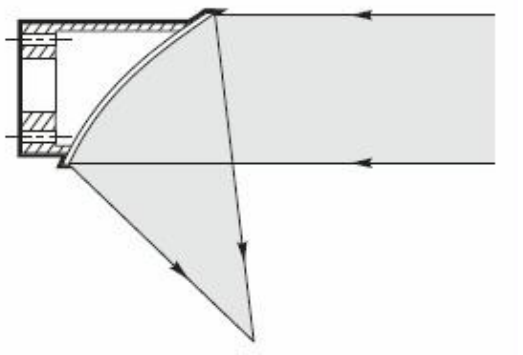

b) Reflection of an off-axis paraboloidal

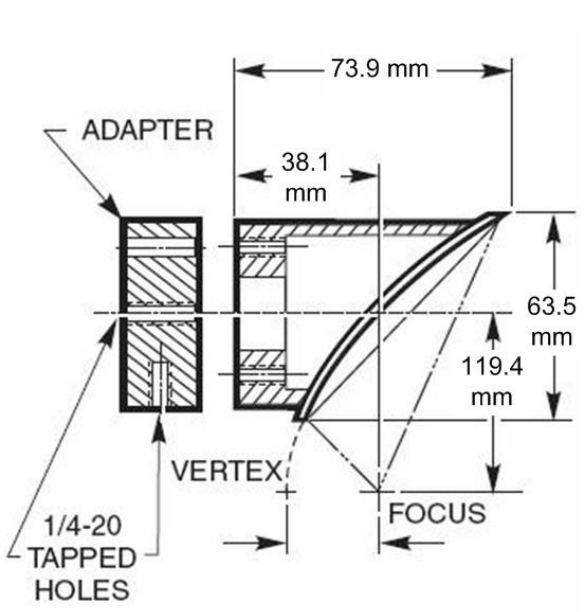

c) Off-axis parabolic mirror dimensions

Figure A.2: Off-axis paraboloidal reflector screens based on figures from [107]

Geometric measurement components

The layout of the vertical and horizontal slits on the slit wheel is illustrated in Figure A.3. The slits 1 to 3 are the vertical slits and slit 4 to 5 are the horizontal ones.

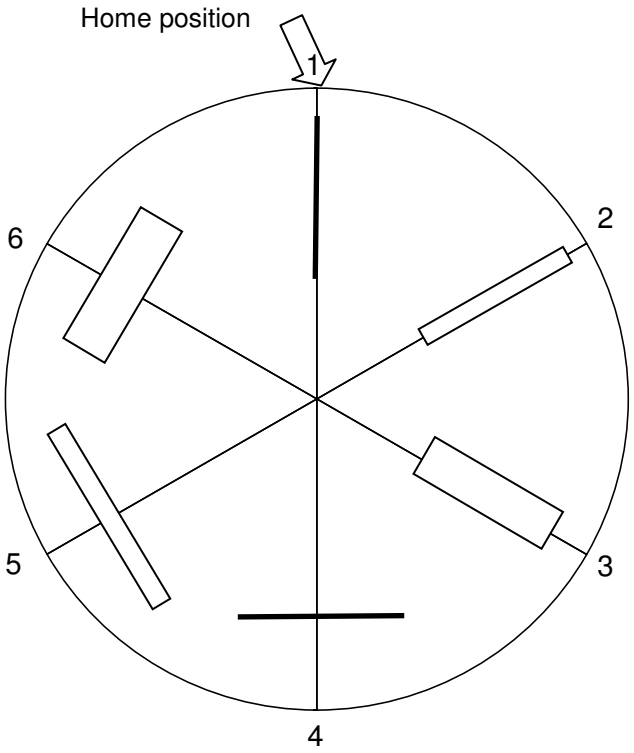

Figure A.3: Layout of the vertical and horizontal slits on the wheel [108]

Radiometric measurement components

The possible lamp combinations of the large integrating sphere are listed In Table A.1 and Figure A.4 shows the arrangement of the lamps in the large integrating sphere. Two power units operate two lamps (see lamp 8 and lamp18 as well as lamp 2 and lamp 10).

Table A.1: Lamp combinations of the large sphere

Combination no.	Complete wattage	Rack no.	Lamp no.	Lamp combination
1	**90**	2	**2, 10**	**2*45 W**
2	**135**	6, 2	**2,10,6**	**3*45 W**
3	**180**	2, 18	**2,10,8,18**	**4*45 W**
4	**200**	3, 11	**3,11**	**2*100 W**
5	**300**	3,11,17	**3,11,17**	**3*100 W**
6	**400**	3,7,11,17	**3,7,11,17**	**4*100 W**
7	**600**	1,9,14	**1, 9, 14**	**3*200 W**
8	**800**	1,9,11,14,17	**1, 9,11,14,17**	**3*200 W + 2*100 W**
9	**1000**	1,5, 9 ,11,14,17	**1, 5,9,11,14,17**	**4*200 W + 2*100 W**
10	**1200**	1,3 ,5 ,7,9,11,14,17	**1, 3, 5, 7, 9, 11, 14, 17**	**4*200 W + 4*100**
11	**1625**	1,2 ,3 ,5 ,6 ,7,9,11,12, 14,17,18	**1, 2, 3, 5, 6, 7, 8, 9, 10, 11, 12, 14, 17, 18**	**5*200 W + 4*100 W + 5*45 W**
12	**2025**	1,2,3,4,5,6,7,9,11,12, 13,14,17,18	**1, 2, 3, 4, 5, 6, 7, 8, 9, 10, 11, 12, 13, 14, 17, 18**	**7*200 W + 4*100 W + 5*45 W**

Appendix A

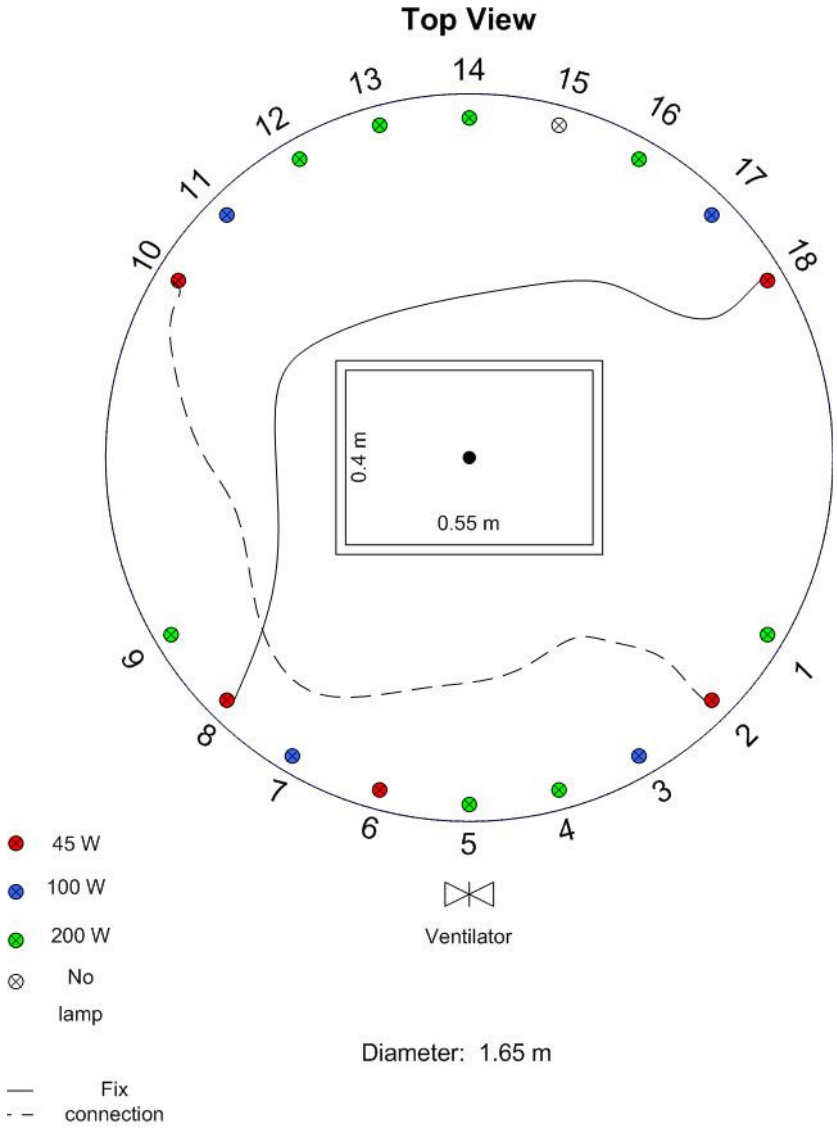

Figure A.4: Lamp arrangement of the large sphere

Small integrating sphere

Figure A.5 shows the radiance and the uncertainty of the small integrating sphere. The sphere was calibrated at PTB in November 2007. The uncertainty (U) is 1% in the wavelength range from 390 nm to 1700 nm. The uncertainty increases in the shorter and longer wavelength range (see top of Figure A.5).

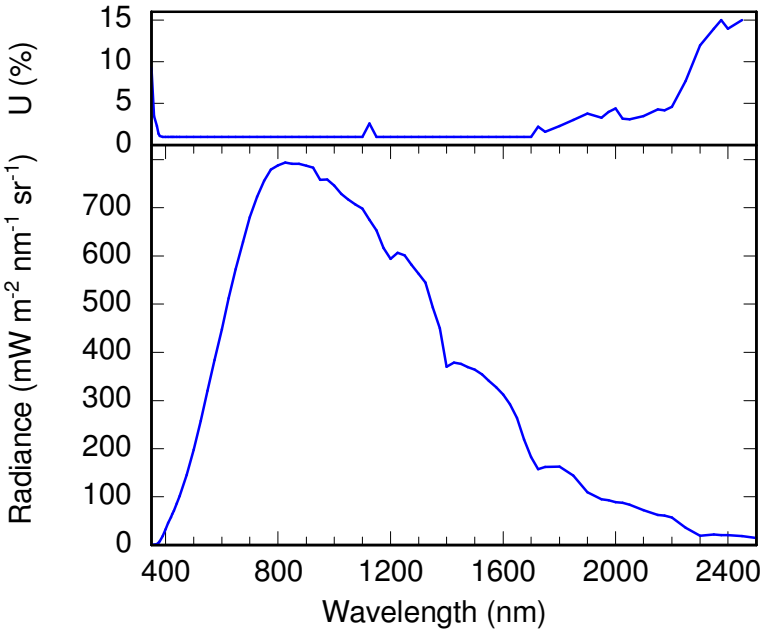

Figure A.5: Spectral radiance and uncertainty of the small sphere, calibrated in Nov. 2007 [34]

Table A.2: Absolute diffraction efficiencies of the gratings

Wavelength (nm)	**Absolute diffraction efficiencies (%)**
430	40 - 45
500	70 - 75
600	70 - 75
700	50
800	40 - 45
900	35 - 40

Appendix B. Additional Software Information

Table B.3: INI-files of the modules *Slave*, *Master* and *Sensor*

Module	Content
Slave	Network settings, hardware COM ports
	Environmental data thresholds, default values for the emulation mode
	Setup times for the different devices
	Monochromator correction equations
	Lamp combination list of the large sphere
	Speed of the axes of the folding mirror
Master	File names and name spaces of the different XML schemata
	File names of the different log files
	Network settings for the communication with the *Slave* module
	IDL settings
	Default parameter values for the different sensors
Sensor(s)	COM port, timeout and directory

Table B.4: Procedures used in the spectral characterisation analysis process

Name of the IDL procedure	Description
chbmo00_015_get_logs_data	Reads the measurement data and *Slave* and *Sensor* log data
chbmo00_008_read_slaveorsensordata: file:monochromator_settings.txt	Reads the monochromator wavelength calibration values
chbmo00_017_read_powermeter_measurements	Reads the monochromator output values
chbmo00_016_calculate_pixel_number	Calculate the spatial pixel number according to the viewing angle
chbm03_004_gaussfit	Gaussian function
chbm00_014_print_wmf	Print Gaussian curves of 5 channels

Table B.5: Procedures used in the geometric characterisation analysis process (across and along track LSF)

Name of the IDL procedure	Description
chbmo00_018_read_textfile input file: chbmo01_001_log.txt	Read analysis log template
chbmo00_015_get_logs_data	Reads the measurement data and *Slave* and *Sensor* log data
chbmo00_008_read_slaveorsensordata: file:slitwheel_settings.txt	Reads the collimator and slit wheel settings
chbmo03_002_get_environment_data	Read the laboratory ambient data
chbmo00_017_read_powermeter_measurements	Reads the monochromator output values
chbmo00_016_calculate_pixel_number	Calculate the spatial pixel number according to the viewing angle
chbm03_004_gaussfit	Gaussian function
chbm00_014_print_wmf	Print Gaussian curves of 5 channels

Table B.6: Procedures used in the radiometric characterisation analysis process

Name of the IDL procedure	Description
chbmo00_015_get_logs_data	Reads the measurement data and *Slave* and *Sensor* log data
chbmo00_008_read_slaveorsensordata	Reads the transmittance values of the neutral density filter
chbmo00_017_read_powermeter_measurements	Reads the monochromator output values
chbmo00_024_radiometric_dark_corrected_cube	Corrects the nadir measurement data by subtracting the dark current data and create a cube file
chbm03_004_gaussfit	Gaussian function
chbm00_014_print_wmf	Print Gaussian curves of 5 channels

Figure B.6 illustrates an example of the *Slave* software interface. The figure shows all names and data types of the relevant parameters of the "sensor" device group.

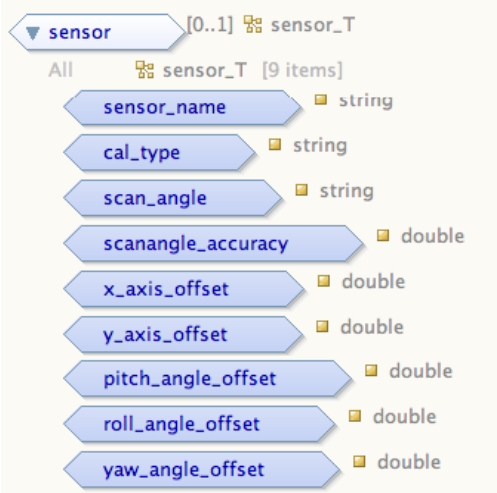

Figure B.6: Parameters and data types of the Slave interface group "sensor" ([55])

IDL functions

The IDL Gaussian function "GAUSSFIT" was modified by a return value for the status of the fit function. This value is used for error control. The used IDL function, implemented in IDL, is:

(B-1)

$$z = \frac{\lambda - A_1}{\sigma}$$

where

λ: wavelength (nm)

A_1: centre of the Gaussian function (nm)

σ: standard deviation of the Gaussian function (nm)

$$f(\lambda) = A_0 * \exp(\frac{-z^2}{2}) + A_3$$

(B-2)

where

λ : wavelength (nm)

A_0 : height of the Gaussian function (DN)

A_3 : constant term (DN)

Master module

The names, units and descriptions of the interface parameters of the Slave are listed in Table B.7.

Table B.7: Slave interface parameter list

Device group	Parameter	Units	Description
global	pressure	hPa	returns the air pressure
	temperature	°C	returns the temperature inside the laboratory
	humidity	%	returns the humidity inside the laboratory
	weathersta_updatetime	ms	measurement time cycle of the weather station
	ambient_light	lux	returns the ambient light
	amlight_updatetime	ms	measurement time cycle of the ambient light
	software_mode	-	auto=automatic, demo=demonstration
	light	-	room light status: 0=no light, 1 = light can be on
	comments	-	comments from the operator
	date	-	returns the date
	time	-	returns the time (local)
	measurement_time	sec	planned measurement time
	setup_time	sec	estimated time for the setup of the devices
	request_id	-	id of the current *Master* request
	status	-	returns the status of whole CHB hardware: 0=off, 1=on
	error_code	-	error code
	error_message	-	error message
sensor	sensor_name	-	specify sensor (AISA, ROSIS, APEX, …)
	cal_type	-	calibration mode: geo=geometrical, spec=spectral, rad=radiometric, pol=polarisation
	scan_angle	°	scan angle of the instrument
	scanangle_ accuracy	°	returns the scan angle accuracy
	x_axis_offset	°	x-axis difference between the home position of the mirror and the optical axis of the sensor
	y_axis_offset	°	y-difference between mirror home position and sensor optical axis
	pitch_angle_offset	°	pitch angle of the sensor relative to nadir
	roll_angle_offset	°	roll angle of the sensor relative to nadir
	yaw_angle_offset	°	yaw angle of the sensor relative to nadir

Device group	Parameter	Units	Description
folding mirror	height	mm	distance between folding mirror and sensor slit (altitude of entrance pupil)
	cal_mode	-	calibration mode: spec=spectral, geo=geometrical
	filterarm_angle	°	mounted filter: none=no filter, pol=polarisation filter
	filter_number		number of polarisation filter
	filter_orientation	°	orientation of the polarisation filter
	mirror_yposition	mm	y-position of the mirror relative to home position
	mirror_angle	°	angle of the mirror relative to nadir position
	status	-	returns the status of the folding mirror: 0=off, 1=on
	error_code	-	error code
	error_message	-	error message
Monochro-mator	turret	-	Returns the number of the turret
	lamp_source	-	lamp type
	lamp_voltage	V	settings power-supply of the lamp
	lamp_current	A	settings power-supply of the lamp
	shutter	-	shutter status: 0=close, 1=open
	wavelength	nm	wavelength
	filter_number	-	position of the filter in the wheel
	entrance_slit_type	-	entrance slit type: man=manual, mot=motorised
	entrance_slit_width	µm	entrance slit width in 2 µm steps
	entrance_slit_height	mm	entrance slit height 15 mm
	exit_slit_type	-	exit slit type: man=manual, mot=motorised
	exit_slit_width	µm	exit slit width
	exit_slit_height	mm	exit slit height, manual slit 1, 2, 4, 10
	exit_filter	-	position of the filter in the wheel
	grating	-	number of the grating
	lines	1/mm	returns the lines per mm
	blaze	nm	returns the blaze wavelength
	status	-	returns the status of the monochromator: 0=off, 1=on
	error_code	-	error code
	error_message	-	error message
collimator	slit_number	-	slit number
	slit_angle	°	angle of current slit relative to wheel home position
	lamp_source	-	lamp type
	lamp_voltage	V	settings power-supply of the lamp
	lamp_current	A	settings power-supply of the lamp
	input	-	input device (other can be e.g. photo diode)
	status	-	returns the status of the collimator: 0=off, 1=on
	error_code	-	error code
	error_message	-	error message
integrating sphere	diameter	m	diameter of the integrating sphere
	lamp_combination	-	See Table A.1
	filter_list	-	list of the used transmission filters
	lamp_list	-	list of the used lamps
	target	-	info about used reflectance target

Device group	Parameter	Units	Description
	diode_updatetime	ms	measurement time cycle for photodiode
	status	-	returns the status of the integrating sphere: 0=off, 1=on
	error_code	-	error code
	error_message	-	error message

Figure B.7 shows the GUI for sensor settings for the ROSIS sensor in the *Master* software. In general the IP address of the computer is necessary for the *Master* software, on which the sensor commodity offers its service. Each implemented sensor has its own dialog because every sensor has other settings. For example, AISA has a shutter that can be closed; ROSIS has no shutter but a specific mirror position for dark measurements. The *Master* software opens the necessary GUI of the selected sensor.

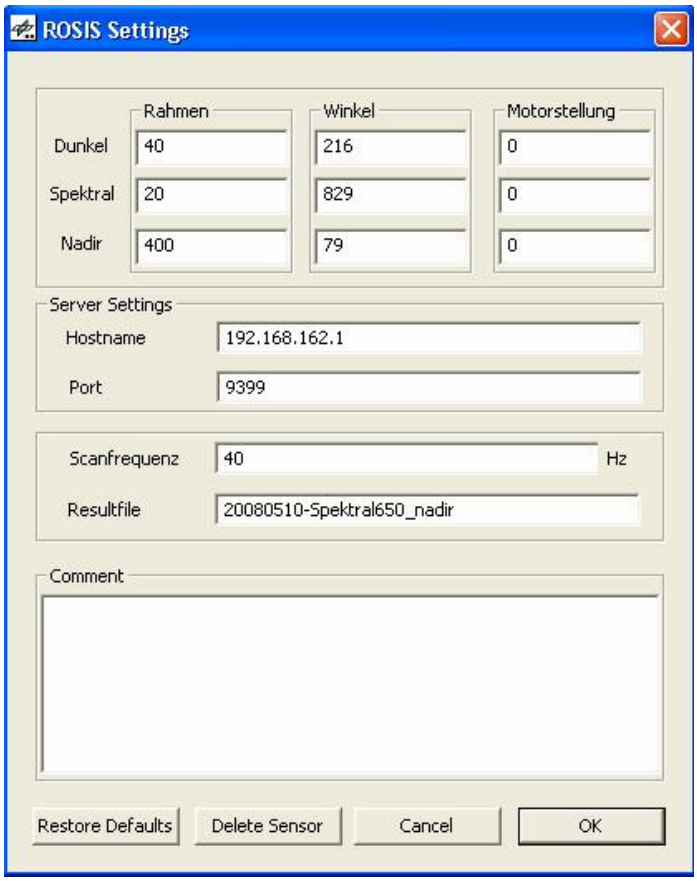

Figure B.7: ROSIS sensor configuration GUI

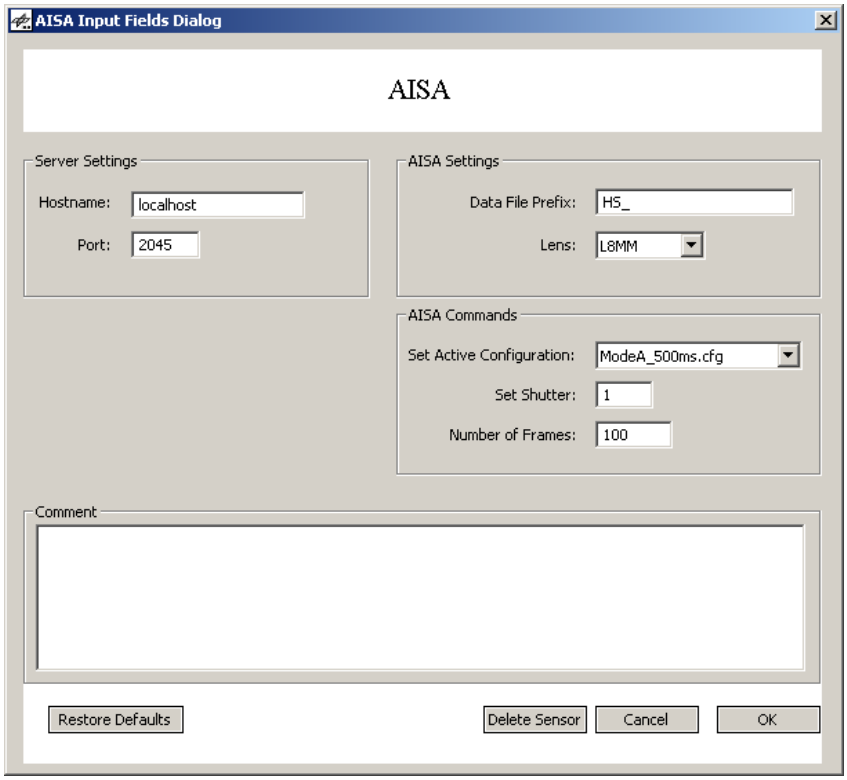

Figure B.8: AISA sensor configuration GUI

The dialog for the step action collection is shown in Figure B.9. It is possible to collect, to delete or to change actions. The order of the step actions can be changed with the "*Move up"* or "*Move down"* button on the right side by marking the chosen action. The flow sequence of the actions is thereby from top to bottom.

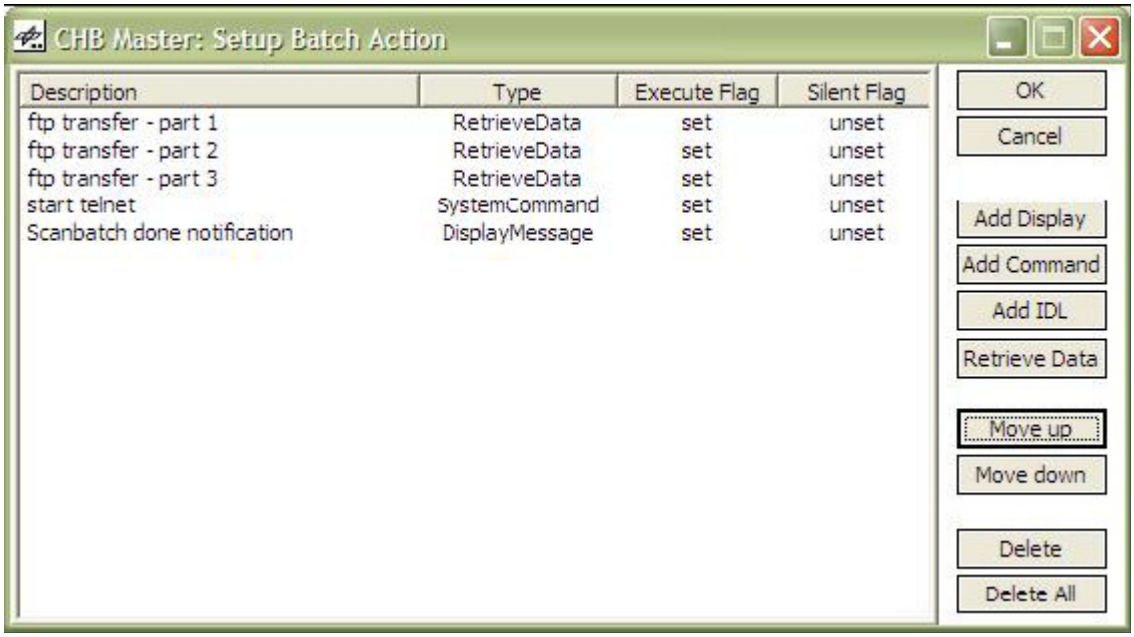

Figure B.9: *Master* Step Action GUI

Appendix B

Figure B.10: *Master* logging dialog

Figure B.11 illustrates the GUI for the selection and execution of measurements.

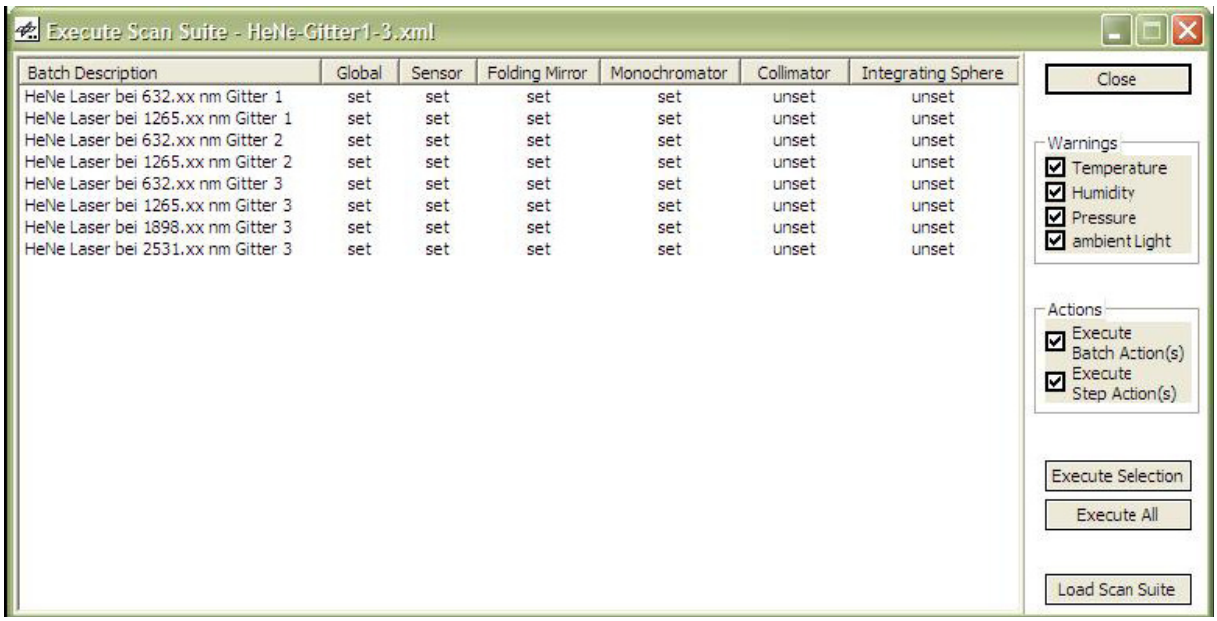

Figure B.11: *Master* GUI for the execution of measurements

The different data transfer possibilities of the sensor data in the *Master* module are listed in Table B.8.

Table B.8: Data transfer possibilities in the *Master* Software:

Local Copy	The copy command can be used if the *Sensor* and *Master* software runs on the same computer or if the data folder is shared on the sensor computer. Parameters of the copy command are the source and the destination path.
File Transfer Protocol (FTP)	If the *Sensor* and *Master* software are running on different PCs the recorded data can be copied with FTP. The *Master* uses the “GNU Wget [109]” program for the access and copy of data. Needed parameters are the user name and its password on the FTP server, the IP address and port number as well as the source path and destination path.
Hypertext Transfer Protocol (HTTP)	The *Master* software uses the existing “GNU Wget [109]” program for the data transfer. The needed parameters are the IP address of the sensor computer, the HTTP port number and the source and destination path.

Slave module

The content of the *Slave* observer function is shown in Figure B.12. The web page is divided into three parts. The left side comprises the requested device settings and the right side contains the current settings of the devices as well as error information. The frame at the bottom shows the current messages for the operator.

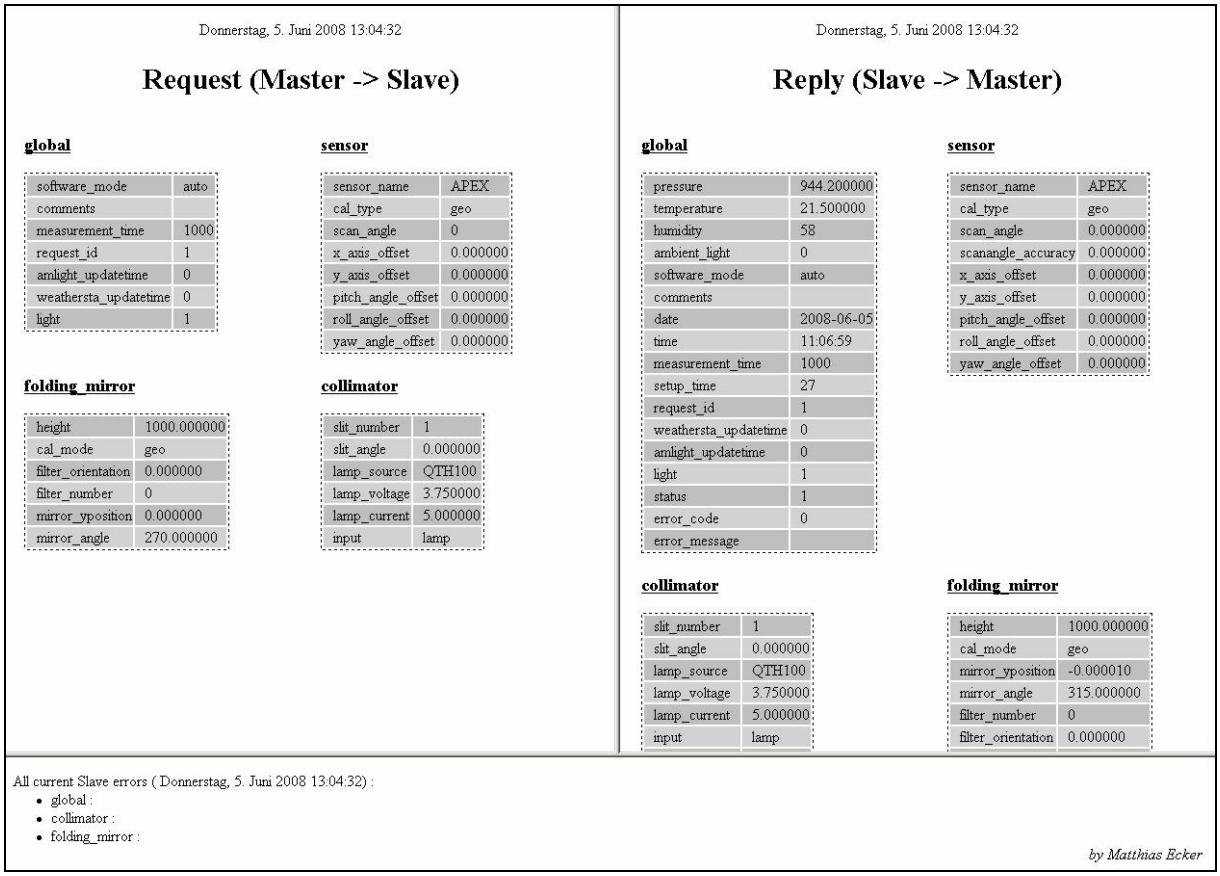

Figure B.12: Content of the web page of the *Slave* Observer

Figure B.13 illustrates the GUI for the monitoring of the environmental data. The monitoring can be switched on as well as the alert function for the illuminance meter and weather station.

Appendix B

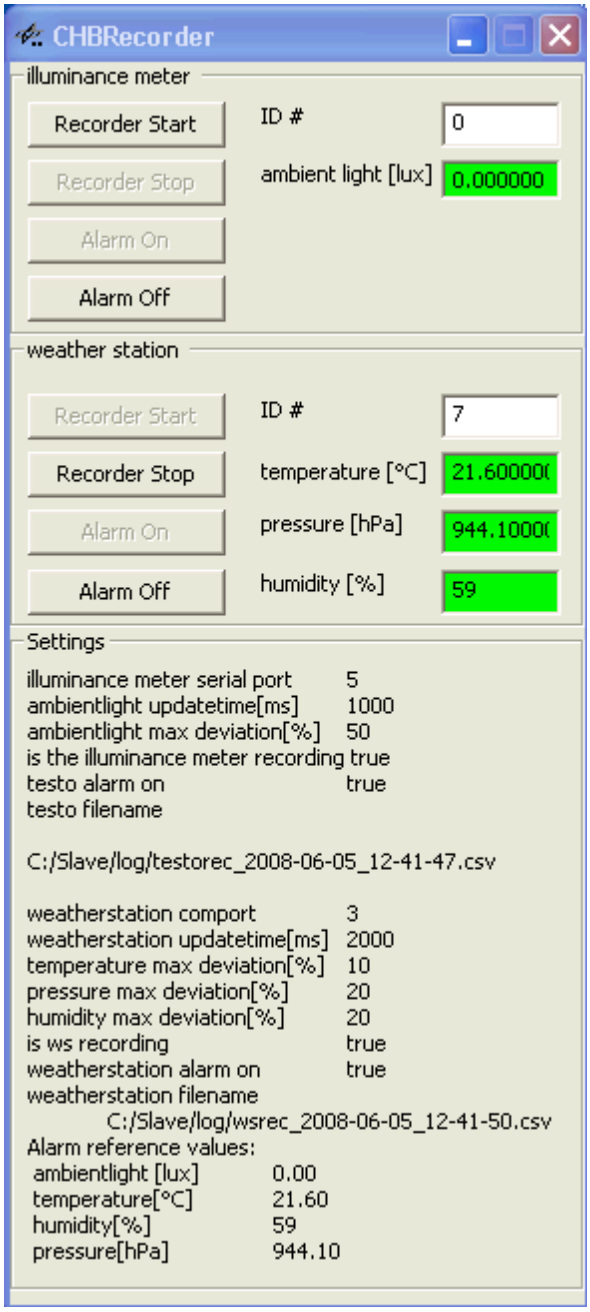

Figure B.13: Monitoring of the environmental data

Appendix C. Analysis Results

Table C.9 contains the wavelength calibration values of the monochromator. The values were determined for the gratings of turret 2 during the monochromator calibration in March 2008 [110].

Table C.9: Monochromator calibration values for the gratings of turret 2 (calibrated 2008-03-26)

Grating no.	Offset (nm)	Gain	Standard deviation (nm)
1	-0.08105	$3.3227 \cdot 10^{-4}$	0.142
2	-0.23935	$1.9384 \cdot 10^{-4}$	0.105
3	0.35757	$-1.2918 \cdot 10^{-4}$	0.077

Geometric Characterisation Results

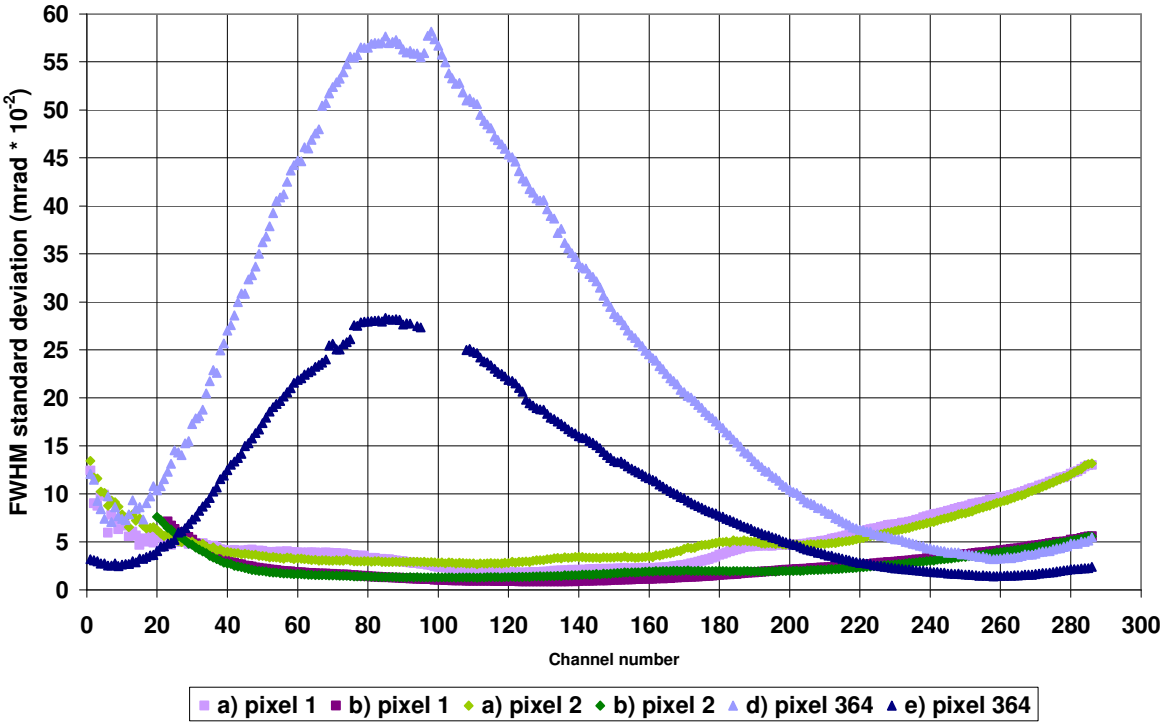

Figure C.14: Standard deviation of the FWHM values of the different measurements and pixels

Appendix C

AISA across track LSF measurement results

Table C.10 contains the across track measurement results for AISA at nine spatial positions (see chapter 6.4.2).

Table C.10: AISA across track LSF measurement results of channel 250 and different spatial pixels

Pixel number	Viewing angle (°)	FWHM (°)	FWHM (mrad)	Sampling distance (°)
1	25.745	0.192	3.351	
2	25.668	0.258	4.503	0.077
3	25.559	0.303	5.288	0.109
72	16.527	0.276	4.817	
73	16.391	0.273	4.765	0.136
113	10.930	0.278	4.852	
114	10.793	0.273	4.765	0.137
152	5.520	0.277	4.835	
153	5.379	0.274	4.782	0.141
191	0.068	0.289	5.044	
192	-0.072	0.283	4.939	0.140
230	-5.388	0.271	4.730	
231	-5.526	0.269	4.695	0.138
269	-10.777	0.259	4.520	
270	-10.913	0.258	4.503	0.136
310	-16.357	0.281	4.904	
311	-16.493	0.277	4.835	0.136
362	-23.154	0.284	4.957	
363	-23.281	0.282	4.922	0.127
364	-23.407	0.280	4.887	0.126

The following figure contains the AISA FWHM standard deviations for four spatial pixel and all channels consistent to the viewing angles plotted in Figure 6.22.

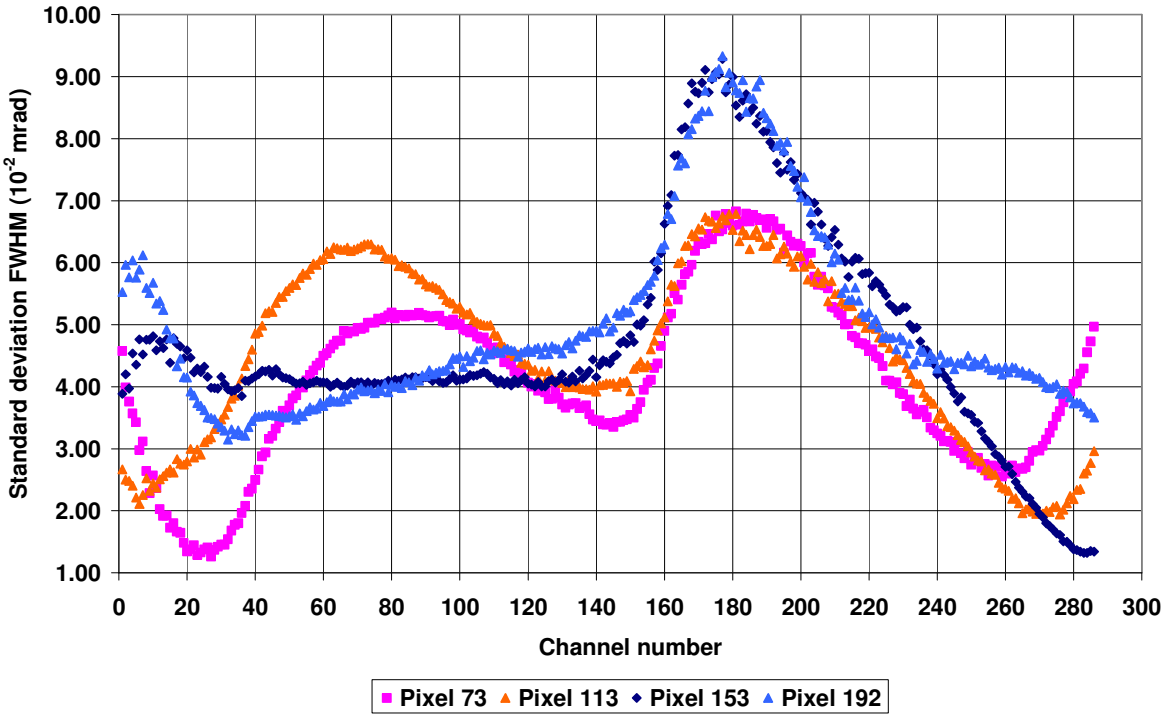

Figure C.15: AISA standard deviation for FWHM of the across track LSF for several pixels

The following picture is an exemplary measurement result of pixel 153 and channel 196.

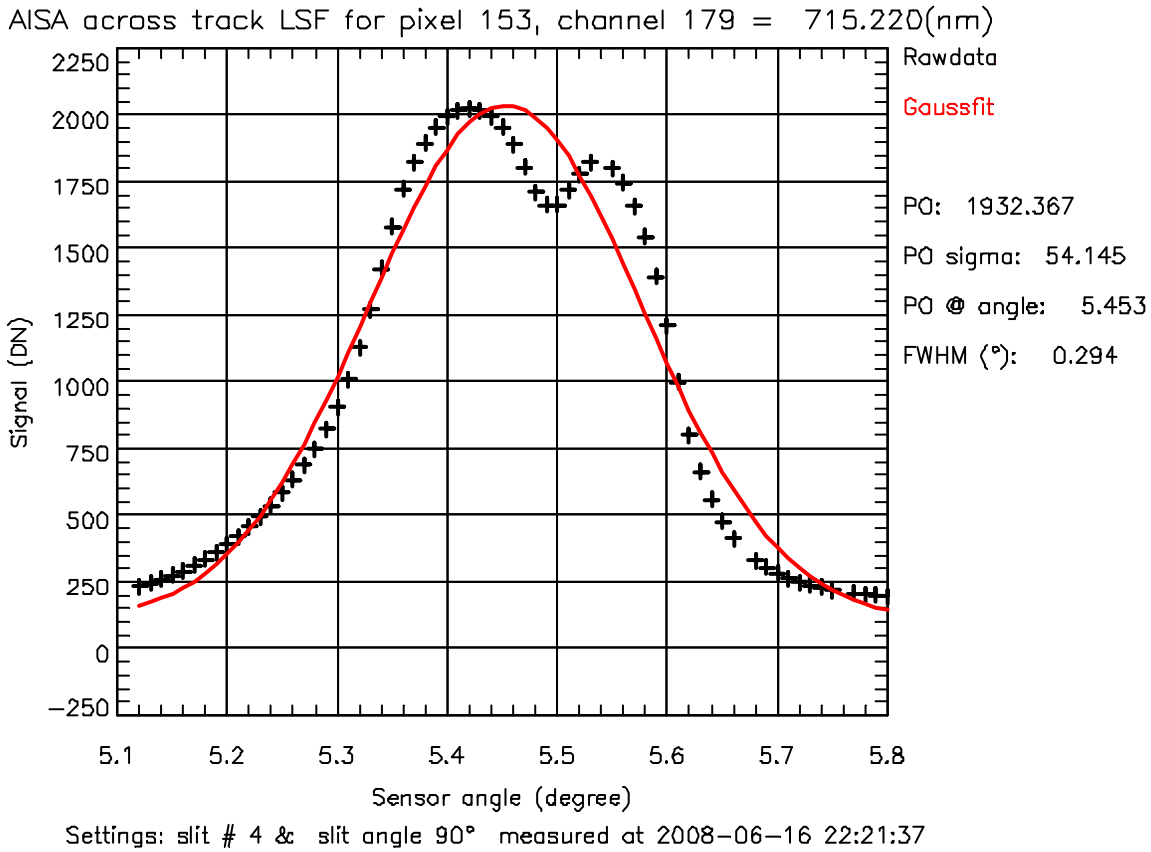

Figure C.16: AISA across track LSF measurement result of pixel 153 and channel 179

Appendix C

Spectral Characterisation Results

Figure C.17 illustrates the analysis results of measurement number 1 of Table 6.7 of AISA. The difference between the centre wavelengths of the intensity corrected (419.766 nm) and non intensity corrected (419.773 nm) is 0.007 nm. The FWHM values are 1.528 nm (uncorrected) and 1.579 nm for the intensity corrected.

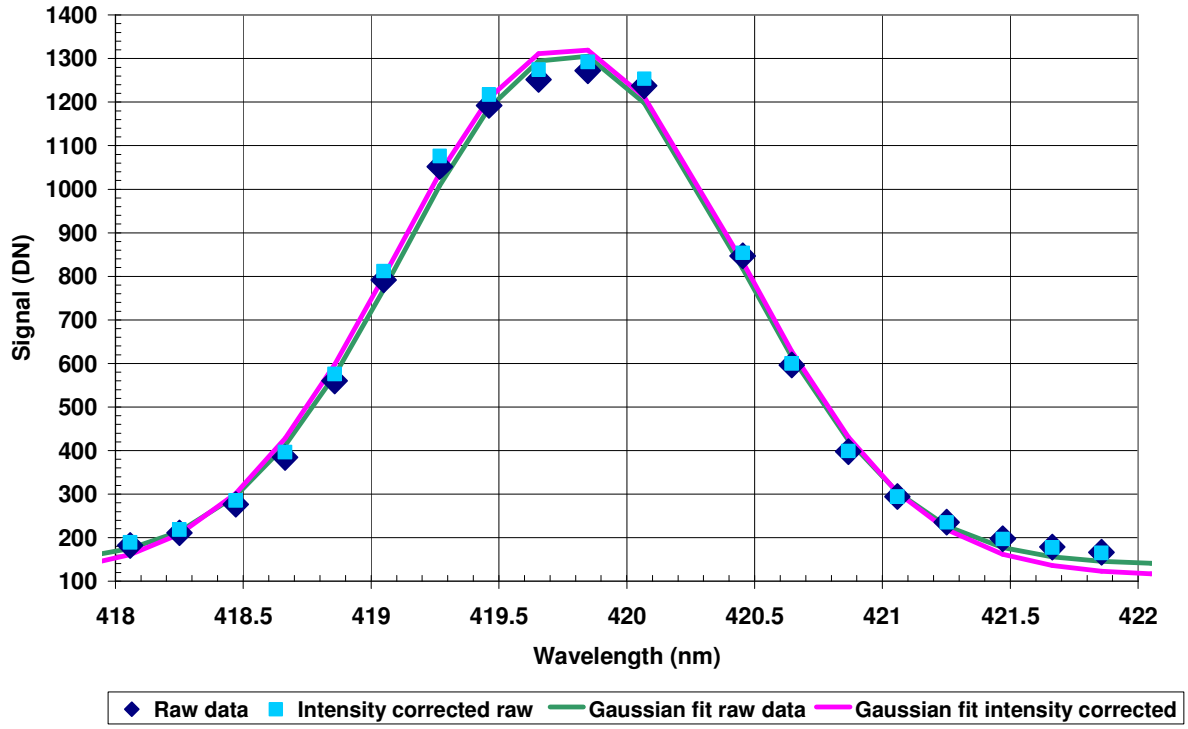

Figure C.17: Comparison of channel 1 none corrected and intensity corrected data of AISA (pixel 192)

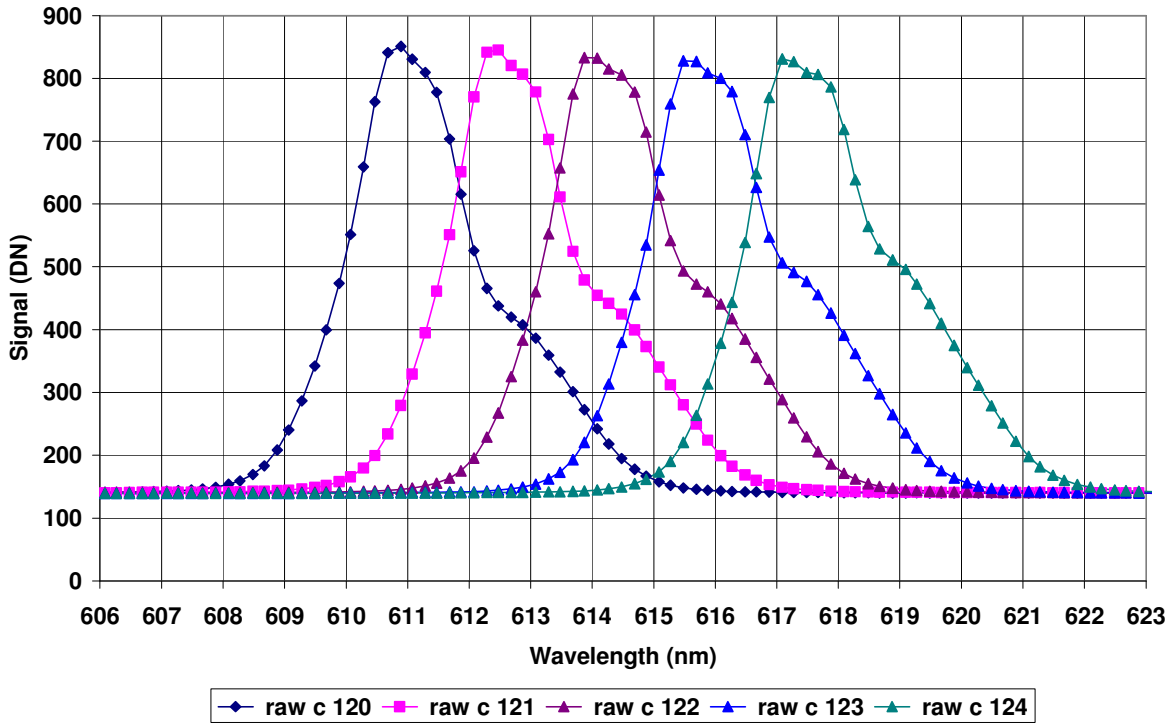

Figure C.18: Recorded data of the AISA nadir pixel for the channels 120 to 124 (measurement e))

Table C.11: Results of the spectral characterisation of channel 1 to 35 at nadir position of AISA

Channel #	Centre wavelength (nm)	FWHM (nm)	Std. dev Centre wavelength (nm)	Std. dev FWHM (nm)	Offset (DN)	Sampling distance (nm)	Overlap (%)
1	419.773	1.528	0.002	0.002	138	-	-
2	421.240	1.521	0.002	0.002	139	1.467	1.9
3	422.706	1.517	0.002	0.002	139	1.466	1.8
4	424.171	1.519	0.002	0.002	139	1.465	1.8
5	425.647	1.543	0.002	0.002	139	1.476	1.8
6	427.144	1.575	0.002	0.002	139	1.497	2.0
7	428.653	1.602	0.002	0.002	139	1.509	2.6
8	430.180	1.642	0.002	0.002	139	1.527	3.0
9	431.716	1.677	0.002	0.002	139	1.537	3.8
10	433.251	1.684	0.001	0.002	139	1.535	4.5
11	434.791	1.737	0.001	0.001	139	1.540	5.3
12	436.351	1.799	0.002	0.002	140	1.560	6.2
13	437.923	1.855	0.001	0.001	139	1.572	7.5
14	439.515	1.873	0.001	0.001	140	1.592	7.9
15	441.088	1.883	0.001	0.001	139	1.573	8.8
16	442.639	1.895	0.001	0.001	140	1.551	9.8
17	444.181	1.923	0.001	0.001	139	1.541	10.6
18	445.719	1.954	0.001	0.001	140	1.538	11.5
19	447.243	1.967	0.001	0.001	139	1.524	12.5
20	448.761	1.988	0.001	0.001	140	1.518	13.2
21	450.272	2.016	0.001	0.001	139	1.511	14.0
22	451.783	2.064	0.001	0.001	139	1.511	14.9
23	453.314	2.126	0.001	0.001	139	1.532	15.5
24	454.861	2.193	0.001	0.001	140	1.547	16.5
25	456.430	2.245	0.001	0.001	140	1.570	17.1
26	458.010	2.290	0.001	0.001	140	1.579	17.9
27	459.587	2.320	0.001	0.001	139	1.577	18.7
28	461.169	2.358	0.001	0.001	139	1.582	19.3
29	462.761	2.403	0.001	0.001	140	1.592	19.8
30	464.374	2.459	0.001	0.001	140	1.613	20.2
31	465.993	2.506	0.001	0.001	139	1.619	21.1
32	467.604	2.516	0.001	0.001	139	1.611	21.8
33	469.202	2.505	0.001	0.001	139	1.598	22.2
34	470.787	2.519	0.001	0.001	139	1.585	22.6
35	472.369	2.528	0.001	0.001	139	1.582	22.9

Appendix C

Table C.12: AISA centre wavelengths and FWHM of the channels 79, 80 and 81 of seven spatial pixels

	Channel no.	Spatial pixel number						
		74	114	153	192	231	270	309
Centre wavelength (nm)	79	544.7	544.1	543.6	543.4	543.5	543.7	544.8
	80	546.4	545.8	545.3	545.1	545.2	545.4	546.5
	81	548.0	547.4	547.0	546.8	546.9	547.0	548.2
FWHM (nm)	79	3.50	3.32	3.33	3.42	3.48	3.98	4.74
	80	3.51	3.29	3.30	3.44	3.50	4.00	4.80
	81	3.51	3.34	3.32	3.39	3.50	3.98	4.74

Table C.13: AISA measurement date, measuring time, number of data points for the spectral characterisation measurements of Table 6.7

	Measurement date	Duration (hh:mm)	Duration (min.)	Number of data points	sec/100 frames for one data point
a	2008-03-19	5:50	350	501	42
b	2008-03-20	1:36	96	151	38
c	2008-03-18	3:00	180	250	43
d	2008-03-25	2:45	165	225	44
e	2008-03-17	4:43	283	350	49
f	2008-03-13	1:40	100	150	40
g	2008-03-13	0:40	40	62	39
h	2008-03-13	6:35	395	538	44
i	2008-03-14	4:40	280	350	48
j	2008-03-17	2:15	135	200	41
Total		**33:44**	**2024**	**2777**	**43**

Table C.14: AISA measurement date, measuring time, number of data points for the spectral characterisation measurements of Table 6.14

	Measurement date	Duration (hh:mm)	Duration (min.)	Number of data points	sec/100 frames for one data point
a	2008-06-23	00:40	40	60	40.0
b	2008-06-23	00:39	39	60	39.0
c	2008-06-23	00:40	40	60	40.0
d	2008-06-23	00:39	39	60	39.0
e	2008-06-24	00:40	40	60	40.0
f	2008-06-24	00:39	39	60	39.0
g	2008-06-24	00:39	39	60	39.0
Total		**04:36**	**276**	**420**	**39.4**

Table C.15: ROSIS measurement date, measuring time, number of data points of the spectral characterisation measurements of Table 6.12

	Measurement date	Duration (hh:mm)	Duration (min.)	Number of data points	sec / 100 frames	sec / 500 frames
a	2008-09-11	00:15	15	31	5.8	29.0
b	2008-09-15	00:08	8	17	5.6	28.2
c	2008-09-15	00:18	18	38	5.7	28.4
d	2008-09-16	00:04	4	17	2.8	14.1
e	2008-09-17	00:20	20	45	2.7	13.3

Table C.16: ROSIS analysis results of measurement c) and e) for different spatial pixels and channels

	Pixel number	Channel number	Centre wavelength (nm)	σ (nm)	FWHM (nm)	σ (nm)	Spectral sampling interval (nm)
c	18	27	493.845	0.023	5.221	0.025	—
		28	497.898	0.021	5.168	0.023	4.053
		29	501.872	0.021	5.043	0.023	3.974
		30	505.767	0.023	4.974	0.025	3.895
e	259	80	696.312	0.041	6.796	0.051	—
		81	700.555	0.039	6.950	0.052	4.243
		82	704.838	0.036	7.121	0.046	4.283

Radiometric Measurements Results

Transmittance (see Figure C.19) of the 64 fold filter measured with the two-beam spectrometer Varian CARY-1. With this spectrometer the transmittance in the wavelength range from 190 nm to 900 nm with 1 nm resolution can be determined by comparing the reference beam with the measurement beam [102]. The measurements are performed in October 2005. An increase of the signal noise is remarkable for wavelength higher than 850 nm.

Appendix C

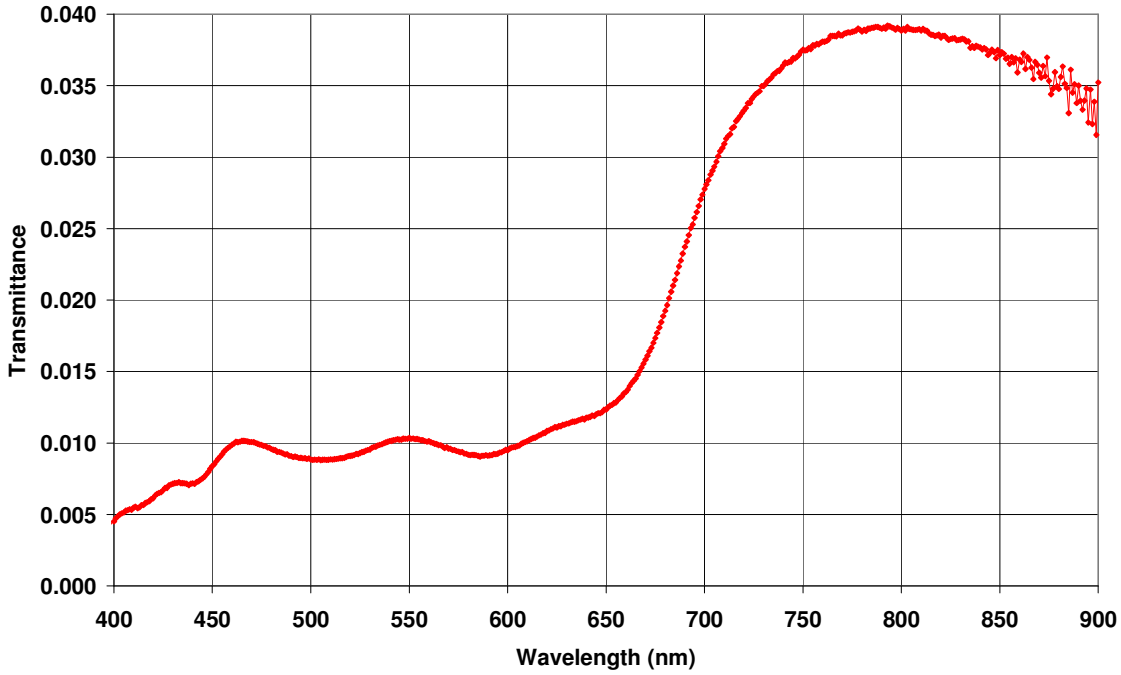

Figure C.19: Transmittance of the AISA 64-fold filter

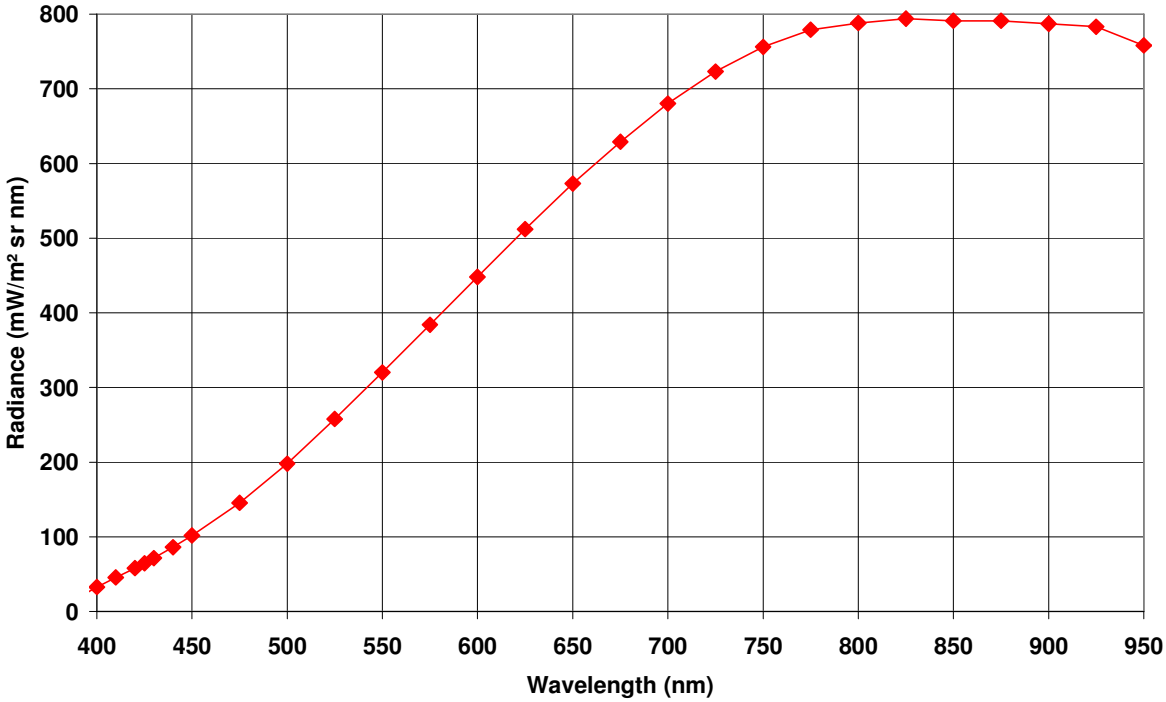

Figure C.20: Spectral radiance of small integrating sphere

References

1. S. A. Morain and A.M. Budge, Eds., *Post-Launch Calibration of Satellite Sensors*, *Proc. of the International Workshop on Radiometric and Geometric Calibration, 2-5 December 2003, Gulfport, Mississippi, USA*, ISPRS Book Series, Vol. 2. Leiden, London, New York, Philadelphia, Singapore: A. A. Balkema Publishers, 2004.
2. P.M. Teillet et al., "Importance of Data Standardization for Generating High Quality Earth Observation Products for Natural Resource Management," *Canada Centre for Remote Sensing – Earth Sciences Sector*, Oct. 2004. [Online]. Available: http://wgcv.ceos.org/docs/ceos/CCRS-Cal-Impact-Report-2004.pdf. [Accessed: 2008-11-20].
3. Committee on Earth Observation Satelittes (CEOS), "Working Group on Calibration and Validation," 2009. [Online]. Available: http://www.ceos.org/index.php?option=com_content&view=category&layout=blog&id=75&Itemid=116. [Accessed: 2009-12-05].
4. P. Strobl, P. Schötz, H.-R. Böhl, and J. Fries, Jochen, "Calibration of Airborne Optical Sensors at DLR - Facilities and Methods," in *Proc. of the 3rd EARSeL Workshop on Imaging Spectroscopy*, Herrsching, Germany, 13-16 May, 2003, pp. 36–49.
5. J. B. Campbell, *Introduction to Remote Sensing*, 2nd ed. New York: Guilford Press, 1996.
6. R. K. Vincent, *Fundamentals of Geological and Environmental Remote Sensing*. Upper Saddle River, New Jersey: Prentice Hall, 1997, pp. 84-95.
7. European Space Agency (ESA) – Earthnet Online, "PROBA," 2008. [Online]. Available: http://earth.esa.int/missions/thirdpartymission/proba.html. [Accessed: 2008-10-05].
8. F. Lehmann et al., "The Digital Airborne Imaging Spectrometer DAIS 7915, Hyperspectral Applications with a New Sensor," in *Proc. of ISSSR* ,1995, CD-ROM.
9. P. Strobl, "Entwicklung von Verfahren zur Datenaufbereitung und Kalibrierung eines abbildenden Spektrometers am Beispiel des DAIS 7915," Ph.D. dissertation, University of Potsdam, Potsdam, Germany, Scientific Technical Report STR00/12, 2000.
10. P. Strobl, A. Müller, D. Schläpfer, and M. E. Schaepman, "Laboratory calibration and inflight validation of the Digital Airborne Imaging Spectrometer DAIS 7915," in *Proc. of SPIE*, vol. 3071, 1997, pp. 225-236.
11. R. Müller and D. Oertel, "Laboratory Calibration of DAIS-7915 for Systematic Data Correction," German Aerospace Center (DLR): Weßling, Germany, Rep. DLR IB 552-5/95, 1995.
12. T. Cocks, S. Jenssen, R. A. Stewart, I. Wilson, and T. Shields, "The HyMap airborne hyperspectral sensor: the system, calibration and performance," in *Proc. of the 1st EARSeL Workshop on Imaging Spectroscopy*, Zurich, Switzerland, 6-8 October,1998, pp. 37–43.

References

13. B. Kunkel, F. Bechlinger, D. Viehmann, H. van der Piepen, and R. Doerffer, “ROSIS iaging spectrometer and its potential for ocean parameter measurements (airborne and spaceborne),” *International Journal of Remote Sensing (IJRS)*, vol. 12, iss. 4, pp. 753-761, 1991.
14. P. Gege, D. Beran, W. Mooshuber, J. Schulz, and H. van der Piepen, „System analysis and performance of the new version of the imaging spectrometer ROSIS,” in *Proc. of the 1st EARSeL Workshop on Imaging Spectroscopy*, Zurich, Switzerland, 6-8 October,1998, pp. 29–35.
15. M. Riedmann, “Laboratory Calibration of the Compact Airborne Spectrographic Imager (CASI-2)”, 2003. [Online]. Available: http://www.soton.ac.uk/%7Eepfs/resources/pdf_pubs/MRCasiCal.pdf. [Accessed: 2005-05-13].
16. Specim, “aisa EAGLE hyperspectral sensor”. [Online]. Available: http://www.specim.fi/media/pdf/product-brochures/aisa-products-ver3-08.pdf. [Accessed: 2008-11-21].
17. I. Baarstad, T. Løke, and P. Kaspersen. “ASI – A new airborne hyperspectral imager,” in *Proc. of the 4th EARSeL Workshop on Imaging Spectroscopy*, Warsaw, Poland, 26-29 April, 2005, pp. 107–110.
18. N. Oppelt and W. Mauser, "The Airborne Visible / Infrared Imaging Spectrometer AVIS: Design, Characterization and Calibration," *Sensors,* vol. 7, no. 9, pp. 1934-1953, September 2007. [Online]. Available: MDPI, doi: 10.3390/s7091934. [Accessed: 2009-03-31].
19. K. I. Itten et al., "APEX - the Hyperspectral ESA Airborne Prism Experiment," *Sensors* vol. 8, no. 10, pp. 6235-6259, October 2008. [Online]. Available: MDPI, doi: 10.3390/s8106235. [Accessed: 2008-10-22].
20. A. Müller et al., “ARES: a new reflective/emissive imaging spectrometer for terrestrial applications,” in *Proc. of SPIE*, vol. 5574, 2004, pp. 120-127.
21. B. Suhr, P. Gege, J. Nieke, K. I. Itten, and G. Ulbrich, “Calibration facility for airborne imaging spectrometers,” in *Proc. of SPIE*, vol. 5978, 2005, pp. 225-233.
22. T. G. Chrien and T. Rubin, “Calibration and Valdidation of Imaging Spectrometer Data,” in *2nd Int. Airborne Remote Sensing Conference and Exhibition, ERIM, San Francisco*, 1996.
23. Australian Government - National Measurement Institute, “International measurement,” 22 Sep 2009. [Online]. Available: http://www.measurement.gov.au/IM/Pages/home.aspx. [Accessed: 2009-10-20].
24. NERC Field Spectroscopy Facility, “FSF home page,” 2009. [Online]. Available: http://fsf.nerc.ac.uk/. [Accessed: 2010-01-27].
25. Onera, “Theorical and Applied Optics: Facilities (DOTA),” 2009. [Online]. Available: http://www.onera.fr/dota-en/facilities.php. [Accessed: 2010-01-25].
26. Japan Aerospace Exploration Agency - Earth Observation Research Center (JAXA, EORC), “Advanced Land Observing Satellite (ALOS)”. [Online]. Available: http://www.eorc.jaxa.jp/ALOS/en/index.htm. [Accessed: 2010-01-25].

27. Centre Spatial de Liège (CSL), “Space Activities, Non Space Activities and Services,” 2010. [Online]. Available: http://www.csl.ulg.ac.be/. [Accessed: 2010-01-26].
28. NASA Jet Propulsion Laboratory, “An Overview of MISR Calibration Objectives,” 2008. [Online]. Available: http://www-misr.jpl.nasa.gov/mission/calib.html. [Accessed: 2010-01-26].
29. Rupert Müller, M. Lehner, Rainer Müller, P. Reinartz, M. Schroeder, and B. Vollmer, “A program for direct georeferencing of airborne and spaceborne line scanner images,” in *Proc. of the ISPRS Commission I Symposium*, vol. XXXIV, part 1, 2002, pp. 148-153.
30. J. Schulz, “Systemtechnische Untersuchungen an dem abbildenden Spektrometer ROSIS-01 zur Erfassung und Interpretation der Meeresfarben,” Ph.D. dissertation, Forschungsbericht 97-08. Weßling, Germany: German Aerospace Center (DLR), Institut für Optoelektronik, 1997.
31. P. Gege and W. Mooshuber, “Electronic Performance of the Imaging Spectrometer ROSIS-03,” in *Proc. of the ISPRS Joint Workshop: Sensors and Mapping from Space*, Hannover, Germany, 1997, pp. 49-67.
32. R. Richter, A. Mueller, M. Habermeyer, S. Dech, K. Segl, and H. J. Kaufmann, “Spectral and radiometric requirements for the airborne thermal imaging spectrometer ARES,” *International Journal of Remote Sensing (IJRS)*, vol. 26, iss. 15, pp. 3149-3162, 2005.
33. J. Nieke et al., “Calibration methodology for the airborne dispersive pushbroom imaging spectrometer (APEX),” in *Proc. of SPIE*, vol. 5570, 2005, pp. 445-452.
34. P. Gege et al., “Calibration facility for airborne imaging spectrometers,” *ISPRS Journal of Photogrammetry and Remote Sensing*, vol. 64, iss. 4, pp. 387-397, July 2009.
35. M. E. Schaepman, “Calibration of a Field Spectroradiometer,” Ph. D. dissertation, Remote Sensing Series, Vol. 31. Zurich, Switzerland: Remote Sensing Laboratories, University of Zurich, 1998.
36. Specim, “AISA airborne imaging spectrometer,” 2001. [Online]. Available: http://www.specim.fi. [Accessed: 2001-01-19].
37. P. Strobl, H. Schwarzer, J. Fries, P. Schötz, and H.-R. Böhl, “APEX-CHB Preliminary Design Report,” German Aerospace Center (DLR), Weßling, Germany, Rep. APEXCHB-DLR-REPP004, 2004.
38. G. Ulbrich, “Calibration Home Base for APEX - Statement of Work,” Rep. EEM-FI/2001-12-568/GU/gu, 2001.
39. K.-H. Sümnich, “Vorrichtung zur Kalibrierung eines optischen Instrumentes mit einem fotoelektrischen Detektor,” German Patent, DE 102 18 947 A1, 2002.
40. P. Gege et al., “APEX-CHB Final Report,” German Aerospace Center (DLR), Weßling, Germany, Rep. APEXCHB-DLR-REPP006, 2007.
41. Newport, “Oriel MS257 ¼ m Monochromator and Imaging Spectrograph,” 2010. [Online]. Available: http://search.newport.com/?q=*&x2=sku&q2=77700. [Accessed: 2010-01-28].

References

42. B. Suhr, J. Fries, P. Gege, and H. Schwarzer, “APEX calibration facility: status and first commissioning results,” in *Proc. of SPIE*, vol. 6361, 2006, pp. 636110-1 – 636110-9.
43. Newport, “Infrared Elements for Oriel Light Sources,” 2007. [Online]. Available: http://www.newport.com/store/genproduct.aspx?id=378507&lang=1033&Section=Pricing. [Accessed: 2007-11-21].
44. Testo, “testo 545: Beleuchtungsstärke-Messgerät,” 2009. [Online]. Available: http://www.testo.de/online/abaxx-?$part=PORTAL.DEU.ContentDesk&$event=show-from-menu&categoryid=1209443. [Accessed: 2010-01-28].
45. Meilhaus Electronic, “USB & mobile Messtechnik – Temperatur-Messung: Mini-Datenlogger Zuckerwürfel”. [Online]. Available: http://www.meilhaus.org/downloadserver/zwcv/german/me-zw_3_07d.pdf. [Accessed: 2010-01-28].
46. DLR, “IT-Sicherheitspolitik des DLR,” Deutsches Zentrum für Luft- und Raumfahrt (DLR),” Nov. 2001.
47. M. Ecker, “Automatisierung einer optoelektronischen Kalibriereinrichtung,” thesis, Landshut University of Applied Sciences, Landshut, Germany, 2007.
48. Microsoft Developer Network (MSDN), “Visual C++ Libraries: MFC Library Reference,” 2008. [Online]. Available: http://msdn.microsoft.com/en-us/library/d06h2x6e(VS.71).aspx. [Accessed: 2008-06-05].
49. Oxford Brookes University, “History of the Web,” 2002. [Online]. Available: http://www.w3c.rl.ac.uk/primers/history/origins.htm. [Accessed: 2008-06-27].
50. Microsoft Developer Network (MSDN), “Windows TCP/IP Stack Components: Application Layer,” 2008. [Online]. Available: http://msdn.microsoft.com/en-us/library/aa505920.aspx. [Accessed: 2008-02-11].
51. World Wide Web Consortium (W3C), “Extensible Markup Language (XML),” 2009-04-16. [Online]. Available: http://www.w3.org/XML/. [Accessed: 2008-06-05].
52. World Wide Web Consortium (W3C), “XML Schema,” 2010-01-12. [Online]. Available: http://www.w3.org/XML/Schema. [Accessed: 2010-01-28].
53. The Apache Software Foundation, “Xerces-C++ XML Parser,” 2007. [Online]. Available: http://xerces.apache.org/xerces-c/. [Accessed: 2008-06-06].
54. L. Thomason, Y. Berquin, and A. Ellerton, “TinyXml Documentation 2.5.1,” 2006-08-18. [Online]. Available: http://www.grinninglizard.com/tinyxmldocs/index.html. [Accessed: 2008-06-05].
55. S. Leistenschneider, “Software zur automatisierten Kalibrierung optischer Sensoren,” thesis, Munich University of Applied Sciences, Munich, Germany, 2007.
56. World Wide Web Consortium (W3C), “XHTML™ 1.0 The Extensible HyperText Markup Language (Second Edition),” 2002. [Online]. Available: http://www.w3.org/TR/xhtml1/. [Accessed: 2010-01-28].
57. World Wide Web Consortium (W3C), “The Extensible Stylesheet Language Family (XSL),” 2009-11-13. [Online]. Available: http://www.w3.org/Style/XSL/. [Accessed: 2010-01-28].

58. The Apache Software Foundation, “Xalan-C++ version 1.10,” 2004. [Online]. Available: http://xml.apache.org/xalan-c/. [Accessed: 2008-06-04].
59. OWIS, “Microstep Controller SM32 – User Manual,” OWIS GmbH, Staufen, Germany, SM32UM0100-02E, 2005.
60. ORIEL, “Programming Manual for MS257,” ORIEL Instruments, Stratford, CT, USA, 77700B-M, 1994.
61. L.O.T.-Oriel Groupe Europe, “Pen-Ray Line Sources,”. [Online]. Available: http://www.lot-oriel.com/site/site_down/ls_calibration_deen15.pdf. [Accessed: 2008-08-31].
62. Newport, “Oriel Pencil Style Calibration Lamps,” 2008. [Online]. Available: http://www.newport.com/file_store/PDFs/tempPDFs/e5395_Oriel-Pencil-Style-Calibration-Lamps.pdf. [Accessed: 2008-04-09].
63. Berg, I., “muParser library,” 2006. [Online]. Available: http://muparser.sourceforge.net. [Accessed: 2010-01-28].
64. Lavrsen, K., “Open2300,” 2006. [Online]. Available: http://www.lavrsen.dk/twiki/bin/view/Open2300/WebHome. [Accessed: 2008-12-01].
65. World Wide Web Consortium (W3C), “HTTP - Hypertext Transfer Protocol,” 2008. [Online]. Available: http://www.w3.org/Protocols/. [Accessed: 2008-06-05].
66. World Wide Web Consortium (W3C), “Document Object Model (DOM),” 2005-01-19. [Online]. Available: http://www.w3.org/DOM/. [Accessed: 2008-06-05].
67. M. Goubeau, “Automatisierung des Hyperspektralsensors AISA für den Feld- und Laboreinsatz,” thesis, TU München, Munich, Germany, 2007.
68. SPECIM, “AISA Airborne Imaging Spectrometer: User’s Manual, Version 1.2,” Spectral Imaging Ltd. (SPECIM), Oulu, Finland, 1997.
69. SPECIM, “AISA Airborne Imaging Spectrometer: User’s Manual, Version 3.0,” Spectral Imaging Ltd. (SPECIM), Oulu, Finland, March 2001.
70. SPECIM, “AISA Airborne Imaging Spectrometer: Raw Data Format Description, Version 1.7,” Spectral Imaging Ltd. (SPECIM), Oulu, Finland, July 1997.
71. R. Bärs, L. Watson, and O. Weatherbee, “AISA as a tool for timely commercial remote sensing,” in *Proc. of the 4th International Airborne Remote Sensing Conference and Exhibition / 21st Canadian Symposium on Remote Sensing*, Ottawa, Canada, 1999, pp. I-239 – I-246.
72. J. Okkonen and F. Plassmeier, “Interface protocol between airobotics navigation computer and Specim AISA sensor head control computer, version 1.6,” Spectral Imaging Ltd., Oulu, Finland and airobotics GmbH, Bremen, Germany, 2001.
73. J. R. Schott, *Remote Sensing: The Image Chain Approach*, New York: Oxford University Press, 1997, pp. 148-189.
74. H.J. Kramer, *Observation of the Earth and its Environment*, 2nd ed. Berlin, Germany: Springer-Verlag, 1994, pp. 311-312.
75. H. S. Chen, *Remote Sensing Calibration Systems: An Introduction*, Vol. 142, Hampton, Virginia, USA: A. Deepak Publishing, 1997.

References

76. G. R. Hopkinson, T. M. Goodman, and S.R. Prince, *A Guide to the Use and Calibration of Detector Array Equipment*, Vol. PM142. Bellingham, Washington, USA: SPIE Press Book, 2004.
77. A. Stewart and T. Cocks, “ARES User's Manual – Draft,” Integrated Spectronics Pty Ltd., Castle Hill, Australia, Rep. DLR-MAN-DOC-User-002, iss. 1, 2006.
78. F. Dell'Endice, J. Nieke, D. Schläpfer, and K. I. Itten, „Scene-based method for spatial misregistration detection in hyperspectral imagery,” *Applied Optics*, vol. 46, iss. 15, pp. 2803-2816, May 2007.
79. D. Schläpfer, J. Nieke, and K. I. Itten, “Spatial PSF Nonuniformity Effects in Airborne Pushbroom Imaging Spectrometry Data,” *IEEE Trans. on Geoscience and Remote Sensing*, vol. 45, no. 2, pp. 458-468, February 2007.
80. J. Nieke, D. Schläpfer, F. Dell’Endice, J. Brazile, and K. I. Itten, “Uniformity of Imaging Spectrometry Data Products,” *IEEE Trans. on Geoscience and Remote Sensing*, vol. 46, no. 10, pp. 3326-3336, October 2008.
81. E.J. Milton, N. Fox, and S. Mackin, “Calibration, validation and the NERC Airborne Remote Sensing Facility,” in *Annual Conference of the Remote Sensing and Photogrammetry Society, Aberdeen, Scotland*. Nottingham, UK, Remote Sensing and Photogrammetry Society, Sept. 2004. [Online]. Available: http://eprints.soton.ac.uk/20399/. [Accessed: 2010-01-26].
82. National Research Council Canada, „NRC Institute for National Measurement Standards (NRC-INMS),” 2010-01-15. [Online]. Available: http://www.nrc-cnrc.gc.ca/eng/ibp/inms.html. [Accessed: 2010-01-26].
83. Physikalisch-Technische Bundesanstalt (PTB), “Abteilung 4 – Optik,” 2010-01-22. [Online]. Available: http://www.ptb.de/de/org/4/_index.htm. [Accessed: 2010-01-26].
84. The National Physical Laboratory (NPL), “The UK’s National Measurement Institute,” 2010. [Online]. Available: http://www.npl.co.uk/. [Accessed: 2010-01-26].
85. National Institute of Standards and Technology (NIST), “Calibration Services,” 2010-01-15. Online]. Available: http://ts.nist.gov/MeasurementServices/Calibrations/index.cfm. [Accessed: 2010-01-26].
86. Bureau International des Poids et Mesures (BIPM), “The International Bureau of Weights and Measures”. [Online]. Available: http://www.bipm.org/en/bipm/. [Accessed: 2010-01-26].
87. ALLSTAR Network, Section 5.1 - The Axes of Rotation,” 2004. Online]. Available: http://www.allstar.fiu.edu/aero/flight51.htm. [Accessed: 2010-01-26].
88. P. Gege et al., “CHB Handbook,” German Aerospace Center (DLR), Weßling, Germany, Rep., iss. 0.1, 2007.
89. D. Oertel and B. Zhukov, *On-ground calibration facility and calibration algorithms for wide-angle imaging and videospectrometric airborne sensor in the VIS-TIR spectral range*, Forschungsbericht DLR-FB 93-44. Weßling, Germany: DLR, Institut für Optoelektronik, 1993.

90. F. D. van der Meer and S. M. de Jong, eds, *Imaging Spectrometry: Basic Principles and Prospective Applications*, Vol. 4, Dordrecht, the Netherlands: Kluwer Academic Publishers, 2001, pp. 31–43.
91. ASD Inc., “FR Sampling Interval and Spectral Resolution,” 1999. [Online]. Available: http://www.asdi.com/FR-Sampling-Interval-Spectral-Resolution.pdf. [Accessed: 2008-03-23].
92. Labsphere, “A Guide to Reflectance Coatings and Materials”. [Online]. Available: http://www.labsphere.com/data/userFiles/A%20Guide%20to%20Reflectance%20Coatings%20and%20Materials.pdf. [Accessed: 2008-07-05].
93. SPECIM, “AISA Sensor Head Calibration Test Report: Schneider CNG 1.4/8 mm lens,” Spectral Imaging Ltd. (SPECIM): Oulu, Finland, July 2000.
94. SPECIM, “AISA Sensor Head Calibration Test Report: Schneider CNG 1.4/23 mm lens,” Spectral Imaging Ltd. (SPECIM): Oulu, Finland, July 2000.
95. Schneider Optics, “Cinegon 1.4/8.0 mm: Performance Data,” Schneider Optics, Inc.: New York, USA, 2000.
96. Schneider Optics, “Xenoplan 1.4/23 mm: Performance Data,” Schneider Optics, Inc.: New York, USA, 2000.
97. B. M. Braam, J. T. Okkonen, M. Aikio, K. Makisara, and J. F. Bolton, “Design and first test results of the Finnish airborne imaging spectrometer for different applications (AISA),” in *Proc. of SPIE*, vol. 1937, 1993, pp. 142-151.
98. M. Damm, “Charakterisierung und Korrektur von Streulicht in einem flugzeuggetragenen Hyperspektralsystem,” thesis, Mittweida University of Applied Sciences, Mittweida, Germany, 2007.
99. P. Gege et al., “ROSIS Handbook,” German Aerospace Center (DLR), Weßling, Germany, internal report, iss. 0.22, 2008.
100. F. Yutian, “ROSIS-03 Report 10/03 - 12/03,” German Aerospace Center (DLR), Weßling, Germany, 2003.
101. S. Thiemann, P. Strobl, P. Gege, N. Stahl, W. Mooshuber, and H. van der Piepen, “Das abbildende Spektrometer ROSIS,” in *21.Jahrestagung der Deutschen Gesellschaft für Photogrammetrie und Fernerkundung (DGPF)*, Band 10, Sept. 2001, pp. 147-153.
102. S. Jackschath, “Charakterisierung des Hyperspektralsensors AISA und dessen Umbau zu einem Feldmessgerät,” thesis, TU München, Munich, Germany, 2005.
103. P. Mouroulis and M.M. McKerns, “Pushbroom imaging spectrometer with high spectroscopic data fidelity,” SPIE Optical Engineering, vol. 39, no. 3, pp. 808-816, March 2000.
104. Airobotics, “Hyperspektralscanner AISA: Technische Details,” airobotics GmbH: Bremen, Germany, 2004.
105. SPECIM, “AISA Airborne Imaging Spectrometer: Viewing geometry check Ver. 1.0,” Spectral Imaging Ltd. (SPECIM): Oulu, Finland, January 2001.

References

106. Leica Geosystems, “Leica PAV30: Gyro-Stabilized Camera Mount,” 2002. [Online]. Available: http://www.aerial-survey-base.com/pdfs/Cameras_PDF/Leica/PAV30_Brochure.pdf. [Accessed: 2010-01-27].
107. Newport, “Ellipsoidal and Paraboloidal Reflectors”. [Online]. Available: http://www.newport.com/file_store/PDFs/tempPDFs/e5530_Ellipsoidal-and-Paraboloidal-Reflectors.pdf. [Accessed: 2007-11-26].
108. B. Suhr, *Bedienungsanleitung für die Steuerung des Spaltrades*, German Aerospace Center (DLR), IFM, Weßling, Germany, 2006.
109. Free Software Foundation, Inc., “GNU Wget,” 2008-02-07. [Online]. Available: http://www.gnu.org/software/wget/. [Accessed: 2008-06-05].
110. B. Suhr and J. Fries, “Monochromator Calibration Measurement Report,” German Aerospace Center (DLR), IFM, Weßling, Germany, March 2008.